International
Progress Report

IPR-02-41

Äspö Hard Rock Laboratory

Groundwater flow, mixing and geochemical reactions at Äspö HRL

Task 5. Äspö Task Force on groundwater flow and transport of solutes

A.Luukkonen
E. Kattilakoski

VTT Building and Transport & VTT Energy, Finland

April 2001

Svensk Kärnbränslehantering AB
Swedish Nuclear Fuel
and Waste Management Co
Box 5864
SE-102 40 Stockholm Sweden
Tel +46 8 459 84 00
Fax +46 8 661 57 19

Äspö Hard Rock
Laboratory

Report no.	No.
IPR-02-41	F65K
Author	Date
Luukkonen, Kattilakoski	01-04-01
Checked by	Date
Margit Snellman, Amio Hautojärvi	02-04-30
Approved	Date
Christer Svemar	02-11-19

Äspö Hard Rock Laboratory

Groundwater flow, mixing and geochemical reactions at Äspö HRL

Task 5. Äspö Task Force on groundwater flow and transport of solutes

A.Luukkonen

E. Kattilakoski

VTT Building and Transport & VTT Energy, Finland

April 2001

Keywords: Groundwater flow, solute transport, coupled hydrogeochemistry, chemistry, mixing, mole balance, Äspö, Task 5

FOREWORD

This report summarises the work by the Posiva Oy modelling group, performed within Task #5. The general backgrounds and objectives of the project are shortly concluded in the abstract. The report is made up of five parts with the following titles and authors:

Part I. Groundwater flow, mixing and geochemical reactions at Äspö Hard Rock Laboratory – Executive summary. A. Luukkonen and E. Kattilakoski.

Part II. Mixing proportions of brine, glacial, meteoric and Baltic Sea waters in the Äspö tunnel. E. Kattilakoski.

Part III. Groundwater mixing and geochemical reactions – An inverse-modelling approach. A. Luukkonen.

Part IV. Mixing proportions of glacial, Litorina, altered, saline, meteoric and Baltic Sea waters in the Äspö tunnel. E. Kattilakoski and A. Luukkonen.

Part V. Modelling questionnaire for Task #5. E. Kattilakoski and A. Luukkonen.

ABSTRACT

The Task #5 project was a part of the Äspö task force on modelling of groundwater flow and transport of solutes. The aim of the Task #5 was to compare and eventually integrate hydrochemistry and hydrogeology. At the launch of the project, it was stated that the results and methods developed in the project would be useful for an assessment of the stability of the hydrodynamic and hydrochemical conditions for any future repository site located in a crystalline bedrock environment. The first objective of the task was to assess the consistency of groundwater flow models and hydrochemical mixing-reaction models through comparison of hydraulic and chemical data as a function of Äspö tunnel construction. The ultimate objective was to develop a procedure for integration of hydrological and hydrochemical information.

The starting point for consistency comparisons, and integration of hydrological and hydrochemical information is how the mixing fractions and initial boundary conditions of the reference water types are extracted from the geochemical data. Two optional methods for this extraction were available. The results of the first method were delivered for all Task #5 modelling groups, and it classifies the geochemical data with reference of four different water types: brine (highly saline water), glacial melt (water from the Pleistocene glacier), meteoric (1960's precipitation estimate) and the present Baltic Sea water. Posiva Oy's modelling group developed the second method for geochemical data interpretations. The second method classifies the geochemical data with reference of seven different water types: saline, preglacial altered (shallow altered mixed water), glacial melt, Litorina Sea (relic fresh seawater), postglacial altered (shallow altered seawater), meteoric (shallow altered fresh water) and the Baltic Sea water (present fresh seawater).

The hydrodynamical modelling code, used in the flow-transport simulations, couples the residual pressure and salinity fields to solve the groundwater flow and solute transport equations defined for the study volume. Mixing fractions are transported in the simulations like any solute. No geochemical reactions are taken into account during transport. Initial conditions (hydrological and geochemical) on the boundaries and within the study volume give the starting values for the calculations. The consistencies between the simulated mixing fractions (groundwater flow model) and the observed mixing fractions (hydrochemical mixing-reaction model) at specific control points are attempted to reach by modifying hydrological parameters within the study model suitably. The second geochemical modelling method used in the studies allows assessment of net-geochemical reactions along a flow path after a simulation; fulfilling the hydrological-geochemical integration demand with a loose one-step process.

The two optional geochemical data extraction methods and the simulation results with the two alternative geochemical boundary conditions show significant discrepancies. Differences in results can be pointed to geochemical extraction methods and inadequate hydrological definition of the model volume. These discrepancies as such strongly point out the need of integrated view in repository site investigations.Posiva

SAMMANFATTNING

Task 5-projektet var en del av Äspös samarbete om modellering av grundvattenflöde och transport av lösningar. Syftet med Task 5 var att jämföra och slutligen integrera hydrokemi och hydrogeologi. Vid uppstarten av projektet bestämdes att resultat och metoder som utvecklats i projektet skulle vara användbara för en utvärdering av hydrokemiska och hydrologiska förhållandens stabilitet på varje framtida förvarsplats i kristallint berg. Det första målet med projektet var att utvärdera stabiliteten hos modeller för grundvatten och modeller för hydrokemiska blandningsreaktioner genom jämförelse med hydrauliska och kemiska data som en funktion av drivningen av Äspörampen. Det slutliga målet var att utveckla ett sätt att integrera hydrogeologisk och hydrokemisk information.

Utgångspunkten för jämförelsen av överensstämmelsen och integreringen av hydrologisk och hydrokemisk information är hur blandfraktionerna och ursprungliga randvillkor hos referensvattnet sammanställs med hjälp av geokemiska data. Två alternativa metoder för denna sammanställning var tillgängliga. Resultatet med den första metoden spreds till alla modellgrupper i Task 5. Metoden klassificerar geokemiska data med hänsyn till fyra olika vattentyper: saltlake (vatten med hög salthalt), glacialt smältvatten (vatten från den pleistocena perioden), meteoriskt vatten (1960-talets nederbördsuppskattning) och det nuvarande Östersjövattnet. Posiva Oys modellgrupp utvecklade den andra metoden för geokemisk datatolkning. Metod nummer två klassificerar geokemiska data med hänsyn till sju olika vattentyper: salt, förglacialt förändrat (grunt förändrat blandat vatten), glacialt smältvatten, Litorinavatten (relikt sött havsvatten), postglacialt förändrat (grunt förändrat havsvatten), meteoriskt (grunt förändrat sött vatten) och Östersjövatten (nuvarande sött havsvatten).

Den hydrodynamiska koden, som användes i flödes-transportsimuleringen, kopplar kvarvarande tryck-och salthaltsfält för att lösa flöde av grundvatten och transport av lösningar, vilka definierats för den studerade volymen. Blandade fraktioner transporteras i simuleringen som vilken annan lösning som helst. Ingen geokemisk reaktion antas ske under transporten. Ursprungliga förhållanden (hydrologiska och geokemiska) längs ränderna och inom den studerade volymen ger startvärdena för beräkningarna. Man försöker uppnå överensstämmelse mellan de simulerade blandningsfraktionerna (flödesmodell för grundvatten) och de observerade blandningsfraktionerna (model för hydrokemisk blandningsreaktion) i specifika kontrollpunkter genom att modifiera hydrologiska parametrar på ett lämpligt sätt i de studerade modellerna. Den andra geokemiska modellmetoden som användes i studierna tillåter analys av slutstadiet av geokemiska reaktioner längs en flödesväg efter en simulering och fullföljer de hydrologiska-geokemiska integrationskraven med en öppen enstegsprocess.

De två alternativa metoderna för sammanställning av geokemiska data och simuleringsresultat med de två alternativa geokemiska randvillkoren visar signifikant avvikelse. Skillnader i resultat kan härledas till geokemiska sammanställningsmetoder och otillräckliga hydrologiska definitioner av modellvolymen. Dessa avvikelser påtalar tydligt behovet av en integrerad syn vid platsundersökningar.

TABLE OF CONTENTS

Part I

EXECUTIVE SUMMARY

EXECUTIVE SUMMARY

Introduction

Background and objectives

The SKB Task #5 plan presented in Autumn ’97 outlined the primary rationale for the studies presented here in three separate reports following this summary. The fundamental aims of the Task were to compare and to develop procedures for integration of hydrological and hydrochemical information, which could be used for assessment of potential disposal sites. It was stressed that integration of hydrochemistry and hydrology should be a prime objective of each modelling group.

The objective of the Task was also to assess the consistency of groundwater flow models and hydrochemical mixing-reaction models through integration and comparison of hydraulic and chemical data obtained before, during and after the Äspö tunnel construction. This objective was met by simulating hydrological-hydrochemical changes with two separate approaches, and by comparing results from these to each other. The first coupling attempt of hydrological-hydrochemical changes was based on groundwater mixing fractions calculated with the M3 method (Laaksoharju et al., 1999), and the other was based on the results obtained with an inverse modelling method. The basics of the hydrological simulations and the principles of both the geochemical calculation methods are shortly introduced in the following, as well as the benefits and the deficiencies of the simulation results.

The objectives of the Task motivated the development of an inverse hydrochemical-modelling tool (as first referred to by Plummer et al., 1983) for the Äspö site. The inverse modelling tool attempts to meet the requirements set in the Task #5 plan. It identifies the original (or reference) groundwater types based on the palaeo-evolution of the site, identifies the mixing portions of the reference water types in each obtained and studied water sample, and evaluates the effects of net-geochemical reactions during the reference water mixings. Perhaps most importantly, however, “the inverse modelling approach” introduces the forward predictive tool for taking into account reactions in hydrological simulations.

Groundwater flow modelling

Model concepts and formulation

The mathematical formulation of groundwater flow (Bear, 1979; Huyakorn & Pinder, 1983; de Marsily, 1986) and transport in the dual porosity medium (Huyakorn et al., 1983) comprises three coupled partial differential equations with non-linearities. Two of them describe the flow of water with variable density and the amount of mass transported with flowing water in the water-bearing fractures. The third equation describes the amount of mass transported by diffusion in the matrix blocks.

The flow and transport in the water-bearing fractures are coupled by the density and the Darcy velocity. This results in a system of two non-linear partial differential equations that can rarely be solved analytically. The equations describing the amount of mass transported with flowing water in the water-bearing fractures and by diffusion in the matrix blocks are coupled by the continuity of the diffusive mass flux at the interface of the fracture and the matrix block. The finite element code FEFTRA was used in this work for the numerical solution (Taivassalo et al., 1991; Löfman & Taivassalo, 1993; Laitinen, 1995).

The finite element method with linear elements was employed. The conventional Galerkin technique (Huyakorn & Pinder, 1983) was applied to the flow equation. In order to avoid the numerical problems related to highly convective cases the transport equation was solved using the streamline-upwind/Petrov-Galerkin (SUPG) method (Brooks and Hughes, 1992; implemented in FEFTRA by Laitinen, 1995). The conventional Galerkin method was applied to the diffusion equation in the matrix blocks.

In the coupled cases non-linearities were treated by the Picard iteration scheme (Huyakorn & Pinder, 1983), which applies the finite element procedure for the flow and the transport equation sequentially. At the end of each iteration sweep the concentration values were updated using an underrelaxation scheme. This way the oscillations of concentration changes from iteration to iteration were reduced. No iteration was needed in the mixing calculations of a single water type, which utilised the previously simulated residual pressure and concentration fields.

An initial estimate for the nodal values of the residual pressure and the concentration at the beginning of the first iteration sweep of each time step was obtained by using a linear time extrapolation formula.

The mass matrices resulting from the finite element formulation of the flow and transport equations were formed by a lumping procedure. In practical problems this leads to a more stable solution than with a ”consistent” matrix.

The Gauss-Seidel method (Atkinson, 1988; Laitinen, 1994) was used to solve the matrix equation in the mixing calculations. In the coupled calculations the conjugate gradient method (Atkinson, 1988; Laitinen, 1994) was used to solve the finite element formulation of the flow equation for residual pressure and the Gauss-Seidel method to solve the finite element formulation of the transport equation for concentration.

Simulation model

All the certain, probable and possible structures proposed by Rhén et al. (1997) were included in the model (Figure 1). The hydraulic connections were established as given by Rhén et al. (1997, Fig. 6-31 and Table A2-6). The depth of the model is 1500 m.

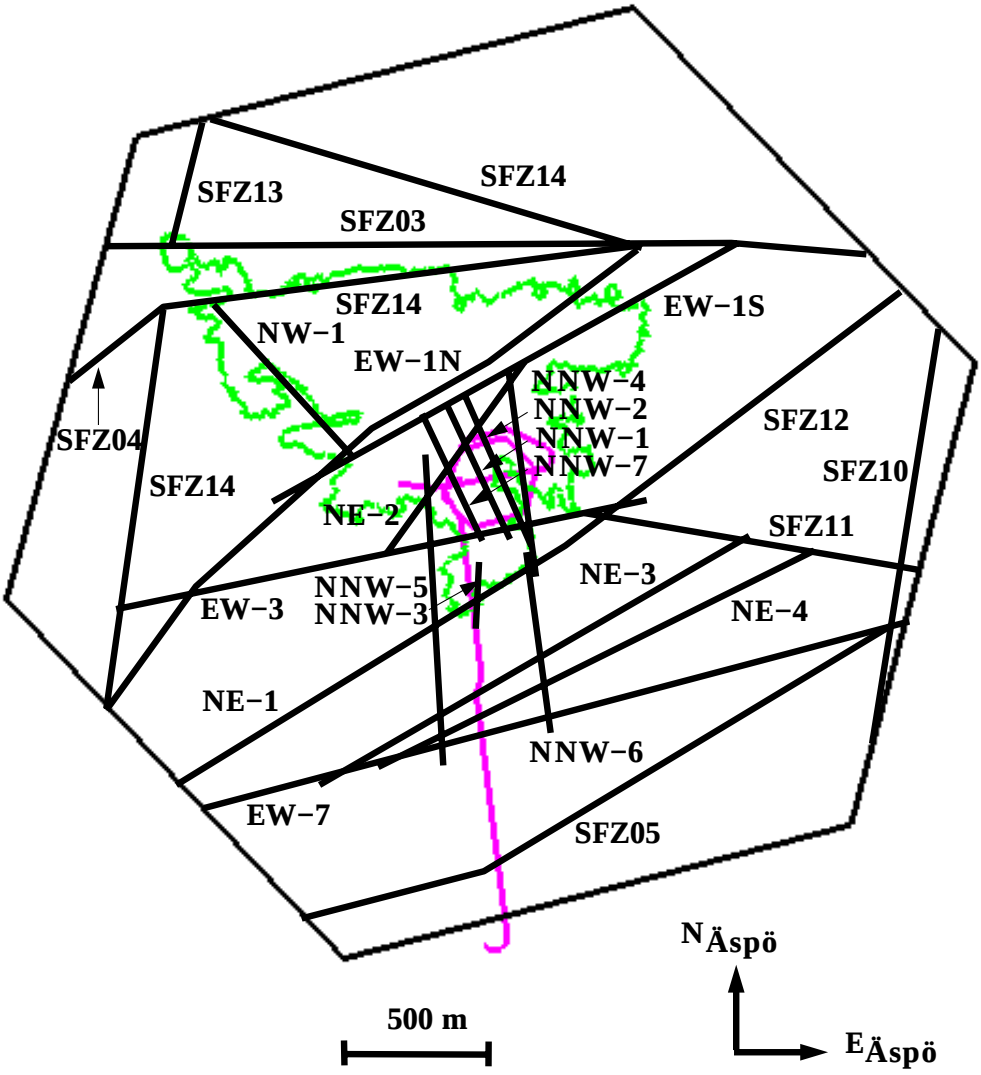

Figure 1. Modelling area and fracture zones at the surface. The coastline of the Äspö Island and the tunnel are also shown.

The properties of the hydraulic units were taken from the work by Rhén et al. (1997) when available. Modifications concerning the shallow depth transmissivities of the fracture zones (except for SFZ05) in the dry land areas and the deep part transmissivities of the zones SFZ05, SFZ12 and NNW-8 were done in the inverse-modelling based hydrological simulations. In these simulations four site scale hydraulic rock mass domains (Rhén et al., 1997) were included in the model.

The finite elements for the rock blocks are linear hexahedrals and wedges. Triangles and quadrangles are used for the fracture zones. The mesh contains 58 224 three-dimensional elements and 13 443 two-dimensional elements.

Seventeen time steps were chosen. They cover the period from the natural conditions until December 1996.

The tunnel and shaft advance was modelled by giving a residual pressure boundary condition for the flow equation and a flow rate boundary condition for the transport equation to the nodes describing the tunnel and shafts in each time step.

In the M3-based simulations the model was calibrated to fit the freshwater head measured in the boreholes KAS02—KAS09, KAS12 and KAS14. The tunnel and shaft boundary conditions given in those simulations were not modified in the inverse-modelling based simulations.

The tunnel was modelled without modifying the hydraulic conductivity of the rock around it. The residual pressure boundary condition in the tunnel and the shaft was fixed on the basis of the freshwater head measured in the nearmost borehole sections. In order to get an insight into the residual pressure boundary condition to be assigned to the nodes pertaining to the tunnel, the measured freshwater heads from borehole sections at certain times (Forsmark and Rhén, 1994) were assigned to the nearest nodes of the tunnel phase. In case many values were obtained in one node an average was calculated. The measured values not farther than 75 metres away the tunnel were used.

In each time step the nodes representing the tunnel and the shaft were grouped according to the measurement sections determined by the weirs. The flow rate measured at the weir was then uniformly divided between the nodes. In the coupled calculations of residual pressure and concentration the flow rate boundary condition for the transport equation was modified in each time step in accordance with the measurements during the tunnel construction.

The initial concentration boundary condition was defined in accordance with the chemical modelling and with the natural conditions which prevailed before the tunnel construction. In the inverse-modelling based hydrological simulations the chloride distributions given in the land and sea areas differ. The concentration boundary conditions initially given in the interior nodes were released in the first time step. The initial residual pressure boundary condition throughout the model was calculated from the concentration distribution. In the first time step the residual pressure in the interior and bottom nodes was released. Zero residual pressure was applied at the sea level, while groundwater table was specified over the land.

In the second time step the progress of the tunnel was taken into account for the first time. The groundwater table boundary condition at the surface of the model was released. A flow rate boundary condition giving an infiltration of about 20 mm/a in the shaft area was given for the flow equation in the nodes depicting the land.

Low freshwater heads were measured in the uppermost packed-off sections of the borehole KAS02. Thus, relatively low residual pressure corresponding to the freshwater head $h_{0,shaft}(z)$ = -80 m was assigned to the nodes representing the shaft. However, the model is not fully capable of producing the low freshwater head measured in the borehole KAS02. The first modelling stage of the shaft in November 1992 impairs the fit between the model result and the measurements (Figure 2).

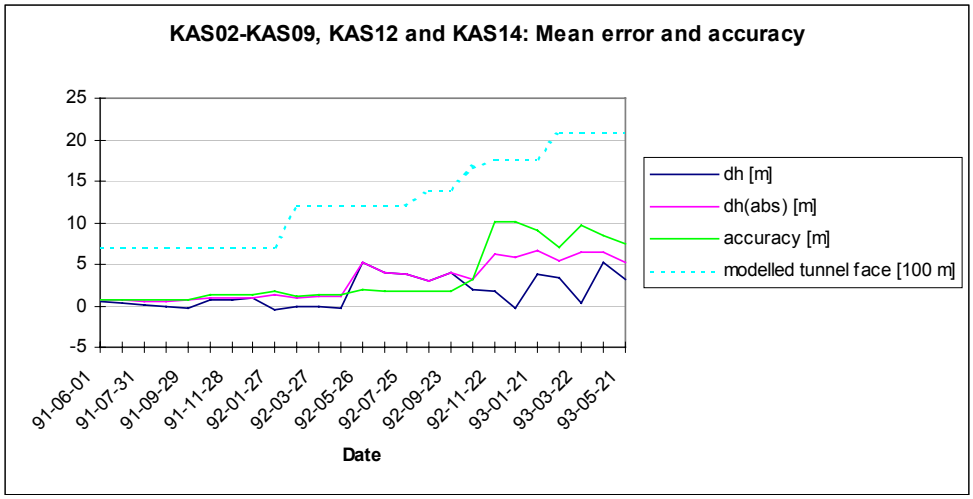

Figure 2. Mean error and accuracy (m) in the boreholes KAS02–KAS09, KAS12 and KAS14 as function of time (M3-based simulations).

In the hydrological simulations the mixing fractions of the reference water types were transported like conservative parameters. The transport equations of the different groundwater types were solved using the previously simulated residual pressure and concentration fields. The initial concentration boundary condition for the transport equations of the different water types was given in each node on the basis of the geochemical modelling. The boundary condition given initially in an interior node was released in the first time step.

The groundwater flow modelling aimed to the determination of the mixing proportions. The simulated mixing proportions give tools to interpret the actual sample compositions for locations of interest.

Geochemical estimations

The M3 method (e.g. Laaksoharju et al., 1999) and the inverse modelling approach (e.g. Pitkänen et al., 1999a) distinctly differ from each other in several respects. At a general level the M3 solution is based statistically on the total number of measured values

comprising the data set while the inverse approach is analytically based on studies of individual samples. Principally, because of the different choice of reference water types the results of the calculation methods can be compared only if the mixing fraction results of both methods are converted back to *chemical composition estimates* of the samples.

Principles of the M3 and inverse modelling approaches

Essentially, the M3 method is a process where all obtained samples and the selected reference water types are put together into a principal component analysis. The variables involved in the calculations are Na, K, Ca, Mg, HCO_3, Cl, SO_4, ^3H, δ^2H and $\delta^{18}O$, and the total variation of this data set is summarised with two principal components (PC_1 and PC_2). According to Laaksoharju et al. (1999) M3 aims to calculate how *mixing* and *reactions* have affected the obtained groundwater samples.

The inverse modelling approach utilises traditional geochemical modelling tools and methods (e.g. Plummer et al., 1994; Parkhurst & Appelo, 1999). The purpose of the inverse geochemical modelling is to determine the kind of initial water samples and geochemical reactions involved, and what reaction amounts are needed in order to produce an existing final water composition. The current modelling approach chains this method sample by sample, and systematically goes through the whole data set sample material used for the studies. Ultimately, the aim is to answer the questions: what kind of *mixtures* of reference water types and how large net geochemical *reactions* are needed to produce each sample composition of the studied data set.

Choice of reference water types

In the M3 method, the reference water types chosen define a polygon on the PC_1 vs. PC_2 plot. All obtained samples are supposed to plot within this polygon (Laaksoharju et al., 1999). The logic is clear, if a sample is mixture of the reference water types, it should not plot outside the polygon. The M3 calculations have been used to interpret the regional groundwater geochemistry from the Äspö Hard Rock Laboratory region (e.g. Laaksoharju & Wallin, 1997; Laaksoharju et al., 1999).

In the inverse modelling approach, the choice of reference water types requires interpretation of the palaeohydrology and palaeogeochemistry of the study area. The relevant succession of historic events constrains the calculations since during each historical period specific reference water types may infiltrate the bedrock. In contrast to M3, no compositional rules are set, i.e. a reference composition may plot also within the data set to be studied.

A simplified history of the Äspö site is presented in Figure 3. The Quaternary history of the island has been divided into four main, hydrogeochemically significant stages that cover the present, Litorina Sea, glacial and preglacial ages.

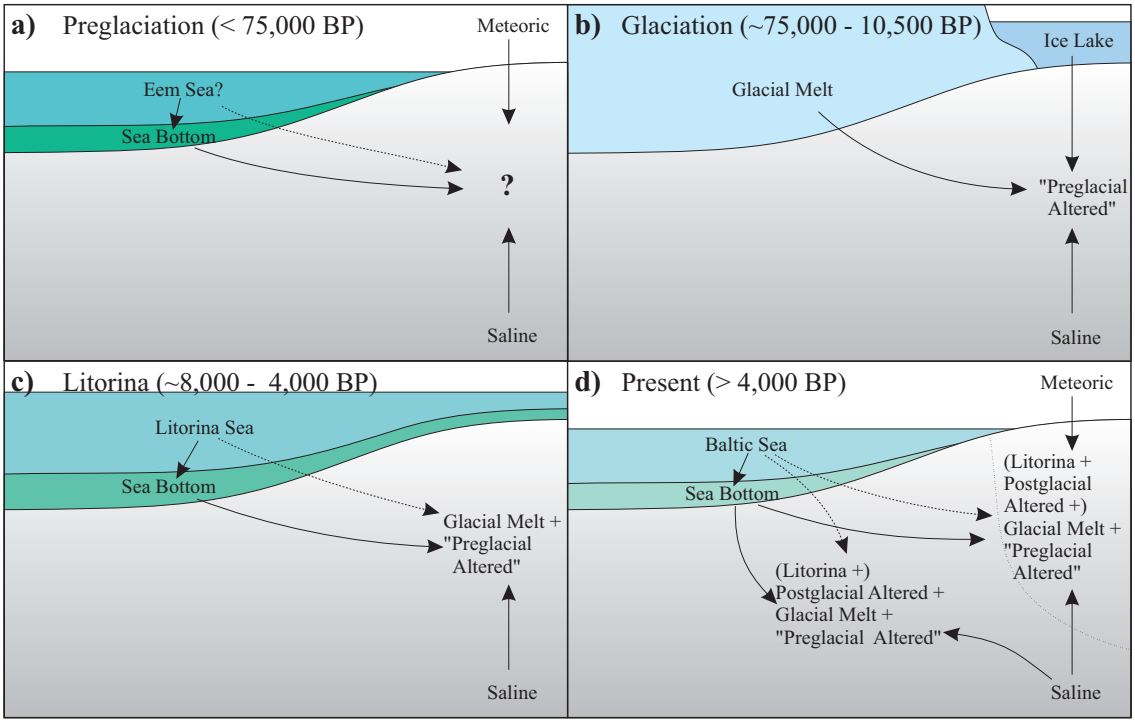

Figure 3. Quaternary history of the Äspö area, based on analyses of geochemical data and interpretations of the Quaternary history of the Fennoscandian Shield (e.g. Eronen, 1988; Laaksoharju & Wallin, 1997). Only periods considered significant for groundwater evolution at the Äspö site are presented.

Figure 4 illustrates the differences between the reference water compositions chosen for the M3 and inverse approaches. The Baltic Sea and glacial melt water compositions selected are practically similar. However, the meteoric reference used in the M3 method is an estimate of 1960's precipitation (Laaksoharju & Wallin, 1997), while in the inverse approach it is dilute shallow level groundwater from the centre of the Äspö Island. The difference between these two meteoric references is minimal if measured with conservative variables (Fig. 4) but quite important if non-conservative variables are studied. Significant reactions occur while fresh rainwater (e.g. 1960's precipitation) infiltrates into the bedrock and becomes dilute shallow level bedrock groundwater. As an example the highest alkalinity concentrations (affecting PC_1 and PC_2 orientations) found from Äspö are present in shallow level bedrock, until concentrations decrease step by step with depth. The inverse approach attempts to take into account this gradual fade out, but this is not possible for the M3 approach which combines the abrupt increase and the gradual fade thus loosing the reaction path which leads to a change in the meteoric water composition.

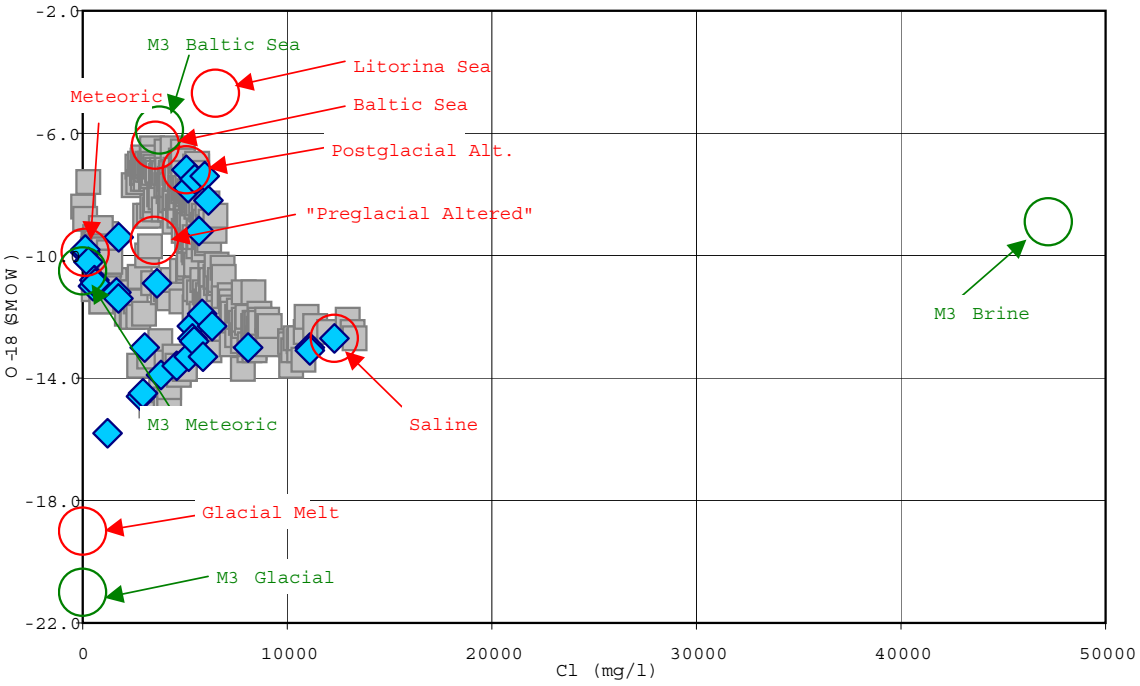

Figure 4. Reference water types of the M3 (green circles), the inverse approach (red circles), undisturbed samples before the tunnel construction (blue diamonds) and disturbed samples during and after the tunnel construction (grey squares) from Äspö in the Cl-^{18}O plot.

An important difference in the approaches is how the saline reference type has been chosen. The M3 method uses a brine sample (depth –1656 m) found from the main land at Laxemar (Laaksoharju & Wallin, 1997), while the inverse approach uses the most saline undisturbed sample (depth –914 m) found below the Äspö Island. The compositional gap between these two is clearly visible in Figure 4. From the viewpoint of this present exercise it is likely that the excavated Äspö laboratory system causes an effective flow system that probably does not extend any deeper downwards from the tunnel construction than it is away from the ground level. Since the laboratory tunnel extends to a depth of 450 m, a saline reference water from a depth of 914 m seems reasonable.

For the current modelling exercise the M3 calculation is based on four reference types (1960's precipitation, Baltic Sea, glacial melt water, and brine). For the inverse approach, seven reference types have been used (Fig. 4).

M3-based results

The mixing ratios simulated at the control points and at certain cutting planes were compared with those from the M3 model (Gurban et al., 1998). As regards to the mixing ratios at the control points, the character of the brine water seems steady, except in the

prediction section (tunnel length > 3000 m), where it is mildly increasing. The glacial water decreases since it is a relict component in present-day groundwater conditions. The meteoric water generally increases. The overall character of the Baltic water seems quite steady. These results are fairly well in line with those by Gurban et al. (1998). As an example of the results, Figure 5 shows the comparison of the simulated mixing ratios with the M3 estimates at the control point SA2074A.

The tunnel construction has caused the upconing of the brine water, the decrease of the relict glacial water and the increase of the mixing ratios of the meteoric and Baltic waters in the tunnel area. These M3-based simulations show the essential role of the dispersion lengths as regards to the mixing ratios at the control points. Also, the infiltration from the sea had to be restricted.

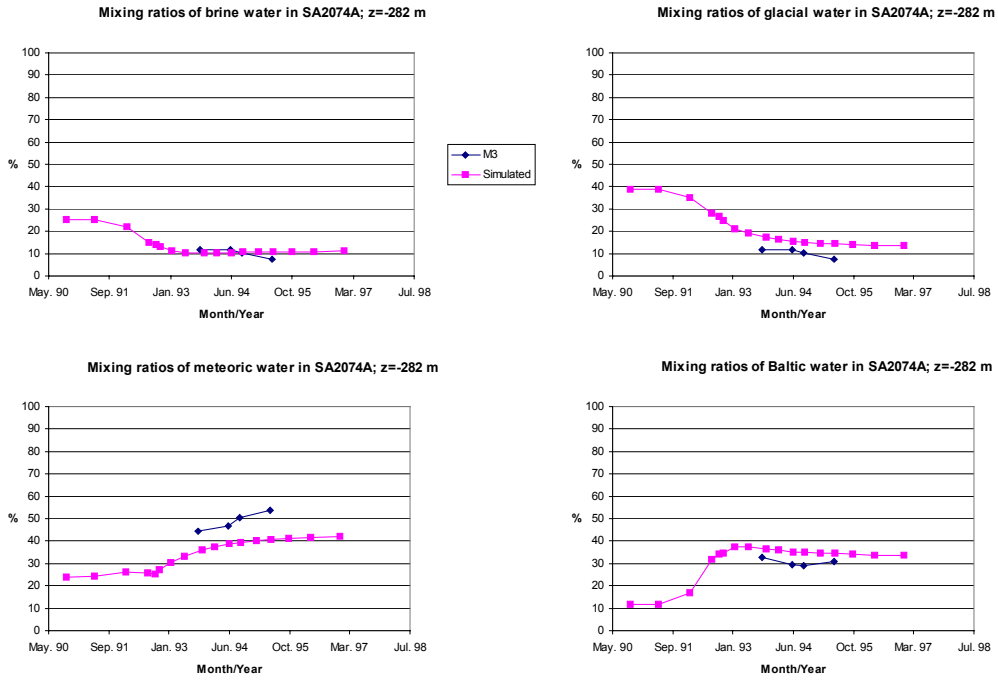

Figure 5. The mixing ratios of brine, glacial, meteoric and Baltic water in SA2074A as a function of time.

In summary, the M3 estimations indicate calm geochemical changes or practically static geochemical conditions during the period that the Äspö tunnel excavations gradually change the initial undisturbed hydrological–geochemical conditions into the disturbed conditions. Similarly, the M3-based simulations produce smooth trends that coincide in most cases relatively well with the M3 estimations. This easily leads to the conclusion that hydrological simulations during disturbed conditions calibrate closely to *observed* geochemical values. However, it is well to remember that these values are not observations but statistically calculated results from the actual observed values.

From the hydrological simulation point of view, the calm changes or almost static conditions are convenient. After the boundaries and the initial conditions are calibrated, conservative and broadly distributed conductivity areas delineate the system, i.e. the whole system reflects more or less an equivalent continuum model.

Inverse-modelling based results

The inverse estimation results give the impression of more brisk geochemical changes in response to the system disturbance (Fig. 6). In most cases there are three distinct water sources (meteoric, Baltic Sea, saline) potentially intruding into a control point. Other water type fractions tend to diminish as a function of time as they do not have any extensive sources.

On the whole, the inverse modelling based simulations give good or fair results at shallow depths compared to the estimated mixing fraction results. By suitably adjusting the surface boundary conditions and the transmissivities the shallow problems usually have been solved. The adjustments of the node types were generally necessary because of the coarseness of the model, and the re-estimations of the transmissivity values usually were necessary because of a lack of measurement values. At depth two major problems can be pointed out in the simulations. At certain control points the difference between the estimations and simulations begins systematically to increase after the control point actually experiences the effect of the neighbouring open tunnel. At least in one case it seems that the hydrological model may behave too stiffly in time compared to the geochemically estimated fractions.

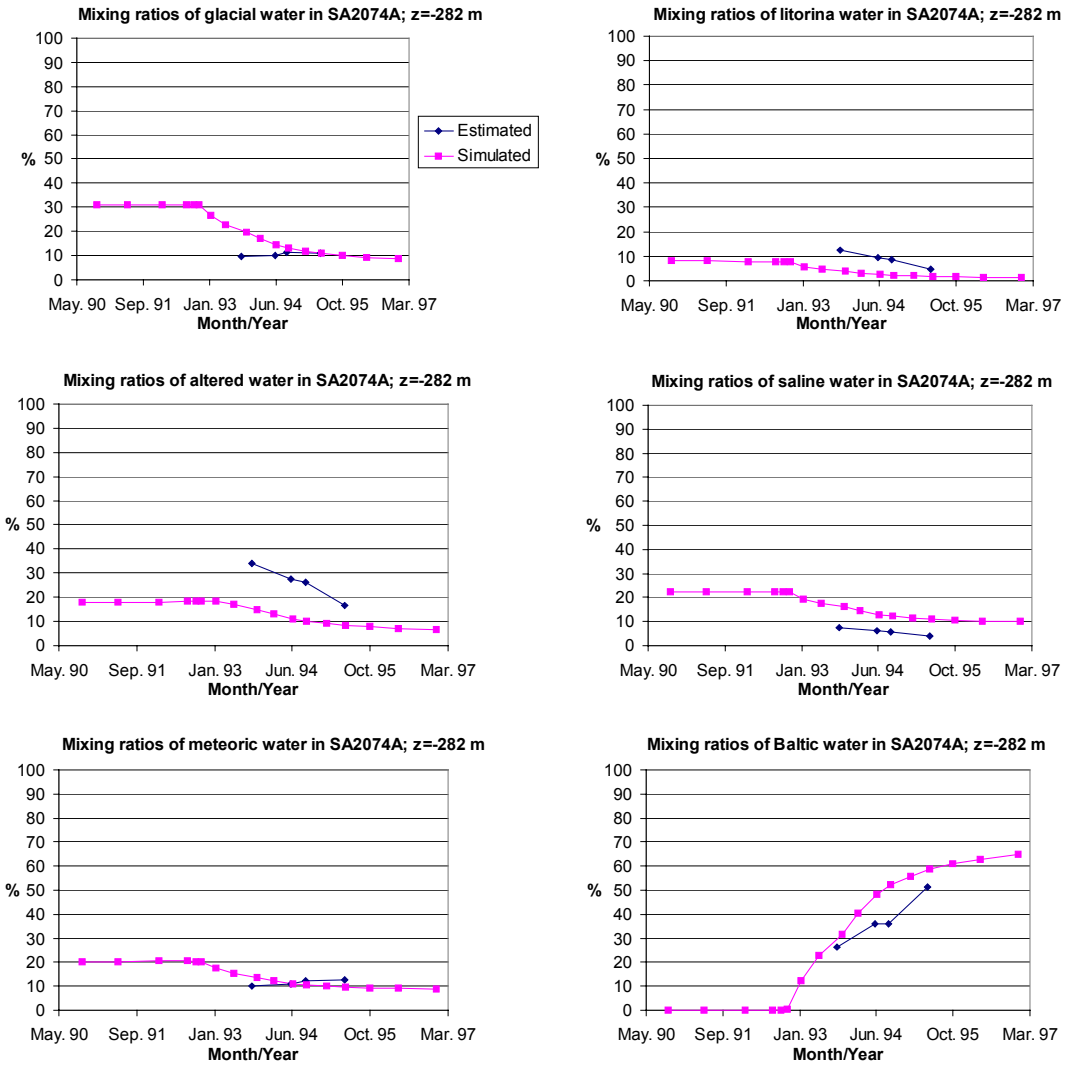

Figure 6. The mixing ratios of glacial, Litorina, altered, saline, meteoric and Baltic water in SA2074A as a function of time.

There are a couple of factors that may explain these discrepancies. A primary concern is that the hydrological properties of the individual structures taken into account in the model are not correctly calibrated. Only eight calibration points with time-series data were used for the model calibrations. In four deep points the calibrations were not successful. It is also likely that the fracture zones of the Äspö site have spatial properties that cannot be bypassed only with simple generalisations, and more consideration should be given to the structural relations.

In the case of a conductive fracture zone, the physical dimensions of mechanically weak rock and the hydrologically conductive zone are frequently considered as equal, though the former always has clearly larger dimensions than the latter. Usually, this happens simply because only the mechanically weak zone can be easily measured during the geological mapping. The fracture zone thicknesses used in the current simulations vary from 5 m to 50 m the average being around 20 m. Currently, the fracture zones have

been taken into account as more conductive equivalent continuums within a less conductive block of bedrock. However, this approach maybe is defective and the fracture zones should be modelled as fracture networks where interconnected fractures form highly conductive pipes within fracture zones.

There was also a conceptual problem in the hydrological simulation process itself (concerning the M3-based simulations as well). The mixing fractions for each reference water type had to be calculated in separate independent runs. As a consequence the initial results collected and summed up for a certain sample did not necessarily add up to 100 % but frequently to some figure over 100 %. This problem was addressed mainly by adjusting the dispersion lengths and ultimately recalculating the initial mixing fractions to 100 %. In all, however, this problem is basically related to the hydrological properties of the structures that were noted already above as a primary concern.

Conclusions

Realistic, site-scale hydrological simulations are demanding tasks, there are several traps and sources of uncertainties. Nevertheless, the Äspö site with extensive data sets from both undisturbed and disturbed conditions is an exceptional target for these studies. The open tunnel condition, causing considerable drawdown on a scale beyond any formal interference tests, gives possibilities to simulate and fit spatial hydrological properties and relations of fracture zones in the geological site model.

Similarly, it can be said that attempts to incorporate or couple hydrogeochemistry into site-scale hydrological simulations are challenging tasks. The geochemical modelling tools can be sensitive instruments that sum up information from the behaviour of several analysed chemical components. If this extracted information contains conservative parameters such as mixing fractions, the geochemical modelling then actually produces natural tracers for the hydrological simulations.

The M3 modelling tool probably does not describe the Äspö open tunnel conditions sensitively. Despite the deep aerial drawdown caused by the tunnel, the estimated mixing fractions behave smoothly as a function of time. This can be explained by the nature of the chosen input parameters, for example, to keep the M3 calculations simple, only the four main reference groundwaters were used. Other factors, such as discarding 20–30 % of the primary variation in the data set by using just two principal components, albeit the most important components, also have contributed to the decrease in sensitivity. The hydrological model calibrates more conveniently to the geochemical estimates behaving stiffly. At the same time, however, both the stiffly behaving mixing fraction estimates and the calmly acting simulation results unnecessarily hide or give averages of the hydrological information which are too generalised to relate to fracture zones.

Contrary to M3 the inverse modelling exercise has involved a more detailed approach with the result that a greater sensitive response to groundwater change due to tunnel excavation has been possible. In addition, the inverse approach proposes a method to take into account geochemical reactions in the hydrological forward simulations, i.e.

there is a loose one-step forward coupling between hydrochemistry and hydrology taking into account net-geochemical changes when a final water is made up from the reference water types.

There are, however, problems in the inverse approach based simulations as well. At depth, the simulations exhibit either a systematically growing difference to the geochemically estimated values, or hint to an exaggerated stiffness of the hydrological model. These difficulties raised three principal questions: “are the hydrological properties of the fracture zones correctly estimated at depth, are the structural relations between the fracture zones correctly defined, and is the open tunnel effect taken correctly into account in the hydrological model?”

Furthermore, at least the following aspects include notable uncertainties in the FEFTRA mixing model: (i) In addition to the hydraulic conductivity of the rock and the transmissivities and widths of the fracture zones there is high uncertainty in the fracture spacing and the dispersion lengths. (ii) The extensions of many fracture zones are uncertain. (iii) The modelling of the tunnel and shaft by merely specifying pressure and flow rate boundary conditions to the nodes. (iv) The applicability of the constant in-time pressure and concentration conditions in the model boundaries. (v) The infiltration in the Äspö Island and through the sea bottom.

References

Atkinson, K. E., 1988. An Introduction to Numerical Analysis. John Wiley & Sons, Inc., New York. ISBN 0-471-50023-2, Second Edition.

Bear, J., 1979. Hydraulics of Groundwater. McGraw-Hill, Israel.

Brooks, A. N. & Hughes, T. J. R., 1992. Streamline Upwind/Petrov-Galerkin Formulations for Convection Dominated Flows with Particular Emphasis on the Incompressible Navier-Stokes Equations. Computer Methods in Applied Mechanics and Engineering, 32, pp. 199-259.

Eronen, M., 1988. A scrutiny of the late Quaternary history of the Baltic Sea. Geological Survey of Finland, Special Paper 6, Espoo, 11–18.

Forsmark, T. & Rhén, I., 1994. SKB - ÄSPÖ HARD ROCK LABORATORY. Information for Numerical Modelling 1994. PR 25-94-16

Gurban, I., Laaksoharju, M. & Andersson, C., 1998. Influences of the Tunnel Construction on the Groundwater Chemistry at Äspö. Hydrochemical Initial and Boundary Conditions: WP D1, WP D2. Part 2. Äspö Hard Rock Laboratory, IPR-02-59. (in press)

Huyakorn, P. S., Lester, B. H. & Mercer, J. W., 1983. An Efficient Finite Element Technique for Modelling Transport in Fractured Porous Media, 1, Single Species Transport. Water Resources Research, vol. 19, no. 3, pp. 841-854.

Huyakorn, P. S. & Pinder, G. F., 1983. Computational Methods in Subsurface Flow. Academic Press INC, Orlando.

Laaksoharju, M. & Wallin, B., eds..1997. Evolution of the groundwater chemistry at the Äspö Hard Rock Laboratory. Proceedings of the second Äspö International Geochemistry Workshop, June 6-7, 1995. Stockholm, Sweden: Swedish Nuclear Fuel and Waste Management Co., International Cooperation Report 97-04.

Laaksoharju, M., Skårman, C. & Skårman, E., 1999. Multivariate mixing and mass-balance (M3) calculations, a new tool for decoding hydrogeochemical information. Applied Geochemistry 14, 861–871.

Laitinen, M., 1994. Developing an Iterative Solver for the FEFLOW Package. VTT Energy, Espoo. Technical Report, POHJA-2/94. (in Finnish)

Laitinen, M., 1995. Modelling Convection Dominated Transport Problems with Improved Galerkin Finite Element Formulations. Technical Research Centre of Finland, Espoo. VTT Julkaisuja - Publikationer 804. (in Finnish)

Löfman J. & Taivassalo V., 1993. FEFLOW 1.10 – Solving of Coupled Equations for Flow, Heat and Solute Transport. Report YJT-93-30, Nuclear Waste Commission of Finnish Power Companies, Helsinki. (in Finnish)

de Marsily, G., 1986. Quantitative Hydrogeology — Groundwater Hydrology for Engineers. Academic Press INC, Orlando.

Parkhurst, D.L. & Appelo, C.A.J., 1999. User's guide to PHREEQC (Version 2) – A computer program for speciation, batch-reaction, one dimensional transport, and inverse geochemical calculations. Denver, USA: U.S. Geological Survey, Water-Resources Investigations Report 99-4259, 312 p.

Pitkänen, P., Löfman, J., Koskinen, L., Leino-Forsman, H., Snellman, M., 1999a. Application of mass-balance and flow simulation calculations to interpretation of mixing at Äspö, Sweden. Applied Geochemistry 14, 893–905.

Plummer, L.N., Parkhurst, D.L. & Thorstenson, D.C., 1983. Development of reaction models for ground-water systems. Geochimica et Cosmochimica Acta 47, 665–686.

Plummer, L.N., Prestemon, E.C., and Parkhurst, D.L., 1994. An interactive code (NETPATH) for modeling NET geochemical reactions along a flow PATH. Version 2.0. Reston, USA: U.S. Geological Survey, Water-Resources Investigations Report 94-4169, 130 p.

Rhén, I. (ed.), Gustafson, G., Stanfors, R. & Wikberg, P., 1997. ÄSPÖ HRL — Geoscientific Evaluation 1997/5. Models Based on Site Characterization 1986-1995. SKB TR 97-06.

Taivassalo, V., Koskinen, L. & Mészáros, F., 1991. Further Development of the FEFLOW Code for Transient Simulations. Work Report 91-14, Teollisuuden Voima Oy (TVO), Helsinki. (in Finnish)

Part II

Task 5 — Mixing Proportions of Brine, Glacial, Meteoric and Baltic Sea Waters in the Äspö Tunnel

Eero Kattilakoski

VTT Energy

March 2001

SUMMARY

Task 5 (Impact of the tunnel construction on the groundwater system at Äspö, a hydrological-hydrochemical model assessment exercise) aims for the comparison and ultimate integration of hydrochemistry and hydrogeology. This work concerned with the groundwater flow modelling part of Task 5. No chemical reactions were modelled, only mixing. The simulation time steps covered the period from the natural conditions until the completion of the tunnel and shafts.

The flow model was constructed by including the hydrologic connections recognised during the tunnel construction. The observed properties of water and bedrock were included in the simulation model. The initial salinity boundary condition was fixed in accordance with the observations of the groundwater composition. The hydraulic data gained from boreholes was utilised to confirm the boundary condition in the tunnel.

The FEFTRA code was used to solve both the coupled equations of residual pressure and concentration and the transport equations of the different water types. The dual porosity transport model was applied to the equations of the different groundwater types, which were solved using the previously simulated residual pressure and salinity fields. The initial concentration boundary condition for the transport equations of the different water types was given in the basis of geochemical M3 estimations. Detailed performance measures were used for the presentation of the results.

The mixing ratios simulated at the control points and at certain cut planes were compared with the M3 estimations. As regards to the mixing ratios in the control points, the future condition of the brine water seems steady, except in the prediction section (tunnel length > 3000 m), where it is mildly increasing. The glacial water decreases, because it is a relict component in the present-day groundwater conditions. The meteoric water generally increases. The overall future condition of the Baltic water seems quite steady. These results are fairly well in line with the M3 estimations. The tunnel construction caused the upconing of the brine water, the decrease of the relict glacial water and the increase of the mixing ratios of the meteoric and Baltic waters in the tunnel area. This work showed the essential role of the dispersion lengths as regards to the simulated mixing ratios at the control points. Also, the infiltration from the sea had to be restricted.

TABLE OF CONTENTS

1 INTRODUCTION

1.1 Background

Task 5 (Impact of the tunnel construction on the groundwater system at Äspö, a hydrological-hydrochemical model assessment exercise) aims for the comparison and ultimate integration of hydrochemistry and hydrogeology. The consistency of groundwater flow models and hydrochemical mixing-reaction models is assessed through the integration and comparison of hydraulic and chemical data obtained before and during the tunnel construction. The modelling task will be useful for a stability assessment of the hydrodynamic and hydrochemical conditions at Äspö. A specific objective is the development of a procedure for the integration of hydrological and hydrochemical information which could be used for disposal site assessments — especially in a crystalline bedrock environment. (Wikberg, 1998)

In the modelled present-day conditions (Laaksoharju and Wallin (eds.), 1997) in the uppermost 250 m of the bedrock the calculated dominating mixing portion (> 30 %) is that of meteoric water. The dominating mixing portion is generally less than 50 % of the whole groundwater composition: the remaining part consists of various mixing portions of the other reference waters. At greater depths a brackish—saline water consisting of proportions of present and ancient Baltic Sea water and glacial melt water occurs at the depth of 250—600 m. Below this level the saline water still contains proportions of glacial water and brine water. The tunnel construction caused a withdrawal and especially a decrease of the mixing portions of the glacial component, because it is a relict water.

1.2 Objectives

This work concerns with the groundwater flow modelling part of Task 5. No chemical reactions have been modelled, only mixing (see Appendix B). The simulation time steps cover the period from the natural conditions until the completion of the tunnel and shafts.

The flow model was constructed by including the hydrologic connections recognised during the tunnel construction. The observed properties of water and bedrock were included in the simulation model. The initial salinity boundary condition was fixed in accordance with the observations of the groundwater composition. The hydraulic data gained from boreholes was utilised to confirm the boundary condition in the tunnel.

The FEFTRA code (formerly known as FEFLOW) is used to solve both the coupled equations of residual pressure and concentration and the transport equations of the different water types. The dual porosity transport model is applied to the equations of the different groundwater types, which are solved

using the previously simulated residual pressure and salinity fields. The simulated mixing ratios are compared with those from geochemical M3 estimations (Gurban et al., 1998). Detailed performance measures (Rhén, Smellie and Wikberg, 1998) will be used for the presentation of the results.

2 MODEL CONCEPTS AND FORMULATION

2.1 Governing equations

The mathematical formulation of flow and transport in the *dual porosity* medium comprises three coupled and non-linear partial differential equations. Two of them describe the flow of water with variable density and the amount of mass transported with flowing water in the water-bearing fractures. The third equation describes the amount of mass transported by diffusion in the matrix blocks. The mathematical formulation of the dual porosity approach is explained in detail by Löfman and Taivassalo (1995) and Löfman (1996).

The flow equation is expressed in terms of the residual pressure p — the actual pressure minus the hydrostatic component of freshwater (e.g., Bear, 1979; de Marsily, 1986):

$$\nabla \cdot (\frac{\rho \mathbf{k}}{\mu}(\nabla p - (\rho - \rho_0)\mathbf{g})) = \frac{S_S}{g}\frac{dp}{dt} + \phi\frac{d\rho}{dt} - \rho_{in}Q_{in} + \rho Q_{out}\,, \qquad (2.1)$$

where

p	is the residual pressure (Pa),
ρ	is the density of water (kgm^{-3}),
ρ_0	is the freshwater density (kgm^{-3}),
μ	is the viscosity of water (kgm^{-1}s^{-1}),
$\boldsymbol{k}$	is the permeability tensor of the medium (m^2),
$\boldsymbol{g}$	is the gravitational acceleration (ms^{-2}),
S_S	is the specific storage of the medium (m^{-1}),
ϕ	is the total porosity (-),
ρ_{in}	is the density of the inflowing water (kgm^{-3}),
Q_{in}	is the term for sources (s^{-1}) and
Q_{out}	is the term for sinks (s^{-1}).

The permeability tensor $\boldsymbol{k}$ in Eq. (2.1) can be expressed in terms of the hydraulic conductivity $\boldsymbol{K}$ (m/s):

$$\mathbf{k} = \frac{\mathbf{K}\mu}{\rho g}\,. \qquad (2.2)$$

In the dual porosity approach Eq. (2.1) describes the flow in the water-bearing fractures.

The equation describing mass transport in the water-bearing fractures is as follows (Huyakorn et al., 1983):

$$\nabla \cdot (\mathbf{D}\nabla c) - \nabla \cdot (\mathbf{q}c) + Q_{in}c_{in} - Q_{out}c + (1 - \phi_f)\Gamma = \phi_f \frac{\partial c}{\partial t}\,, \qquad (2.3)$$

where c is the concentration of the solute (g/l),
$\boldsymbol{D}$ is the hydrodynamic dispersion coefficient, which includes dispersion and diffusion (m^2s^{-1}),
$\boldsymbol{q}$ is the Darcy velocity (ms^{-1}),
Q_{in} is the term for sources (s^{-1}),
c_{in} is the concentration in the inflowing water (g/l),
Q_{out} is the term for sinks (s^{-1}),
ϕ_f is the flow (fracture) porosity (-) and
Γ is the rate of solute transfer from the matrix block to the fracture ($kgm^{-3}s^{-1}$).

The components of the hydrodynamic dispersion tensor in Eq. (2.3) are

$$D_{ij} = \varepsilon_T |\mathbf{q}| \delta_{ij} + (\varepsilon_L - \varepsilon_T) \frac{q_i q_j}{|\mathbf{q}|} + \phi_d D_0 \delta_{ij} , \tag{2.4}$$

where ε_L is the longitudinal dispersion length (m),
ε_T is the transversal dispersion length (m),
δ_{ij} is the Kronecker delta function (-),
ϕ_d is the diffusion porosity (-) and
D_0 is the molecular diffusion coefficient in water (m^2s^{-1}).

The Darcy velocity $\boldsymbol{q}$ in Eq. (2.3) in terms of the residual pressure p is

$$\mathbf{q} = -\frac{\mathbf{k}}{\mu} (\nabla p - (\rho - \rho_0)\mathbf{g}) . \tag{2.5}$$

The mass transport in the matrix blocks can be described with a one-dimensional diffusion equation

$$\frac{\partial}{\partial z'} (D_e' \frac{\partial c'}{\partial z'}) = \phi' \frac{\partial c'}{\partial t} , \tag{2.6}$$

where c' is the concentration of the solute (g/l),
D_e' is the effective diffusion coefficient (m^2s^{-1}) and
ϕ' is the porosity in the matrix blocks (-).

In accordance with Archie's law (Valkiainen, 1992), the connection between the effective diffusion coefficient and the porosity in the matrix blocks can be stated as

$$D_e' = 0.71 \cdot D_0 \phi'^{1.58} . \tag{2.7}$$

Equations (2.3) and (2.6) are coupled by the continuity of the diffusive mass flux at the interface of the fracture and the matrix block. For a rectangular matrix block unit the rate of solute transfer from the matrix block to the fracture is

$$\Gamma = -\frac{1}{a}(D'_e \frac{\partial c'}{\partial z'}\Big|_{z'=a}), \tag{2.8}$$

where a (m) is half the fracture spacing, i.e., half the matrix block thickness.

2.2 Numerical tool

The flow equation (2.1) and the transport equation (2.3) are coupled by the density ρ and the Darcy velocity **q** (Eq. (2.5)). This results in a system of two non-linear partial differential equations that can rarely be solved analytically. The finite element code FEFTRA was used in this work for the numerical solution (Löfman, 1996).

The finite element method with linear elements was employed. The conventional Galerkin technique was applied to the flow equation (2.1). In order to avoid the numerical problems related to highly convective cases the transport equation (2.3) was solved using the streamline-upwind/Petrov-Galerkin (SUPG) method (Brooks and Hughes, 1992; implemented in FEFTRA by Laitinen, 1995). The conventional Galerkin method was applied to the diffusion equation (2.6) in the matrix blocks.

In the coupled cases non-linearities were treated by the Picard iteration scheme (Huyakorn and Pinder, 1983), which applies the finite element procedure for both the flow and the transport equation sequentially. At the end of each iteration sweep the pressure and concentration values are updated using an underrelaxation scheme. This way the oscillations of concentration changes from iteration to iteration are reduced. No iteration was needed in the mixing calculations of a single water type, which utilised the previously simulated residual pressure and salinity fields.

An initial estimate for the nodal values of the residual pressure and the concentration at the beginning of the first iteration sweep of each time step was obtained by using a linear time extrapolation formula.

The mass matrices resulting from the finite element formulation were formed by a diagonalization procedure known as ”lumping” (Huyakorn and Pinder, 1983). In practical problems this leads to a more stable solution than with a ”consistent” matrix.

The Gauss-Seidel method (Laitinen, 1994) was used to solve the matrix equation (2.3) in the mixing calculations. In the coupled calculations the conjugate gradient method was used to solve the finite element formulation of Equation (2.1) for residual pressure and the Gauss-Seidel method to solve the finite element formulation of Equation (2.3) for concentration.

3 SIMULATION MODEL

3.1 Geometric framework

All the certain, probable and possible structures proposed by Rhén et al. (1997) were included in the model.

The regional zones SFZ05 and SFZ12 have dip angles of about 70 degrees. The other regional zones are vertical. All the regional zones extend to the depth of 1500 m.

The local zones were defined as quadrangles with corner points as proposed by the three points given by Rhén et al. (1997). The vertical zones were extended to the depth of 1500 m (except NNW-8, which extends to the depth of 700 m).

The hydraulic connections were established as given by Rhén et al. (1997, Fig. 6-31 and Table A2-6).

The definitions of the zones SFZ07 and EW-1N were combined: thus, the zone EW-1N has a regional extension in the model (Fig. 5.1). The geometry of the zone NE-1 was combined with the geometry of SFZ12. The directions of the zones NE-3 and NE-4 were approximated with the average values of X, Y and Z given. In addition, NE-3 was connected with SFZ11 and EW-7.

The zone EW-1S was given an extension as far as SFZ07 and SFZ03. The assumed hydraulic connection of EW-1S with the zones NNW-1, NNW-2 and NNW-4 was formed. EW-3 stops at SFZ14 and SFZ12. The zone EW-7 was continued as far as SFZ12 and SFZ10.

The zones NE-2 and EW-1S were connected. The conductor NW-1 is assumed to terminate to the south at EW-1N. The conductor NNW-4 intersects with EW-1S and SFZ12. In the southern end, NNW-5 was connected with NE-4 and NNW-6 with EW-7. NNW-7 forms a connection with EW-3 and EW-1S. In addition, NNW-7 was extended to the depth of 191 m.

The coordinates of the fracture zones included in the flow model are shown in Appendix A.

3.2 Finite element mesh

The finite elements for the rock blocks are linear hexahedrals and wedges. The base mesh formed by these elements is approximately the same as in the study by Mészáros (1996). Triangles and quadrangles are used for the fracture zones. The mesh contains 58 224 three-dimensional elements and 13 443 two-dimensional elements.

The element mesh extends from the sea level to the depth of 1500 m (as in Mészáros, 1996).

3.3 Material properties

The properties of water and bedrock employed in the simulations are shown in Table 3.1.

Table 3.1. Properties of water and bedrock used in the simulations.

Symbol	Parameter	Value	Reference
μ	Viscosity	$1.0 \cdot 10^{-3}$ kgm^{-1}s^{-1}	Lide (1990)
ρ_0	Freshwater density	998.585 kgm^{-3}	
D_0	Molecular diffusion coefficient	$1.0 \cdot 10^{-9}$ m^{2}s^{-1}	Löfman and Taivassalo (1995)
a_C	Density dependence on salinity	0.741	Rhén et al. (1997) p. 183
ε_L	Longitudinal dispersion length [1)]	1000 m	
ε_T	Transversal dispersion length [2)]	100 m	
ϕ_d	Diffusion porosity	$3.5 \cdot 10^{-3}$	
ϕ'	Porosity in the matrix blocks	$3.5 \cdot 10^{-3}$	Rhén et al. (1997) p. 22, p. 403
C_{vh}	Coefficient for dependence between the volume and hydraulic apertures	10	Vieno et al. (1992)

1) 5000 m for NE-2, NNW-1, NNW-2, NNW-4, NNW-5, NNW-7

2) 500 m for NE-2, NNW-1, NNW-2, NNW-4, NNW-5, NNW-7

The properties of the fracture zones are shown in Table 3.2 (Rhén et al., 1997). The transmissivities T (m^2/s), the widths of the zones (m), storage coefficients S (-), the fracture spacings $2a_0$ (m), the fracture apertures $2b$ (m) and the flow porosities ϕ_f (-) at the surface are shown.

Rhén et al. (1997) give the linear relationship between $\log_{10}T$ and $\log_{10}S$. They notice that the relation seems to give unrealistic low S values for very low T values. For that reason, for S the value $\max(1.0 \cdot 10^{-6}; aT^b)$ is used in this work. There are also few points for the regression which makes the relation mentioned above uncertain. However, the variability in S values is probably relatively large.

An assumption is made on the depth dependence of the spacing of the water-bearing fractures:

$$2a = 2a_0 2^{-\frac{z}{500}}, \tag{3.1}$$

where $2a_0$ (m) is the fracture spacing on the surface.

The fracture aperture $2b$ (m) is given as a function of the fracture spacing $2a$ (m) and the hydraulic conductivity K as follows (Taivassalo and Saarenheimo, 1991)

$$2b = C_{vh}\left(\frac{12\mu}{\rho_0 g} K 2a\right)^{1/3}, \tag{3.2}$$

where C_{vh} (Vieno et al., 1992) is the coefficient for the dependence between the volume and the hydraulic fracture aperture, μ the viscosity of water (Lide, 1990), ρ_0 the freshwater density and g the gravitational acceleration (9.81 m/s^2).

The flow porosity ϕ_f (-) is given as follows (as in Löfman, 1996)

$$\phi_f = \frac{b}{a+b}. \tag{3.3}$$

The transmissivity of the zone EW-3 has a depth dependence (Rhén et al., 1997 A2:14)

$$T = T_0 \cdot 10^{cd}, \tag{3.4}$$

where T_0 is the transmissivity at the ground surface given in Table 3.2, c is the coefficient for the depth dependence (-3.9·10^{-3} m^{-1}) and d is the depth (m).

Table 3.2. Properties of fracture zones. The transmissivity of the zone EW-3 has a depth dependence as given in Eq. (3.4). The transmissivity of the uppermost elements of the fracture zones below the sea is T=9.3·10^{-9} m^2/s (supposed width 30 m).

Zone	T (m^2/s) according to Rhén et al., 1997 (Mean)	T (m^2/s), modified	width of zone (m) according to Rhén et al., 1997	S (-) Rhén et al., 1997 p. 214-215	max (1.0·10^{-6}; S)	$2a_0$ (m) Rhén et al., 1997 p. 117	$2b$ (m) at model surface	ϕ_f (-) at model surface
SFZ01	3.0·10^{-6}		20	4.3·10^{-7}	1.0·10^{-6}	0.05	2.1·10^{-4}	4.2·10^{-3}
SFZ02	1.0·10^{-4}		20	6.7·10^{-6}	6.7·10^{-6}	0.05	6.7·10^{-4}	1.3·10^{-2}
SFZ03	3.0·10^{-6}		20	4.3·10^{-7}	1.0·10^{-6}	0.05	2.1·10^{-4}	4.2·10^{-3}
SFZ04	3.0·10^{-6}		20	4.3·10^{-7}	1.0·10^{-6}	0.05	2.1·10^{-4}	4.2·10^{-3}
SFZ05	1.0·10^{-4}		20	6.7·10^{-6}	6.7·10^{-6}	0.05	6.7·10^{-4}	1.3·10^{-2}
SFZ06	3.0·10^{-6}		20	4.3·10^{-7}	1.0·10^{-6}	0.05	2.1·10^{-4}	4.2·10^{-3}
SFZ08	3.0·10^{-6}		20	4.3·10^{-7}	1.0·10^{-6}	0.05	2.1·10^{-4}	4.2·10^{-3}
SFZ09	3.0·10^{-6}		20	4.3·10^{-7}	1.0·10^{-6}	0.05	2.1·10^{-4}	4.2·10^{-3}

Table 3.2. (cont.) Properties of fracture zones. The transmissivity of the zone EW-3 has a depth dependence as given in Eq. (3.4). The transmissivity of the uppermost elements of the fracture zones below the sea is T=9.3·10^{-9} m^2/s (supposed width 30 m).

zone	T (m^2/s) according to Rhén et al., 1997 (Mean)	T (m^2/s), modified	width of zone (m) according to Rhén et al., 1997	S (-) Rhén et al., 1997 p. 214-215	max (1.0·10^{-6}; S)	$2a_0$ (m) Rhén et al., 1997 p. 117	$2b$ (m) at model surface	ϕ_f (-) at model surface
SFZ10	1.0·10^{-4}		20	6.7·10^{-6}	6.7·10^{-6}	0.05	6.7·10^{-4}	1.3·10^{-2}
SFZ11	3.0·10^{-6}		20	4.3·10^{-7}	1.0·10^{-6}	0.05	2.1·10^{-4}	4.2·10^{-3}
SFZ12/ NE-1	2.2·10^{-4}		20	1.6·10^{-5}	1.6·10^{-5}	0.05	8.8·10^{-4}	1.7·10^{-2}
SFZ13	3.0·10^{-6}		20	4.3·10^{-7}	1.0·10^{-6}	0.05	2.1·10^{-4}	4.2·10^{-3}
SFZ14	3.0·10^{-6}		20	4.3·10^{-7}	1.0·10^{-6}	0.05	2.1·10^{-4}	4.2·10^{-3}
SFZ15	1.0·10^{-4}		20	6.7·10^{-6}	6.7·10^{-6}	0.05	6.7·10^{-4}	1.3·10^{-2}
EW-1N/ SFZ07	5.2·10^{-7}		30	1.1·10^{-7}	1.0·10^{-6}	0.05	1.0·10^{-4}	2.0·10^{-3}
EW-1S	1.2·10^{-5}		30	1.3·10^{-6}	1.3·10^{-6}	0.05	2.9·10^{-4}	5.8·10^{-3}
EW-3	1.7·10^{-5} (T_0)		15	1.3·10^{-6}	1.3·10^{-6}	0.05	4.1·10^{-4}	8.2·10^{-3}
EW-7	1.5·10^{-5}		10	1.5·10^{-6}	1.5·10^{-6}	0.05	4.5·10^{-4}	8.9·10^{-3}
NE-2	1.2·10^{-7}		5	3.4·10^{-8}	1.0·10^{-6}	0.05	1.1·10^{-4}	2.3·10^{-3}
NE-3	3.2·10^{-4}		50	1.7·10^{-5}	1.7·10^{-5}	0.05	7.3·10^{-4}	1.4·10^{-2}
NE-4	3.1·10^{-5}		40	2.7·10^{-6}	2.7·10^{-6}	0.05	3.6·10^{-4}	7.2·10^{-3}
NW-1	4.1·10^{-7}		10	8.9·10^{-8}	1.0·10^{-6}	0.05	1.4·10^{-4}	2.7·10^{-3}
NNW-1	8.6·10^{-6}	3.0·10^{-5} (Svensson, 1997)	20	2.6·10^{-6}	2.6·10^{-6}	0.05	4.5·10^{-4}	8.9·10^{-3}
NNW-2	2.4·10^{-5}	2.1·10^{-6} (Mean – st. dev)	20	1.1·10^{-6}	1.1·10^{-6}	0.05	1.9·10^{-4}	3.7·10^{-3}
NNW-3	2·10^{-5} (Table A2-7)		20	1.9·10^{-6}	1.9·10^{-6}	0.05	3.9·10^{-4}	7.8·10^{-3}
NNW-4	6.5·10^{-5}		10	4.8·10^{-6}	4.8·10^{-6}	0.05	7.4·10^{-4}	1.4·10^{-2}
NNW-5	4.0·10^{-6}		20	5.3·10^{-7}	1.0·10^{-6}	0.05	2.3·10^{-4}	4.6·10^{-3}
NNW-6	1.4·10^{-5} (Table A2-7)		20	1.4·10^{-6}	1.4·10^{-6}	0.05	3.5·10^{-4}	7.0·10^{-3}
NNW-7	7.5·10^{-6}	8.0·10^{-5} (Svensson, 1997)	20	5.6·10^{-6}	5.6·10^{-6}	0.05	6.3·10^{-4}	1.2·10^{-2}
NNW-8	8.4·10^{-6}	8.0·10^{-6}	20	9.2·10^{-7}	1.0·10^{-6}	0.05	2.9·10^{-4}	5.8·10^{-3}

The properties of the rock are shown in Table 3.3. The specific storage S_S (m^{-1}) is derived from a linear relationship between $\log_{10}K$ and $\log_{10}S_S$ given by Rhén et al. (1997).

Table 3.3. Properties of rock.

rock	K (m/s) Rhén et al., 1997 p. 365, 219	S_S (m^{-1}) Rhén et al., 1997 p. 241-242	$2a_0$ (m) Rhén et al., 1997 p. 131	$2b$ (m) at model surface	ϕ_f (-) at model surface
	$9.3 \cdot 10^{-9}$	$8.4 \cdot 10^{-7}$	0.45	$1.7 \cdot 10^{-4}$	$3.8 \cdot 10^{-4}$

3.4 Boundary conditions

Seventeen time steps were chosen. They cover the period from the natural conditions until December 1996 (Table 3.4).

Table 3.4. The modelling period with comments on the tunnel and shaft updating.

Step	Date	Tunnel face (m)	Comments on modelling
0	0.5 years before 1.10.1990	0	Start of modelling period
1	1.10.1990	0	
2	21.05.1991	696	First tunnel updating, release of groundwater table over the land
3	10.02.1992	1212	
4	10.08.1992	1398.8	
5	05.10.1992	1672.5	
6	10.11.1992	1774	First updating of shafts
7	11.02.1993	2100	
8	03.06.1993	2600.1	
9	03.11.1993	2604	No updating of tunnel
10	16.02.1994	2998.8	Second updating of shafts
11	16.06.1994	3192.3	
12	16.09.1994	3600	

Table 3.4. (cont.) The modelling period with comments on the tunnel and shaft updating.

13	24.01.1995	3600	Last updating of shafts
14	25.05.1995	3600	
15	24.10.1995	3600	
16	24.04.1996	3600	
17	23.12.1996	3600	

The tunnel and shaft advance is modelled by giving a residual pressure boundary condition for the flow equation (Eq. (2.1)) and a flow rate boundary condition for the transport equation (Eq. (2.3)) to the nodes describing the tunnel and shafts in each time step (see Section 4).

3.4.1 Solving of pressure and salinity fields

The fixing of the initial salinity boundary condition is described in Section 4.2.

The density of saline water (kg/m^3) is given by the following equation (Rhén et al., 1997)

$$\rho = \rho_0 + a_C S, \tag{3.5}$$

where ρ_0 is the freshwater density (998.585 kg/m^3), a_C is the coefficient of the density dependence on the salinity (0.741) and S is the salinity (g/l).

Thus, the hydraulic pressure (Pa) can be expressed as

$$p = p_{fresh}(d) + a_C g \int_0^d S(d_z)\, dd_z\,, \tag{3.6}$$

where p_{fresh} is the freshwater pressure, g is the gravitational acceleration (9.81 m/s^2) and d is the depth (m).

The residual pressure (Pa) is

$$p_{res} = a_C g \int_0^d S(d_z)\, dd_z\,. \tag{3.7}$$

The initial (t=0) pressure boundary condition for each node of the element mesh under the sea level is calculated with Eq. (3.7), after the initial salinity

distribution has been determined (Section 4.2). Zero residual pressure is applied at the sea level, while groundwater table is specified over the land.

In the first time step the pressure and salinity boundary conditions given in the interior nodes of the element mesh are released. The pressure boundary condition in the bottom nodes is also released, because it would not be consistent with the salinity.

In the second time step the progress of the tunnel is taken into account for the first time. The groundwater table boundary condition at the surface of the model is released (see Table 3.4). A flow rate boundary condition giving an infiltration of about 20 mm/a in the shaft area is given for the flow equation in the nodes depicting the land. The application of an infiltration boundary condition of 100 mm/a over the land areas would result in the freshwater head maximum of over 60 metres in Äspö, Laxemar and Mjälen in this time step.

3.4.2 Transport of water types

The initial concentration boundary condition for the transport equations of the different water types is given on the basis of the M3 (Multivariate Mixing and Mass balance) estimations done by Gurban et al. (1998). Their M3 modelling started by comparing the groundwater compositions in the data from the Äspö Hard Rock Laboratory. The measured groundwater composition was supposed to be a result of modern and ancient water—rock interactions and mixing processes. Thus, waters with similar compositions were assumed to have a similar origin and have undergone similar mixing and reaction processes. The comparison of several groundwater constituents was performed in an optimum way by using multivariate techniques (principal component analysis, PCA). The result of the comparison was used to construct an ideal mixing model between the groundwater samples which seem to participate in the groundwater system studied. The ideal mixing model employed different reference waters (brine, glacial, meteoric and Baltic) that the other waters are compared with. Table 3.5 shows the concentrations of the main constituents Na, K, Ca, Mg, HCO_3, Cl and SO_4 in the 100 % mixing ratios of the different water types.

Table 3.5. The concentrations of the main constituents (mg/l) in the different groundwater types identified in Äspö.

Main constituents (mg/l)							Water type			
Na	K	Ca	Mg	HCO_3	Cl	SO_4	Brine	Glacial	Meteoric	Baltic
8500	45.5	19300	2.12	14.1	47200	906	100.0%	0.0%	0.0%	0.0%
0.17	0.4	0.18	0.1	0.12	0.5	0.5	0.0%	100.0%	0.0%	0.0%
0.4	0.29	0.24	0.1	12.2	0.23	1.4	0.0%	0.0%	100.0%	0.0%
1960	95	93.7	234	90	3760	325	0.0%	0.0%	0.0%	100.0%

The mixing portions (%) were calculated on the basis of the linear distances of a sample to the reference waters. The relevance of the chosen ideal mixing model was then tested by predicting the concentrations of the water conservative elements such as Cl and O^{18}. As soon as the model was calibrated to predict the concentrations of the conservative elements fairly well, the concentrations of the non-conservative elements were calculated. The deviation between the result from the ideal mixing model and the measurements could be used to show the effects from groundwater reactions. The calculated mixing portions of each sample were interpolated to a grid covering from west to east Laxemar, Äspö, Ävrö and Mjälen.

The identified mixing ratios (Gurban et al., 1998) are used to determine the initial concentration of each water type in the nodes of the element mesh used in this work. For example, in the point (Easting, Northing, elevation) = (2200.3; 5880.1; -1500.0) Gurban et al. (1998) give the following mixing ratios: brine 97.1 %, glacial 3.2 %, meteoric 0 % and Baltic water 1.7 %. In the mixing calculations presented here chloride is used to identify the water types. Thus, according to the concentrations given in Table 3.5 for Cl, the concentrations of the water types in the point mentioned above are approximately the following: brine 45.8 g/l, glacial 0.016 mg/l, meteoric 0 g/l and Baltic 63.9 mg/l.

The boundary condition given in an interior node is then released in the first time step.

4 CALIBRATION

4.1 Introduction

The model was calibrated to fit the freshwater head measured in the boreholes KAS02—KAS09, KAS12 and KAS14 and also the measured flow into the tunnel and the shaft.

The tunnel was modelled without modifying the hydraulic conductivity of the rock around it. The residual pressure boundary condition in the tunnel and the shaft was fixed on the basis of the freshwater head measured in the nearmost borehole sections. In order to get an insight into the boundary condition to be assigned to the nodes pertaining to the tunnel, the measured freshwater heads from borehole sections at certain times (Forsmark and Rhén, 1994) were assigned to the nearest nodes of the tunnel phase. In case many values were obtained in one node an average was calculated. The measured values not farther than 75 metres away the tunnel were used.

In the calibration the model was also given an initial salinity boundary condition in accordance with the natural conditions which prevailed before the tunnel construction.

4.2 Salinity

The initial salinity boundary condition was defined in accordance with the chemical modelling by Gurban et al. (1998). They present the concentrations of the main constituents Na, Ca, HCO_3, Cl and SO_4 prior to the tunnel construction extracted from an interpolation grid. The interpolation in their model was based on the measured data. Their model domain covers an area with the surface coordinates as following: (-300; 5600), (-300; 8121), (3450.44; 5600), (3450.44; 8121). The depth of the box is 1500 m.

Zero salinity was used over the land due to the freshwater flow into the groundwater system. This is caused by the hydraulic gradient of the water table of the Äspö island. The salinity used at the sea level was 6 g/l.

The following linear, approximate salinity distribution (Table 4.1) on the vertical sides of the model was fixed on the basis of the chloride data by Gurban et al. (1998). The distribution was used to assign each node on the vertical sides with a salinity boundary condition. Thus, the residual pressure boundary condition (Eq. 3.7) prevailing on the lateral edges throughout the simulation could be given consistently with the salinity. The approximate salinity in Table 4.1 is not exactly the salinity implied by the mixing fractions. The approximate salinity distribution is needed to define the consistent pressure boundary condition on the vertical edges, however.

The justification for the salinity distribution (Table 4.1) can be given as follows: (1) The total salinity is 1.7 times the chloride concentration (Rhén et al., 1997; Fig. 7-25). (2) The measured salinities are from the surface parts as far as about 950 metres depth (Fig. 4.2). A salinity not much more than the chloride concentration was used below that depth level. A chloride concentration of 47.2 g/l was measured from the borehole KLX02 (Gurban et al., 1998). (3) The salinity of about 10 g/l was measured at the depth of about 450 m in the tunnel area from the boreholes KAS02 and KAS06 (Rhén et al., 1997; Fig. 6-20).

An initial value for the salinity in each node inside and in the bottom of the mesh used in this work was assigned with the chloride concentration from the nearest point in the model by Gurban et al. (1998). In the first time step the interior boundary conditions were released.

Table 4.1. Salinity on the vertical edges.

Depth (m)	Salinity (g/l) on vertical edges
0	6.0
200	6.0
450	10.0
725	11.6
950	18.0
1100	25.0
1500	45.0

4.3 Residual pressure

The initial residual pressure boundary condition throughout the vertical boundaries of the model was calculated from the salinity in Table 4.1 using Eq. 3.7. In order to get a reasonable result in the boreholes before the tunnel construction a somewhat different salinity distribution was used to calculate the initial residual pressure boundary condition (Eq. 3.7) in the interior and the bottom nodes of the element mesh. Deviating from the distribution on the vertical edges (Table 4.1) the salinity for this calculation was 3 g/l at the surface and 5 g/l at the depth of 200 m.

In the first time step the residual pressure boundary conditions in the interior and bottom nodes were released.

The freshwater head used to calculate the residual pressure boundary condition prevailing in the tunnel nodes is depicted in Figure 4.1. The lowering of the curve in the depth interval 284—348 m is based on a calibration result in the boreholes KAS05—KAS08.

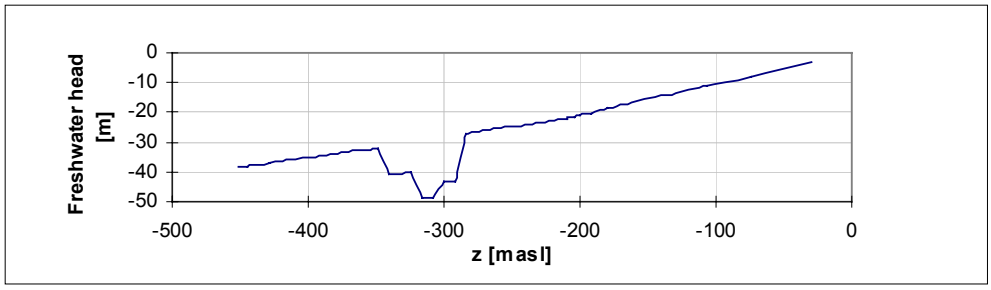

Figure 4.1. The freshwater head (m) used to calculate the residual pressure boundary condition in the tunnel nodes.

The low freshwater head measured in the uppermost packed-off sections of the borehole KAS02 was tried to catch up by assigning the residual pressure corresponding to the freshwater head

$$h_{0,shaft}(z) = -80 \text{ m} \tag{4.1}$$

to the nodes representing the shaft.

The freshwater hydraulic head measured from the boreholes and the residual pressure are related as follows:

$$p_{res}(z) = \rho_0 g h_0(z)\,, \tag{4.2}$$

where ρ_0 is the freshwater density (998.585 kg/m^3), g is the gravitational acceleration (9.81 m/s^2) and $h_0(z)$ is the freshwater head (m) given in the basis of the borehole measurements.

The simulated and measured salinities in the boreholes KAS02—KAS09, KAS11—KAS14, KAS16 and KBH02 before the tunnel construction are shown in Figure 4.2, while the simulated and measured freshwater head in the boreholes KAS02—KAS09, KAS12 and KAS14 as function of time are shown in Figure 4.3. In spite of the relatively low residual pressure boundary condition assigned to the nodes depicting the shaft, the model is not fully capable of producing the low freshwater head measured in the borehole KAS02.

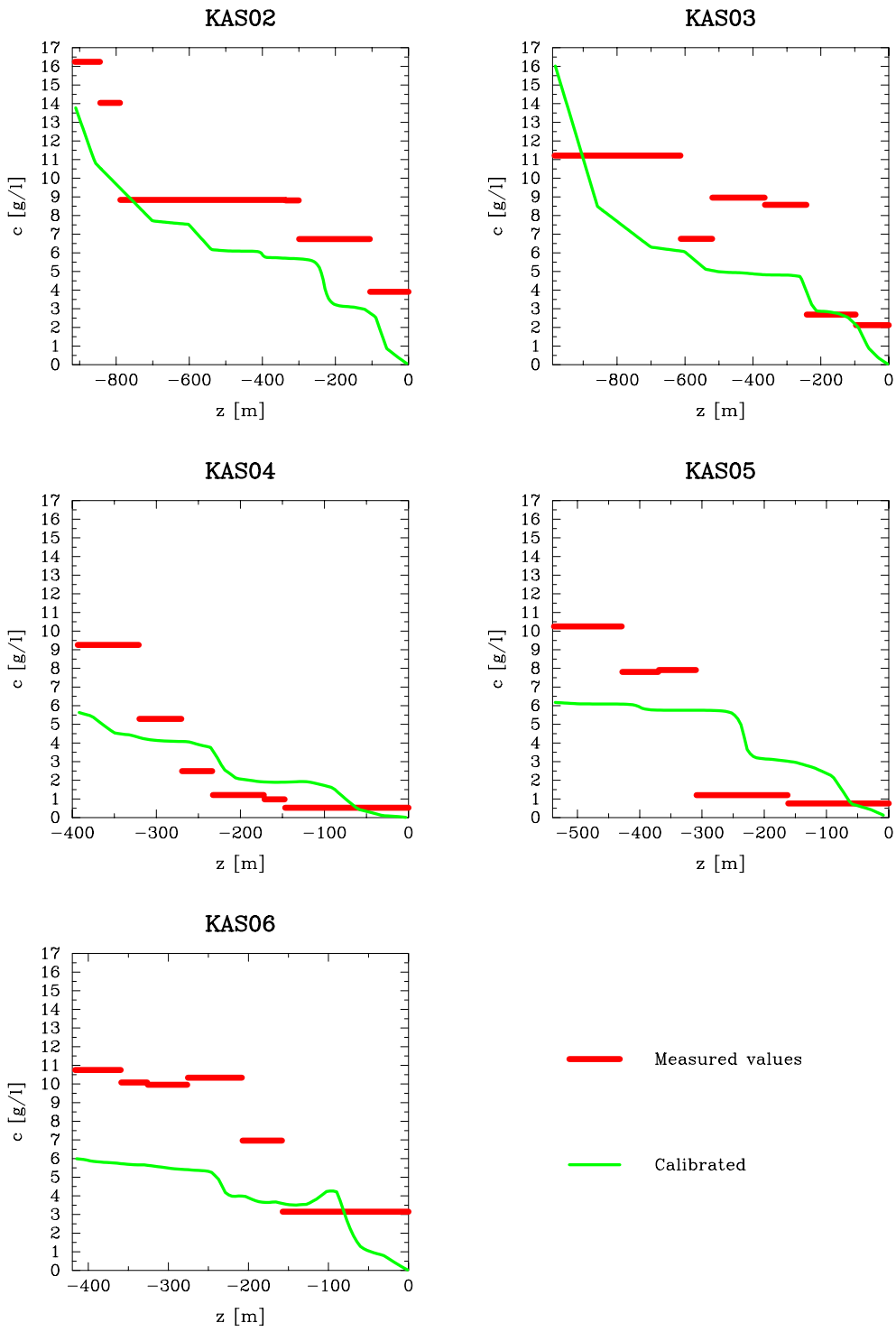

Figure 4.2. Simulated and measured salinities (g/l) in the boreholes KAS02—KAS06 before the tunnel construction.

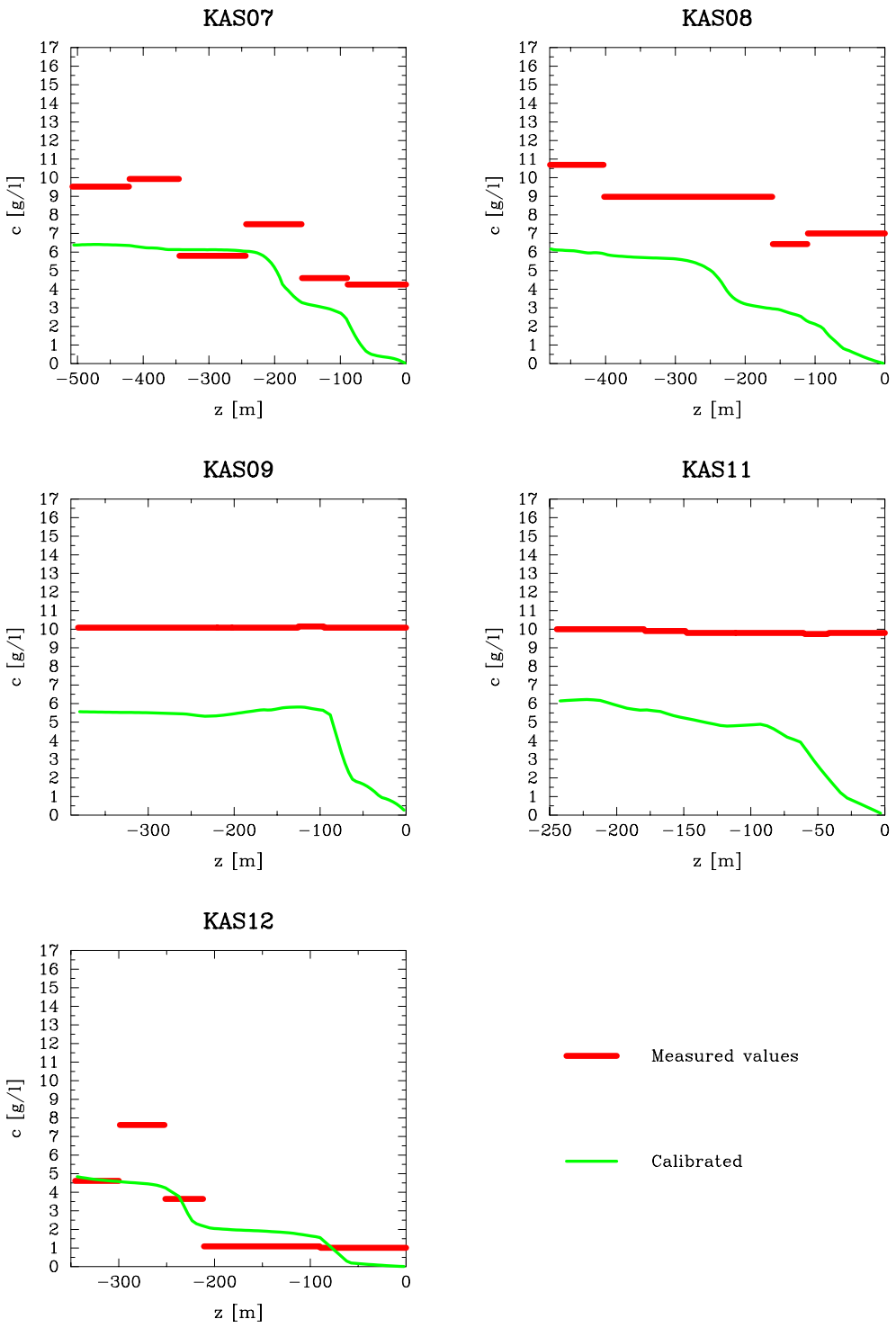

Figure 4.2. (cont.) Simulated and measured salinities (g/l) in the boreholes KAS07—KAS09, KAS11 and KAS12 before the tunnel construction.

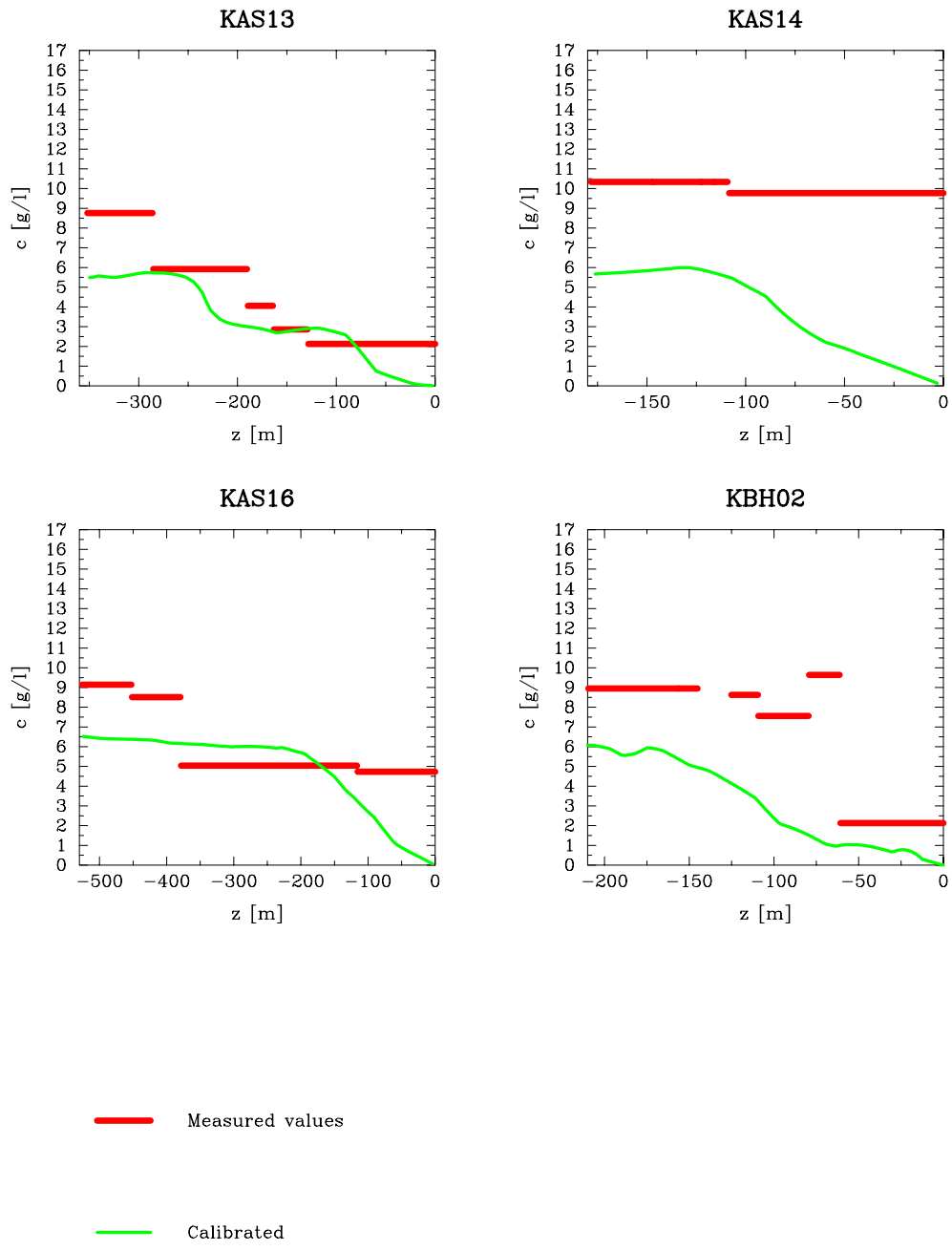

Figure 4.2. (cont.) Simulated and measured salinities in the boreholes KAS13, KAS14, KAS16 and KBH02 before the tunnel construction.

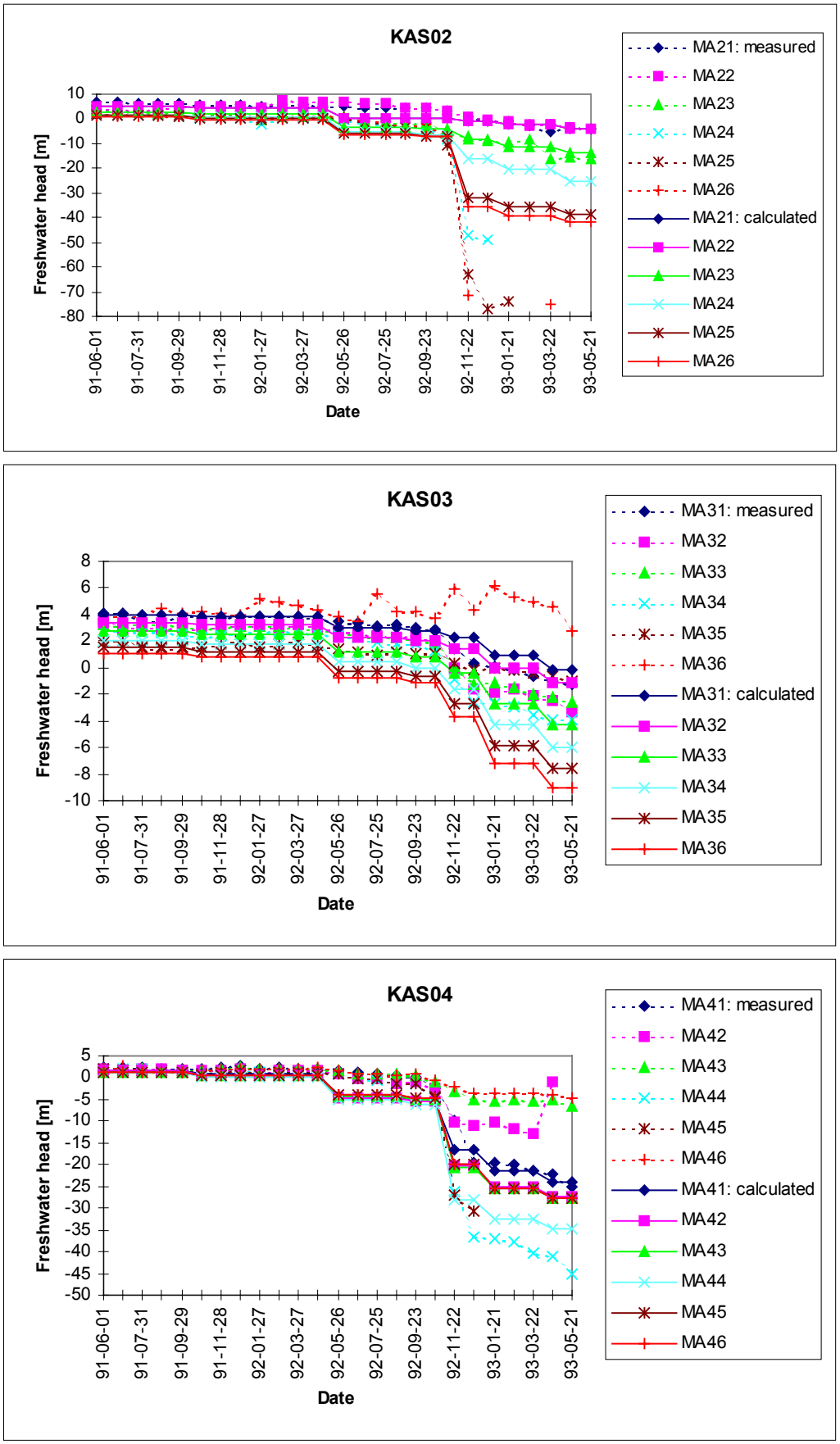

Figure 4.3. Simulated and measured freshwater head (m) in the boreholes KAS02—KAS04 as function of time.

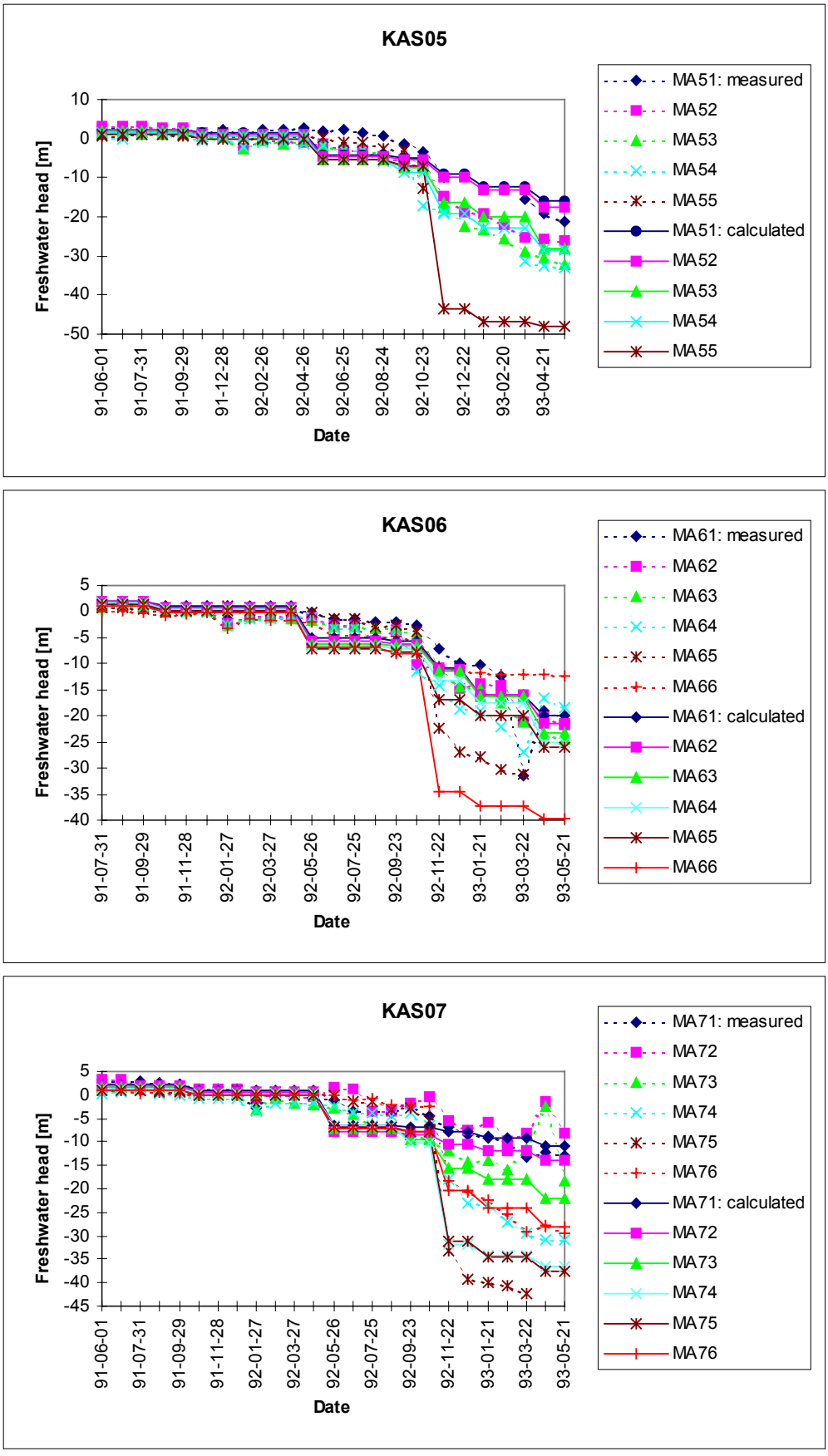

Figure 4.3. (cont.) Simulated and measured freshwater head (m) in the boreholes KAS05—KAS07 as function of time.

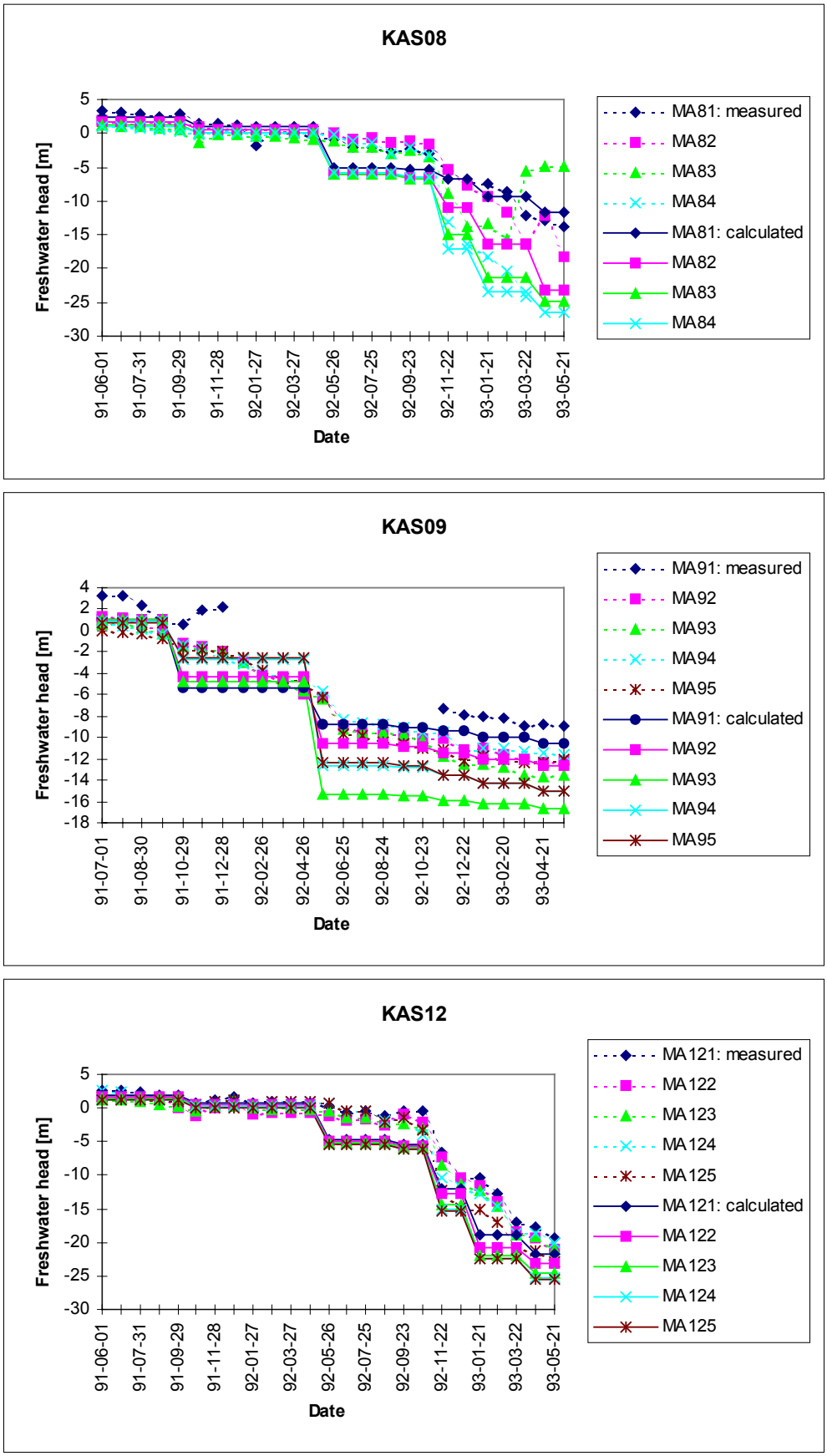

Figure 4.3. (cont.) Simulated and measured freshwater head (m) in the boreholes KAS08, KAS09 and KAS12 as function of time.

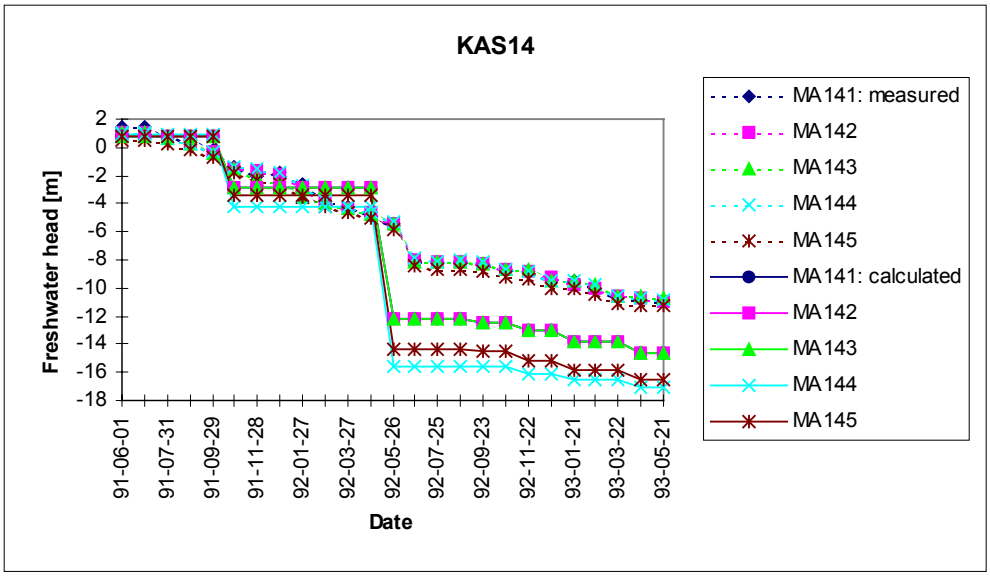

Figure 4.3. (cont.) Simulated and measured freshwater head (m) in the borehole KAS14 as function of time.

4.4 Inflow

Details about the flow measurements can be found in SKB PR 25-95-28, App. 2:4. The flow rates have also been presented by Rhén et al. (1997) (App. 2). However, minor adjustments of the flow rates reported by Rhén et al. (1997) and in SKB PR 25-95-28 have been made after August 1995 in the data delivered.

In each time step the nodes representing the tunnel and the shaft were grouped according to the measurement sections determined by the weirs. The flow rate measured at the weir was then uniformly divided between the nodes. In the coupled calculations of residual pressure and salinity the flow boundary condition was given for the transport equation in each time step after the first tunnel updating.

As suggested, the actual measurements at MA1659G, MA2587G and MA3384G have not been used in the modelling. Tunnel F (parallel and close to tunnel A, approximately section 3400-3510 m) being not modelled, the flow rate in MF0061G was added to MA3411G (50 %) and MA3426G (50 %).

4.5 Mean error and accuracy

The mean error and accuracy are defined as follows (Rhén, Smellie and Wikberg, 1998):

MEAN ERROR

$$dh = \frac{\sum_{i=1}^{n} (h_i^m - h_i^c)}{n}, \tag{4.3}$$

$$dh(abs) = \frac{\sum_{i=1}^{n} \left| h_i^m - h_i^c \right|}{n}, \tag{4.4}$$

ACCURACY

$$Dh = \sqrt{\frac{\sum_{i=1}^{n} (h_i^m - h_i^c - dh)^2}{n-1}}, \tag{4.5}$$

where n is the number of points with measured data used to compare with calculated points, h piezometric level (freshwater head) in metres above sea level (masl). Index m refers to a measured value and c to a calculated one.

These quantities are depicted in the following Figure 4.4 in the boreholes KAS02—KAS09, KAS12 and KAS14 separately and in all the boreholes concurrently. The first modelling stage of the shaft in November 1992 impairs the fit between the model result and the measurements especially in the boreholes KAS02—KAS06. This effect can also be seen in the last figure showing the performance measures calculated from all the borehole results.

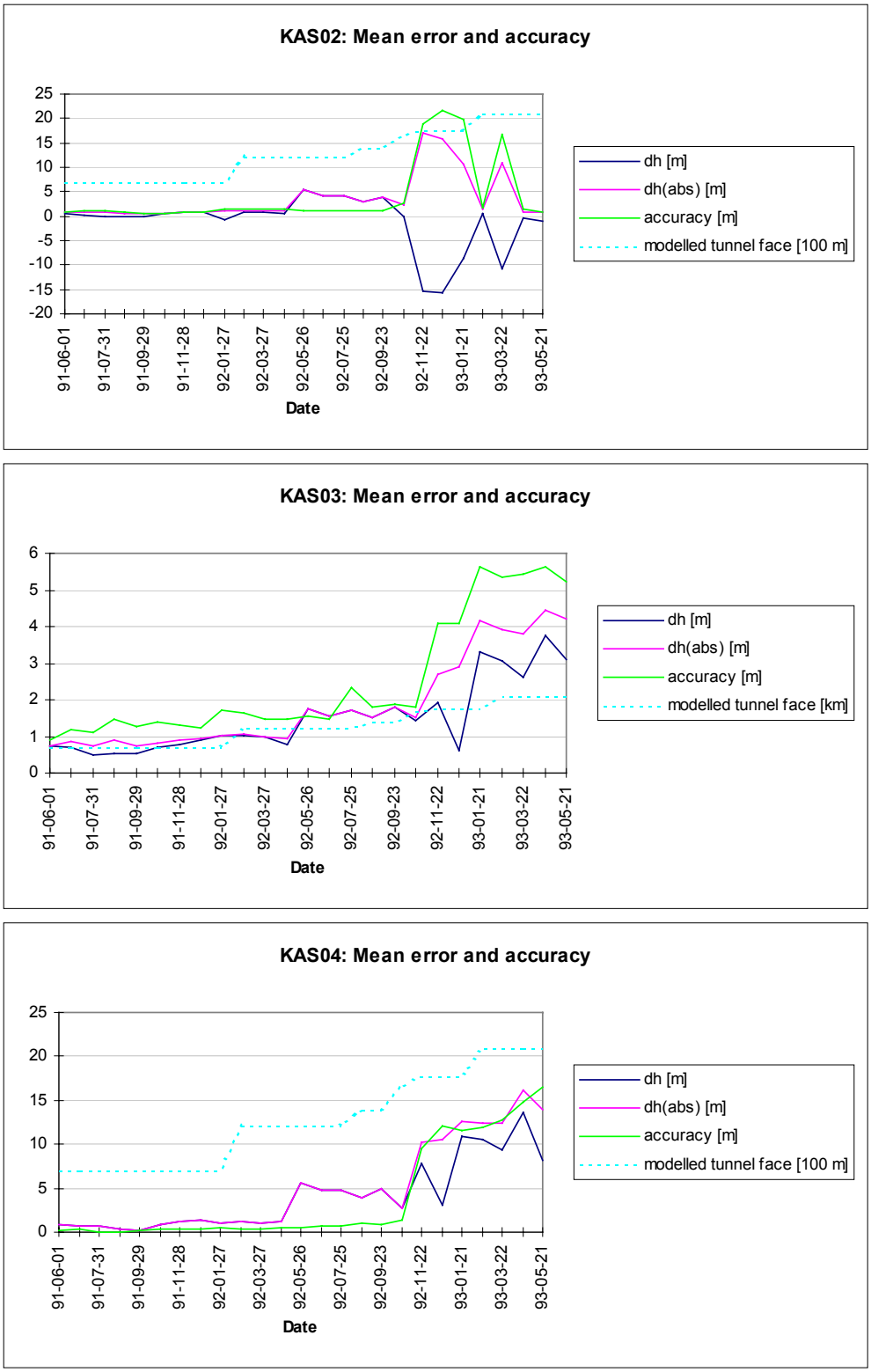

Figure 4.4. Mean error and accuracy (m) in the boreholes KAS02—KAS04 as function of time.

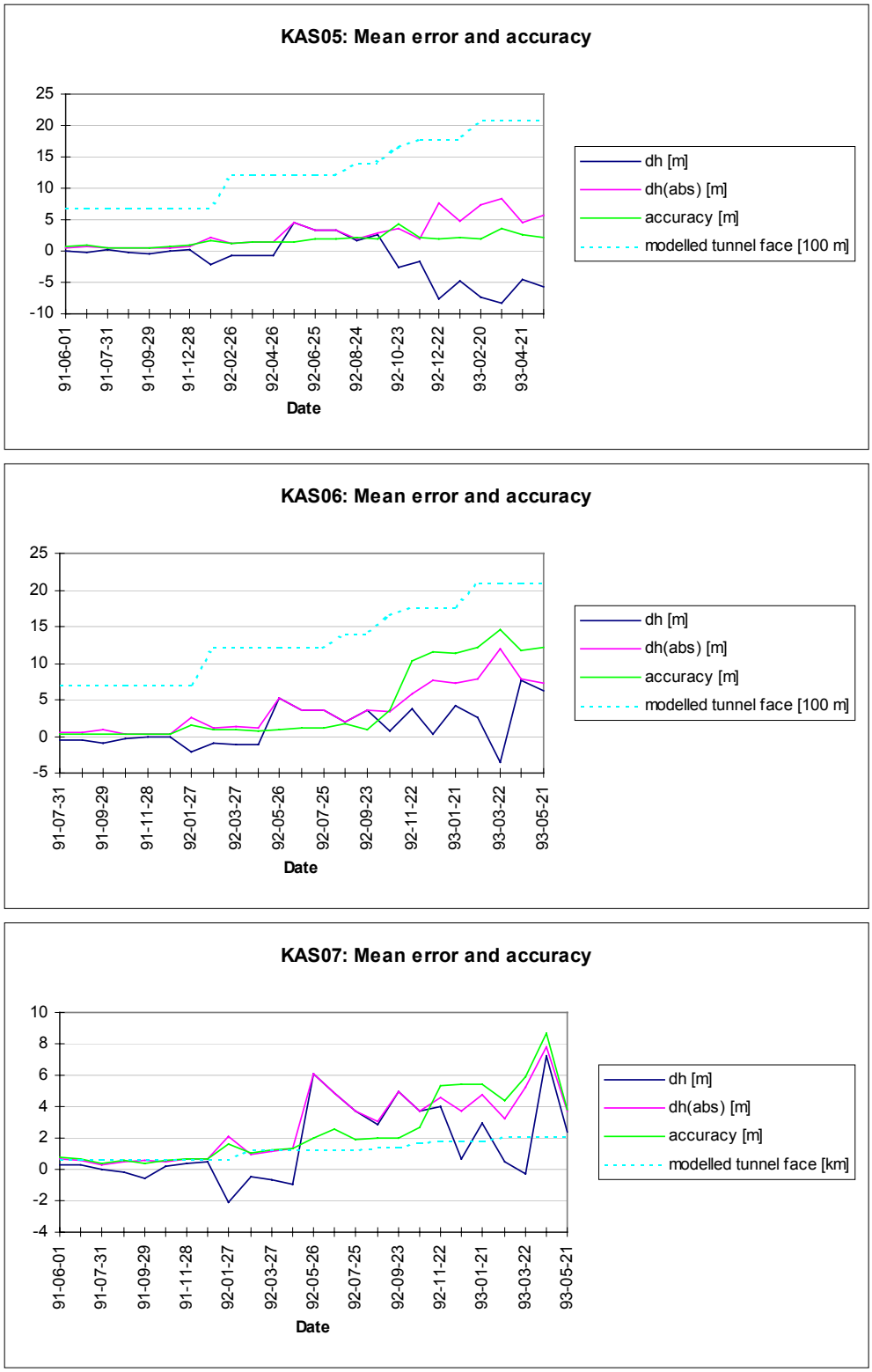

Figure 4.4. (cont.) Mean error and accuracy (m) in the boreholes KAS05—KAS07 as function of time.

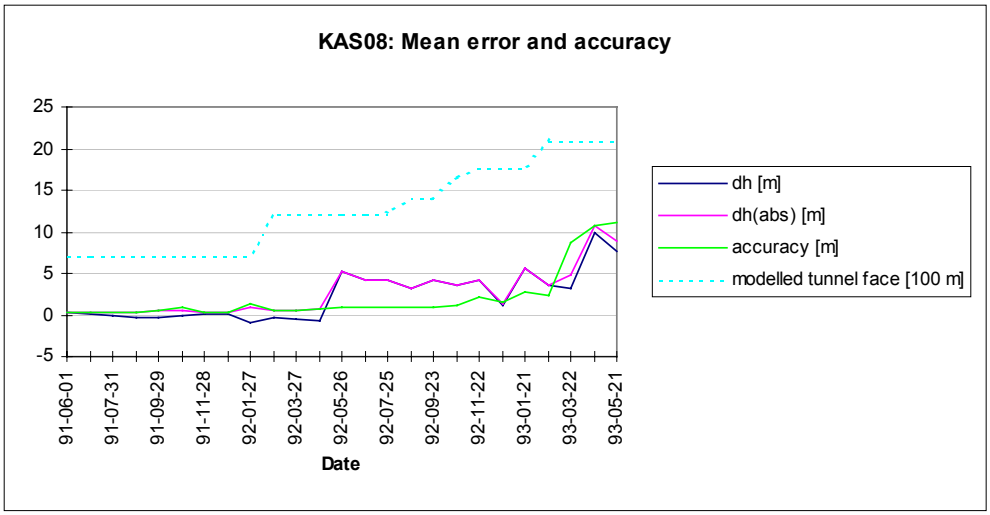

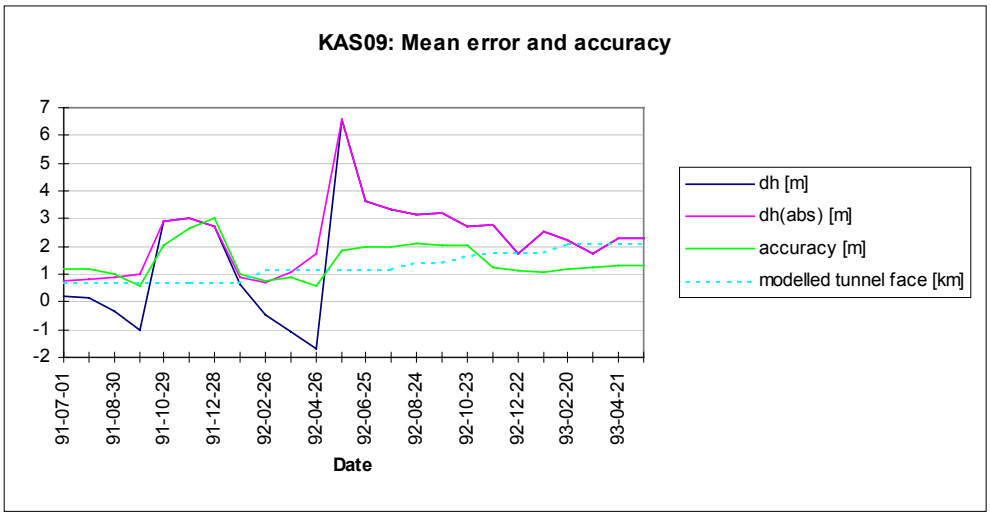

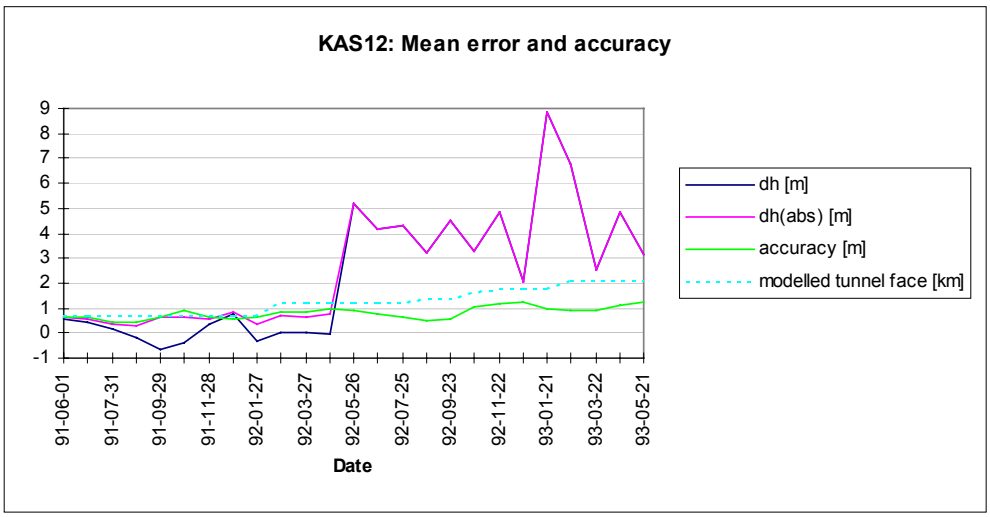

Figure 4.4. (cont.) Mean error and accuracy (m) in the boreholes KAS08, KAS09 and KAS12 as function of time.

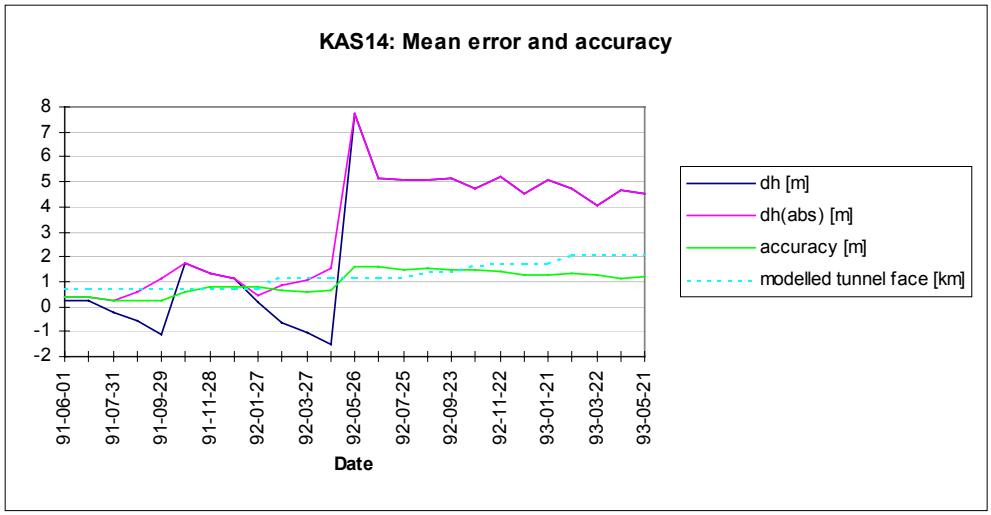

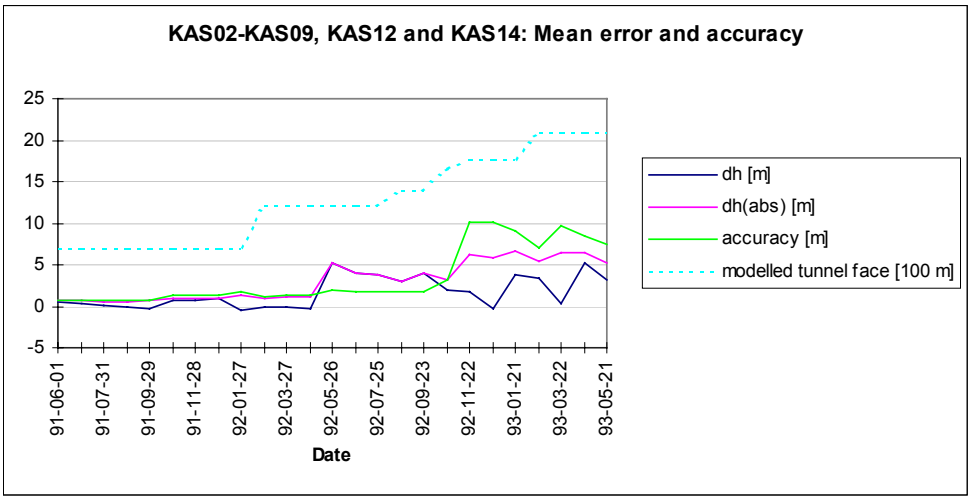

Figure 4.4. (cont.) Mean error and accuracy (m) in the borehole KAS14 and in the whole model as function of time.

5 MAIN RESULTS

5.1 Introduction

In this work, the flow equation is expressed in terms of the residual pressure. The flow direction can not generally be determined from the residual pressure contours, except in a freshwater zone (see Eq. (2.5)).

The surface boundary condition for four tunnel face positions (1400 m, 2100 m, 3000 m and 3600 m) is shown in Figure 5.1 as freshwater head (m). It depicts the groundwater table in the surroundings of the Äspö island. The lowering of the groundwater table also in the area of Hålö, Ävrö and Mjälen to be seen clearly for the tunnel face position 1400 m is due to the withdrawal of the tunnel and the infiltration boundary condition applied over the land. The effect of the shaft boundary condition (Sections 4.3 and 4.4) can be seen to be very strong after the first modelling step of the shaft when the tunnel face was at 1774 metres (see Table 3.4).

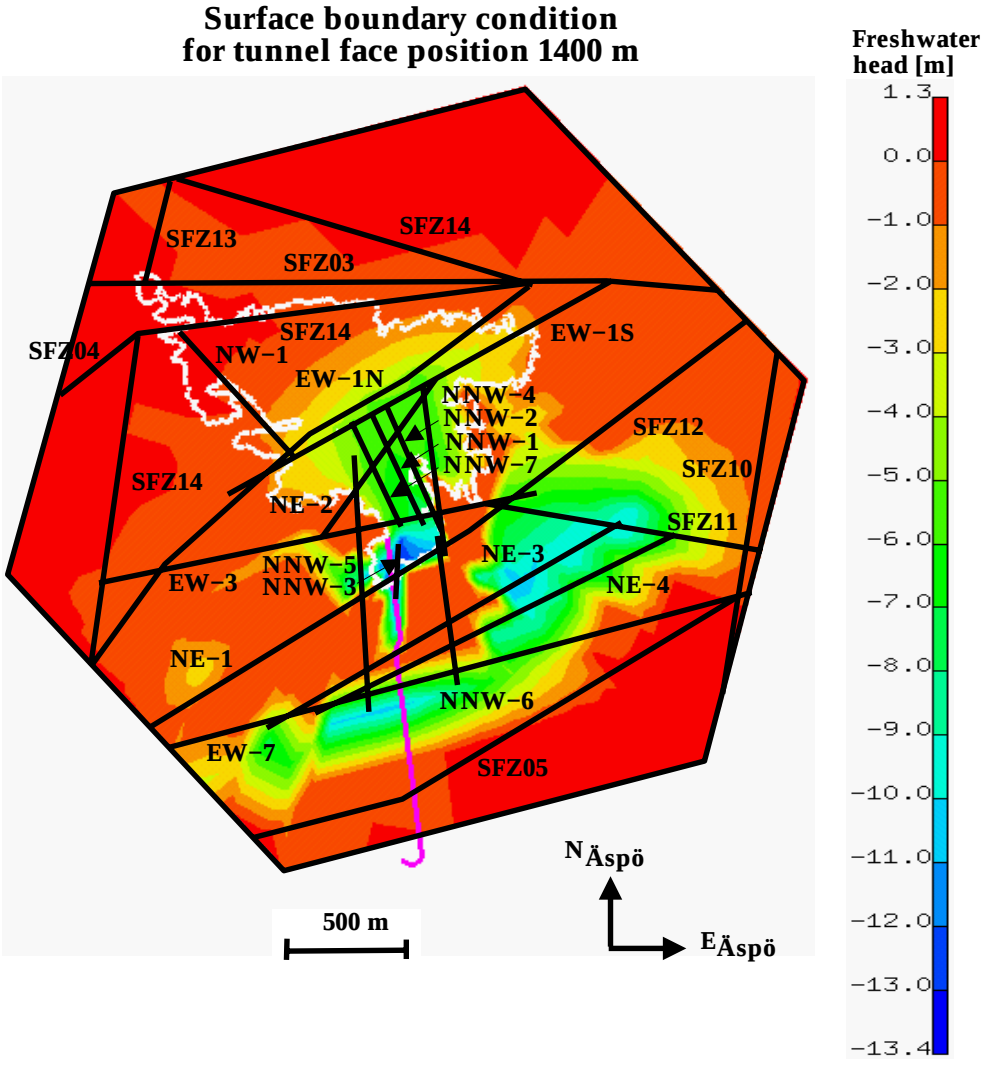

Figure 5.1. Surface boundary condition for tunnel face position 1400 m.

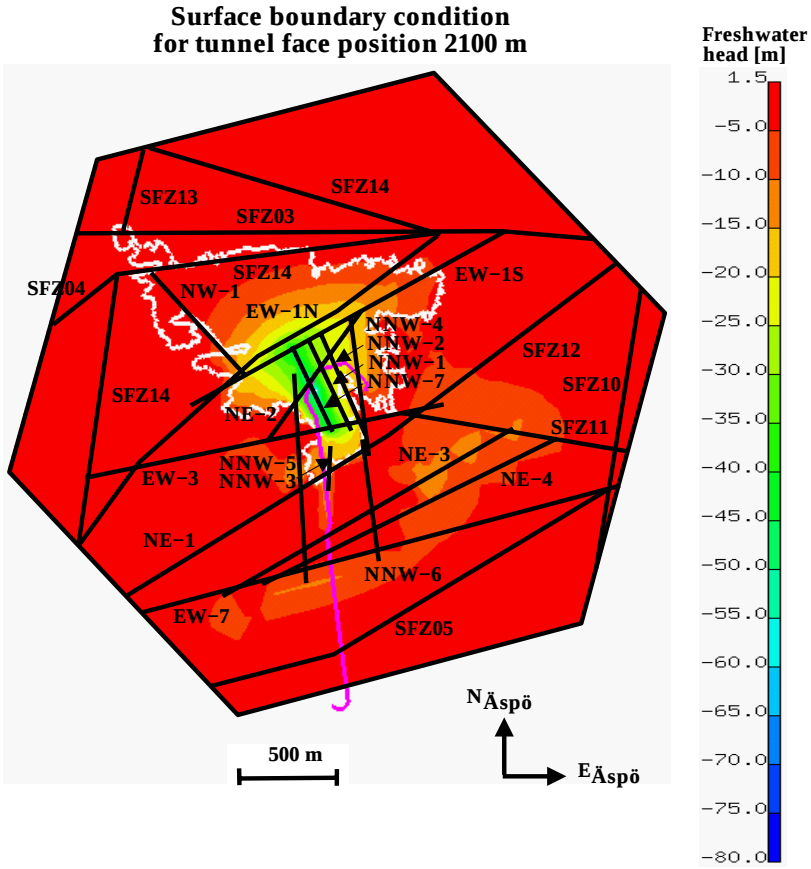

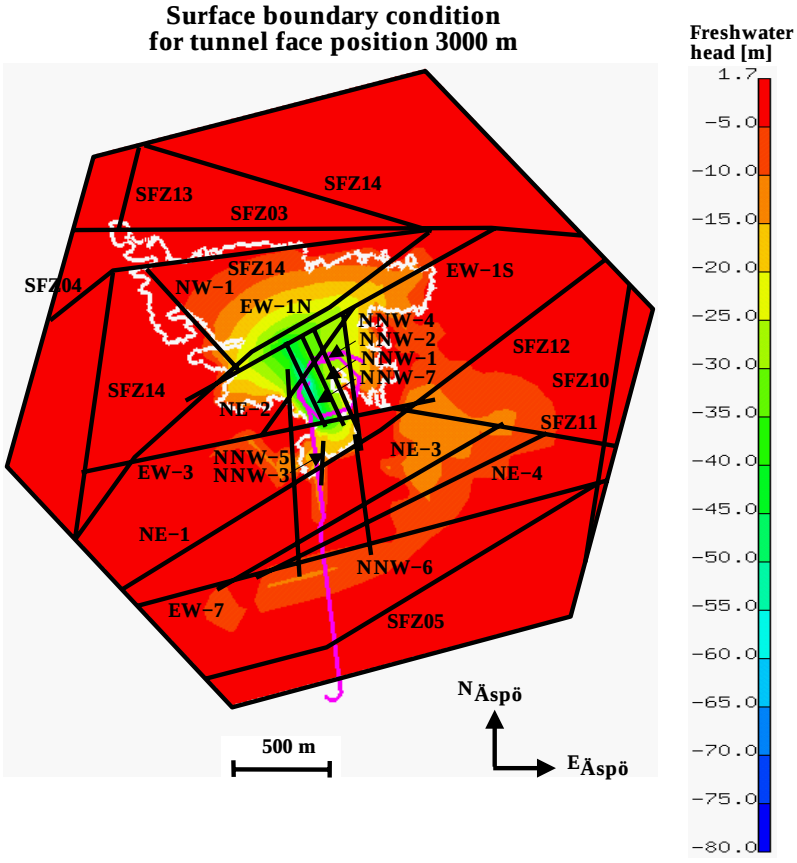

Figure 5.1. (cont.) Surface boundary condition for tunnel face positions 2100 m (top) and 3000 m (bottom).

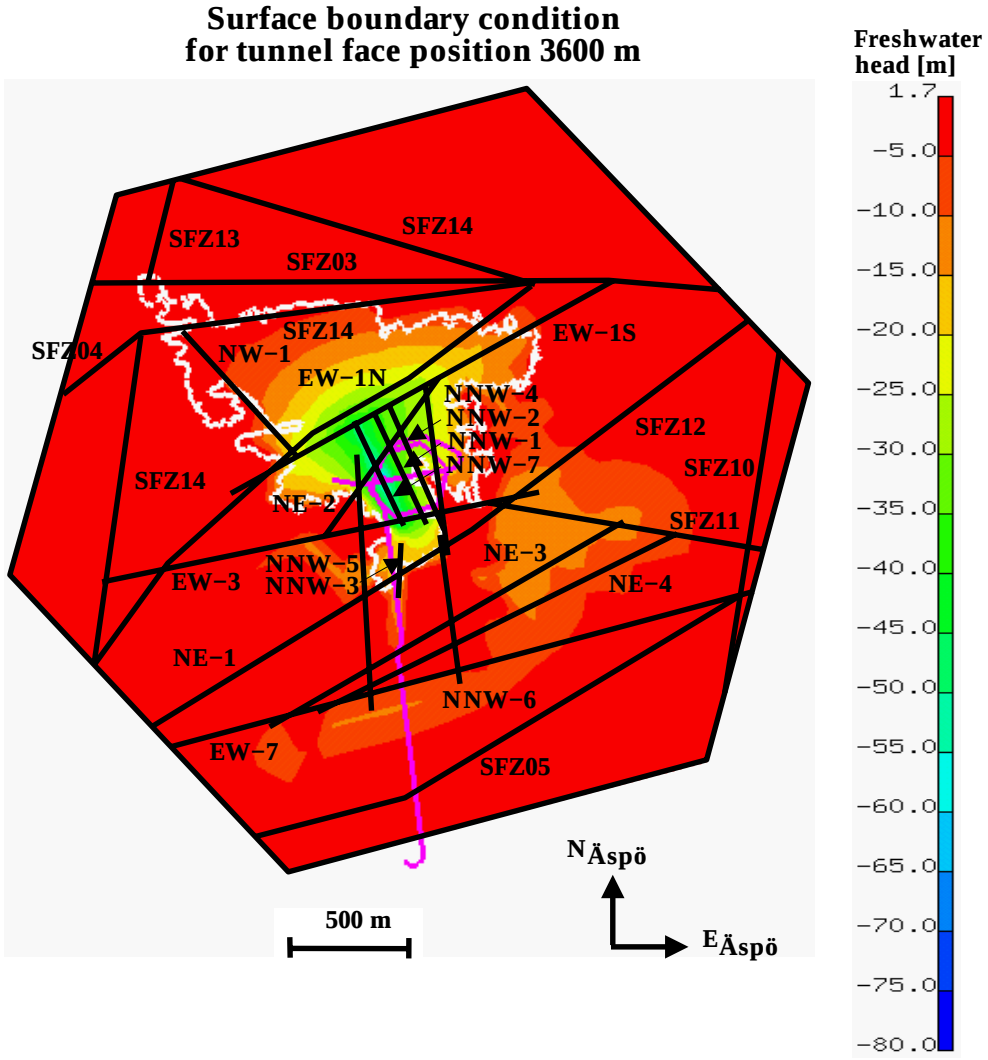

Figure 5.1. (cont.) Surface boundary condition for tunnel face position 3600 m.

5.2 Mixing ratios at control points

In the mixing calculations the transport equations of the different groundwater types were solved using the previously simulated residual pressure and salinity fields (Fig. 5.2).

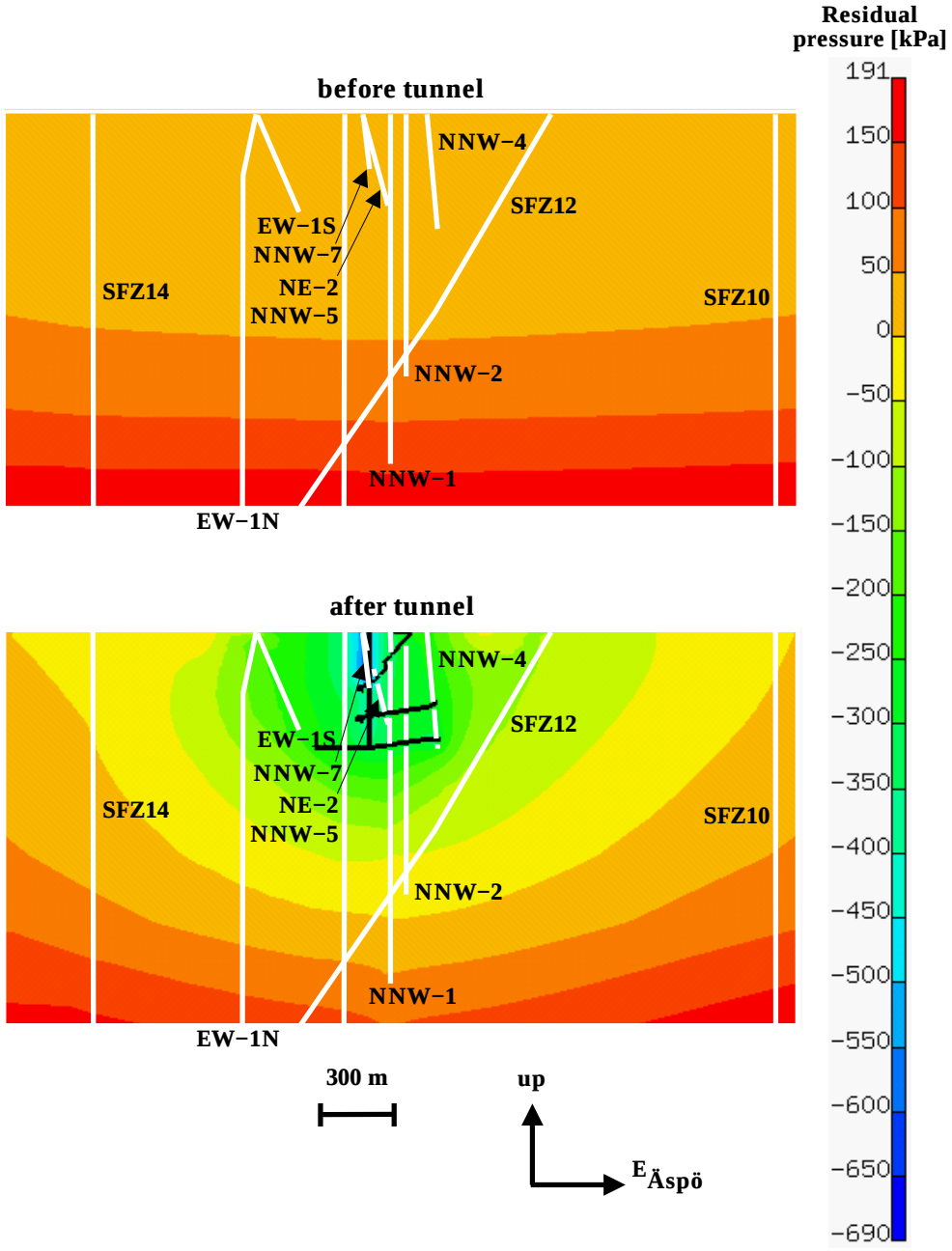

Figure 5.2. Residual pressure (kPa) on an east—west trending cut plane through the control point KA3110A before and after the tunnel construction.

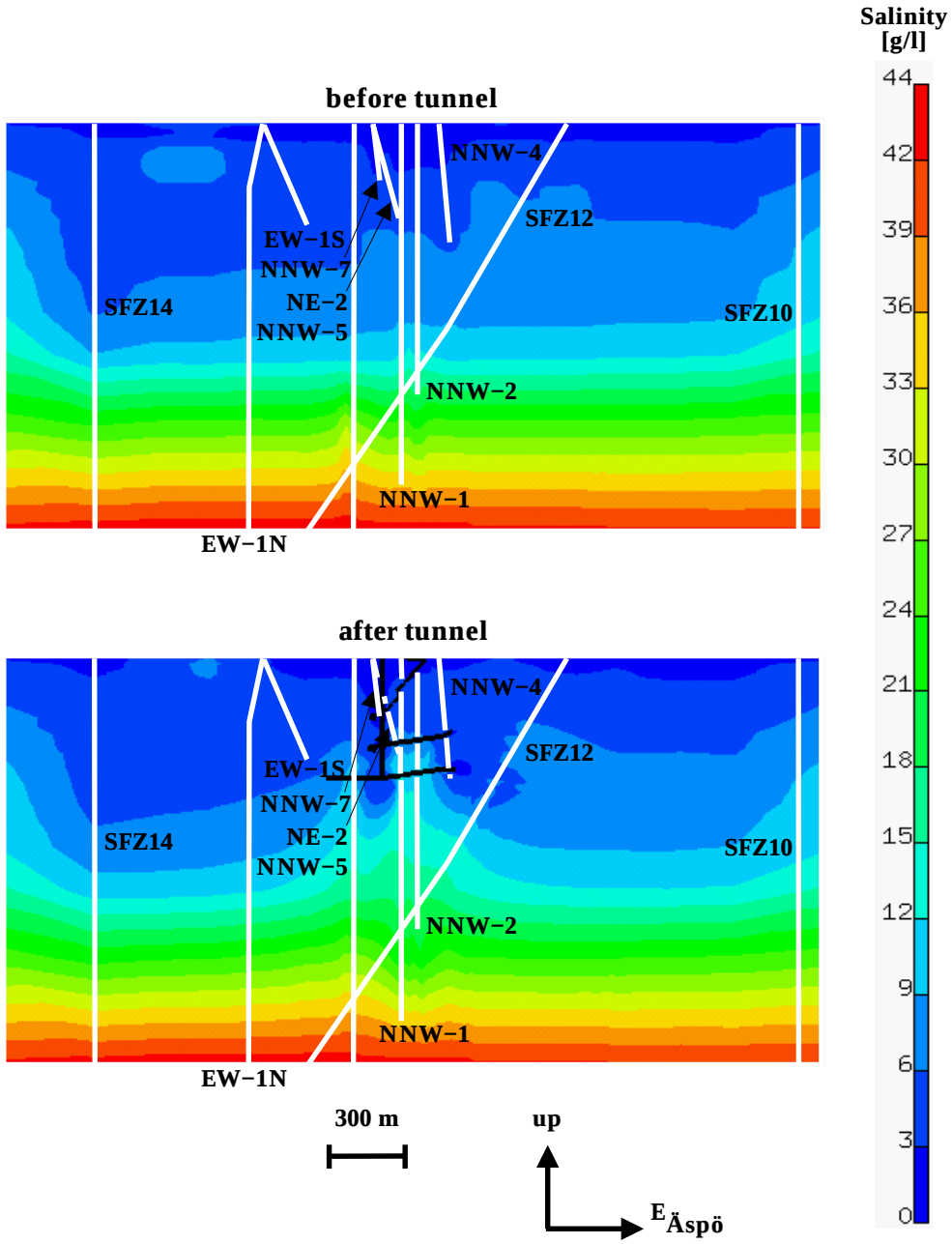

Figure 5.2. (cont.) Salinity (g/l) on an east—west trending cut plane through the control point KA3110A before and after the tunnel construction.

The model was firstly solved by using the dispersion lengths 1000 m and 100 m for the longitudinal and transversal dispersion lengths, respectively. This did not lead to a reasonable fit with the mixing ratios estimated from the measurements (Gurban et al., 1998).

The model was improved by decreasing the infiltration from the sea by lowering the transmissivity of the uppermost elements of the fracture zones below the sea to the value T=9.3·10^{-9} m^2/s (supposed width 30 m). This was expected to have an effect on the simulated mixing ratios especially in the control points SA0813B, SA0850B and SA1229A. To enhance the similarity of the pattern of the estimated (M3) and the simulated mixing

ratios in the control points SA2074A and SA2783A, the dispersion lengths of the fracture zones NE-2, NNW-1, NNW-2, NNW-4, NNW-5 and NNW-7 situated in the tunnel area were increased fivefold (see Table 3.1). In all, this was an advance. The result in the control point SA2783A was not yet reasonable, however.

Next the mixing result in the control point SA2783A (in the interpreted position of the fracture zone NNW-2) was considered. The transmissivities were modified in three cases.

In the first case the transmissivities of the fracture zones EW-3, NE-2, NE-1, NNW-1, NNW-7 and NNW-8 were taken as in Model 96 (Rhén et al. 1997, Table 8-1). The transmissivity of the zone NNW-2 was T=2.1·10^{-6} m^2/s (see Table A2-8 in Rhén et al. 1997). Two results were compared: firstly, the model with the dispersion lengths 1000 m and 100 m for the longitudinal and transversal dispersion lengths of all the fracture zones, respectively, secondly, the model with the dispersion lengths of the fracture zones NE-2, NNW-1, NNW-2, NNW-4, NNW-5 and NNW-7 modified as described above. The mixing ratios in the control points were compared between these results. The latter was found better on the basis of the better fit between the estimated and the simulated mixing ratios in the control point SA2074A. The latter result in the control point SA2783A was also better than in the case simulated before the transmissivity modifications. In these results the performance measures got worse, however.

In the second case only the transmissivity of the zone NNW-2 was modified to the value T=2.1·10^{-6} m^2/s (see Table A2-8 in Rhén et al. 1997). As regards to the mixing results in the control points and the performance measures, this was not considerably better than the case without transmissivity modifications.

Finally, in the third case, the transmissivities of the fracture zones EW-3, NE-2, SFZ12 (combined with NE-1) and NNW-8 were taken as in Model 96 (Rhén et al. 1997, Table 8-1). The transmissivity of the zone NNW-2 was T=2.1·10^{-6} m^2/s (see Table A2-8 in Rhén et al. 1997). The transmissivities of the zones NNW-1 and NNW-7 were restored to retain the calibration result in the borehole KAS02. This led to a somewhat better mixing result in the control point SA2783A than in the case without transmissivity modifications. Also the overall mixing result and the perfomance measures were quite reasonable.

If the topography also outside the Äspö island is included, the mixing ratios in the control points and the performance measures in the case without transmissivity modifications do not change considerably. This is due to the great, extensive effect of the Äspö tunnel prevailing.

Figures 5.3—5.7 depict the mixing ratios of brine, glacial, meteoric and Baltic water in the control points KR0012B, SA0813B, SA1229A, SA2074A and SA2783A as function of time. The model result (Cal. 10) is compared to the result of the geochemical M3 estimations (Gurban et al.,

1998). Figures 5.8 and 5.9 show the comparison in the control points outside the Äspö tunnel, namely KAS03 (section 533—626 m) and KAS07 (section 501—604 m). Figures 5.10—5.12 show the mixing ratios in the control points KA3005A, KA3110A and KA3385A of the prediction section 2900—3600 m of the tunnel. Table 5.1 summarizes the single results in the control points KAS03 (section 609—623 m; preinvestigations), SA0850B and SA1327B.

In KR0012B (Fig. 5.3) the mixing ratio of meteoric water is too low and the mixing ratio of Baltic water too high compared to the model by Gurban et al. (1998). In this boundary area the model can't describe the effect of the tunnel very well due to the large element size. Thus, in this work the flow from underneath the tunnel possibly is too high in the vicinity of the control point KR0012B. Looking at the calculation results from the beginning of year 1995 onward (Figures 5.4, 5.5, 5.7, 5.10—5.12), one can predict the future conditions of the different water types at the control points. Generally, the brine water seems to remain steady, except in the prediction section (Figures 5.10—5.12), where it is mildly increasing. The glacial water decreases, because it is a relict component in the present-day groundwater conditions. In the control point KA3385A the future condition of the glacial component seems nearly unvarying. The meteoric water generally increases. In the control points SA2783A and KA3385A it remains steady in the near future, however. The overall future condition of the Baltic water seems quite steady. These results are fairly well in line with those by Gurban et al. (1998).

Figure 5.13 shows the mixing ratios of each water type on an east—west trending cut plane through the control point KA3110A before and after the tunnel construction (time steps 1 and 13, respectively (see Table 3.4)). The tunnel construction caused the upconing of the brine water, the decrease of the relict glacial water and the increase of the mixing ratios of the meteoric and Baltic waters in the tunnel area.

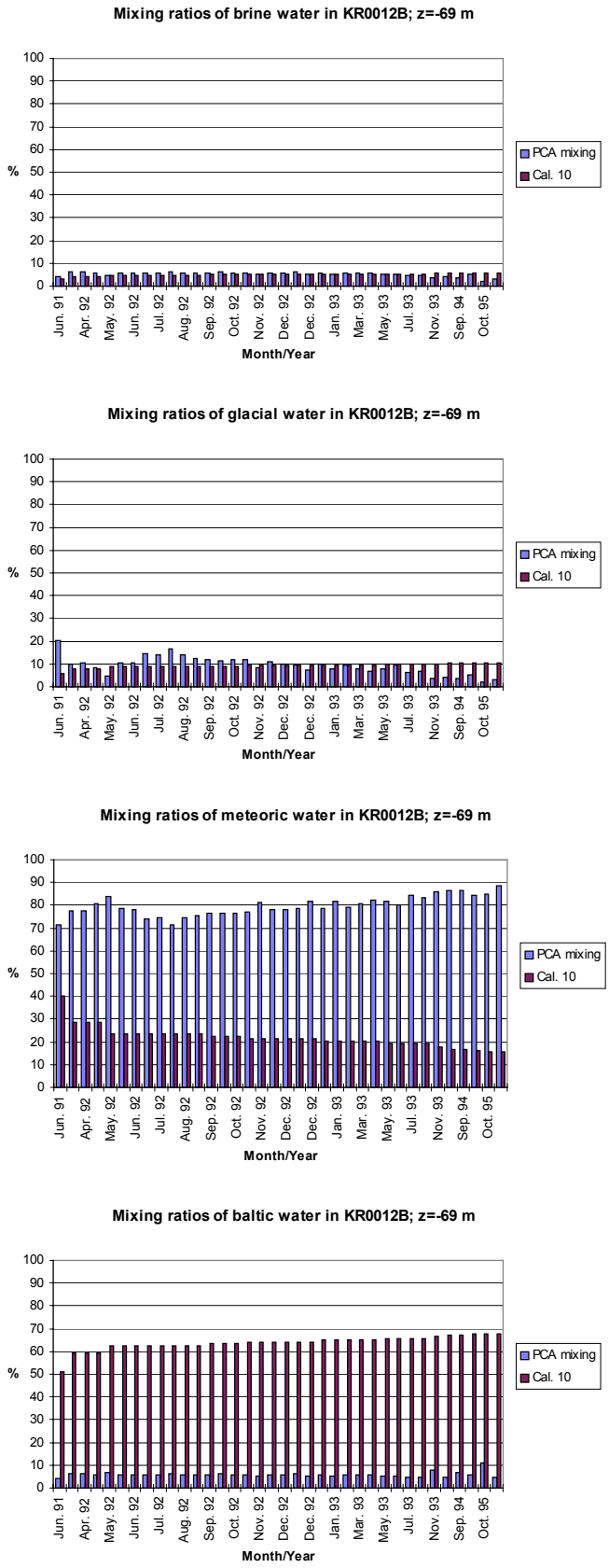

Figure 5.3. The mixing ratios of brine, glacial, meteoric and Baltic water in KR0012B as function of time.

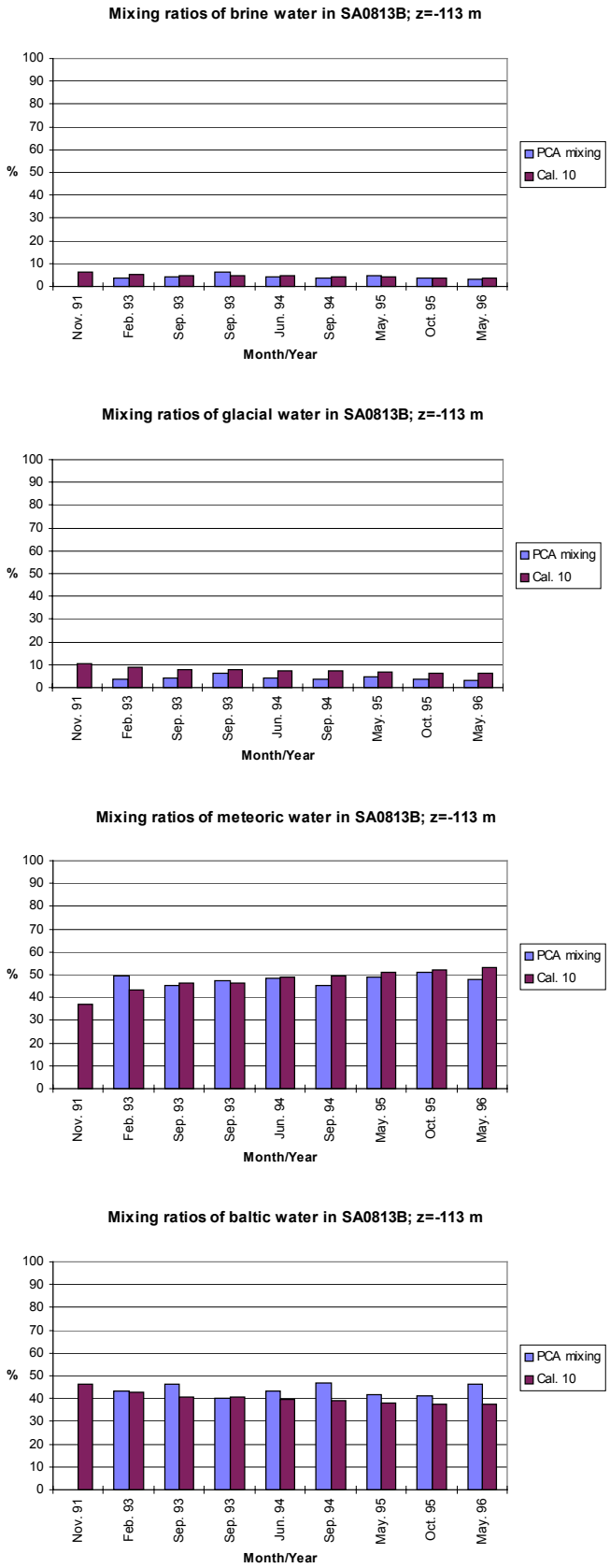

Figure 5.4. The mixing ratios of brine, glacial, meteoric and Baltic water in SA0813B as function of time.

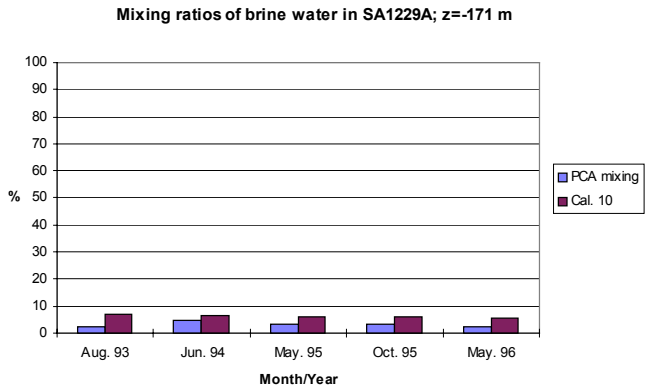

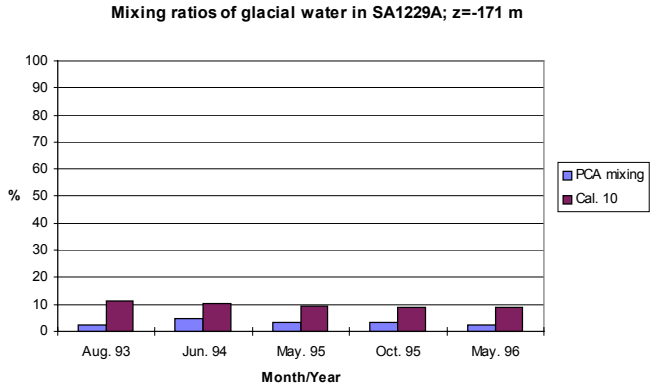

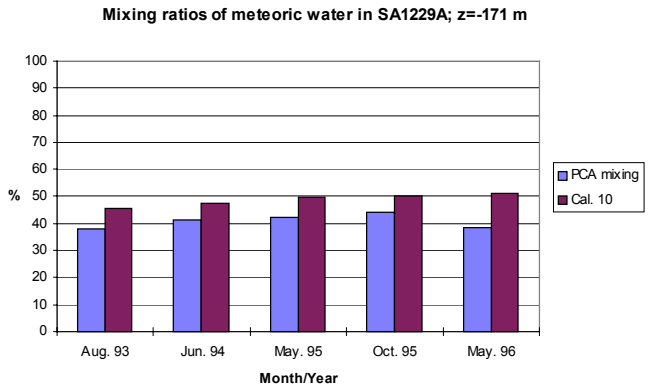

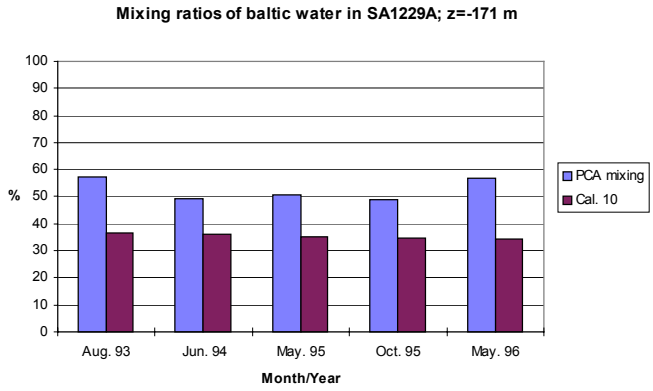

Figure 5.5. The mixing ratios of brine, glacial, meteoric and Baltic water in SA1229A as function of time.

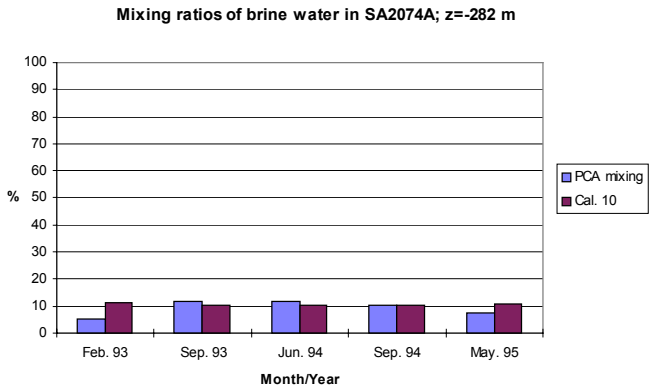

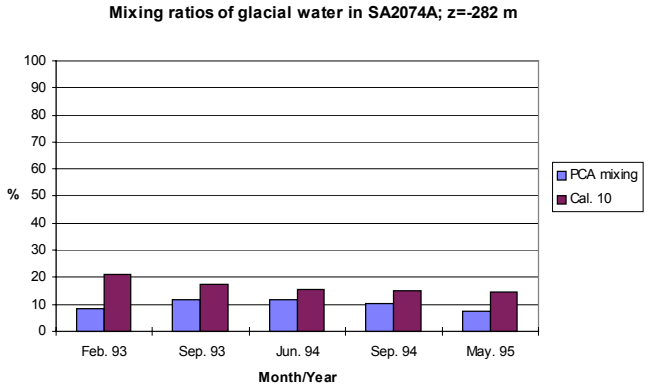

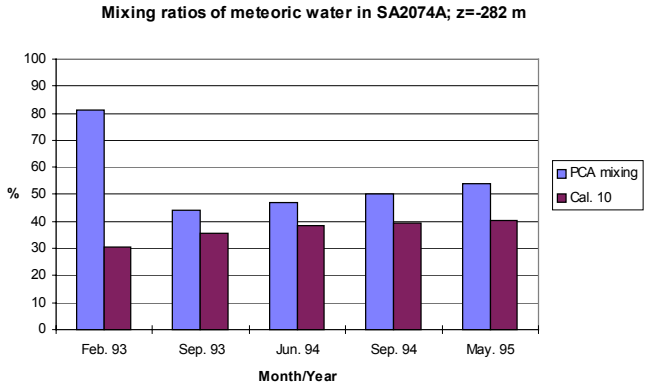

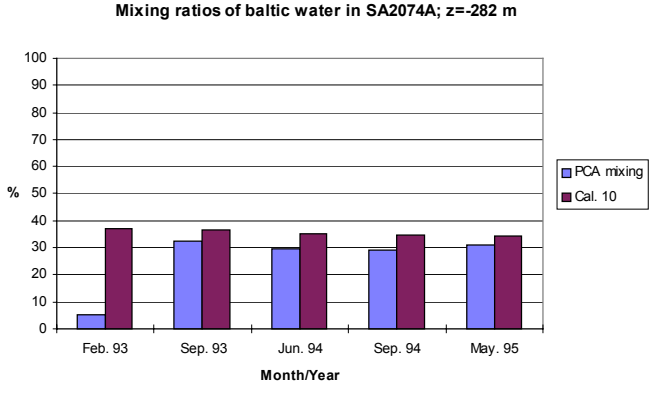

Figure 5.6. The mixing ratios of brine, glacial, meteoric and Baltic water in SA2074A as function of time.

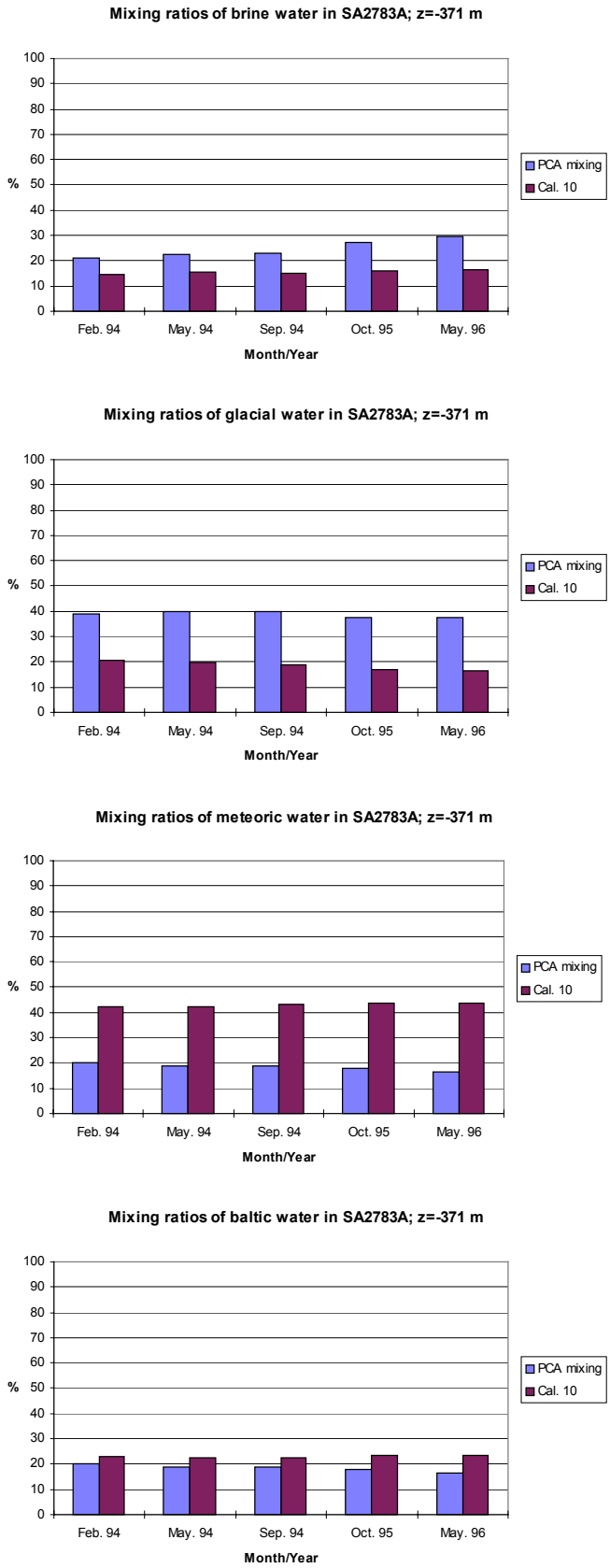

Figure 5.7. The mixing ratios of brine, glacial, meteoric and Baltic water in SA2783A as function of time.

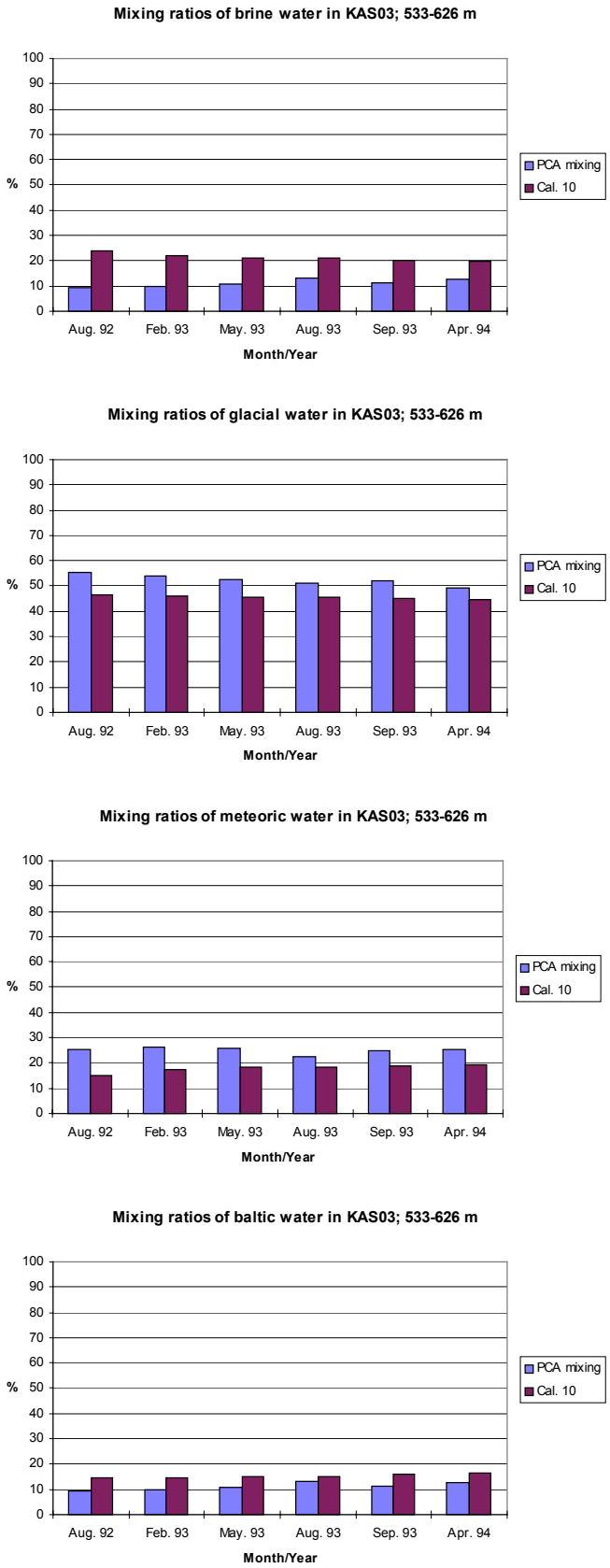

Figure 5.8. The mixing ratios of brine, glacial, meteoric and Baltic water in KAS03 (section 533—626 m) as function of time.

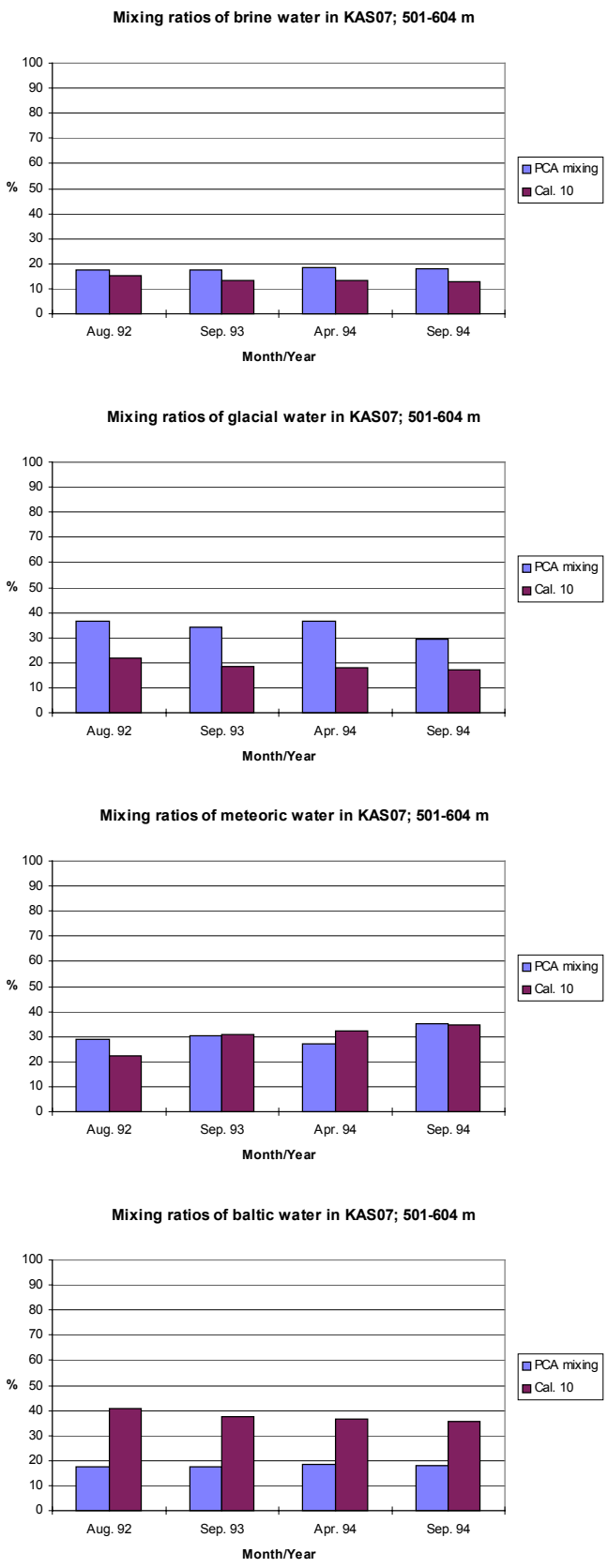

Figure 5.9. The mixing ratios of brine, glacial, meteoric and Baltic water in KAS07 (section 501—604 m) as function of time.

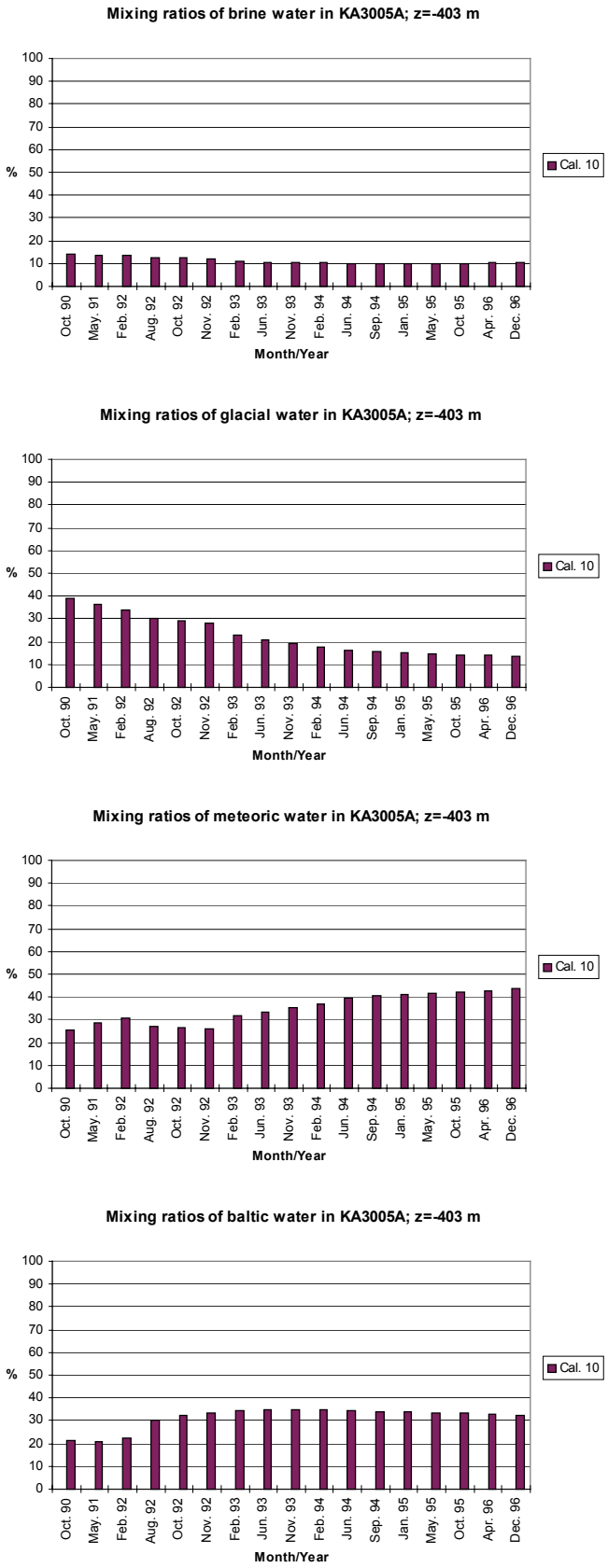

Figure 5.10. The mixing ratios of brine, glacial, meteoric and Baltic water in KA3005A as function of time.

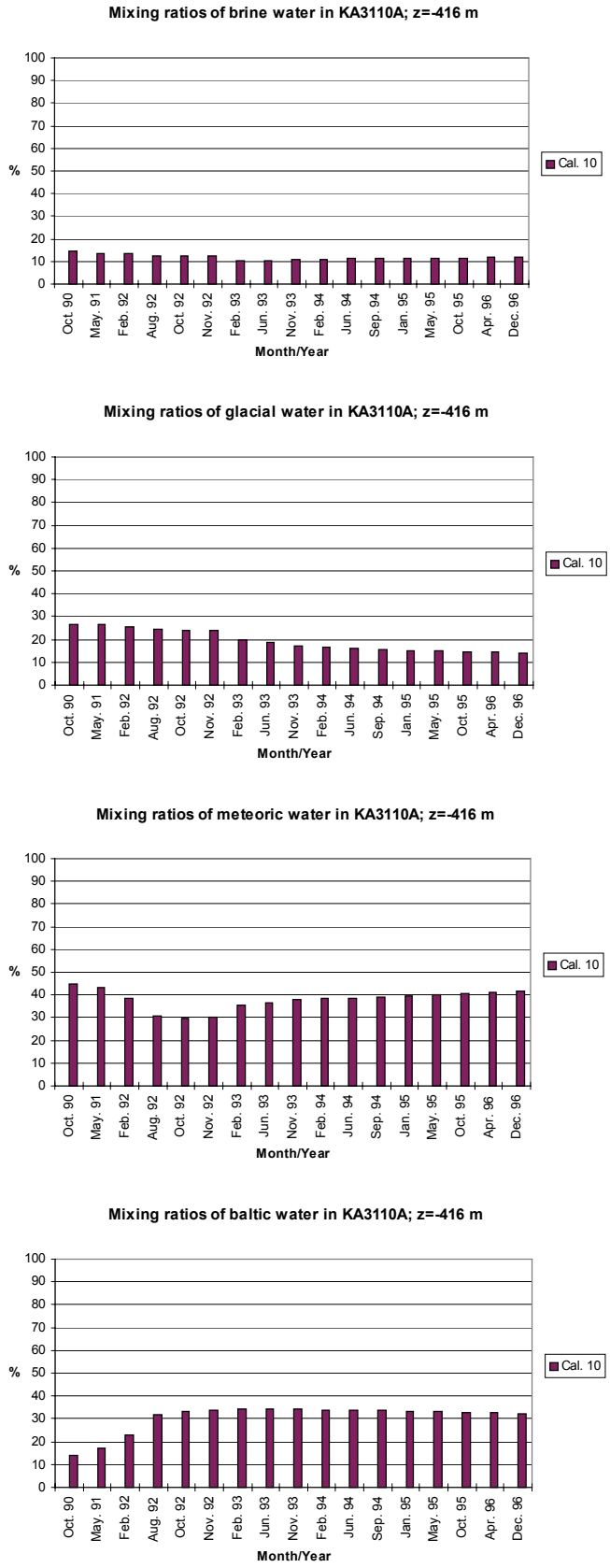

Figure 5.11. The mixing ratios of brine, glacial, meteoric and Baltic water in KA3110A as function of time.

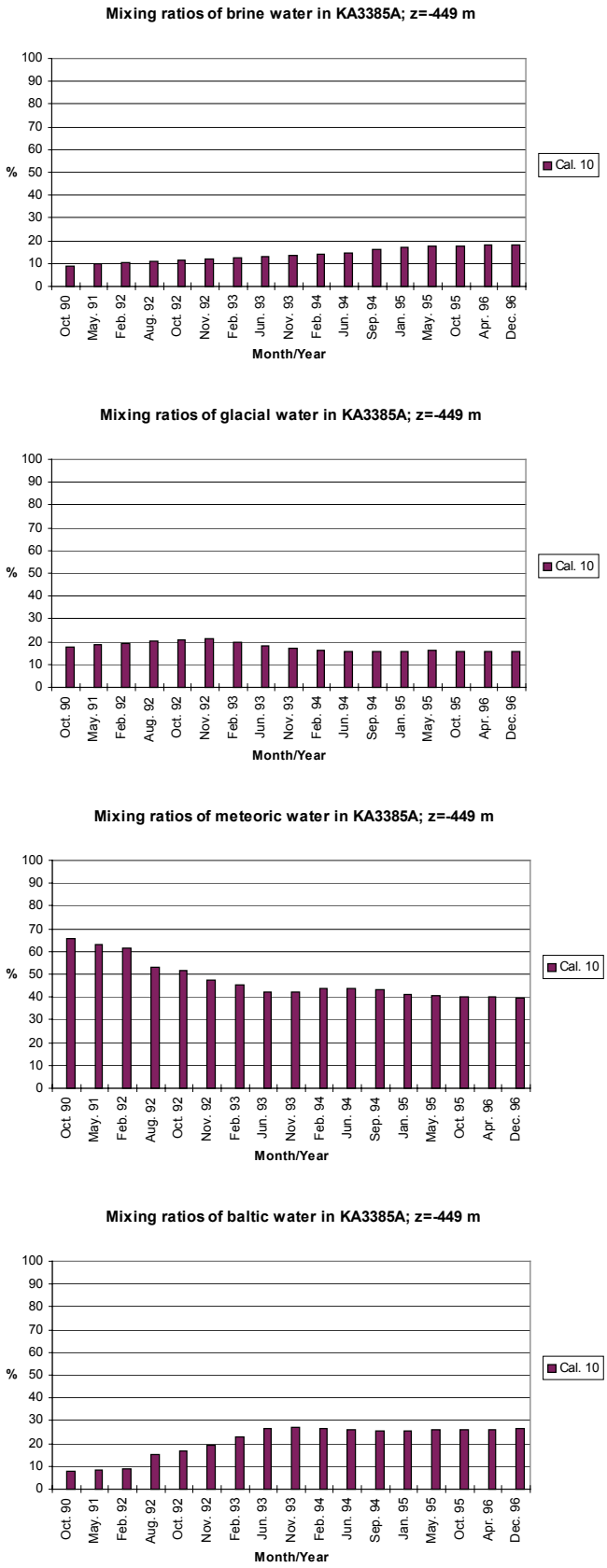

Figure 5.12. The mixing ratios of brine, glacial, meteoric and Baltic water in KA3385A as function of time.

Table 5.1. The mixing ratios of brine, glacial, meteoric and Baltic water in KAS03 (section 609—623 m; preinvestigations), SA0850B and SA1327B.

	PCA mixing (Gurban et al., 1998)					Cal. 10			
	Date	*Brine*	*Glacial*	*Meteoric*	*Baltic*	*Brine*	*Glacial*	*Meteoric*	*Baltic*
KAS03	*Sep. 88*	17	51	16	16	24	48	14	14
SA0850B	*Aug. 91*	10	10	47	33	8	13	26	54
SA1327B	*Oct. 92*	7	7	51	35	9	16	35	40

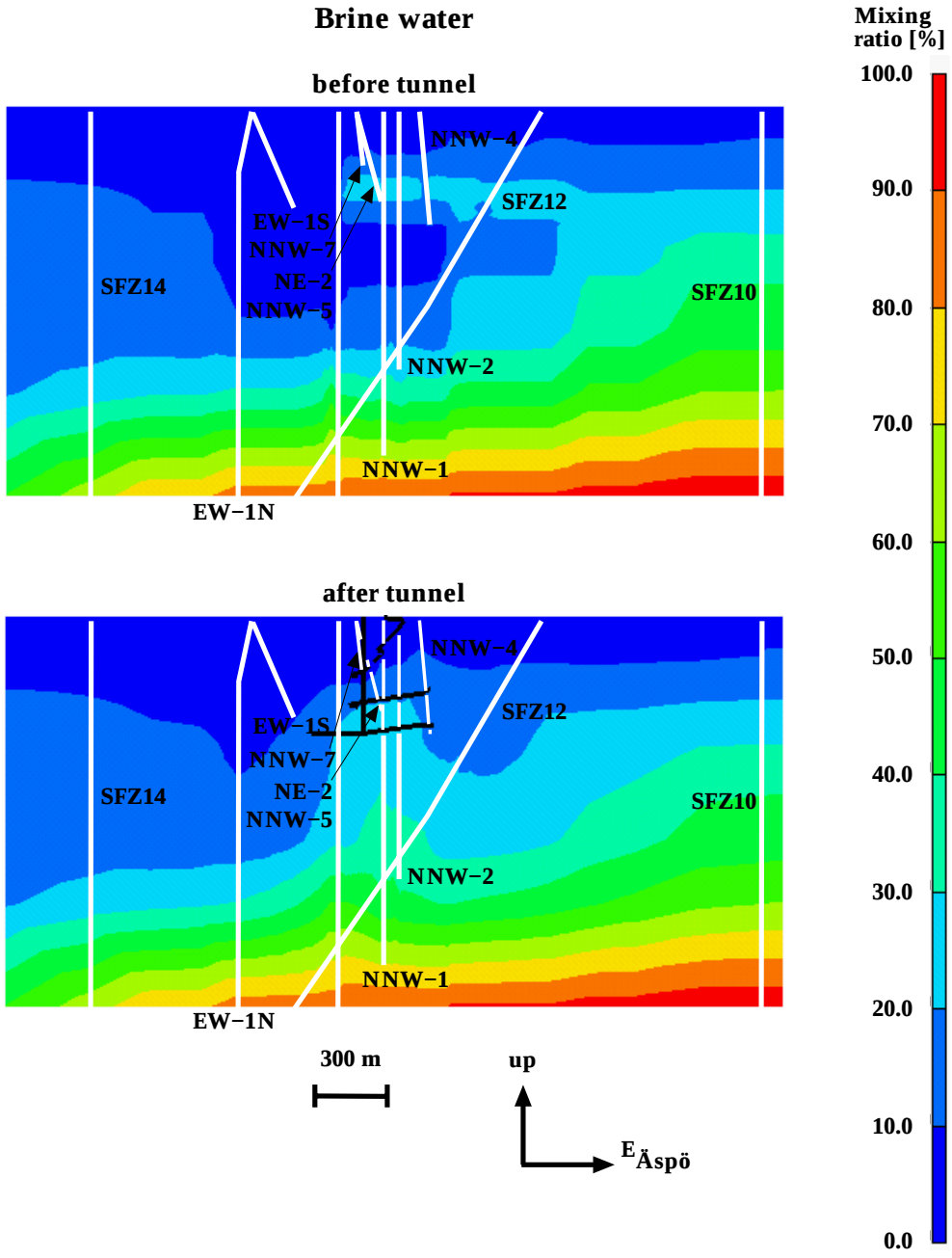

Figure 5.13. The mixing ratio of brine water on an east—west trending cut plane through the control point KA3110A before and after the tunnel construction.

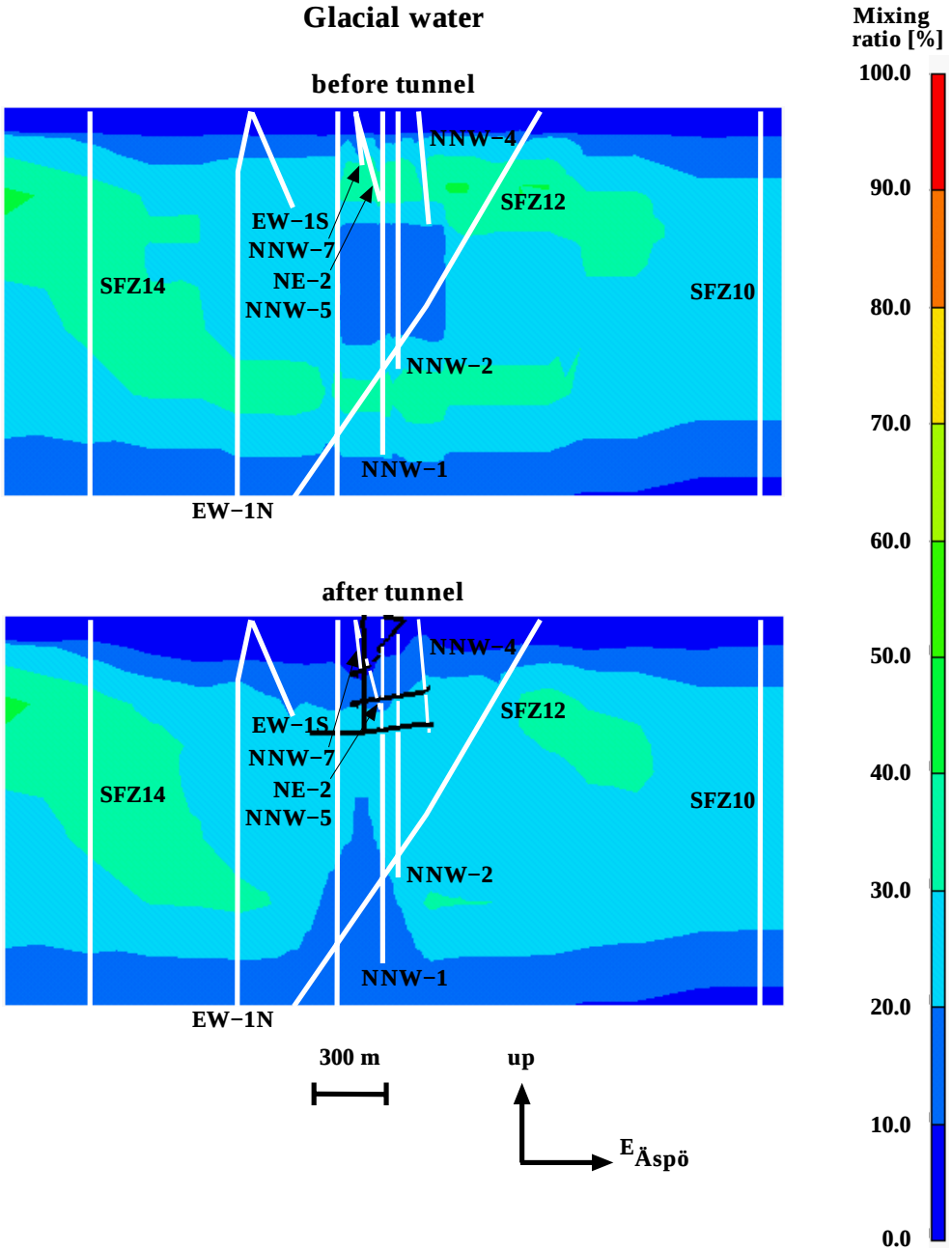

Figure 5.13. (cont.) The mixing ratio of glacial water on an east—west trending cut plane through the control point KA3110A before and after the tunnel construction.

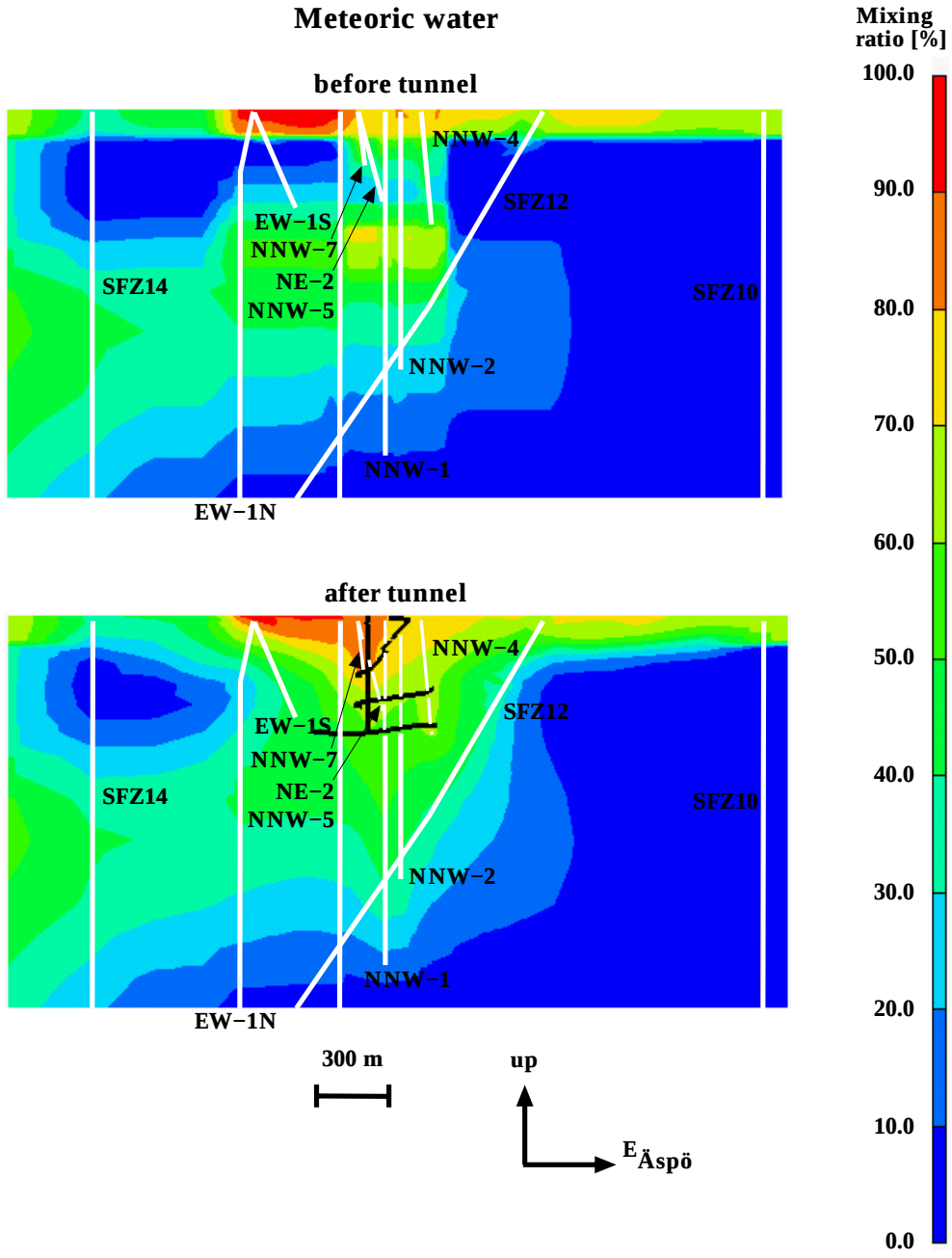

Figure 5.13. (cont.) The mixing ratio of meteoric water on an east—west trending cut plane through the control point KA3110A before and after the tunnel construction.

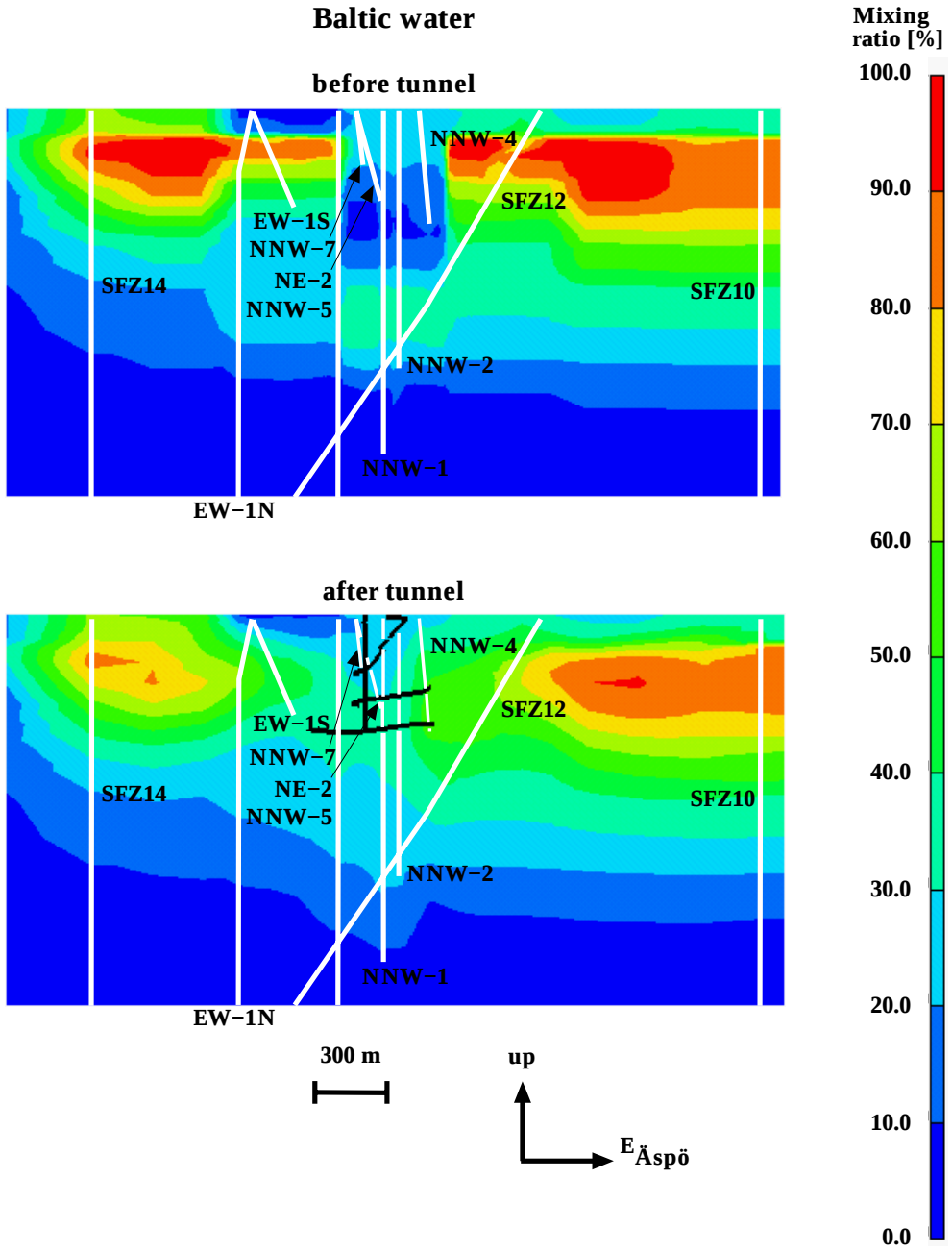

Figure 5.13. (cont.) The mixing ratio of Baltic water on an east—west trending cut plane through the control point KA3110A before and after the tunnel construction.

5.3 Flow pattern to control points

Figure 5.14 shows some flow paths to the tunnel and to the control points outside the tunnel in the tunnel front positions 1400 m, 2100 m, 3000 m and 3600 m. The paths were computed using the residual pressure and salinity fields for the time steps in question. The paths can be used to show from where the water coming to the control points originates.

The water to the control point KR0012B in all the tunnel front positions in question (1400 m, 2100 m, 3000 m and 3600 m) originates outside the southern vertical edge of the model. To the control points SA0813B and SA0850B water flows from the ground level. Also to SA1229A in the tunnel front positions 1400 m, 2100 m and 3600 m water flows from the ground level. In the tunnel front position 3000 m it flows from the vertical edge of the model. To SA1327B in the tunnel front position 2100 m water flows from the ground level. In the later positions it originates outside the vertical edge of the model. The other calculated paths to the tunnel originate outside the vertical boundaries of the model. Also, the water to the later control points (KA1755A, SA2783A and KA3385A) flows very deep (~1000 m) from the vertical edges of the model. The water to the control section of KAS03 north—west of the tunnel area before the tunnel construction originates outside the model bottom. Then, within the tunnel construction the water to the control section of KAS03 flows from the vertical edge of the model.

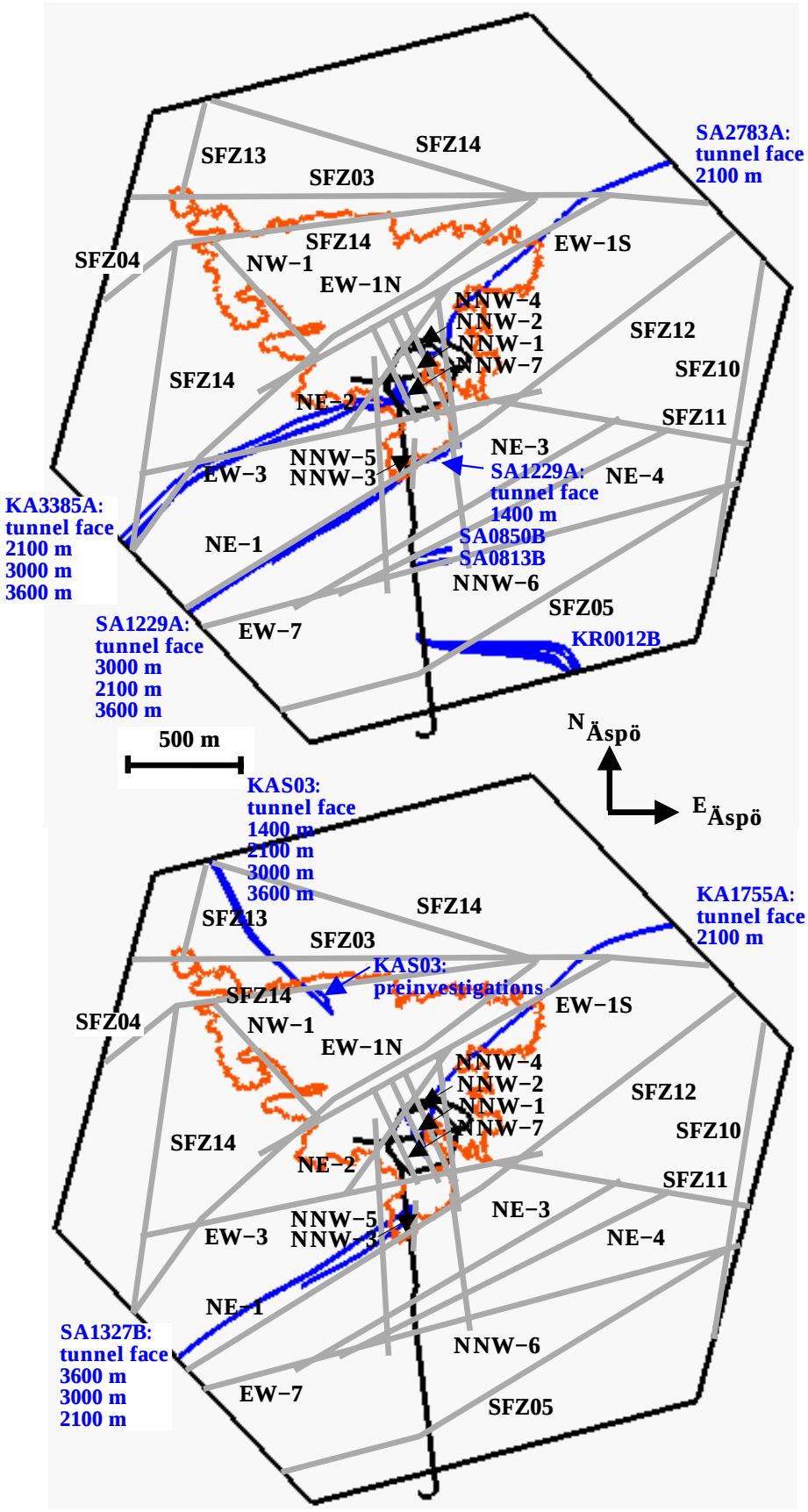

Figure 5.14. Projections of flow paths to the control points on a horizontal plane. The coastline of the Äspö island, the fracture zones at the surface and the model boundaries are also shown.

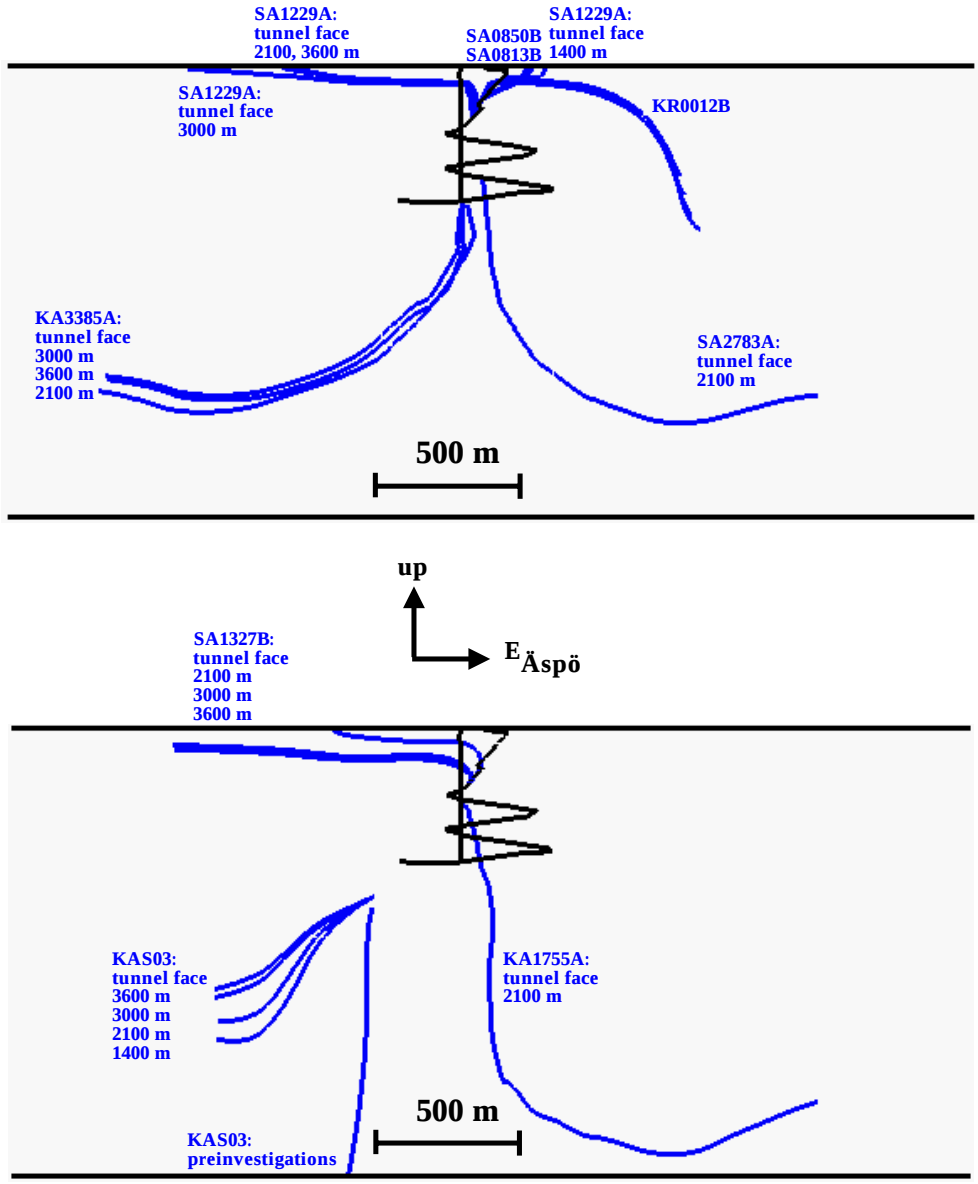

Figure 5.14. (cont.) Projections of flow paths to the control points on an east—west trending cut plane.

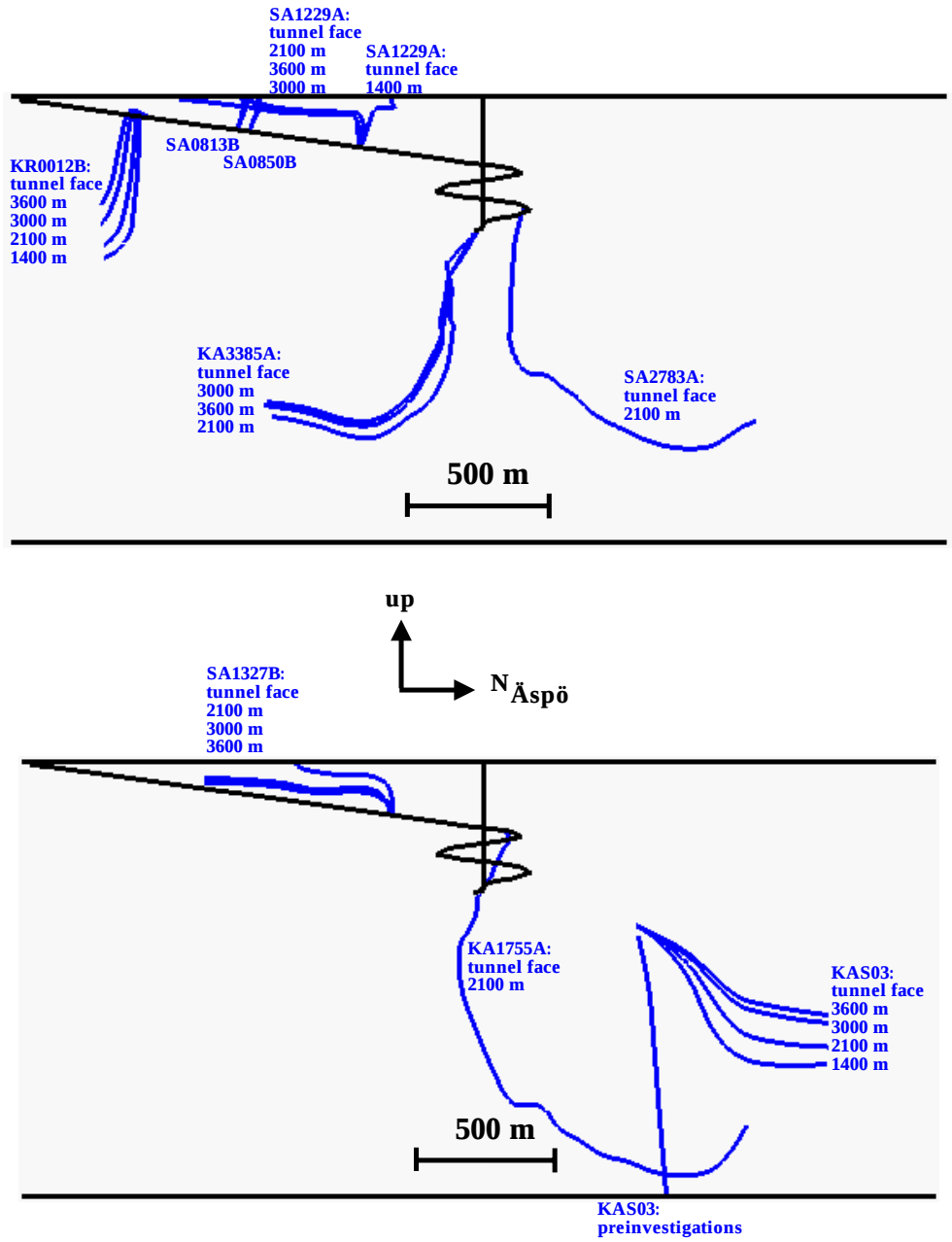

Figure 5.14. (cont.) Projections of flow paths to the control points on a north—south trending cut plane.

6 COMPARISON AND CONSISTENCY CHECK

This work concerned with the groundwater flow modelling part of Task 5. No chemical reactions were modelled, only mixing. The simulation time steps covered the period from the natural conditions until the completion of the tunnel and shafts.

The residual pressure and salinity fields were simulated first. In the mixing calculations the transport equations of the different groundwater types were solved using these fields. The modelling work is summarized in Appendix B.

The initial concentration boundary condition for the transport equations of the different water types was given on the basis of the geochemical M3 estimations done by Gurban et al. (1998). The mixing ratios were simulated at the control points and at certain cut planes. The hydraulic modelling in this work gave quite similar results to the M3 estimations. This work showed the essential role of the dispersion lengths as regards to the simulated mixing ratios at the control points. After all, the values for the dispersion lengths are quite poorly known. Also, the infiltration from the sea had to be restricted.

The mixing ratios simulated in this work and the mixing ratios from the M3 estimations (Gurban et al., 1998) still differ. Figure 6.1 sketches the error sources in the mixing simulations. The error in the initial conditions for the different water types is due to the M3 uncertainties and the interpolations. It may still change during the simulations due to the uncertainties in the other parts of the FEFTRA mixing model (pressure and salinity fields, later boundary conditions, properties, geometry, numerical solution).

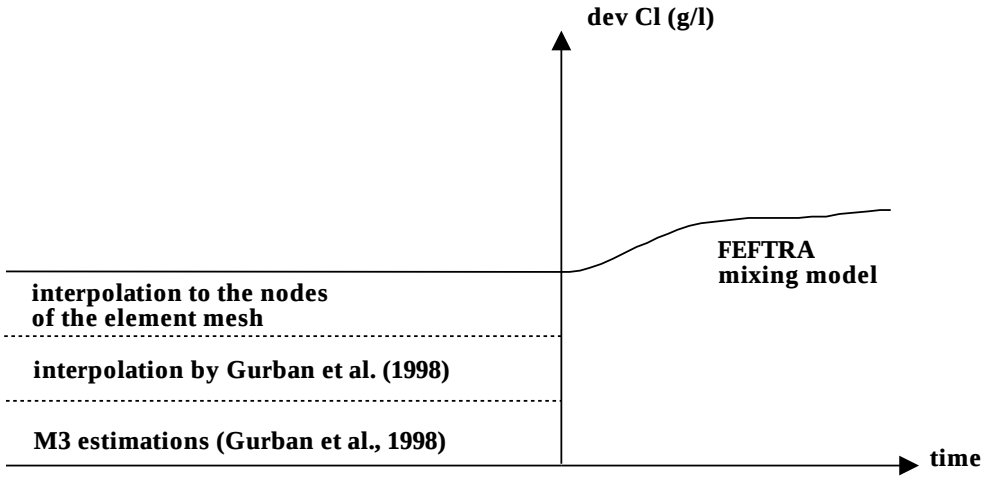

Figure 6.1. The error sources in the mixing simulations due to the initial conditions for the different water types and the other parts of the FEFTRA mixing model.

The following aspects have to be included in the uncertainties of the FEFTRA mixing model:

- The inaccuracy of the boundary conditions in later time steps.
- The material properties provide with variation possibilities. In addition to the dispersion lengths ε_L and ε_T mentioned above, there is high uncertainty in the hydraulic conductivity of the rock K, the transmissivities T and the fracture spacing $2a$.
- The depth extensions of many fracture zones are uncertain.
- Numerical inaccuracy.

REFERENCES

J Bear, 1979. Hydraulics of Groundwater. McGraw-Hill, Israel.

A N Brooks and T J R Hughes, 1992. Streamline Upwind/Petrov-Galerkin Formulations for Convection Dominated Flows with Particular Emphasis on the Incompressible Navier-Stokes Equations. Computer Methods in Applied Mechanics and Engineering, 32, pp. 199-259.

T Forsmark and I Rhén, 1994. SKB - ÄSPÖ HARD ROCK LABORATORY. Information for Numerical Modelling 1994.

I Gurban, M Laaksoharju and C Andersson, 1998. Influences of the Tunnel Construction on the Groundwater Chemistry at Äspö. Hydrochemical Initial and Boundary Conditions: WP D1, WP D2. Part 2. Äspö Hard Rock Laboratory, IPR-02-59. (in press)

P S Huyakorn, B H Lester and J W Mercer, 1983. An Efficient Finite Element Technique for Modelling Transport in Fractured Porous Media, 1, Single Species Transport. Water Resources Research, vol. 19, no. 3, pp. 841-854.

P S Huyakorn and G F Pinder, 1983. Computational Methods in Subsurface Flow. Academic Press INC, Orlando.

M Laaksoharju and B Wallin (eds.), 1997. Evolution of the Groundwater Chemistry at the Äspö Hard Rock Laboratory. Proceedings of the Second Äspö International Geochemistry Workshop, June 6-7, 1995. SKB International Cooperation Report SKB ICR 97-04. Stockholm, Sweden.

M Laitinen, 1994. Developing an Iterative Solver for the FEFLOW Package. Technical Report, VTT Energy, POHJA-2/94, Espoo (in Finnish).

M Laitinen, 1995. Modelling Convection Dominated Transport Problems with Improved Galerkin Finite Element Formulations. Technical Research Centre of Finland, Espoo. VTT Julkaisuja - Publikationer 804. (in Finnish)

D R Lide (ed.), 1990. CRC Handbook of Chemistry and Physics. 71st Edition 1990-1991. CRC Press Inc., Boston.

J Löfman, 1996. Groundwater Flow Modelling at the Olkiluoto Site. Flow under Natural Conditions. Posiva Oy, Helsinki. Work report PATU-96-76e.

J Löfman and V Taivassalo, 1995. Simulations of Pressure and Salinity Fields at Äspö. SKB ICR 95-01.

G de Marsily, 1986. Quantitative Hydrogeology — Groundwater Hydrology for Engineers. Academic Press INC, Orlando.

G de Marsily, 1986. Quantitative Hydrogeology — Groundwater Hydrology for Engineers. Academic Press INC, Orlando.

F Mészáros, 1996. Simulation of the Transient Hydraulic Effect of the Access Tunnel at Äspö. Äspö International Cooperation Report ICR 96-06.

I Rhén (ed.), G Gustafson, R Stanfors and P Wikberg, 1997. ÄSPÖ HRL — Geoscientific Evaluation 1997/5. Models Based on Site Characterization 1986-1995. SKB TR 97-06.

I Rhén, J Smellie and P Wikberg, 1998. Äspö HRL Task Force on Modelling of Groundwater Flow and Transport of Solutes. Task 5, Performance Measures, Version 1. November 1998.

U Svensson, 1997. A Site Scale Analysis of Groundwater Flow and Salinity Distribution in the Äspö Area. SKB TR 97-17.

V Taivassalo and A Saarenheimo, 1991. Groundwater Flow Analysis for the VLJ Repository. Nuclear Waste Commission of Finnish Power Companies, Helsinki. YJT-91-10.

M Valkiainen, 1992. Diffusion in the Rock Matrix — A Review of Laboratory Tests and Field Studies. Nuclear Waste Commission of Finnish Power Companies, Report YJT-92-04, Helsinki.

T Vieno, A Hautojärvi, L Koskinen and H Nordman, 1992. TVO-92 Safety Analysis of Spent Fuel Disposal. Nuclear Waste Commission of Finnish Power Companies, Helsinki. YJT-92-33E.

P Wikberg, 1998. Äspö Task Force on Modelling of Groundwater Flow and Transport of Solutes. Plan for Modelling Task # 5: Impact of the Tunnel Construction on the Groundwater System at Äspö, a Hydrological-Hydrochemical Model Assessment Exercise. Äspö Hard Rock Laboratory Progress Report HRL-98-07.

EW-1N

-3570.0	2545.0	0.0
-480.0	5285.0	0.0
-480.0	5285.0	-1600.0
-3570.0	2545.0	-1600.0
-480.0	5285.0	0.0
905.0	6525.0	0.0
905.0	6525.0	-1600.0
-480.0	5285.0	-1600.0
905.0	6525.0	0.0
1215.0	6950.0	0.0
1215.0	6950.0	-1600.0
905.0	6525.0	-1600.0
1215.0	6950.0	0.0
1614.4	7359.1	-327.4
1614.4	7359.1	-1600.0
1215.0	6950.0	-1600.0
1215.0	6950.0	0.0
1614.4	7359.1	-327.4
1811.5	7482.0	0.0
1215.0	6950.0	0.0
1811.5	7482.0	0.0
2197.1	7698.3	0.0
2000.0	7575.4	-327.4
1614.4	7359.1	-327.4
1614.4	7359.1	-327.4
2000.0	7575.4	-327.4
2000.0	7575.4	-1600.0
1614.4	7359.1	-1600.0
2000.0	7575.4	-1600.0
2000.0	7575.4	-327.4
2690.0	8080.0	0.0
2690.0	8080.0	-1600.0
2690.0	8080.0	0.0
2197.1	7698.3	0.0
2000.0	7575.4	-327.4
2690.0	8080.0	0.0

EW-1S

1453.1	7217.4	0.0
3006.0	8088.1	0.0
3138.2	8076.0	-369.5
1339.7	7067.6	-369.5

EW-3

2703.6	7229.1	0.0
938.8	6863.0	0.0
920.1	6751.4	-542.2
2166.5	7010.0	-542.2

EW-7

743.3	6075.7	0.0
279.4	5913.4	-231.8
3571.8	6795.9	-231.8
3590.5	6838.9	0.0

NE-2

1829.9	7038.5	0.0
2325.1	7720.0	0.0
2389.6	7671.5	-349.4
1718.4	6747.8	-349.4

NE-3

1621.3	6288.3	0.0
1290.7	6171.2	-227.6
2939.8	7123.4	-227.6
3040.3	7107.6	0.0

NE-4

1818.6	6349.8	0.0
3267.3	7064.3	0.0
3368.7	7044.4	-228.3
1905.5	6322.8	-228.3

NW-1

1257.6	7882.0	0.0
1725.7	7373.8	0.0
2091.3	7607.4	-246.6
1447.6	8306.2	-246.6

NNW-1

2033.4	7551.8	0.0
2240.6	7104.5	0.0
2374.7	6814.7	-1600.0
2161.3	7275.6	-1600.0

NNW-2

2091.2	7583.1	0.0
2300.2	7106.1	0.0
2300.2	7106.1	-319.2
2184.3	7370.7	-1144.1

NNW-3

2143.6	7025.4	0.0
2136.9	6812.9	0.0
2136.9	6812.9	-1600.0
2143.6	7025.4	-1600.0

NNW-4

2240.2	7668.4	0.0
2286.2	7609.0	-436.7
2340.9	7178.9	-436.7
2328.3	6975.0	0.0

NNW-5

1962.8	7394.1	0.0
2025.1	6348.5	0.0
2025.1	6348.5	-1600.0
1962.8	7394.1	-1600.0

NNW-6

2298.7	7058.1	0.0
2382.9	6464.0	0.0
2382.9	6464.0	-1600.0
2298.7	7058.1	-1600.0

NNW-7

1988.5	7486.7	-191.2
1957.1	7515.0	0.0
2146.8	7105.3	0.0
2180.4	7072.3	-191.5

NNW-8

1540.0	8060.0	-300.0
2030.0	7570.0	-300.0
2030.0	7570.0	-700.0
1540.0	8060.0	-700.0

SFZ01

-3190.0	13380.0	0.0
-1475.0	12910.0	0.0
-1475.0	12910.0	-1600.0
-3190.0	13380.0	-1600.0
-1475.0	12910.0	0.0
760.0	12380.0	0.0
760.0	12380.0	-1600.0
-1475.0	12910.0	-1600.0
760.0	12380.0	0.0
2620.0	12000.0	0.0
2620.0	12000.0	-1600.0
760.0	12380.0	-1600.0
2620.0	12000.0	0.0
4760.0	11620.0	0.0
4760.0	11620.0	-1600.0
2620.0	12000.0	-1600.0
4760.0	11620.0	0.0
8550.0	10950.0	0.0
8550.0	10950.0	-1600.0
4760.0	11620.0	-1600.0

SFZ02

-1095.0	14250.0	0.0
-1475.0	12910.0	0.0
-1475.0	12910.0	-1600.0
-1095.0	14250.0	-1600.0
-1475.0	12910.0	0.0
-1830.0	11760.0	0.0
-1830.0	11760.0	-1600.0
-1475.0	12910.0	-1600.0
-1830.0	11760.0	0.0
-2050.0	10640.0	0.0
-2050.0	10640.0	-1600.0
-1830.0	11760.0	-1600.0
-2050.0	10640.0	0.0
-2190.0	9760.0	0.0
-2190.0	9760.0	-1600.0
-2050.0	10640.0	-1600.0
-2190.0	9760.0	0.0
-2380.0	8905.0	0.0
-2380.0	8905.0	-1600.0
-2190.0	9760.0	-1600.0
-2380.0	8905.0	0.0
-2570.0	8310.0	0.0
-2570.0	8310.0	-1600.0
-2380.0	8905.0	-1600.0
-2570.0	8310.0	0.0
-3025.0	7285.0	0.0
-3025.0	7285.0	-1600.0
-2570.0	8310.0	-1600.0
-3025.0	7285.0	0.0
-3571.0	5335.0	0.0
-3571.0	5335.0	-1600.0
-3025.0	7285.0	-1600.0
-3571.0	5335.0	0.0
-3740.0	4690.0	0.0
-3740.0	4690.0	-1600.0
-3571.0	5335.0	-1600.0
-3740.0	4690.0	0.0
-3950.0	3620.0	0.0
-3950.0	3620.0	-1600.0
-3740.0	4690.0	-1600.0
-3950.0	3620.0	0.0
-4140.0	2640.0	0.0
-4140.0	2640.0	-1600.0
-3950.0	3620.0	-1600.0

SFZ03

-4140.0	8785.0	0.0
-2570.0	8310.0	0.0
-2570.0	8310.0	-1600.0
-4140.0	8785.0	-1600.0
-2570.0	8310.0	0.0
-1950.0	8210.0	0.0
-1950.0	8210.0	-1600.0
-2570.0	8310.0	-1600.0
-1950.0	8210.0	0.0
-1330.0	8120.0	0.0
-1330.0	8120.0	-1600.0
-1950.0	8210.0	-1600.0
-1330.0	8120.0	0.0
1120.0	8070.0	0.0
1120.0	8070.0	-1600.0
-1330.0	8120.0	-1600.0
1120.0	8070.0	0.0
1120.0	8070.0	-1600.0
2690.0	8080.0	-1600.0
2690.0	8080.0	0.0
2690.0	8080.0	0.0
3000.0	8085.0	0.0
3000.0	8085.0	-1600.0
2690.0	8080.0	-1600.0
3000.0	8085.0	0.0
3710.0	8020.0	0.0
3710.0	8020.0	-1600.0
3000.0	8085.0	-1600.0
3710.0	8020.0	0.0
5200.0	7900.0	0.0
5200.0	7900.0	-1600.0
3710.0	8020.0	-1600.0
5200.0	7900.0	0.0
5800.0	7930.0	0.0
5800.0	7930.0	-1600.0
5200.0	7900.0	-1600.0
5800.0	7930.0	0.0
8330.0	8000.0	0.0
8330.0	8000.0	-1600.0
5800.0	7930.0	-1600.0

SFZ04

-5240.0	3520.0	0.0
-3740.0	4690.0	0.0
-3740.0	4690.0	-1600.0
-5240.0	3520.0	-1600.0
-3740.0	4690.0	0.0
-3050.0	5285.0	0.0
-3050.0	5285.0	-1600.0
-3740.0	4690.0	-1600.0

-3050.0	5285.0	0.0
-2570.0	5570.0	0.0
-2570.0	5570.0	-1600.0
-3050.0	5285.0	-1600.0
-2570.0	5570.0	0.0
-590.0	6670.0	0.0
-590.0	6670.0	-1600.0
-2570.0	5570.0	-1600.0
-590.0	6670.0	0.0
200.0	7160.0	0.0
200.0	7160.0	-1600.0
-590.0	6670.0	-1600.0
200.0	7160.0	0.0
1095.0	7860.0	0.0
1095.0	7860.0	-1600.0
200.0	7160.0	-1600.0

SFZ05

-5310.0	2880.0	0.0
-1000.0	5140.0	0.0
-754.1	4651.1	-1503.5
-5048.5	2399.3	-1503.5
-1000.0	5140.0	0.0
-754.1	4651.1	-1503.5
2316.6	5474.2	-1503.5
2165.0	6000.0	0.0
2165.0	6000.0	0.0
2316.6	5474.2	-1503.5
3800.8	6340.3	-1503.5
3520.0	6810.0	0.0
3520.0	6810.0	0.0
3800.8	6340.3	-1503.5
7133.0	7974.4	-1503.5
5800.0	7930.0	0.0

SFZ06

-1950.0	8210.0	0.0
-760.0	8830.0	0.0
-760.0	8830.0	-1600.0
-1950.0	8210.0	-1600.0
-760.0	8830.0	0.0
-50.0	9140.0	0.0
-50.0	9140.0	-1600.0
-760.0	8830.0	-1600.0
-50.0	9140.0	0.0
715.0	9360.0	0.0
715.0	9360.0	-1600.0
-50.0	9140.0	-1600.0
715.0	9360.0	0.0
2285.0	9450.0	0.0
2285.0	9450.0	-1600.0
715.0	9360.0	-1600.0
2285.0	9450.0	0.0
4285.0	9740.0	0.0
4285.0	9740.0	-1600.0
2285.0	9450.0	-1600.0
4285.0	9740.0	0.0
5595.0	9920.0	0.0
5595.0	9920.0	-1600.0
4285.0	9740.0	-1600.0

5595.0	9920.0	0.0
8330.0	10230.0	0.0
8330.0	10230.0	-1600.0
5595.0	9920.0	-1600.0

SFZ08

-70.0	3095.0	0.0
2380.0	2260.0	0.0
2380.0	2260.0	-1600.0
-70.0	3095.0	-1600.0
2380.0	2260.0	0.0
2785.0	2190.0	0.0
2785.0	2190.0	-1600.0
2380.0	2260.0	-1600.0
2785.0	2190.0	0.0
6545.0	1240.0	0.0
6545.0	1240.0	-1600.0
2785.0	2190.0	-1600.0

SFZ09

1165.0	1570.0	0.0
2380.0	2260.0	0.0
2380.0	2260.0	-1600.0
1165.0	1570.0	-1600.0
2380.0	2260.0	0.0
2810.0	2525.0	0.0
2810.0	2525.0	-1600.0
2380.0	2260.0	-1600.0
2810.0	2525.0	0.0
7240.0	4640.0	0.0
7240.0	4640.0	-1600.0
2810.0	2525.0	-1600.0

SFZ10

2670.0	1260.0	0.0
2785.0	2190.0	0.0
2785.0	2190.0	-1600.0
2670.0	1260.0	-1600.0
2785.0	2190.0	0.0
2810.0	2525.0	0.0
2810.0	2525.0	-1600.0
2785.0	2190.0	-1600.0
2810.0	2525.0	0.0
3550.0	7000.0	0.0
3550.0	7000.0	-1600.0
2810.0	2525.0	-1600.0
3550.0	7000.0	0.0
3710.0	8020.0	0.0
3710.0	8020.0	-1600.0
3550.0	7000.0	-1600.0
3710.0	8020.0	0.0
4285.0	9740.0	0.0
4285.0	9740.0	-1600.0
3710.0	8020.0	-1600.0
4285.0	9740.0	0.0
4760.0	11620.0	0.0
4760.0	11620.0	-1600.0
4285.0	9740.0	-1600.0
4760.0	11620.0	0.0
5050.0	13000.0	0.0
5050.0	13000.0	-1600.0
4760.0	11620.0	-1600.0

SFZ11

2512.7	7182.4	0.0
3550.0	7000.0	0.0
3550.0	7000.0	-1600.0
1665.9	7331.3	-1600.0
3550.0	7000.0	0.0
3810.0	6975.0	0.0
3810.0	6975.0	-1600.0
3550.0	7000.0	-1600.0
3810.0	6975.0	0.0
7570.0	6165.0	0.0
7570.0	6165.0	-1600.0
3810.0	6975.0	-1600.0

SFZ12

3899.5	8448.2	-1503.5
3760.2	8080.1	0.0
3367.2	8446.5	-1503.5
3899.5	8448.2	-1503.5
2420.0	7070.0	0.0
2212.8	7576.5	-1503.5
3367.2	8446.5	-1503.5
3760.2	8080.1	0.0
2212.8	7576.5	-1503.5
2420.0	7070.0	0.0
-706.0	5145.9	0.0
-992.9	5611.9	-1503.5

SFZ13

-50.0	9140.0	0.0
1230.0	8500.0	0.0
1230.0	8500.0	-1600.0
-50.0	9140.0	-1600.0
1230.0	8500.0	0.0
1120.0	8070.0	0.0
1120.0	8070.0	-1600.0
1230.0	8500.0	-1600.0

SFZ14

905.0	6525.0	0.0
1095.0	7860.0	0.0
1095.0	7860.0	-1600.0
905.0	6525.0	-1600.0
1095.0	7860.0	0.0
2670.0	8070.0	0.0
2670.0	8070.0	-1600.0
1095.0	7860.0	-1600.0
2670.0	8070.0	0.0
1230.0	8500.0	0.0
1230.0	8500.0	-1600.0
2670.0	8070.0	-1600.0

SFZ15

2285.0	9450.0	0.0
2620.0	12000.0	0.0
2620.0	12000.0	-1600.0
2285.0	9450.0	-1600.0
2620.0	12000.0	0.0
2810.0	13430.0	0.0
2810.0	13430.0	-1600.0
2620.0	12000.0	-1600.0

Control point	Date	M3 estimation (%)				Hydrological simulation (%)			
		Brine	Glacial	Meteoric	Baltic	Brine	Glacial	Meteoric	Baltic
KR0012B	19.Jun.91	4.2	20.2	71.4	4.2	3.2	5.9	39.9	50.9
KR0012B	08.Apr.92	6.3	10	77.5	6.3	4.4	7.9	28.4	59.3
KR0012B	22.Apr.92	6.1	10.3	77.4	6.1	4.4	7.9	28.4	59.3
KR0012B	06.May.92	5.7	8.1	80.6	5.7	4.4	7.9	28.4	59.3
KR0012B	20.May.92	4.6	4.6	84.1	6.6	4.9	8.8	23.6	62.6
KR0012B	03.Jun.92	5.5	10.5	78.5	5.5	4.9	8.8	23.6	62.6
KR0012B	26.Jun.92	5.7	10.3	78.3	5.7	4.9	8.8	23.6	62.6
KR0012B	08.Jul.92	5.9	14.5	73.7	5.9	4.9	8.8	23.6	62.6
KR0012B	21.Jul.92	5.8	14.1	74.3	5.8	4.9	8.8	23.6	62.6
KR0012B	06.Aug.92	6	16.5	71.5	6	4.9	8.8	23.6	62.6
KR0012B	18.Aug.92	5.7	14.3	74.3	5.7	4.9	8.8	23.6	62.6
KR0012B	03.Sep.92	5.8	12.7	75.6	5.8	4.9	8.8	23.6	62.6
KR0012B	17.Sep.92	5.8	11.8	76.6	5.8	5.1	9.1	22.3	63.6
KR0012B	30.Sep.92	6	11.4	76.7	6	5.1	9.1	22.3	63.6
KR0012B	12.Oct.92	5.7	11.8	76.8	5.7	5.1	9.1	22.3	63.6
KR0012B	28.Oct.92	5.6	11.8	77	5.6	5.2	9.2	21.6	64.0
KR0012B	10.Nov.92	5.3	8.3	81.2	5.3	5.2	9.2	21.6	64.0
KR0012B	24.Nov.92	5.5	10.7	78.3	5.5	5.2	9.2	21.6	64.0
KR0012B	02.Dec.92	5.8	10.1	78.2	5.8	5.2	9.2	21.6	64.0
KR0012B	10.Dec.92	6.1	9.2	78.6	6.1	5.2	9.2	21.6	64.0
KR0012B	21.Dec.92	5.4	7.4	81.8	5.4	5.2	9.2	21.6	64.0
KR0012B	04.Jan.93	5.7	10.1	78.4	5.7	5.3	9.5	20.3	64.9
KR0012B	19.Jan.93	5.3	7.6	81.7	5.3	5.3	9.5	20.3	64.9
KR0012B	07.Feb.93	5.7	9.4	79.3	5.7	5.3	9.5	20.3	64.9
KR0012B	17.Mar.93	5.7	7.7	80.9	5.7	5.3	9.5	20.3	64.9
KR0012B	24.Mar.93	5.6	6.7	82.2	5.6	5.3	9.5	20.3	64.9
KR0012B	16.May.93	5.3	7.9	81.6	5.3	5.4	9.7	19.1	65.7
KR0012B	11.Jun.93	5	9.6	80.4	5	5.4	9.7	19.1	65.7
KR0012B	05.Jul.93	4.6	6.2	84.5	4.6	5.4	9.7	19.1	65.7
KR0012B	16.Aug.93	4.9	6.8	83.4	4.9	5.4	9.7	19.1	65.7
KR0012B	08.Nov.93	3.4	3.4	85.7	7.6	5.6	10.0	18.0	66.4
KR0012B	10.Aug.94	4.2	4.2	86.7	4.9	5.8	10.4	16.5	67.3
KR0012B	05.Sep.94	3.4	3.4	86.3	6.8	5.8	10.4	16.5	67.3
KR0012B	18.May.95	5	5	84.5	5.5	5.9	10.5	15.9	67.6
KR0012B	10.Oct.95	2.2	2.2	85	10.7	5.9	10.6	15.7	67.8
KR0012B	21.May.96	3.1	3.1	88.8	4.9	6.0	10.6	15.6	67.9
SA0813B	06.Nov.91	0	0	0	0	6.2	10.4	37.1	46.4

Control point	Date	M3 estimation (%)				Hydrological simulation (%)			
		Brine	Glacial	Meteoric	Baltic	Brine	Glacial	Meteoric	Baltic
SA0813B	07.Feb.93	3.7	3.7	49.5	43.1	5.4	8.8	43.3	42.5
SA0813B	07.Sep.93	4.1	4.1	45.5	46.2	4.8	7.9	46.5	40.8
SA0813B	29.Sep.93	6.4	6.4	47.2	40.1	4.8	7.9	46.5	40.8
SA0813B	07.Jun.94	4.1	4.1	48.4	43.4	4.4	7.3	48.7	39.6
SA0813B	05.Sep.94	3.9	3.9	45.2	47	4.3	7.1	49.5	39.1
SA0813B	17.May.95	4.8	4.8	48.9	41.5	3.9	6.6	51.3	38.2
SA0813B	12.Oct.95	3.9	3.9	50.9	41.4	3.8	6.3	52.2	37.7
SA0813B	21.May.96	3	3	47.8	46.2	3.6	6.1	53.1	37.2
SA0850B	20.Aug.91	10.2	10.2	46.7	32.8	7.7	12.9	25.7	53.7
SA1229A	24.Aug.93	2.4	2.4	38.2	57.1	6.9	11.2	45.4	36.5
SA1229A	07.Jun.94	4.8	4.8	41.1	49.3	6.5	10.3	47.3	35.9
SA1229A	18.May.95	3.4	3.4	42.3	50.9	6.0	9.3	49.7	35.0
SA1229A	11.Oct.95	3.5	3.5	44	49	5.9	9.0	50.3	34.7
SA1229A	21.May.96	2.4	2.4	38.3	56.8	5.8	8.8	51.2	34.2
SA1327B	15.Oct.92	7	7	51.4	34.7	9.3	16.3	34.9	39.5
SA2074A	05.Feb.93	5.1	8.3	81.4	5.1	11.1	21.2	30.5	37.2
SA2074A	28.Sep.93	11.6	11.6	44.2	32.5	10.5	17.3	35.8	36.4
SA2074A	07.Jun.94	11.9	11.9	46.9	29.4	10.5	15.6	38.6	35.3
SA2074A	06.Sep.94	10.3	10.3	50.3	29	10.6	15.2	39.3	34.9
SA2074A	18.May.95	7.6	7.6	53.9	31	10.7	14.4	40.6	34.3
SA2783A	14.Feb.94	21.2	38.9	20	20	14.6	20.5	42.1	22.8
SA2783A	17.May.94	22.4	40	18.8	18.8	15.3	19.8	42.3	22.7
SA2783A	07.Sep.94	22.9	39.8	18.7	18.7	15.2	18.9	43.2	22.7
SA2783A	25.Oct.95	27.2	37.4	17.7	17.7	16.1	16.9	43.7	23.3
SA2783A	20.May.96	29.4	37.7	16.5	16.5	16.3	16.5	43.6	23.6
KAS07	31.Aug.92	17.3	36.4	29.1	17.3	15.2	22.0	22.2	40.6
KAS07	06.Sep.93	17.7	34.2	30.4	17.7	13.3	18.5	30.7	37.4
KAS07	12.Apr.94	18.3	36.3	27.1	18.3	13.2	17.8	32.2	36.7
KAS07	06.Sep.94	17.8	29.3	35	17.8	13.0	16.9	34.7	35.5
KAS03	19.Aug.92	9.6	55.6	25.2	9.6	23.7	46.7	15.1	14.6
KAS03	07.Feb.93	10	53.8	26.2	10	22.2	46.0	17.1	14.6
KAS03	16.May.93	10.7	52.6	26	10.7	21.3	45.5	18.1	15.0
KAS03	16.Aug.93	13.1	51.1	22.6	13.1	21.3	45.5	18.1	15.0
KAS03	07.Sep.93	11.5	52.3	24.7	11.5	20.4	45.0	18.8	15.8
KAS03	12.Apr.94	12.8	49.2	25.2	12.8	19.8	44.5	19.2	16.4
KAS03	03.Sep.88	17.1	50.9	16	16	23.9	48.2	13.6	14.4

Control point	Date	Hydrological simulation (%) Brine	Glacial	Meteoric	Baltic
KA3005A	01.Oct.90	14.1	39.1	25.6	21.1
KA3005A	21.May.91	13.7	36.5	28.7	20.9
KA3005A	10.Feb.92	13.3	33.7	30.6	22.4
KA3005A	10.Aug.92	12.6	30.0	27.0	30.4
KA3005A	05.Oct.92	12.4	29.3	26.3	32.0
KA3005A	10.Nov.92	12.1	28.3	26.3	33.4
KA3005A	11.Feb.93	10.8	22.9	31.7	34.6
KA3005A	03.Jun.93	10.5	21.0	33.4	35.1
KA3005A	03.Nov.93	10.5	19.2	35.4	35.0
KA3005A	16.Feb.94	10.4	17.6	37.2	34.9
KA3005A	16.Jun.94	10.0	16.2	39.5	34.3
KA3005A	16.Sep.94	9.9	15.7	40.4	34.0
KA3005A	24.Jan.95	10.0	15.1	41.2	33.7
KA3005A	26.May.95	10.0	14.7	41.8	33.4
KA3005A	25.Oct.95	10.2	14.3	42.4	33.2
KA3005A	24.Apr.96	10.2	14.0	42.9	32.9
KA3005A	24.Dec.96	10.4	13.6	43.5	32.5
KA3110A	01.Oct.90	14.5	26.8	44.8	14.0
KA3110A	21.May.91	13.4	26.6	43.1	17.0
KA3110A	10.Feb.92	13.4	25.5	38.4	22.7
KA3110A	10.Aug.92	12.6	24.7	30.8	31.9
KA3110A	05.Oct.92	12.5	24.1	29.8	33.5
KA3110A	10.Nov.92	12.4	23.8	30.1	33.8
KA3110A	11.Feb.93	10.5	20.0	35.2	34.3
KA3110A	03.Jun.93	10.6	18.6	36.2	34.6
KA3110A	03.Nov.93	10.9	17.1	37.8	34.4
KA3110A	16.Feb.94	10.7	16.5	38.8	34.0
KA3110A	16.Jun.94	11.4	16.1	38.7	33.9
KA3110A	16.Sep.94	11.4	15.8	39.0	33.8
KA3110A	24.Jan.95	11.5	15.4	39.6	33.6
KA3110A	26.May.95	11.6	15.0	40.1	33.3
KA3110A	25.Oct.95	11.7	14.7	40.6	33.0
KA3110A	24.Apr.96	11.8	14.3	41.1	32.7
KA3110A	24.Dec.96	12.0	14.0	41.6	32.4

Control point	Date	Hydrological simulation (%) Brine	Glacial	Meteoric	Baltic
KA3385A	01.Oct.90	8.9	17.6	65.7	7.8
KA3385A	21.May.91	9.9	18.8	63.2	8.1
KA3385A	10.Feb.92	10.3	19.3	61.6	8.8
KA3385A	10.Aug.92	11.1	20.2	53.4	15.3
KA3385A	05.Oct.92	11.4	20.6	51.4	16.7
KA3385A	10.Nov.92	12.0	21.2	47.6	19.2
KA3385A	11.Feb.93	12.4	19.7	45.3	22.7
KA3385A	03.Jun.93	12.9	18.3	42.3	26.5
KA3385A	03.Nov.93	13.5	16.9	42.2	27.2
KA3385A	16.Feb.94	14.0	16.0	43.5	26.5
KA3385A	16.Jun.94	14.4	15.5	43.9	26.2
KA3385A	16.Sep.94	16.0	15.6	43.0	25.5
KA3385A	24.Jan.95	17.2	15.9	41.4	25.7
KA3385A	26.May.95	17.6	15.9	40.6	25.9
KA3385A	25.Oct.95	18.0	15.8	40.1	26.1
KA3385A	24.Apr.96	18.2	15.7	39.8	26.3
KA3385A	24.Dec.96	18.3	15.6	39.6	26.5

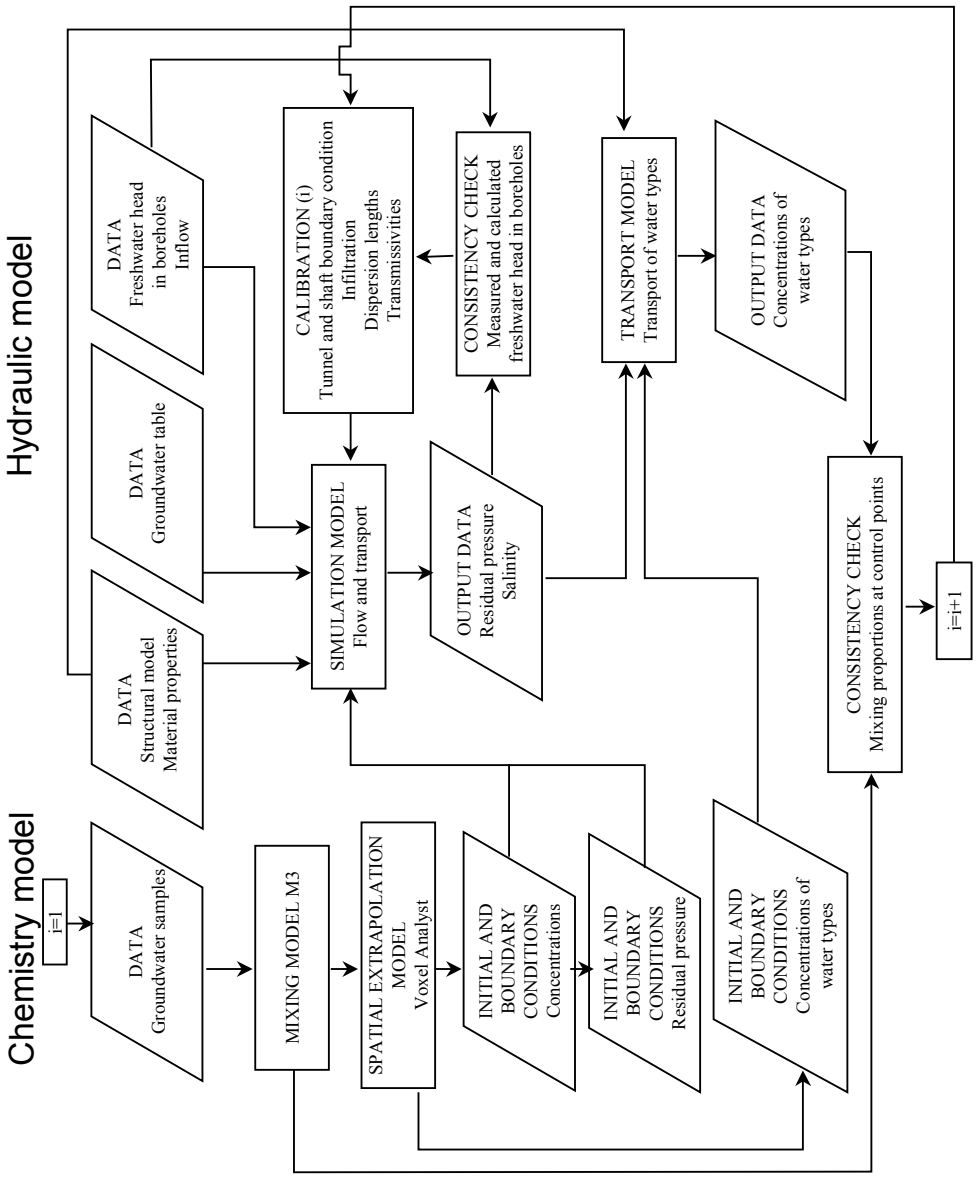
Hydraulic model
Chemistry model
i=1
DATA
Groundwater samples
MIXING MODEL M3
SPATIAL EXTRAPOLATION
MODEL
Voxel Analyst
INITIAL AND
BOUNDARY
CONDITIONS
Concentrations
INITIAL AND
BOUNDARY
CONDITIONS
Residual pressure
INITIAL AND
BOUNDARY
CONDITIONS
Concentrations of
water types
DATA
Structural model
Material properties
DATA
Groundwater table
DATA
Freshwater head
in boreholes
Inflow
SIMULATION MODEL
Flow and transport
CALIBRATION (i)
Tunnel and shaft boundary condition
Infiltration
Dispersion lengths
Transmissivities
OUTPUT DATA
Residual pressure
Salinity
CONSISTENCY CHECK
Measured and calculated
freshwater head in boreholes
TRANSPORT MODEL
Transport of water types
OUTPUT DATA
Concentrations of
water types
CONSISTENCY CHECK
Mixing proportions at control points
i=i+1

Part III

GROUNDWATER MIXING AND GEOCHEMICAL REACTIONS

– AN INVERSE-MODELLING APPROACH

Ari Luukkonen
VTT, Building and Transport, Espoo, Finland

March 2001

Keywords: Äspö, chemistry, groundwater, mixing, mole balance

SUMMARY

The current study makes an attempt to solve the problem of how to determine mixing fractions of identified reference water types and the geochemical reactions related to groundwater mixing processes in collected and analysed samples from Äspö, Sweden. A short review of the alternative M3 geochemical modelling tool is made at the beginning of the report.

The inverse approach solves the mixing problem step by step, following geochemical steady-state assumptions. The calculation method implements an inverse-modelling method where an existing final water composition is reconstructed by mixing a feasible set of initial water samples and letting acceptable geochemical phase reactions modify the conservative initial mixture. The geochemical steady-state assumptions are judged from the mole-transfers needed. A given final water composition must be reached with small, moderate, or otherwise feasible mole transfers. A single reconstruction of final water constitutes a successful "steady-state" step. Steps are chained in the sense that a previous step leads to the following steps, i.e. to find new sets of initial water samples for previous initial water samples, and so on. The steps are ultimately extended to the reference water types, after which mixing fractions of the reference water types in each sample considered in the calculation chain can be solved.

The Äspö groundwater geochemical data is divided into two subsets based on excavations of the Hard Rock Laboratory shafts and tunnels. The undisturbed sample set is used for identifying the reference water types that have been active in Äspö, for describing the general evolution in the bedrock, and for defining the depth relations and distributions of reference water types in the undisturbed Äspö model volume. The disturbed sample set is used for monitoring the effects of tunnel construction on groundwater compositions. The calculation results, for the disturbed condition, indicate that of the reference water types meteoric, fresh Baltic Sea, and deep saline water attempt to intrude into the open tunnel system. The reference water types without an extensive source (pre- and postglacial altered, Litorina, and glacial melt) tend to vanish from the vicinity of the tunnel system.

Contents

List of Figures

List of Tables

1 Introduction

Groundwater geochemical modelling tools are used for a variety of purposes. Problems like determination of the dominating geochemical reactions, quantification of the extent of reactions, and mixing calculations with a set of initial water samples, resulting in a certain final water composition are among the most common ones. Geochemical modelling is usually divided into two general approaches (e.g. Parkhurst & Plummer 1993): (1) inverse modelling, which uses observed groundwater compositions to identify and determine the extent of geochemical reactions, and (2) forward modelling, which uses hypothesised geochemical reactions to predict groundwater compositions. Inverse modelling describes the chemical evolution of groundwater by giving exact estimates of the mixing and geochemical reactions among known initial water compositions needed for reaching a known final water composition. On the contrary, forward modelling starts with known initial water compositions and simulates specified geochemical reactions in order to predict yet unstudied final water composition.

The present study aims to determine step by step, following the steady-state assumption, reference water mixing fractions in groundwater samples collected from the Äspö Hard Rock Laboratory (HRL), and identify the net geochemical reactions required for these reference water mixings. The approach implements inverse modelling, and calculations are carried out on samples taken both before excavation of the HRL tunnels (undisturbed conditions) and afterwards (disturbed conditions). The reference water type mixing fraction results for samples, evaluated in several inverse calculation steps, are considered water-conservative parameters similarly to Cl or ^{18}O concentrations in groundwater. Mixing fractions can be transported like conservative parameters in hydrological simulations, and mole transfer results obtained in the inverse calculations may be coupled indirectly to hydrological transport. The conservative transport results are corrected based on trends (net mole-transfer vs. dominant reference water-type fraction) earlier observed with the known sample set.

This report is a part of international co-operation launched and steered by SKB. Since the M3 geochemical modelling tool (e.g. Laaksoharju et al., 1999a) has been widely used in the earlier SKB studies, a short review of the M3 method is given at the beginning of this report. The differences between the geochemical modelling methods are discussed at the end of the report.

In relation to POSIVA´s Finnish national programme on disposal of high-level waste and spent nuclear fuel, the inverse-modelling method has been favoured as a basic groundwater geochemical modelling tool (e.g. Pitkänen et al. 1999a). The inverse-modelling approach is used for identification of the extent of geochemically feasible reactions as a function of mixing fractions of reference water types.

This study reports only on how inverse calculations are done for Äspö HRL data, and how geochemical boundary conditions are defined for hydrological simulations. The results of such geochemical calculations and their use in hydrological simulations have been reported elsewhere (Kattilakoski & Luukkonen 2000).

2 A review of M3 approach

The M3 method (e.g. Laaksoharju et al., 1999a) and the inverse modelling approach (e.g. Pitkänen et al., 1999a) distinctly differ from each other in several respects. At a general level, the M3 solution is statistical based always on collective analysis of a data set while the inverse approach is analytical based on studies of individual samples. Principally, because of the different choice of reference water types the results of the calculation methods can be compared only if the mixing fraction results of both methods are converted back to *chemical composition estimates* of the samples.

Essentially, the M3 method is a process where all obtained samples and the reference water types needed are put together into a principal component analysis. The variables involved in the calculations are Na, K, Ca, Mg, HCO_3, Cl, SO_4, ^3H, δ^2H and $\delta^{18}O$, and the total variation of this data set is tried to summarise with two principal components (PC_1 and PC_2). According to Laaksoharju et al. (1999a) M3 aims to calculate how *mixing* and *reactions* have affected the obtained groundwater samples.

At first, the method assumes an *ideal mixing model*. The ideal mixing fractions, for each sample, are calculated from the PC_1 vs. PC_2 plot on the basis how the samples score on the plot in relation to the reference water types. Strictly, euclidean distances on the plot defining the mixing fractions lead to two assumptions embedded into the model. Either all the variables involved in the calculations behave conservatively in the mixings or the non-conservative behaviour of the variables mostly concentrate into the statistical non-explained noise not taken into account during the calculation of principal components. The method requires that over 60 % of the variability among the data should be explained (Laaksoharju et al., 1999a). The practice however shows, that neither of the assumptions holds. The PC_1 and PC_2 are oriented, by default, at right angles to each other, and the concentration variations of non-conservative variables distinctly affect their orientation in the variable space.

The second step of the method is to calculate how the *reactions* have affected to each obtained sample. This comes about by evaluating calculated sample compositions from the reference water compositions following the ideal mixing assumption. Calculated and measured concentrations for existing samples are then compared retrospectively. Deviations between measured and calculated values among non-conservative variables are argued to account for contribution of reactions, and deviations among conservative variables such as Cl and $\delta^{18}O$ are supposed to reflect model error (Laaksoharju et al., 1999a). However, possibly due to statistical defocusing of the primary information (some 20–30 % of the variation frequently discarded), no explicit method has not yet been published how to explicitly extract the *reaction information* for hydrological forward simulations. Therefore, if hydrogeological forward simulations produce conservative reference water type mixing fractions, these results can be converted to chemical compositions only with the ideal mixing assumption and without taking into account any chemical reactions.

3 Inverse-modelling approach

3.1 General

The inverse-modelling method is a combination of speciation modelling and mole balance modelling. Speciation modelling, petrographic observations, reactions expected to dominate in a groundwater system, and isotopic data available provide constraints for inverse studies. In accordance with these constraints, mole balance modelling produces quantitative geochemical reactions that reproduce the compositions of the samples and are consistent with any constraints on the reactant phase (e.g. Parkhurst & Plummer 1993, Runnells 1993). The processes of dissolution and precipitation of minerals, gases, and organic matter in addition to ion exchange and oxidation/reduction processes can be presented with the following mole balance formula:

$$\text{Initial water composition(s)} + \text{“reactant phases”} \rightarrow \text{final water composition} + \text{“product phases”} \qquad 3\text{-}1$$

Currently there are two widely used inverse-modelling tools publicly available. NETPATH (Plummer et al. 1994) is capable of handling all normal inverse-modelling routines, but additionally it is equipped with isotope fractionation and isotope exchange tools (^{13}C, ^{14}C, ^{34}S, ^{15}N, ^{87}Sr). Similarly, PHREEQC-2 (Parkhurst & Appelo 1999) handles the normal inverse-modelling routines but in the case of isotopes only aqueous dilution, without explicit fractionation, is considered. PHREEQC-2 has, however, the capability for inverse modelling within specified chemical and isotopic compositional uncertainties. The treatment of analytical uncertainties produces simpler and more robust mole balance models and allows the significance of mixing fractions and mole transfers to be evaluated (Parkhurst 1997).

The current study utilises the PHREEQC-2 modelling tool both because isotopic data from Äspö HRL is limited and because advanced handling of uncertainties is quite a desirable feature in inverse-modelling tasks.

3.2 Calculation constraints

3.2.1 Reacting phases

The geochemical mole transfer reactions considered in this study are dissolution/ precipitation of calcite, consumption of organic matter (CH_2O), dissolution of goethite, precipitation of pyrite, and in detail undefined ion exchange processes among the pairs Na-Ca, Na-Mg and Na-Fe. Mole balance calculations are applicable only for steady-state conditions. In undisturbed conditions it can be assumed that all the above reactions

are active, even the slow dissolution of goethite coupled with reduction of iron. In disturbed conditions hydrological transport is considered to be so fast that goethite dissolution is not possible.

Certain reactions like dissolution of CO_2 (organic respiration) or O_2 (atmospheric) mostly related to undersaturated soil layer above the bedrock have been discarded in this study. The meteoric reference water used in the calculations has been chosen such that these reactions have already affected the water composition.

The processes related to Na, Ca, Mg and Fe have not been defined in detail. More or less likely reacting phases, in addition to normal exchange processes, are montmorillonite, kaolinite and chlorite that are the usual alteration products of feldspars and biotite (Andersson 1996). These mineral phases have not been included in the inverse calculations because Al concentrations in the samples have not been reported. Exchange processes have been further simplified by omitting K, though its aqueous concentrations in samples have been reported. Because of its ion size, potassium is less eager to exchange with Na than the other elements mentioned above (Stumm 1992, Appelo & Postma 1993). Moreover, K is a minor constituent in the montmorillonite-kaolinite-chlorite mineral assemblage. Aqueous concentrations of silica (SiO_2) in samples are reported. However, weathering of montmorillonite, kaolinite, micas and feldspars affect the mole balances of silica, and therefore it has not been included in the calculations.

Anaerobic production of CH_4 (methanogenesis) has not been considered as a reacting phase in the present study. According to the theoretical redox sequence, methane-containing groundwater is usually low in sulphate (Appelo & Postma 1993). However, all deep Äspö groundwater samples are rich in SO_4. In principle, methane consumption (oxidation) coupled with sulphate reduction is a possible process at the Äspö site. However, this reaction cannot be modelled because aqueous CH_4 concentrations are not reported and there is no carbon isotopic evidence to support the reaction.

3.2.2 Analytical data

From the analytical data delivered, reported values on pH, Na, Ca, Mg, Fe_{tot}, HCO_3, Cl, SO_4, and $\delta^{18}O$ for each sample were used for modellings. In the inverse calculations Cl and ^{18}O concentrations were considered as conservative parameters, i.e. these two parameters essentially define mixing fractions among one, two or three initial water samples.

Initially, at the beginning of each modelling calculation, the uncertainty for analytical results of Na, Ca, Mg, Fe_{tot}, HCO_3, Cl and SO_4 was defined to be 7%. Similarly, the uncertainty for pH and $\delta^{18}O$ was defined as 0.07 and 0.1 units, respectively. In certain cases, especially when a final water sample was close in the Cl–$\delta^{18}O$ field to one of the initial water samples, smaller uncertainty limits were used for conservative parameters. Uncertainties for either Cl or $\delta^{18}O$ or both parameters were then tightened to 5% and 0.05 units, respectively.

Furthermore, in the case of a couple of samples, larger uncertainties were inevitable. Larger uncertainties were unavoidable especially for SO_4 (and HCO_3). Used uncertainties from 10% to 30% in these cases may indicate reacting phases not taken into account in the inverse modelling or missing (not sampled) data along a hypothetical flow path between initial and final water samples. Similarly, in a few cases overall uncertainties had to be broadened to 10–20%, which likely indicates missing data along the assumed flow path. All exceptions to the initial uncertainty assumptions are noted in Appendices 1–6.

Results of K, SiO_2, Br, F, Mn, Li, Sr, HS, ^2H and ^3H concentrations were also obtained for many samples. K and SiO_2 were abandoned for the reasons mentioned in the former chapter. Fluorine could be included into the modellings but has no major effect on mole balances, as it can either dissolve or precipitate in small amounts in the currently prevailing groundwater conditions. Tritium results from Äspö have been shown to be erroneous (Nilsson 1999, Laaksoharju et al. 1999b), and the remaining trace parameters contribute little or no information to the current study.

3.2.3 Reference water types

Detailed study of the geochemical data from the Äspö site requires interpretation of the palaeohydrology of the area. A simplified history of the Äspö site has been constructed based on interpretations of the geochemical data (Fig. 3-1). The Quaternary history of the area has been divided into four main, hydrogeochemically significant stages that cover the present, Litorina Sea, glacial and preglacial ages. During each of these periods specific reference water types infiltrated the bedrock.

The recent water types (Fig. 3-1d) considered here are currently recharging meteoric water, and seawater recharging into the bedrock from the present Baltic Sea. Compositions of both meteoric and seawater reference water types are tabulated in Table 3-1.

The meteoric reference was sampled from the middle of the undisturbed Äspö Island and its composition has been reported earlier by Laaksoharju (1988). According to Laaksoharju (1988), HAS05/-56.3m is a representative of a Na-HCO_3 non-saline dilute granitic water that has gained sodium and bicarbonate from surficial weathering processes of plagioclase and calcite, respectively. However, organic respiration in the unsaturated zone has also contributed to the HCO_3 content. In the delivered analytical data, the sample HAS05/-56.3m represents the most dilute undisturbed bedrock groundwater sample (Cl = 119 mg/l) on Äspö Island. The HAS05/-56.3m sample has a relatively high SO_4 content (SO_4 = 118 mg/l) for water originated from a meteoric source. In view of the lack of sulphur isotope data, several sources can be postulated for sulphate, i.e. oxidation of sedimentary sulphides, direct contribution of seawater, and indirect contribution of seawater sulphates (dissolution of adsorbed sulphates from iron hydroxide surfaces - cf. Banwart 1997). Burton & Viani (1997) have suggested the latter to be effective in the shallow, high HCO_3 bedrock environment of the Äspö HRL.

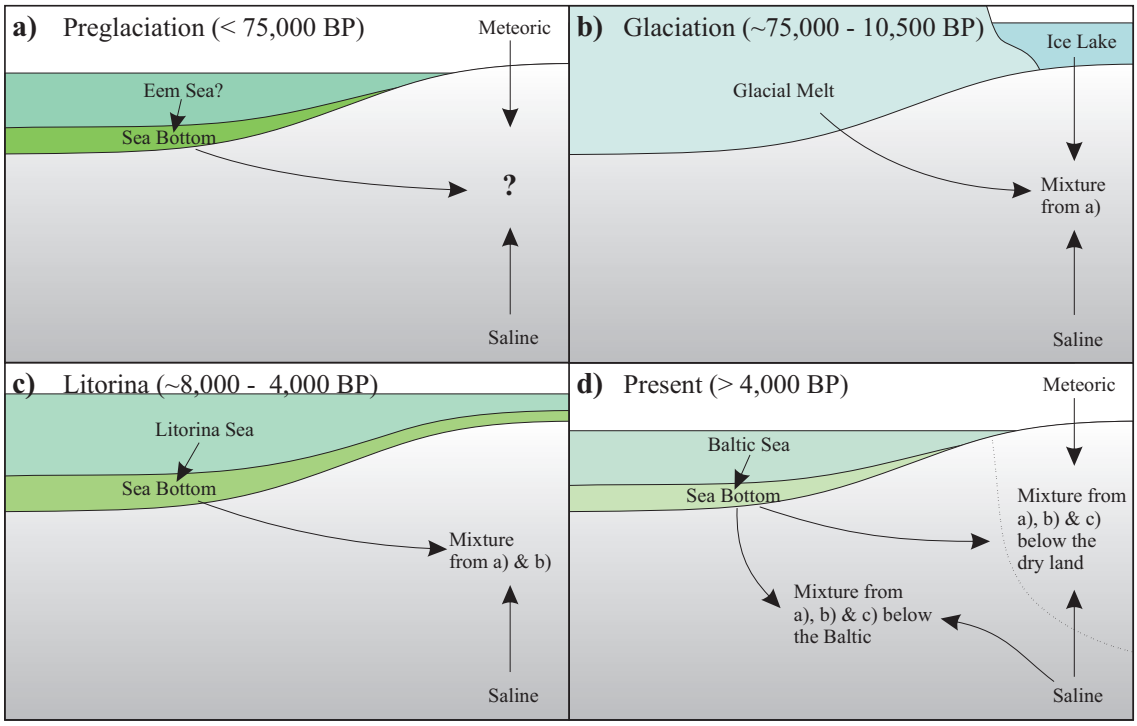

Figure 3-1 Quaternary history of the Äspö area, based on analyses of geochemical data and interpretations of the Quaternary history of the Fennoscandian Shield (e.g. Eronen 1988, Laaksoharju & Wallin 1997). Only periods considered significant for groundwater evolution at the Äspö site are presented.

The seawater reference used is an average of six samples collected from the Baltic during the summers of ’92 and ’93 outside Äspö Island. Sampling IDs and dates are noted in Table 3-1. The used average is somewhat less saline than the earlier used Baltic Sea reference (cf. Laaksoharju & Wallin 1997, p. 32), indicating the dilution of coastal Baltic Sea water consequent to recharge of surficial fresh water from land areas (cf. Luukkonen et al. 1999).

The Litorina stage (Fig. 3-1c - starting about 7,500–7,000 BP) preceding the present stage is clearly identifiable from the hydrogeochemical data. Samples contaminated significantly with Litorina Sea and postglacial altered marine water are characterised by higher salinities than the present Baltic Sea and high $\delta^{18}O$ values.

Based on studies of groundwater salinity, past climate temperature, and discovered subfossil shells in the Hästholmen region of Finland, Kankainen (1986) proposed that $\delta^{18}O$ and Cl values in the Litorina Sea probably initially reached -4.7‰ and 6,500 mg/l, respectively. Laaksoharju & Wallin (1997) estimated $\delta^{18}O$ and Cl values for the Litorina Sea in the Äspö region at -5.0‰ and 6,100 mg/l, respectively. There are, however, also certain fossil indications that at least in the southern part of the Litorina Sea, water was significantly more saline than the presented Cl values indicate (cf. Laaksoharju & Wallin 1997, p. 34). In the present consideration it is assumed that Cl and $\delta^{18}O$ values at the beginning of the Litorina Sea stage in the Äspö region were

roughly similar to those proposed by Kankainen (1986) (cf. Fig. 3-2). The other main element concentrations presented in Table 3-1 were achieved by diluting the estimated global mean ocean water (cf. Pitkänen et al. 1999a for details).

Although the postglacial altered water type is considered here together with the Litorina Sea reference water, a strict time span for this water type (when affected in the Äspö area) cannot be assigned. The postglacial altered water type is a representative of seawater that has been infiltrated through sea bottom sediments (Figs. 3-1c and 3-1d). During infiltration through the bottom, extensive reduction of aqueous sulphate, driven by organic activity and coupled with multiple recycled oxidation-reduction reactions of iron, takes place (cf. Canfield et al. 1993, Wang & Van Chappellen 1996). Similarly, notable complex cation exchange processes occur in the sea bottom causing depletion of Na and Mg, and enrichment of Ca in the recharging water. The postglacial altered reference water composition used (HAS13/-42.0m) is tabulated in Table 3-1. Its Cl content is less than estimated for the Litorina Sea reference but clearly higher than determined for the present Baltic Sea (cf. Fig. 3-2). Therefore the formation of postglacial altered water cannot be restricted to early periods of the Litorina Sea stage. After initiation of the Litorina Sea stage, seawater became diluted towards the present seawater salinity. The Litorina stage lasted until 2,500–2,000 BP. However, as regards Äspö Island, the significant seawater influence ceased when the island rose above sea level some 4,000 years ago (Laaksoharju & Wallin, 1997).

Table 3-1 Reference water types used in the inverse modellings. Meteoric, postglacial altered and saline reference water types are actual undisturbed samples. Reference days in the footnotes are given in relation to the sampling date (Ref. day 0 = 01.01.91).

	Meteoric Water a)	Seawater Average b)	Postglacial Alt. c)	Litorina Sea Approx. d)	Glacial Melt Approx. e)	"Preglacial Altered" f)	Saline g)
pH	8.0	7.7	7.3	7.6	5.8	7.7	8.0
Na	237	1904	1880	3764	0.2	1700	3020
K	4.0	72.7	32.8	134	0.2	(4.0)	7.3
Ca	25.0	90.9	1040	151	0.1	450.0	4380
Mg	6.0	226	219	448	0.1	110.0	49.5
Alkalis	370	85.7	132	92.5	0.2	200	11.0
Cl	119	3562	5070	6500	0.7	3500	12300
SO_4	118	505	136	890	0.1	100	709
Si	5.2	0.3	5.0	1.8	0.0	(4.7)	4.2
Fe	1.6	0.08	2.7	0.002	0.0	1.7	0.08
^{18}O	-9.9	-6.4	-7.2	-4.7	-19.0	-9.5	-12.7

a) HAS05/-56.3m. Reference day -1243
b) Average from 6 samples PASSEA01 (28.8.92) & PASSEA01-05 (7.8.93)
c) HAS13/-42.0m. Reference day -547
d) From Pitkänen et al. (1999a) & refs. therein
e) From Pitkänen et al. (1999a) & refs. therein with reconsidered O-18 value
f) O-18 & Cl values from Pitkänen et al. (1999a). Main component concentrations fitted for samples KAS03/-121.8m (Ref. Day -679), KAS02/-199.8m (Ref. Day -720), KAS03/-239.0 (Ref. Day -856) & KAS02/-881.3 (Ref. Day -700)
g) KAS03/-914.1m. Reference day -657

During *the glacial stage* (Fig. 3-1b) melt water from the Pleistocene ice sheet is considered to have been the dominant source of water recharging into the bedrock. The glacial melt is bound to have been very dilute and poorly buffered water. The main uncertainty centres mostly on the average $\delta^{18}O$ value of the melt. Laaksoharju & Wallin (1997) and Pitkänen et al. (1999a) have assumed almost consistently that the glacial melt had an average $\delta^{18}O$ value of -21‰ – -22‰. Studies of ice sheets from Greenland (e.g. Taylor et al. 1992) indicate distinctly lower $\delta^{18}O$ values for ice (-33– -38‰). However, most of the melt water possibly recharged into the bedrock during the deglaciation period, when the mean annual temperature rose above 0°C and rainwater diluted extreme $\delta^{18}O$ values of melting ice. In the current study the $\delta^{18}O$ value for glacial melt is estimated to be –19‰ (cf. Fig. 3-2). Other estimated concentrations for the glacial melt are listed in Table 3-1.

The preglacial stage (Fig. 3-1a) is the oldest water-recharging period currently considered. Clear signs of a "preglacial altered" water type are not found, and its composition (Table 3-1) is deduced from the Quaternary history of the Äspö region, and on argumentation of the estimated glacial melt composition and the most glacial-type samples analysed from Äspö Island.

At Olkiluoto in Finland, the assumed SO_4 and ^{18}O concentrations in the Litorina Sea and glacial melt, and the existing concentrations in brackish SO_4 groundwater, have led to the interpretation that "preglacial altered" water had $\delta^{18}O$ values of about -11– -10‰ and a Cl concentration of about 3,500 mg/l (Pitkänen et al. 1999a). However, similar reasoning for the Äspö site is not possible, because it seems that a significant part of infiltrated Litorina Sea water has experienced sulphate reduction (resulting in postglacial altered water) during penetration through sea bottom sediments. Moreover, in the Äspö case the altered Litorina Sea water has mixed with a body of SO_4-containing water consisting of glacial, "preglacial altered" and saline reference types.

As Figure 3-1 shows, the "preglacial altered" water was bound to be an admixture from several preglacial sources containing contributions at least from meteoric and saline sources, and probably also from ancient seawater and altered seawater infiltrated through sea bottom sediments.

For current purposes, the Cl and ^{18}O concentrations in "preglacial altered" groundwater were reasoned to be about 3,500 mg/l and -9.5‰, respectively. These estimates approximate the interpretation done in the Olkiluoto studies, and they form the basis for estimations of other element concentrations presented in Table 3-1. The tabulated estimations were calculated with the aid of three distinctly glacial-water-contaminated undisturbed samples (KAS03/-121.8m, KAS03/-239.0m and KAS02/-199.8m) and with one mostly saline reference-water-contaminated sample (KAS02/-881.3m). Locations of these samples in the Cl–^{18}O field are indicated in Figure 3-2. The "preglacial altered" reference composition was iterated gradually in series of PHREEQC-2 calculations where correct directions and feasible reaction amounts in mole transfers judged the step-by-step changes which had occurred in the unknown "preglacial altered" composition. The approximate charge-balance of the estimated water composition was also frequently checked. As shown in Figure 3-2, sample KAS03/-121.8m was assumed to be a binary mixture of initial "preglacial altered" and glacial melt water. Samples KAS03/-239.0m and KAS02/-199.8m were assumed to be ternary mixtures of initial "preglacial altered"

and glacial melt water and a mixed water sample (KAS03/-348.6m). The mostly saline sample KAS02/-881.3m was considered to result from a ternary mixture of "preglacial altered" and glacial melt water, and the saline reference water (sample KAS03/-914.1m).

For *the saline reference water* (KAS03/-914.1m) no strict age relation has been assumed. The source of saline water is considered a large one, and in all saline water there may be present hydrothermal, but diluted, relicts of very old orogenic activities in the Äspö area. Sample KAS03/-914.1m is the most saline ^{18}O-analysed undisturbed sample found below Äspö Island.

3.3 Calculation method

As noted earlier, the calculations of mixing fractions are based on Cl and ^{18}O (with two exceptions where SO_4 has been considered conservative due to a missing ^{18}O value). All other chemical values used in the calculations are subject to mole transfers, i.e. they are dissolved/precipitated from/to reacting phases to satisfy the calculation constraints.

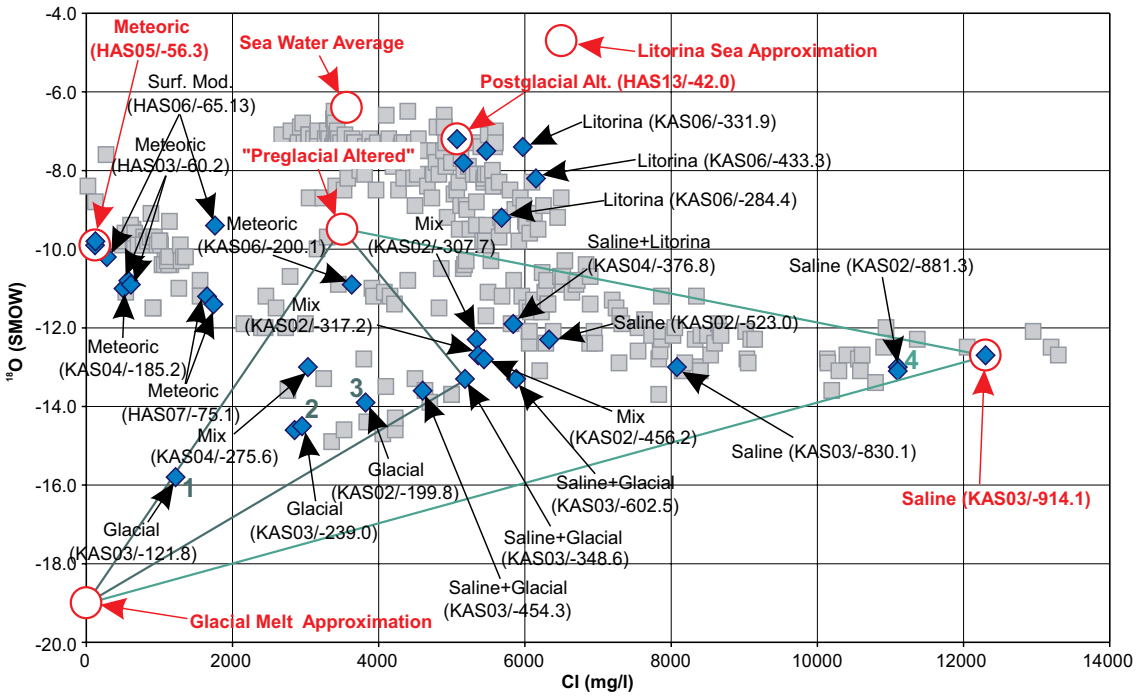

Figure 3-2 Reference water types (red circles), undisturbed samples (blue diamonds) and disturbed samples (grey squares) from the Äspö HRL in the Cl–^{18}O field. Green lines and numbers indicate binary and ternary mixing relations used for estimation of "preglacial altered" water composition (see text for details).

The inverse calculations are done in steps, presuming that the steady-state assumption of chemical reactions is valid. In practice this means that a final water composition can be produced from a realistic set of initial water samples with small, moderate or otherwise feasible mole transfers. The directions of dissolution/precipitation reactions form an important basis for judgement of acceptability of the steady state condition. Such judgements depend strongly on what kind of initial water samples are being mixed together. Say, for example, that we need a significant amount of the meteoric reference HAS05/-56m for mixing; we can assume that mole transfers involve moderate consumption of organic matter (close to ground level organic matter is available) and moderate or strong precipitation of calcite (meteoric reference is high in HCO_3). On the other hand, if in the initial sample set the fresh seawater is the dominating member, we have to assume that the reactions taking place in the sea bottom sediments contribute strongly to the net mole transfers to be calculated. In this case, strong consumption of organic matter, dissolution of calcite, dissolution of Ca and Fe from CaX_2 and FeX_2/goethite, precipitation of Na and Mg to NaX and MgX_2, and precipitation of pyrite can be expected. However, if the saline reference (KAS03/-914.1m) dominates in the initial sample set, only small organic matter consumption (restricted microbial activity at depth) and small overall mole transfers among other dissolved ions may be expected, because saline water is assumed to be well-equilibrated with its environment.

In all, the inverse-modelling approach comprises a multiple exercise based on an attempt to understand the geochemical system along a flow path, and in many cases on trial and error calculations, until the feasible set mole-transfer phases and acceptable set of initial water samples are found for a certain final water. In the current approach, a previous successful (assumed steady-state) step leads to the following step, which is to find new sets of initial water samples for previous initial water samples now considered as final water samples, and so on. These steps are ultimately extended to the reference water types, and then mixing fractions of the reference water types in each sample considered in the calculation chain can be solved.

The idea of the calculation process is presented in Figure 3-3, in which there are five reference water types (REF A … REF E) and seven water samples. The choice of steady-state steps is based on identification of the geochemical affinities for each sample, and finding a suitable initial water assemblage for each of these seven samples (usually one or two suitable initial water samples exhibit a somehow chemically kindred character towards final water). According to Figure 3-3, the following steady-state steps are defined for the samples:

$$S_1 = 0.2*S_2 + 0.5*S_3 + 0.3*\text{REF E} \quad (3\text{-}2)$$
$$S_2 = 0.1*S_3 + 0.5*S_5 + 0.4*\text{REF E} \quad (3\text{-}3)$$
$$S_3 = 0.2*S_4 + 0.4*S_6 + 0.4*\text{REF A} \quad (3\text{-}4)$$
$$S_4 = 0.6*\text{REF B} + 0.4*\text{REF E} \quad (3\text{-}5)$$
$$S_5 = 0.7*\text{REF C} + 0.3*\text{REF D} \quad (3\text{-}6)$$
$$S_6 = 0.4*\text{REF B} + 0.6*\text{REF E} \quad (3\text{-}7)$$
$$S_7 = 0.5*S_1 + 0.4*S_5 + 0.1*\text{REF D} \quad (3\text{-}8)$$

In equations 3-2…3-8, the mixing fraction of each initial water sample is shown with a coefficient. Mole transfers from/to reacting phases are solved simultaneously with the mixing fractions, though mole transfers are not considered here in detail.

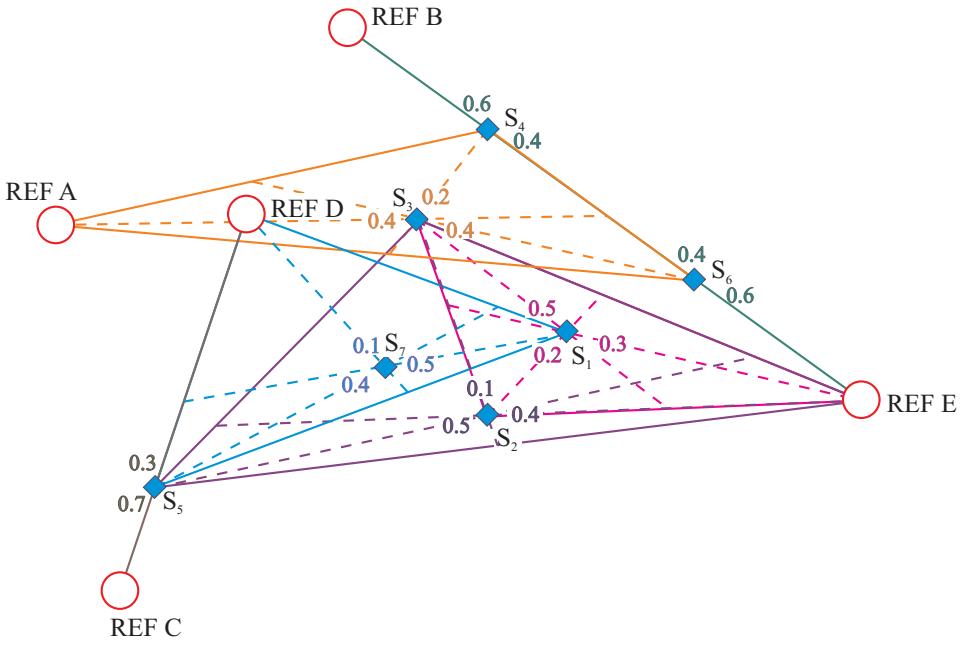

Figure 3-3 Diagrammatic presentation of the stepwise calculation of reference water-type mixing fractions in given water samples. Samples used as initial waters for a certain final water are linked by solid tie-lines. Broken lines illustrate the rough euclidean distance of initial waters from a final water sample. Solid and broken lines, and given mixing fractions related to the same final water sample are given the same colour.

The calculation of mixing fractions of reference water types for each sample from equations 3-2…3-8 is now straightforward. For example, in the case of the first sample, Equations 3-3 and 3-4 are first substituted into Equation 3-2, and then Equations 3-5, 3-6 and 3-7 are substituted into Equation 3-2. For all samples the results are:

$S_1 = 0.20*\text{REF A} + 0.15*\text{REF B} + 0.07*\text{REF C} + 0.03*\text{REF D} + 0.55*\text{REF E}$ 3-9
$S_2 = 0.04*\text{REF A} + 0.03*\text{REF B} + 0.35*\text{REF C} + 0.15*\text{REF D} + 0.43*\text{REF E}$ 3-10
$S_3 = 0.40*\text{REF A} + 0.28*\text{REF B} + 0.32*\text{REF E}$ 3-11
$S_4 = 0.60*\text{REF B} + 0.40*\text{REF E}$ 3-12
$S_5 = 0.70*\text{REF C} + 0.30*\text{REF D}$ 3-13
$S_6 = 0.40*\text{REF B} + 0.60*\text{REF E}$ 3-14
$S_7 = 0.10*\text{REF A} + 0.07*\text{REF B} + 0.32*\text{REF C} + 0.24*\text{REF D} + 0.27*\text{REF E}$ 3-15

As noted in Chapter 2.2.2, analytical uncertainties are included in the calculations. These uncertainties reflect on the mixing fractions as well (cf. Appendices 1–6). In addition to representative mixing fraction results, the calculations give the minimum and maximum fractions possible within the analytical uncertainties given. The minimum and maximum fractions of initial water samples can be inserted in the calculation chain just like the representative values. The minimum and maximum fractions of the reference water types for each sample give the cumulative extreme fractions possible within the analytical uncertainties given to each sample along the calculation chain. Therefore, as the chain of intermediate samples towards the reference water types gets longer, the lower and upper limits of the mixing fractions inevitably become wider for the sample (cf. Figs 4-1 and 4-2, p. 14 and 18). In our example (Fig.

3-3), mixing fraction uncertainties related to sample 1 (S_1) would probably be higher than, for example, uncertainties related to sample 5 (S_5).

The example presented in Figure 3-3 gives an approximate view of the mixing calculations. In practice, the more steps there are close to the reference water types, the more realistic the results are, i.e. pure mixings between two reference waters are better avoided. In summary, our example bears on the current calculation problem. Figure 3-1 (p. 6) gives a schematic overview of groundwater geochemical evolution at Äspö. The earliest mixing among the considered reference water types occurs when the "preglacial altered" and glacial melt mix with each other (Fig. 3-1b). We may assume that in Figure 3-3, REF C presents glacial melt and REF D "preglacial altered" water types. This glacial related assemblage mixes variably with waters related to the saline reference water type, that can be assumed to be a REF E water type in Figure 3-3. Later on, the assemblages composed of a mixture of glacial melt, "preglacial altered" and saline water types mixes variously with water infiltrated from the Litorina Sea. Hence the REF B water in Figure 3-3 could represent the postglacial altered water type infiltrating the bedrock during the Litorina stage (Fig. 3-1c). Finally, mixtures from all earlier contributions mix with meteoric water below the dry land of the Äspö area, and the REF A water type in Figure 3-3 may be related to meteoric water. In conclusion, Figure 3-4 gives a broad overview of how past events are considered to have affected groundwater compositions at shallow depth at Äspö.

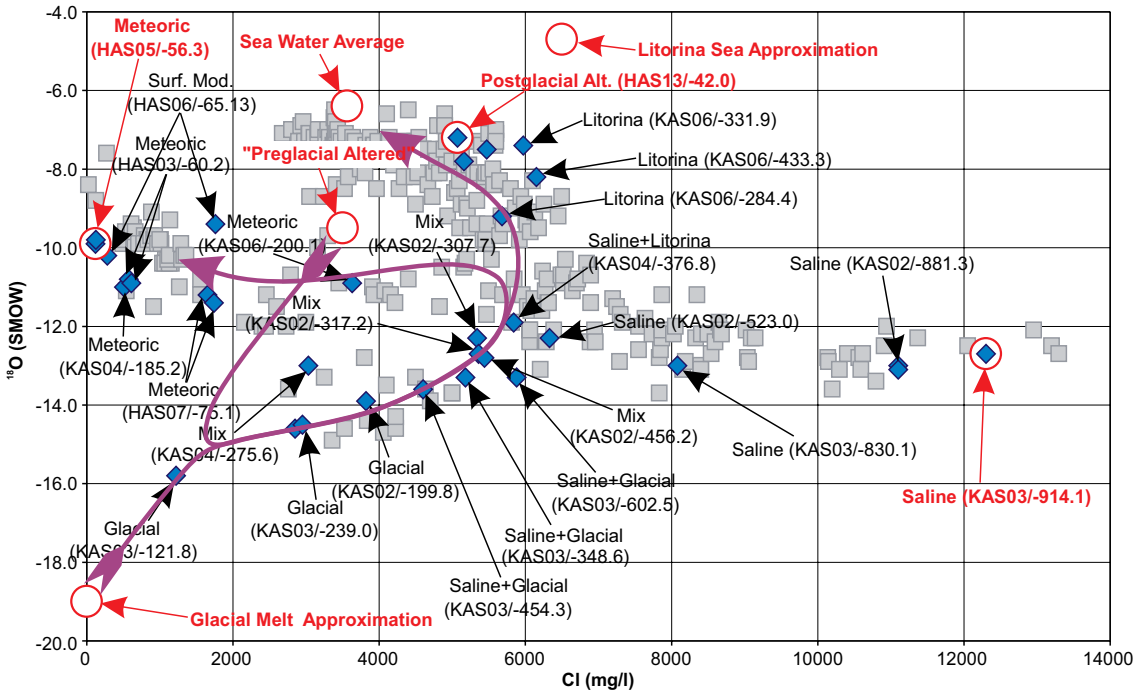

Figure 3-4 Schematic overview of the mixing evolution at shallow depth groundwater in the Äspö area. Violet arrows show assumed evolution trends below sea and land areas.

4 Results

The Äspö groundwater geochemical data are divided into two sets in relation to the excavation of the HRL shafts and tunnels. Tunnel excavations started in October 1990, but for practical reasons the data have been categorised in relation to the date January 1, 1991, when the main tunnel face position was at 263m. The reference days (cf. Appendices 1–6) calculated for each sample are based on this date.

4.1 Undisturbed conditions

The undisturbed samples considered here were collected between August 8, 1987 and June 6, 1990. In all, reference water mixing fractions and mole transfers of reacting phases have been calculated for 25 undisturbed samples. Additionally, three samples (HAS05/-56.3m, HAS13/-42.0m, and KAS03/-914.1m – cf. Chapter 2.2.3) from the undisturbed data were chosen as reference water types. Of the 25 samples, 23 have reported values for the conservative parameters Cl and ^{18}O (cf. Figs. 3-2 and 3-4). However, in order to get more information for interpretation, two additional samples, with only Cl reported, were accepted in the undisturbed calculation effort. In these samples (KAS03/-566m, Day -868; KAS05/-339.5m, Day -209) sulphate reduction was considered negligible, and SO_4 was considered a conservative parameter in addition to Cl.

Based on the judgement rules explained in detail in Chapter 2.3, the chosen undisturbed samples were related to each other. The flow paths for undisturbed samples are presented in Figure 4-1. The flow paths considered here are hypothetical in the sense that no physical path between the interrelated sampling points was required. The aim is to describe the general evolution of water in the bedrock. It is assumed that if stepwise data were available along all physical flow paths related to the chosen undisturbed samples, we would find analogous chemical evolution of groundwater as described here with hypothetical flow paths.

The mixing fractions of the reference water types in the studied 25 undisturbed samples are listed in Table 4-1. The same values, but modified in the sense that preglacial and postglacial altered columns are shown only as a sum column (altered sum), are shown in Table 4-2. The mole transfers required to reach the composition of each final sample from the initial water samples, noted in Figure 4-1, are shown together with the reference water mixing fractions.

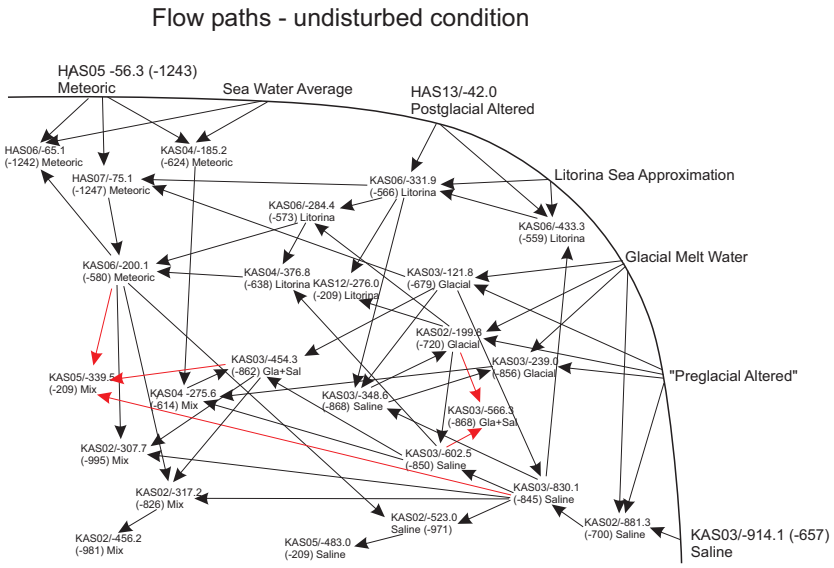

Figure 4-1 Hypothetical flow paths used in mole-transfer modelling. The arch separates reference water types from the rest of the data and roughly interprets their apparent age. Flow paths solved with parameters Cl and ^{18}O are shown with black arrows, paths solved with Cl and SO_4 with red arrows.

Table 4-1 Reference water type mixing fractions (in percent) in the studied undisturbed Äspö water samples. The sampling dates given refer to the date 01.01.91. Estimated minimum and maximum fractions are noted after each representative value. Actual samples used as reference types are shown in green. Sulphate reduction was considered negligible in the samples shown in red.

Sample	Day	Meteoric			Baltic Sea			Postgl. Alt.			Litorina Sea			Glacial Melt			"Pregl. Alt."			Saline			Sum
HAS05/-56.3	**-1243**	**100.0**																					**100.0**
KAS04/-185.2	-624	**87.7**	86.5	90.0	**12.3**	10.0	13.5																100.0
HAS06/-65.1	-1242	**53.5**	52.0	54.1	**27.4**	27.3	27.7	**5.9**	3.1	10.3	**2.5**	0.9	4.0	**5.8**	4.9	7.1	**2.9**	2.1	3.9	**2.1**	1.3	4.1	100.0
HAS07/-75.1	-1247	**41.9**	41.7	42.9				**11.9**	6.7	19.3	**5.0**	2.0	7.4	**26.4**	25.1	26.9	**12.3**	11.6	12.8	**2.4**	1.2	4.0	100.0
KAS06/-200.1	-580	**26.1**	25.6	26.9				**22.8**	11.9	37.5	**9.6**	3.6	14.4	**22.2**	18.9	25.9	**11.1**	8.2	14.2	**8.2**	4.8	14.8	100.0
KAS06/-331.9	-566							**58.0**	32.5	92.7	**24.5**	10.0	35.6	**3.6**	1.4	5.8	**2.0**	0.5	4.2	**11.8**	6.1	19.3	100.0
KAS06/-433.3	-559							**49.7**	36.4	59.1	**23.1**	15.2	30.9	**5.7**	3.1	8.1	**3.2**	1.2	5.9	**18.4**	13.5	27.0	100.0
KAS06/-284.4	-573							**44.6**	24.6	71.8	**18.8**	7.5	27.6	**13.8**	9.1	19.6	**8.3**	2.9	13.3	**14.5**	9.0	24.9	100.0
KAS12/-276.0	-209							**42.9**	21.6	71.1	**18.1**	6.6	27.3	**15.0**	9.5	24.9	**9.1**	3.0	16.8	**14.8**	8.7	28.4	100.0
KAS04/-376.8	-638							**14.1**	7.5	23.8	**5.9**	2.3	9.2	**25.7**	15.9	37.1	**15.3**	5.3	25.4	**39.1**	29.8	58.4	100.0
HAS13/-42.0	**-547**							**100.0**															**100.0**
KAS03/-121.8	-679													**68.4**	68.3	68.4	**31.6**	31.6	31.7				100.0
KAS02/-199.8	-720							**3.4**	1.2	7.7	**1.5**	0.4	3.0	**44.8**	32.8	59.9	**27.6**	10.1	39.7	**22.7**	17.9	41.0	100.0
KAS03/-239.0	-856							**2.1**	0.6	4.3	**0.9**	0.2	1.6	**51.7**	41.1	59.0	**31.6**	21.7	43.4	**13.7**	8.5	22.7	100.0
KAS03/-914.1	**-657**																			**100.0**			**100.0**
KAS02/-881.3	-700													**9.9**	3.2	13.8	**7.1**	0.0	14.0	**83.0**	75.7	96.8	100.0
KAS03/-830.1	-845													**20.8**	14.3	24.1	**11.6**	5.4	17.5	**67.6**	61.6	80.3	100.0
KAS02/-523.0	-971	**7.4**	6.1	8.7				**6.5**	2.8	12.1	**2.7**	0.9	4.7	**21.2**	14.1	26.8	**11.5**	5.6	17.9	**50.7**	42.9	66.0	100.0
KAS05/-483.0	-209	**7.4**	6.1	8.7				**6.5**	2.8	12.1	**2.7**	0.9	4.7	**21.2**	14.1	26.8	**11.5**	5.6	17.9	**50.7**	42.9	66.0	100.0
KAS03/-602.5	-850							**1.4**	0.4	3.7	**0.6**	0.1	1.4	**30.6**	18.8	44.3	**18.1**	6.3	30.3	**49.2**	38.5	72.2	100.0
KAS03/-348.6	-868							**5.5**	2.0	9.4	**2.3**	0.6	3.6	**37.6**	29.5	43.6	**18.4**	13.1	24.2	**36.2**	30.0	50.0	100.0
KAS03/-454.3	-862	**4.1**	2.8	8.6	**0.6**	0.3	1.3	**1.2**	0.3	3.6	**0.5**	0.1	1.4	**37.7**	22.8	55.5	**20.5**	8.9	34.5	**35.4**	24.7	60.4	100.0
KAS03/-566.3	-218							**2.0**	0.6	5.2	**0.9**	0.2	2.0	**34.9**	21.3	52.2	**21.0**	6.9	35.3	**41.2**	30.6	66.5	100.0
KAS04/-275.6	-614	**29.7**	25.2	35.6	**4.2**	2.9	5.3	**1.7**	0.4	4.7	**0.7**	0.1	1.8	**25.3**	11.8	43.7	**15.3**	3.8	29.4	**23.2**	13.4	48.9	100.0
KAS02/-307.7	-995	**14.4**	12.8	16.5	**0.1**	0.0	0.3	**12.0**	5.8	20.8	**5.1**	1.8	8.0	**25.9**	14.4	38.8	**13.7**	6.0	24.2	**28.8**	17.9	57.8	100.0
KAS02/-317.2	-826	**8.2**	7.1	12.4	**0.3**	0.2	0.8	**5.7**	2.8	12.1	**2.4**	0.8	4.6	**31.3**	18.5	46.7	**16.9**	7.4	29.0	**35.1**	22.8	57.8	100.0
KAS02/-456.2	-981	**8.2**	7.1	12.4	**0.3**	0.2	0.8	**5.7**	2.8	12.1	**2.4**	0.8	4.6	**31.3**	18.5	46.7	**16.9**	7.4	29.0	**35.1**	22.8	57.8	100.0
KAS05/-339.5	-209	**10.3**	4.2	20.0	**0.3**	0.0	0.9	**7.9**	1.8	22.0	**3.3**	0.6	8.5	**28.9**	7.7	61.6	**15.5**	3.1	38.3	**33.9**	11.8	79.9	100.0

Table 4-2 Calculated reference water mixing fractions and mole transfers (mmol/l) for the undisturbed samples from Äspö (cf. Appendix 1).

Sample	Day	Meteoric	Baltic	Litorina	Glacial	Alt.Sum	Saline	Calcite	CH_2O	NaX	CaX_2	MgX_2	Goethite	FeX_2	Pyrite	Fe^{+3}	S^{-2}
KAS04/-185.2	-624	0.88	0.12					-2.31	0.34	-2.48	3.75	-1.11	1.38	-1.40		1.38	
HAS06/-65.1	-1242	0.53	0.27	0.02	0.06	0.09	0.02	-1.29	0.19		1.98	-1.26	0.78	-0.71		0.75	
HAS07/-75.1	-1247	0.42		0.05	0.26	0.24	0.02	-1.30	0.23	-0.11		0.78	0.76	-0.73	-0.01	0.76	-0.02
KAS06/-200.1	-580	0.26		0.10	0.22	0.34	0.08	0.08	0.21	-0.09				0.05	-0.06		-0.12
KAS06/-331.9	-566			0.25	0.04	0.60	0.12	-0.03		2.59		-1.29	0.00	0.00		0.00	
KAS06/-433.3	-559			0.23	0.06	0.53	0.18	-0.82	0.12		4.44	-3.93	0.49	-0.51		0.49	
KAS06/-284.4	-573			0.19	0.14	0.53	0.14	-0.31	0.05	0.41			0.20	-0.21		0.20	
KAS12/-276.0	-209			0.18	0.15	0.52	0.15	-0.43	0.07	0.53			0.26	-0.26		0.26	
KAS04/-376.8	-638			0.06	0.26	0.29	0.39	0.01	0.00				0.00			0.00	
KAS03/-121.8	-679				0.68	0.32		0.04	0.02	1.15		-0.57			-0.01	0.00	
KAS02/-199.8	-720			0.01	0.45	0.31	0.23	-2.21	2.77			1.15	1.81	-1.15	-0.66	1.81	-1.33
KAS03/-239.0	-856			0.01	0.52	0.34	0.14	-2.91	2.87	1.87		0.65	2.24	-1.58	-0.66	2.24	-1.32
KAS02/-881.3	-700				0.10	0.07	0.83	-0.28	0.04		0.93	-0.75	0.18	-0.18		0.18	
KAS03/-830.1	-845				0.21	0.12	0.68	-1.23	1.09			0.66	0.90	-0.66	-0.25	0.90	-0.49
KAS02/-523.0	-971	0.07		0.03	0.21	0.18	0.51	-0.47	0.07	1.67		-0.56	0.28	-0.28		0.28	
KAS05/-483.0	-209	0.07		0.03	0.21	0.18	0.51	-0.02	0.07				0.02		-0.02	0.02	-0.04
KAS03/-602.5	-850			0.01	0.31	0.20	0.49	-0.51	0.08	1.89		-0.63	0.31	-0.31		0.31	
KAS03/348.6	-868			0.02	0.38	0.24	0.36	-0.46	0.07	0.53			0.27	-0.27		0.27	
KAS03/-454.3	-862	0.04	0.01	0.00	0.38	0.22	0.35	-0.01	0.00	-0.55		0.27	0.00			0.00	
KAS03/-566.3	-218			0.01	0.35	0.23	0.41			0.00				0.00			
KAS04/-275.6	-614	0.30	0.04	0.01	0.25	0.17	0.23	-0.54	0.08	0.61			0.31	-0.30		0.31	
KAS02/-307.7	-995	0.14	0.00	0.05	0.26	0.26	0.29	-0.61	0.09	0.73			0.38	-0.37		0.38	
KAS02/317.2	-826	0.08	0.00	0.02	0.31	0.23	0.35	-0.02	0.00	-2.07		1.03	0.01			0.01	
KAS02/456.2	-981	0.08	0.00	0.02	0.31	0.23	0.35	-0.22	0.04	0.31			0.16	-0.15		0.16	
KAS05/-339.5	-209	0.10	0.00	0.03	0.29	0.23	0.34	-0.35	0.05	0.37			0.19	-0.19		0.19	

Table 4-3 Pair-wise Spearman rank correlations for the calculation results of Table 4-2. The number of observations used for each correlation is shown with the superscript. Correlations between the reference water types and reacting phases are shown in bold type. Rank correlations with absolute value less than 0.21 and results based on less than four observations have been omitted.

	Meteoric	Baltic	Litorina	Glacial	Alt.Sum	Saline	Calcite	CH_2O	NaX	CaX_2	MgX_2	Goethite	FeX_2	Pyrite	Fe^{+3}	S^{-2}
Meteoric	^{12} 1.00															
Baltic	^{8} 0.52	^{8} 1.00														
Litorina	^{11} 0.35	^{7}-0.60	^{21} 1.00													
Glacial	^{11}-0.36	^{7}-0.31	^{21}-0.75	^{24} 1.00												
Alt.Sum		^{7}-1.00	^{21} 0.67		^{24} 1.00											
Saline	^{11}-0.96	^{7}-0.31	^{21}-0.43		^{23}-0.59	^{23} 1.00										
Calcite	**^{12}-0.73**	**^{8}-0.40**	**^{20} 0.22**			**^{22} 0.27**	^{24} 1.00									
CH_2O	**^{12} 0.84**	**^{8} 0.40**				**^{21}-0.43**	^{23}-0.79	^{23} 1.00								
NaX	**^{10}-0.21**	**^{7}-0.58**						^{16} 0.21	^{18} 1.00							
CaX_2							^{4}-0.40	^{4} 0.40		^{4} 1.00						
MgX_2	**^{6}-0.49**	**^{4}-1.00**	**^{10}-0.44**	**^{13} 0.65**					^{9}-0.38	^{4}-0.80	^{14} 1.00					
Goethite	**^{11} 0.90**	**^{8} 0.40**	**^{19}-0.20**			**^{21}-0.29**	^{22}-0.98	^{21} 0.96		^{4} 0.40	^{13} 0.26	^{22} 1.00				
FeX_2	**^{9}-0.73**	**^{6}-0.54**	**^{17} 0.26**				^{19} 1.00	^{18}-0.82		^{4}-0.40	^{11}-0.44	^{18}-0.99	^{20} 1.00			
Pyrite			**^{5} 0.60**			**^{6}-0.37**	^{7} 0.61	^{7}-0.86	^{4}-0.40		^{5}-0.60	^{5}-0.80	^{5} 0.60	^{7} 1.00		
Fe^{+3}	**^{11} 0.89**	**^{8} 0.40**				**^{21}-0.29**	^{23}-0.98	^{22} 0.96		^{4} 0.40	^{14} 0.30	^{22} 1.00	^{18}-0.99	^{6}-0.89	^{23} 1.00	
S^{-2}			**^{5} 0.60**	**^{6}-0.43**	**^{6}-0.26**	**^{6}-0.37**	^{6} 0.54	^{6}-0.77				^{5}-0.80	^{5} 0.60	^{6} 1.00	^{5}-0.80	^{6} 1.00

The statistical examination of Table 4-2 is a demanding task. There are only 25 observations but 16 variables. Nevertheless, a simple pair-wise Spearman rank correlation matrix from Table 4-2 data is presented in Table 4-3. The rank correlation method has been chosen because, due to missing data (cf. Table 4-2), certain pair-wise correlations inevitably rest on a very small number of observations. Furthermore, due to the overall small number of observations, significant scatter exists among mole-transfer data, which can be diminished with rank correlations. The cost of rank correlations is that the coefficients shown in Table 4-3 have no linear regression slope coefficient interpretation, but give only the "significance" of positive/negative correlation.

The upper left quarter of Table 4-3 shows correlations among the reference water types. Meteoric reference correlates positively with fresh Baltic Sea water. This is a result of biased sampling campaigns; i.e. all bedrock samples have been taken below the dry land of Äspö Island. For this reason the mixing fraction of fresh Baltic Sea water never reaches a high level among undisturbed samples, though logically seawater and meteoric water have independent sources. Sensibly, meteoric reference correlates negatively with saline reference. As regards palaeohydrology, fresh Baltic Sea naturally exhibits a negative correlation to fresh Litorina Sea and "altered sum" (especially postglacial altered, cf. Table 4-1) references, because it replaces these water types during evolution. The palaeohydrological processes bind the Litorina Sea and postglacial reference water types, and also the glacial melt and preglacial reference water types, strongly together (cf. Fig. 3-1 and Table 4-1). The relation between fresh Litorina and the postglacial reference can be seen in Table 4-3, but the relation between glacial and preglacial altered waters remain unclear. However, a positive glacial/ preglacial relation is evident in Table 4-1, but the "altered sum" simplification hides this feature. The fresh Litorina reference correlates negatively with glacial melt, since it replaces melt water in the palaeohydrological evolution. Pre- and postglacial altered references correlate negatively with saline water, because they have mostly infiltrated from the surface and become diluted as a function of depth similarly to meteoric water.

The lower right quarter of Table 4-3 illustrates correlations among mole and redox transfers. Certain variables are by default fully mutually correlated, i.e. redox transfers and reacting phases requiring redox processes (goethite–Fe^{+3} and pyrite–S^{-2}). The source/sink for Fe^{+2} (FeX_2) correlates negatively with goethite for obvious reasons, but also there exists a negative correlation between goethite and pyrite. If dissolution of goethite produces Fe^{+2} and there is available H_2S, through SO_4 reduction or otherwise, the overall reaction results in precipitation of pyrite. Oxidation of organic matter (CH_2O) is the driving force for sulphate and iron reduction, giving the correlations between CH_2O, goethite and pyrite. It is worth noting that from the reference water types meteoric, postglacial altered and "preglacial altered" are all high in Fe^{+2} and additionally high in HCO_3 (cf. Table 3-1). Reaction steps involving any of these water types tend to involve dissolution of organic matter, and precipitation of calcite and pyrite.

The lower left quarter of Table 4-3 attempts to explain the mole-transfer relations related to each reference water type. In accordance with the assumptions made, a high fraction of meteoric reference water promotes dissolution of CH_2O and precipitation of calcite. In the upper bedrock the moderate redox state supports dissolution of goethite,

although due to the relatively high SO_4 concentration in the Äspö meteoric bedrock groundwater, the sulphate reduction is not very evident.

Unfortunately, the fresh Baltic fraction never reaches a high level among the collected undisturbed samples, which would have enabled verification of a distinct SO_4 reduction related to seawater recharge. However, the examination of reference water mixing fractions and primary chemical data of modelled sample compositions indicates that even small fractions of fresh Baltic Sea water give seawater characteristics to the rest of the mole transfers. The precipitation of Na and Mg to NaX and MgX_2 and strong dissolution of Ca from CaX_2 (see Table 4-2, correlations not shown in Table 4-3 due to the small amount of observations) can be interpreted with some controversy from the meteoric reference column. These correlations are, however, distinct and characteristic for seawater in the fresh Baltic reference column.

The Litorina Sea water has mostly been altered during infiltration through sea bottom sediments. Therefore, on the whole, only small mole transfers are found. Samples containing the highest fresh Litorina component contain a doubly high amount of postglacial altered water (cf. Table 4-1) relatively rich in HCO_3 (cf. Table 3-1). Consequently, these samples indicate precipitation of calcite (Table 4-2). A similar type of coupling exists in samples containing glacial and preglacial water (high HCO_3), which also indicates precipitation of calcite.

The saline reference column indicates that as the saline fraction gets higher the dissolution of organic matter and goethite, and the precipitation of calcite, tend to get smaller.

4.1.1 Depth distribution of reference water types

As the examination of the upper left quarter of Table 4-3 already indicated, there are certain distinct depth-related correlations among the undisturbed data set. To examine these relations more closely the calculated mixing fractions have been plotted as a function of depth in Figure 4-2.

According to Figure 4-2, the meteoric and fresh Baltic Sea fractions seem to decrease in an exponential manner as a function of descending depth. Similarly, there appears to be a linear decrease in saline reference fractions as a function of ascending depth. The fresh Litorina Sea fraction always remains at a low level since most Litorina Sea originated groundwater has been altered, and is categorised in the present approach into the postglacial altered fraction. At any rate, there seems to be a small maximum (the regression is Gaussian) in the fresh Litorina component at depth around -350m. In the case of glacial melt and “pre- and postglacial altered” references there are already a considerable scatter of fractions as a function of depth.

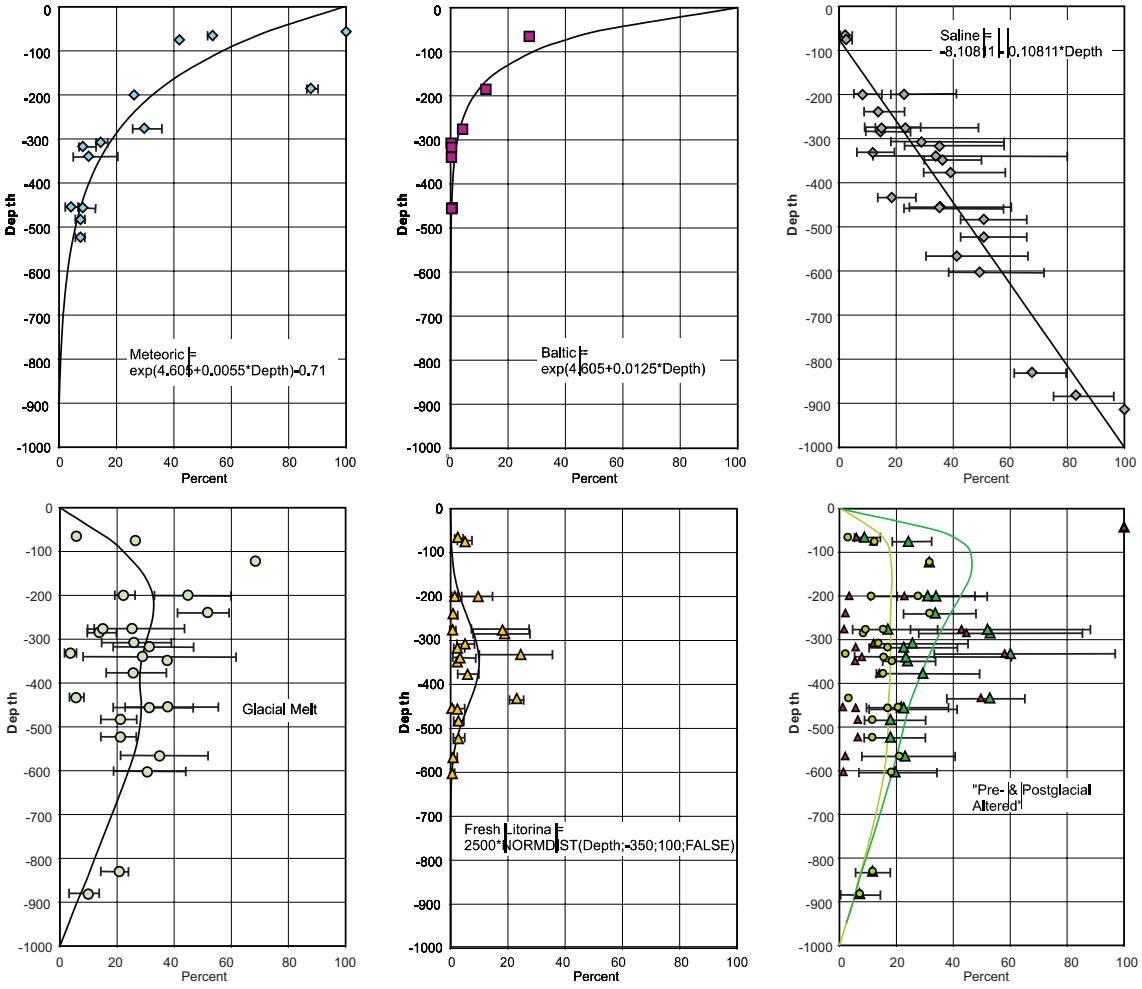

Figure 4-2 Depth distribution of reference water types. Observed mixing fractions of meteoric (blue diamonds), fresh Baltic (violet squares), saline (grey diamonds), glacial melt (light green circles), fresh Litorina (orange triangles), "preglacial altered" (green circles) and postglacial altered (red triangles) references in studied samples. Cumulative extreme mixing fractions stemming from analytical uncertainties of Cl and $\delta^{18}O$ are shown with error bars (cf. Ch. 2.3). The sum of "pre- and postglacial altered" fractions are marked by dark green triangles. Depth distribution regressions are shown with solid lines and further outlined in Figure 4-3.

The regression drawn in the glacial melt diagram (Fig. 4-2) is a visual approximation, which attempts to fit into the observations, and also model to some degree the negative correlation between the fresh Litorina and glacial melt references pointed out in the former Chapter. Compared with observations (cf. Table 4-1 and 4-3), regression considerably smoothens this negative correlation, shown as a local regression minimum in the glacial melt diagram (Fig. 4-2). However, the negative correlation and its depth relation possibly indicate an occasional density turnover phenomenon (younger saline Litorina water penetrates through lighter older glacial melt water) in the fracture zones of Äspö.

The depth distribution of the "preglacial" reference water type is considered in the last diagram of Figure 4-2. Observations are scattered and the regression approximation also includes palaeohydrological simplifications. Observed "preglacial altered" reference fractions are shown with green circles in Figure 4-2, and are closely related to glacial melt fractions. Therefore, the form of the "preglacial" (light green line) regression is bound to be more or less similar to glacial melt regression. According to the palaeohydrological interpretation (Fig. 3-1), the glacial melt and "preglacial altered" reference water types have affected bedrock groundwater compositions both at sea and in the dry land areas of Äspö.

As regards the postglacial altered reference type (red triangles in Fig. 4-2), it can be concluded that in most cases its fractions remain relatively low in the observed samples (cf. Table 4-1). High postglacial fractions are related to samples with a high Litorina component and to a certain set of shallow depth samples. Only one of the shallow depth samples has been used in this study: the postglacial reference water sample HAS13/ -42.0m giving the 100% maximum in the last diagram of Figure 4-2. Considering the palaeohydrological history of postglacial altered water, it is probable that it cannot be strictly related to early periods of the Litorina stage (cf. p. 7), but that new postglacial altered water has continuously developed and infiltrated into the bedrock up until now. In view of this, a simplified interpretation is that the postglacial altered water type has mostly affected the bedrock groundwater compositions in the sea areas of Äspö.

4.1.2 Geochemical boundaries for hydrological simulations

By following the simplifications of the preceding chapter, and making a couple of further assumptions, it is possible to formulate geochemical boundaries for conservative hydrological transport simulations of the Äspö area. However, it has to be kept in mind that the following proposition is based on a biased data set because there are no bedrock groundwater data available from below the sea areas of Äspö.

By assuming that in the land area only meteoric water infiltrates into the bedrock from the ground surface, we can sum up the meteoric, saline, glacial melt and fresh Litorina Sea regression curves from Figure 4-2. The remainder missing from the total of 100% gives us the regression curve for the "preglacial altered" reference type (Fig. 4-3). Similarly, in the sea area, only fresh Baltic Sea is assumed to infiltrate into the bedrock from the sea bottom, and the fresh Baltic Sea, saline, glacial melt and fresh Litorina Sea regression curves are summed up together from Figure 4-2. Now, in the sea area, the remainder missing from the total of 100% gives the sum regression curve (dark green line in Fig. 4-2) for the "pre-and postglacial altered" reference (Fig. 4-3). The "preglacial altered" part of this sum curve is similar to the "preglacial altered" regression curve for the land area. As the last diagram of Figure 4-2 shows, the modelled postglacial regression (the difference between the sum and "preglacial" regressions) attempts to model both the altered early Litorina stage seawater infiltrated down to -600m and more recent altered seawater infiltration. The postglacial altered reference fraction grows gradually with ascending depth, and if the postglacial and the fresh Baltic Sea regressions are summed up together, the sum curve is analogous to the meteoric regression curve shown in Figure 4-2.

Based on the reference water depth fraction relations shown in Figure 4-3, and the estimated Cl content of the reference water types (Table 3-1), the average Cl concentration as a function of depth below the dry land and sea areas of Äspö can be calculated. The Cl concentration distribution gives an estimate of overall salinity (TDS) variations, and the effects of density variations in the hydrological simulations can be calculated. The Cl concentration depth distributions are presented in Figure 4-4. The Cl content below the sea area is higher than below the dry land area. For the dry area, Cl concentrations diminish monotonically as a function of ascending depth, whereas in the sea area, the first 200m below the sea bottom exhibit a roughly constant Cl content. Below -700m Cl concentrations are similar below the sea and dry land areas.

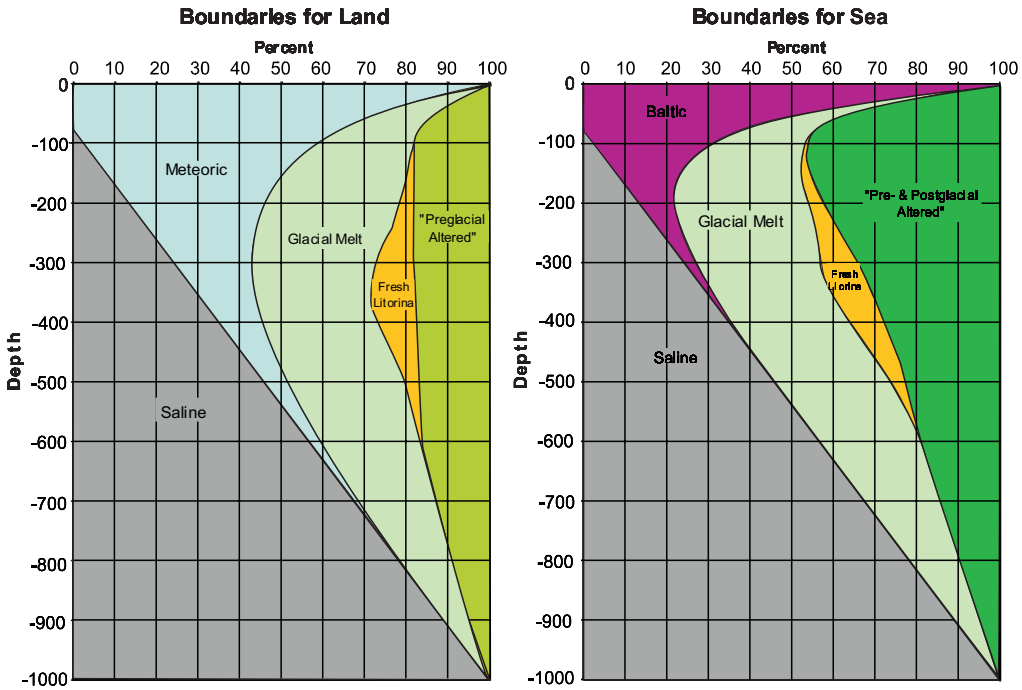

Figure 4-3 Proposed geochemical boundaries as a function of depth for sea and dry land areas of Äspö. Depth distributions of the reference water types summed from the regressions in Figure 4-2. For land areas, the water type sum is 100 – (meteoric + saline + glacial melt + fresh Litorina) = "preglacial altered". For sea areas, the sum is 100 – (fresh Baltic + saline + glacial melt + fresh Litorina) = "pre- and postglacial altered".

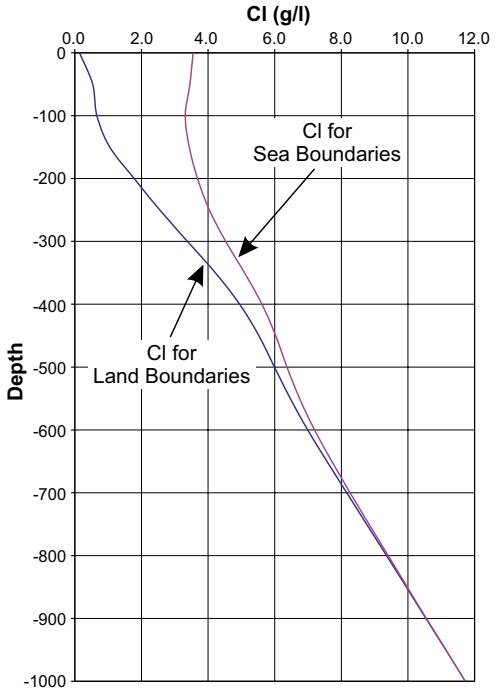

Figure 4-4 Proposed Cl concentration depth distributions for sea and dry land areas of Äspö.

4.2 Disturbed conditions

In the current study, the effects of tunnel construction are monitored with 10 control points. Eight of the control points are located along the main tunnel and two outside the tunnel system. The locations of control points are shown in Figure 4-5 and the basic information given by them is listed in Table 4-4. Disturbed samples, considered in the following, were sampled during the period July 19, 1991 to June 21, 1996.

For control points along the main tunnel, the sampled time series starts after the excavations have passed the sampling location. This means that the farther ahead in the main tunnel the control point is, the less samples are usually available from the control point. Furthermore, though the delivered disturbed data set is extensive for several control points, only the samples with reported values for both Cl and ^{18}O have been accepted for calculations. In all, the chemical characteristics of 75 samples were analysed. However, the Äspö redox zone is emphasised in this data set since 35 of the studied samples are from the control point KR0012B.

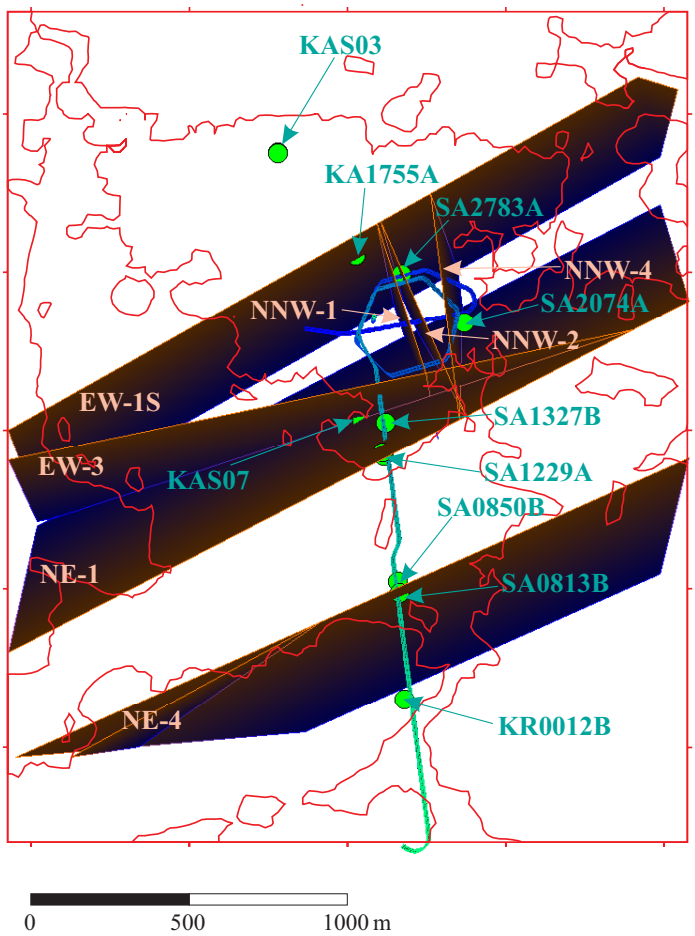

Figure 4-5 Location of the control points used for monitoring the impact of Äspö HRL excavations on bedrock groundwater chemistry.

Table 4-4 Borehole names, sampling sections and relations to fracture zones of the control points monitored as a function of advancing main tunnel excavations of the Äspö HRL.

Along the tunnel

CP	BH name	Depth (m.a.s.l.)	Secup (m)	Seclow (m)	Repr. HCD or HRD	Comments
1	KR0012B	-69.1	5.0	10.6	Redox zone	
2	SA0813B	-112.9	5.6	19.5	NE-4	
3	SA0850B	-117.7	1.0	19.8	NE-4	
4	SA1229A	-171.3	6.0	20.5	NE-1	Appr. 70 m South of the core of NE-1
5	SA1327B	-184.1	6.0	20.3	NE-1	Appr. 30 m North of the core of NE-1
6	KA1755A	-277.6	88.0	160.0	EW-1	Southern branch of EW-1
7	SA2074A	-281.7	6.0	38.7	NNW-4	
8	SA2783A	-371.4	5.8	19.9	NNW-2	Interpreted position of HCD NNW-2

Outside the tunnel

CP	BH name	Depth (m.a.s.l.)	Secup (m)	Seclow (m)	Repr. HCD or HRD	Comments
9	KAS03	-602.5	609.0	623.0		Pre-investigations
9	KAS03	-566.3	533.0	626.0		Construction phase
10	KAS07	-465.0	501.0	604.0	NE-1	Construction phase

CP = Control Point
BH = Borehole
HCD = Hydraulic Conductor Domain
HRD = Hydraulic Rock mass Domain

4.2.1 Control point characteristics

Control point *KR0012B* is located in the redox zone about 70m below ground level at Hålö Island to the south of Äspö (Fig. 4-5). The Cl and ^{18}O concentrations of KR0012B samples are shown in Figure 4-6a. The concentrations indicate quite strong meteoric affinity in all KR0012B samples. Control points *SA0813B and SA0850B* are both related to the fracture zone NE-4 about 115m below sea level between the Hålö and Äspö Islands (Fig. 4-5). According to Figure 4-6b two samples in this data set indicate significant contamination of postglacial altered water. In the control point SA0813A there are also clear signs of fresh Baltic Sea infiltration. Control points SA1229A and SA1327B locate within the fracture zone NE-1 below the southern parts of Äspö Island close to the seashore about 180m below ground level (Fig. 4-5). Figure 4-6c claims clear fresh Baltic Sea infiltration into these control points.

Control points *KA1755A, SA2074A and SA2783A* are all located below Äspö Island within the influence of the spiral part of the Äspö HRL. Control points KA1766A and SA2074A are located approximately 275m below the ground level, but KA1766 is within the EW-1S zone in the middle of the island, while SA2074 is related to the NNW-4 zone close to the seashore. The compositions of KA1755 are saline (Fig. 4-7a) whereas the control point SA2074A indicates contamination from surficial sources. The control point SA2783A is located along the lower spiral of the Äspö HRL within the zone NNW-2 about 370m below the ground level (Fig. 4-5). According to Figure 4-7a, disturbed samples at SA2783A indicate a saline character. Two samples are more saline than the samples from control point SA2074A.

Control points *KAS03 and KAS07* are located outside the tunnel system (Fig. 4-5). Control point KAS03 is in the northern part of Äspö Island about 570m below ground level. KAS03 seems somewhat isolated from the Äspö HRL. However, as Figure 4-7b indicates, construction of the tunnel system causes significant variation in the chemistry of the control point. According to Figure 4-7b, samples from KAS03 seem to contain significant amounts of glacial related water types. Control point KAS07 is located below the straight part of the HRL tunnel about 460m below ground level. KAS07 is situated below Äspö Island quite near the seashore. However, according to Figure 4-7b, the fresh Baltic Sea does not seem to infiltrate the control point. As indicated in Table 4-4, the control points SA1229A, SA1327B and KAS07 are probably all connected to the fracture zone NE-1. The first two control points are contaminated with fresh seawater as a result of excavations (cf. Fig. 4-6c).

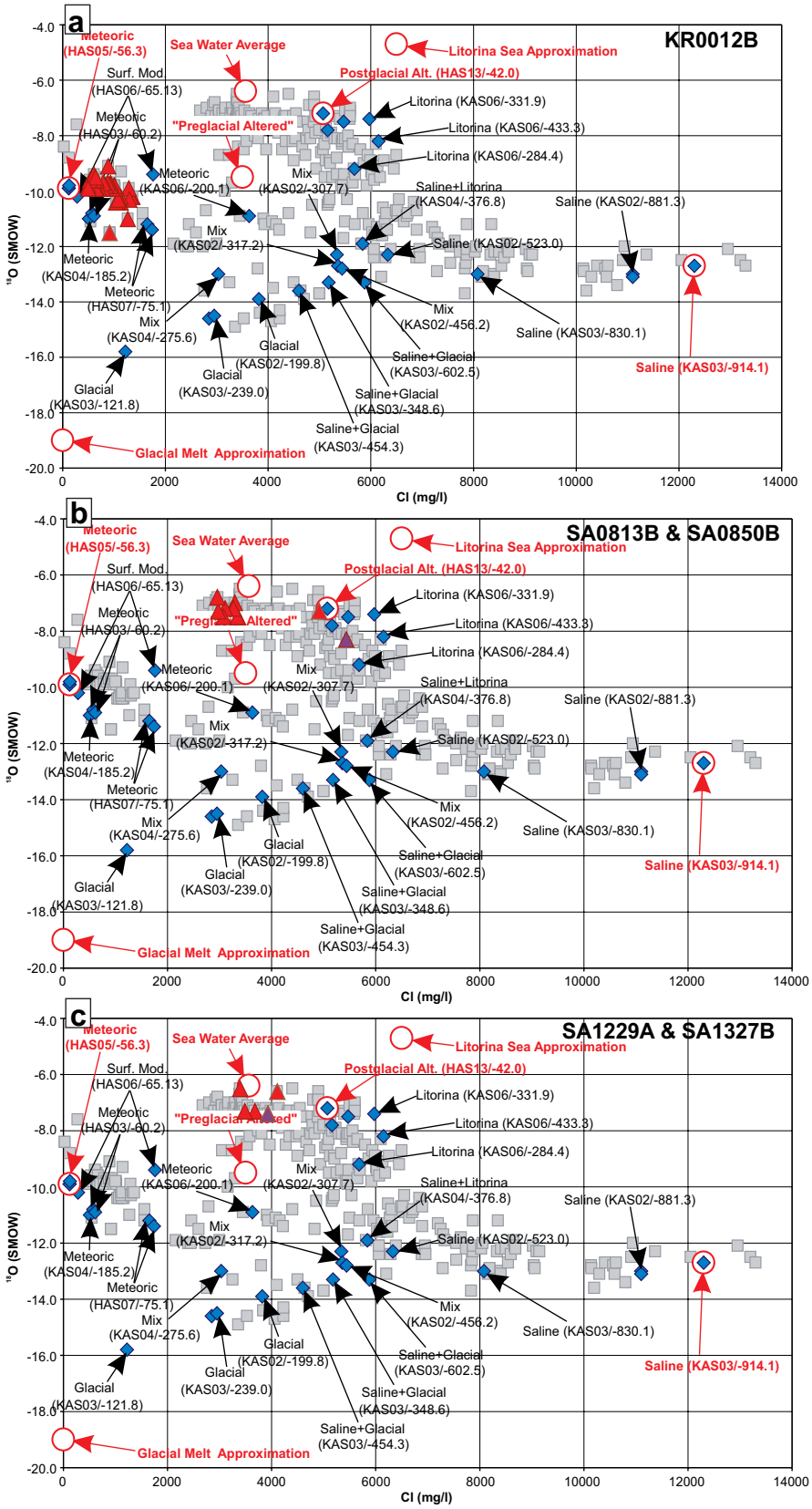

Figure 4-6 Disturbed KR0012B (red triangles – Fig. a), SA0813B (red triangles – Fig. b), SA0850B (purple triangle – Fig. b), SA1229A (red triangles – Fig. c), and SA1327B (purple triangle – Fig. c) samples in the Cl-^{18}O field.

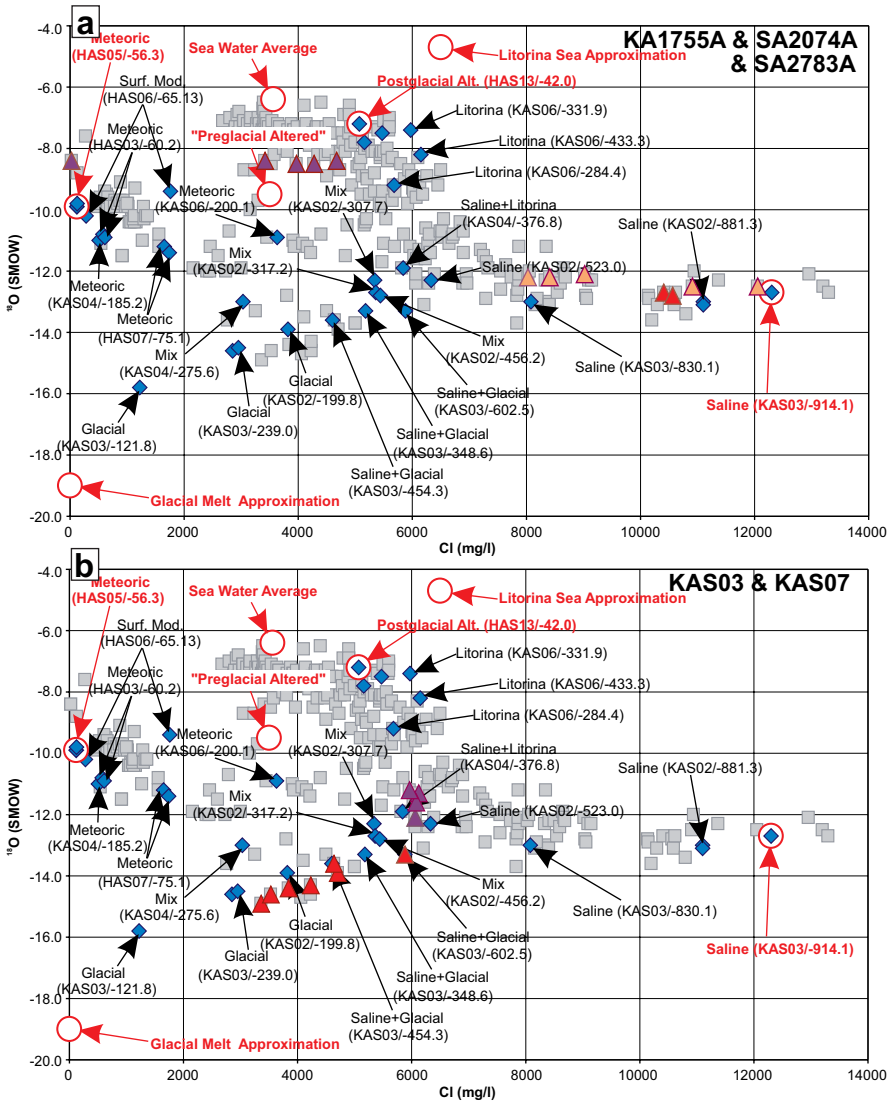

Figure 4-7 Disturbed KA1755A (red triangles – Fig. a), SA2074A (purple triangles – Fig. a), SA2783A (pink triangles – Fig. a), KAS03 (red triangles – Fig. b), and KAS07 (purple triangles – Fig. b) samples in the Cl-^{18}O field.

4.2.2 Evolution of mixing fractions at the control points

The evolution of disturbed mixing fractions of control point *KR0012B* as a function of time is shown in Table 4-5 and Figure 4-8. Initially, in undisturbed conditions (ref. day = 0), the control point is assumed to contain relatively a lot of meteoric water, moderate or low amounts of glacial melt and "preglacial altered" water types, and practically no water from fresh Baltic Sea, Litorina Sea or saline sources. The undisturbed assumption is based on the proposed average conditions for dry land areas presented in Figure 4-3. Therefore, the initial decrease of meteoric water fraction in disturbed conditions is uncertain, though it could be explained for example with a more or less lateral

groundwater flow to the control point (cf. Pitkänen et al. 1999b). However, more importantly the evolution in the disturbed condition shows that meteoric and fresh Baltic Sea water intrude into the control point from surficial sources, and at the same time glacial melt and "preglacial altered" water types begin to diminish. According to the results presented in Figure 4-8, the fraction of meteoric water seems to stabilise to slightly below the 90% level and the Baltic fraction to 10%.

Table 4-5 Reference water type mixing fractions (in percent) in the studied disturbed KR0012B water samples. The sampling dates given refer to the date 01.01.91. Estimated minimum and maximum fractions are noted after each representative value.

Sample	Day	Meteoric			Baltic Sea			Postgl. Alt.			Litorina Sea			Glacial Melt			"Pregl. Alt."			Saline			Sum
KR0012B	169	**55.0**	54.9	55.2				**5.3**	5.3	5.3	**2.2**	2.2	2.2	**24.9**	24.7	25.0	**11.5**	11.4	11.5	**1.1**	1.1	1.1	**100.0**
KR0012B	463	**59.2**	55.1	66.9	**10.3**	7.8	10.8	**6.3**	5.4	6.5	**2.6**	2.3	2.8	**13.9**	12.0	14.5	**6.4**	5.6	6.7	**1.3**	1.1	1.3	**100.0**
KR0012B	477	**62.7**	58.8	67.2	**10.7**	7.5	10.8	**5.5**	5.2	6.2	**2.3**	2.2	2.6	**12.1**	11.5	13.6	**5.6**	5.4	6.3	**1.1**	1.1	1.3	**100.0**
KR0012B	491	**63.6**	62.6	64.4	**12.2**	12.0	12.4	**5.0**	4.9	5.0	**2.1**	2.1	2.1	**11.0**	10.8	11.1	**5.1**	5.0	5.2	**1.0**	1.0	1.0	**100.0**
KR0012B	505	**62.8**	60.7	65.0	**9.2**	6.3	12.2	**5.7**	5.3	6.1	**2.4**	2.2	2.6	**12.7**	11.7	13.6	**5.9**	5.4	6.3	**1.2**	1.1	1.3	**100.0**
KR0012B	519	**64.0**	64.0	64.0				**7.4**	7.4	7.4	**3.1**	3.1	3.1	**16.4**	16.4	16.4	**7.6**	7.6	7.6	**1.5**	1.5	1.5	**100.0**
KR0012B	542	**66.6**	64.8	68.0	**6.3**	5.6	8.3	**5.6**	5.5	5.7	**2.3**	2.3	2.4	**12.3**	12.2	12.7	**5.7**	5.6	5.9	**1.1**	1.1	1.2	**100.0**
KR0012B	554	**68.0**	59.6	76.3	**7.0**	3.2	11.9	**5.1**	4.2	6.0	**2.2**	1.8	2.6	**11.4**	9.4	13.4	**5.3**	4.4	6.2	**1.0**	0.9	1.2	**100.0**
KR0012B	567	**68.3**	64.8	73.5	**6.3**	3.8	9.2	**5.2**	4.6	5.7	**2.2**	1.9	2.4	**11.6**	10.2	12.6	**5.4**	4.7	5.8	**1.1**	0.9	1.2	**100.0**
KR0012B	583	**70.4**	70.3	70.9	**4.4**	3.9	4.5	**5.2**	5.2	5.3	**2.2**	2.2	2.2	**11.5**	11.5	11.6	**5.3**	5.3	5.4	**1.1**	1.1	1.1	**100.0**
KR0012B	595	**71.3**	69.6	74.2	**7.1**	4.7	7.6	**4.4**	4.3	4.9	**1.9**	1.8	2.1	**9.8**	9.5	10.8	**4.6**	4.4	5.0	**0.9**	0.9	1.0	**100.0**
KR0012B	611	**70.1**	69.7	71.1	**5.4**	4.5	5.8	**5.0**	5.0	5.2	**2.1**	2.1	2.2	**11.1**	11.1	11.4	**5.2**	5.1	5.3	**1.0**	1.0	1.1	**100.0**
KR0012B	625	**70.4**	67.1	72.4	**10.9**	10.5	13.3	**3.8**	3.4	4.0	**1.6**	1.4	1.7	**8.5**	7.4	8.8	**3.9**	3.5	4.1	**0.8**	0.7	0.8	**100.0**
KR0012B	638	**71.1**	66.3	74.5	**10.3**	8.1	13.6	**3.8**	3.2	4.2	**1.6**	1.3	1.8	**8.5**	7.1	9.4	**3.9**	3.3	4.3	**0.8**	0.6	0.9	**100.0**
KR0012B	650	**71.4**	67.1	73.9	**10.5**	10.0	13.0	**3.7**	3.2	3.9	**1.6**	1.4	1.7	**8.2**	7.1	8.7	**3.8**	3.3	4.0	**0.8**	0.7	0.8	**100.0**
KR0012B	666	**72.2**	68.1	74.7	**9.3**	7.9	12.6	**3.8**	3.2	4.1	**1.6**	1.4	1.7	**8.4**	7.2	9.1	**3.9**	3.3	4.2	**0.8**	0.7	0.8	**100.0**
KR0012B	679	**72.9**	72.4	73.1	**11.5**	11.5	11.8	**3.2**	3.2	3.2	**1.4**	1.3	1.4	**7.1**	7.0	7.2	**3.3**	3.2	3.3	**0.7**	0.6	0.7	**100.0**
KR0012B	693	**74.7**	73.0	75.5	**9.1**	8.9	11.7	**3.3**	2.9	3.4	**1.4**	1.2	1.4	**7.4**	6.5	7.4	**3.4**	3.0	3.5	**0.7**	0.6	0.7	**100.0**
KR0012B	701	**74.9**	72.6	76.2	**9.2**	8.7	11.4	**3.3**	3.0	3.4	**1.4**	1.3	1.4	**7.2**	6.7	7.6	**3.4**	3.1	3.5	**0.7**	0.6	0.7	**100.0**
KR0012B	709	**77.4**	76.7	78.8	**19.5**	19.1	19.6	**0.6**	0.5	0.7	**0.3**	0.2	0.3	**1.4**	1.2	1.5	**0.7**	0.6	0.7	**0.1**	0.1	0.1	**100.0**
KR0012B	720	**75.5**	74.6	75.9	**10.4**	10.3	11.4	**2.9**	2.7	2.9	**1.2**	1.2	1.2	**6.4**	6.1	6.5	**3.0**	2.8	3.0	**0.6**	0.6	0.6	**100.0**
KR0012B	734	**76.8**	73.5	78.8	**8.2**	7.8	10.9	**3.1**	2.6	3.2	**1.3**	1.1	1.4	**6.8**	5.7	7.1	**3.2**	2.6	3.3	**0.6**	0.5	0.7	**100.0**
KR0012B	749	**76.7**	72.5	79.6	**8.5**	7.6	11.1	**3.0**	2.5	3.3	**1.3**	1.0	1.4	**6.7**	5.5	7.2	**3.1**	2.5	3.4	**0.6**	0.5	0.7	**100.0**
KR0012B	768	**76.4**	72.0	79.5	**8.8**	7.6	11.9	**3.0**	2.4	3.3	**1.3**	1.0	1.4	**6.7**	5.3	7.3	**3.1**	2.5	3.4	**0.6**	0.5	0.7	**100.0**
KR0012B	806	**78.1**	75.6	80.9	**8.6**	5.3	11.0	**2.7**	2.3	3.2	**1.2**	1.0	1.3	**6.0**	5.1	7.1	**2.8**	2.4	3.3	**0.6**	0.5	0.6	**100.0**
KR0012B	813	**77.7**	76.7	78.5	**9.5**	9.3	10.1	**2.6**	2.5	2.7	**1.1**	1.0	1.1	**5.8**	5.5	5.9	**2.7**	2.5	2.8	**0.5**	0.5	0.5	**100.0**
KR0012B	866	**81.4**	79.9	83.0	**5.0**	4.5	5.5	**2.8**	2.6	2.9	**1.2**	1.1	1.2	**6.2**	5.7	6.5	**2.9**	2.7	3.0	**0.6**	0.5	0.6	**100.0**
KR0012B	892	**81.1**	79.1	83.3	**4.7**	4.2	5.9	**2.9**	2.7	3.0	**1.2**	1.1	1.3	**6.4**	6.0	6.7	**3.0**	2.8	3.1	**0.6**	0.6	0.6	**100.0**
KR0012B	916	**84.1**	79.3	89.9	**6.7**	4.3	11.1	**1.9**	1.1	2.4	**0.8**	0.5	1.0	**4.2**	2.4	5.3	**1.9**	1.1	2.5	**0.4**	0.2	0.5	**100.0**
KR0012B	958	**84.1**	73.4	92.5	**10.2**	8.3	16.0	**1.2**	0.0	2.0	**0.5**	0.0	0.8	**2.6**	0.0	4.4	**1.2**	0.0	2.0	**0.2**	0.0	0.4	**100.0**
KR0012B	1042	**85.8**	75.7	93.1	**9.6**	7.7	15.3	**0.9**	0.0	1.8	**0.4**	0.0	0.8	**2.1**	0.0	4.0	**1.0**	0.0	1.8	**0.2**	0.0	0.4	**100.0**
KR0012B	1317	**88.7**	86.3	92.4	**7.1**	5.3	8.3	**0.9**	0.4	1.2	**0.4**	0.2	0.5	**1.9**	0.9	2.6	**0.9**	0.4	1.2	**0.2**	0.1	0.2	**100.0**
KR0012B	1343	**88.1**	80.6	94.0	**7.9**	6.6	13.0	**0.8**	0.0	1.4	**0.4**	0.0	0.6	**1.9**	0.0	3.1	**0.9**	0.0	1.4	**0.2**	0.0	0.3	**100.0**
KR0012B	1598	**85.3**	84.3	87.0	**14.7**	13.0	15.7																**100.0**
KR0012B	1743	**83.2**	78.9	86.9	**10.7**	9.5	13.8	**1.3**	0.6	1.5	**0.5**	0.2	0.6	**2.8**	1.3	3.2	**1.3**	0.6	1.5	**0.3**	0.1	0.3	**100.0**
KR0012B	1967	**87.8**	84.3	90.6	**2.2**	1.6	3.4	**2.0**	1.7	2.3	**0.9**	0.7	1.0	**4.5**	3.7	5.1	**2.1**	1.7	2.3	**0.4**	0.3	0.5	**100.0**

Based on the locations of the control points *SA0813B and SA0850B*, it can be assumed that in the undisturbed condition there is an insignificant amount of meteoric water (no source) and possibly only small amounts of fresh Baltic Sea water (no gradient) mixed with the existing groundwater. The postglacial altered water, slowly infiltrated through the sea bottom, and to a lesser extent the old relict water types (Litorina Sea, glacial melt, preglacial altered and saline), probably dominate the undisturbed groundwater

composition. According to Table 4-6 and Figure 4-8, this reasoning seems valid. The first disturbed samples (ref. day > 0) give distinct fractions for altered water types (here mostly postglacial altered). However, the mixing fractions rapidly change as a function of time. The fresh Baltic Sea, and somewhat surprisingly meteoric water, begin to intrude into the point SA0813B, while the fractions of postglacial altered and Litorina Sea begin to diminish. The meteoric water intrusion into SA0813B may originate either from small islands between Hålö and Äspö, or meteoric water possibly infiltrates from Hålö Island via the fracture zone NE-4. In the time-span considered (Fig. 4-8) it seems that the fresh Baltic Sea and meteoric fractions stabilise around the 75% and 25% level, respectively.

Although the control points *SA1229A and SA1327B* are located below the southern parts of Äspö, these points are easily influenced by seawater. Also the initial undisturbed conditions in Figure 4-8 have been assumed to be similar to those proposed for sea areas in Figure 4-3. According to Table 4-6 and Figure 4-8, the evolution of the control point SA1229A is quite similar to SA0813B. The fresh Baltic Sea fraction increases rapidly while all other reference water types lack a significant source, and begin to diminish. It seems that with time, fresh Baltic Sea water completely replaces all other water types at the point SA1229A.

Table 4-6 Reference water type mixing fractions (in percent) in the studied disturbed SA0850B, SA0813B, SA1327A and SA1229A water samples. The sampling dates given refer to the date 01.01.91. Estimated minimum and maximum fractions are noted after each representative value.

Sample	Day	Meteoric			Baltic Sea			Postgl. Alt.			Litorina Sea			Glacial Melt			"Pregl. Alt."			Saline			Sum
SA0850B	231	**8.3**	7.6	8.9				**67.1**	59.0	70.9	**7.9**	7.7	9.5	**7.8**	7.2	8.5	**3.9**	3.6	4.3	**4.9**	4.7	5.8	**100.0**
SA0813B	309	**1.7**	1.3	2.0	**38.7**	36.2	42.2	**33.2**	31.0	35.2	**14.0**	13.1	14.9	**3.5**	3.0	3.8	**1.8**	1.6	2.0	**7.0**	6.5	7.4	**100.0**
SA0813B	768	**21.0**	20.1	23.0	**62.5**	57.1	63.6	**9.6**	8.7	11.5	**4.1**	3.7	4.9	**0.6**	0.5	0.7	**0.3**	0.3	0.4	**2.0**	1.8	2.3	**100.0**
SA0813B	980	**13.7**	10.1	17.7	**74.3**	65.6	81.3	**7.0**	3.6	11.7	**3.0**	1.5	4.9	**0.4**	0.2	0.7	**0.2**	0.1	0.4	**1.4**	0.7	2.4	**100.0**
SA0813B	1002	**22.5**	20.1	23.5	**59.1**	56.4	63.6	**10.7**	8.7	11.7	**4.5**	3.7	4.9	**0.7**	0.5	0.7	**0.4**	0.3	0.4	**2.2**	1.8	2.4	**100.0**
SA0813B	1253	**19.2**	13.6	23.9	**68.0**	60.9	78.1	**7.4**	3.9	11.6	**3.1**	1.6	4.9	**0.5**	0.2	0.7	**0.3**	0.1	0.4	**1.5**	0.8	2.4	**100.0**
SA0813B	1343	**17.2**	17.2	17.8	**82.9**	82.2	82.9																**100.0**
SA0813B	1597	**27.3**	20.9	30.6	**58.3**	51.1	66.6	**8.3**	6.2	10.6	**3.5**	2.6	4.5	**0.5**	0.4	0.7	**0.3**	0.2	0.4	**1.7**	1.3	2.2	**100.0**
SA0813B	1745	**23.4**	18.7	29.1	**68.4**	57.4	78.3	**4.8**	1.3	9.1	**2.0**	0.6	3.8	**0.3**	0.1	0.6	**0.2**	0.0	0.3	**1.0**	0.3	1.9	**100.0**
SA0813B	1967	**16.0**	15.3	16.8	**80.1**	78.6	84.1	**2.2**	0.4	3.5	**0.9**	0.1	1.5	**0.1**	0.0	0.2	**0.1**	0.0	0.1	**0.5**	0.1	0.7	**100.0**
SA1327A	653	**5.9**	5.8	6.3	**59.7**	59.2	64.9	**15.4**	12.1	16.0	**6.5**	5.1	6.8	**5.7**	5.4	6.0	**2.9**	2.7	3.0	**3.9**	3.2	4.1	**100.0**
SA1229A	966				**68.1**	64.2	72.5	**18.5**	16.0	20.8	**7.8**	6.7	8.8	**1.2**	1.0	1.3	**0.6**	0.6	0.7	**3.8**	3.3	4.2	**100.0**
SA1229A	1253	**4.8**	3.2	5.7	**65.1**	59.4	70.1	**13.8**	9.4	19.3	**5.8**	4.0	8.2	**4.7**	3.1	5.7	**2.4**	1.6	2.9	**3.4**	2.3	4.7	**100.0**
SA1229A	1598	**6.0**	5.1	6.3	**69.8**	65.5	76.2	**9.5**	5.7	12.9	**4.0**	2.4	5.5	**5.3**	4.4	5.8	**2.7**	2.2	2.9	**2.7**	1.8	3.5	**100.0**
SA1229A	1744	**6.4**	5.2	6.4	**75.6**	75.6	80.0	**5.6**	4.5	5.6	**2.4**	1.9	2.4	**5.4**	4.4	5.4	**2.7**	2.2	2.7	**2.0**	1.6	2.0	**100.0**
SA1229A	1967	**0.6**	0.0	1.2	**97.8**	95.6	100	**0.5**	0.0	1.0	**0.2**	0.0	0.4	**0.5**	0.0	1.0	**0.2**	0.0	0.5	**0.2**	0.0	0.4	**100.0**

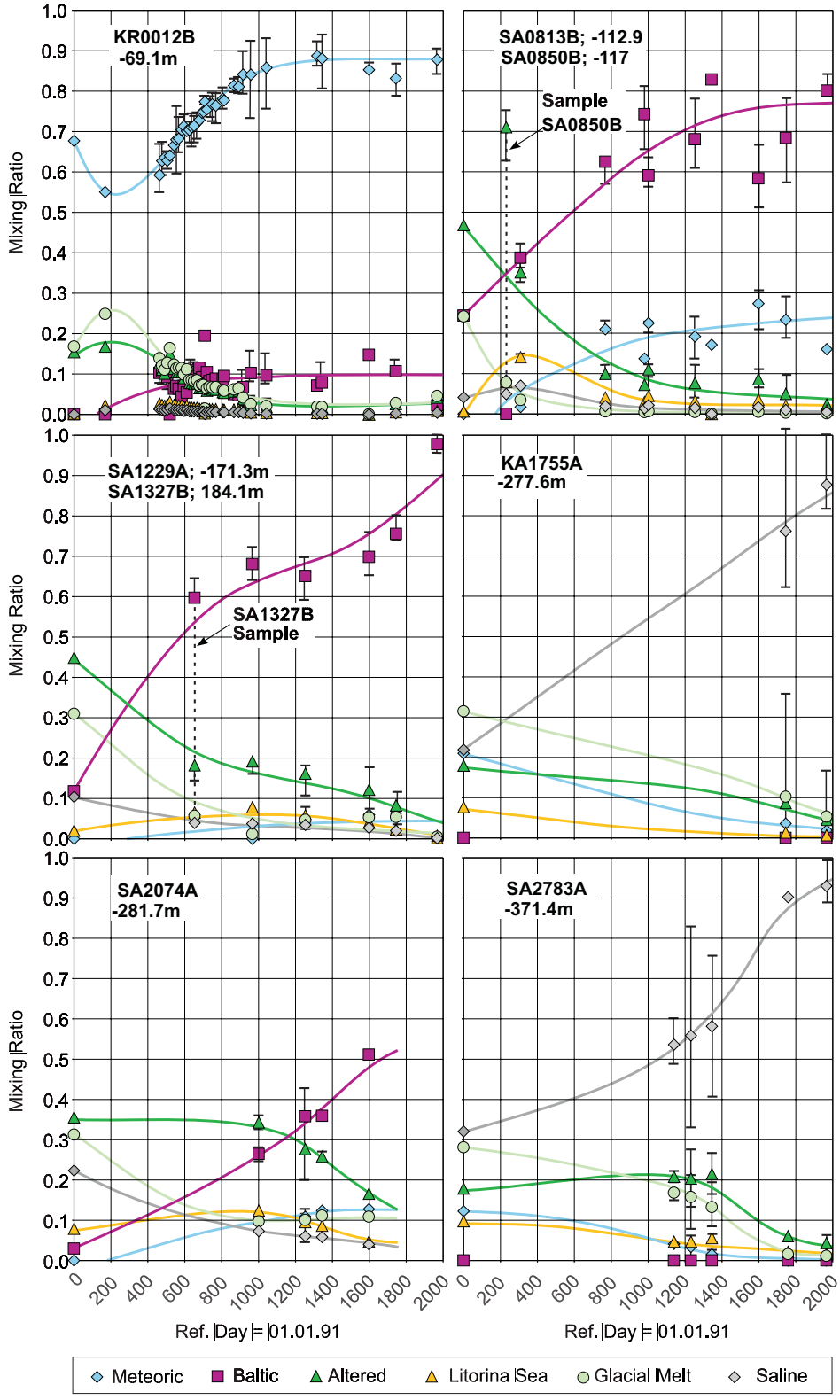

Figure 4-8 Reference water type mixing fractions at control points KR0012B, SA0813B, SA0850B, SA1229A, SA1327B, KA1755A SA2074A and SA2783A as a function of time. Error bars show cumulative maximum errors in mixing fractions. The mixing fractions on the vertical axes (ref. day = 0) are assumed to be undisturbed fractions based on Figure 4-3. Drawn regressions are visual approximations.

There are only two disturbed samples available from the control point *KA1755A* and both samples indicate quite saline character (Table 4-7, Fig. 4-8). The undisturbed boundary assumption (ref. day = 0) for dry land area predicts saline water fraction about to 30% level for the control point, but the studied samples give around 80% fractions of saline water type. All other reference types seem to lack significant sources, and their fractions are diminishing with time.

The control point *SA2074A* has an apparently good structural relation to Baltic Sea like the control points SA1229A and SA1327B. The difference between these points is that SA2074A resides about 100m deeper down in the bedrock than the other two control points. Therefore, it can be expected that seawater intrusion into SA2074A is more peaceful. According Table 4-7 and Figure 4-8, both fresh Baltic Sea and meteoric water are intruding into SA2074A, while the rest reference water type fractions are diminishing with time. In the source data there are in all five disturbed samples with conservative Cl and ^{18}O concentrations available. However, the first sample of this time-series (ref. day = 766) has been considered contaminated in this study (Appendix 5). On the basis of Cl-concentration (cf. Fig. 4-7a) this sample is practically fresh. Furthermore, tunnel excavation reports indicate that on the sampling date the tunnel face position was only three metres away from the sampling point.

In principle control point *SA2783A* could be in connection to sea via structure NNW-2. However, this connection cannot be verified from the disturbed data set indicating that the fracture zone is possibly not a major conductor or extensive in the Äspö bedrock. The SA2783A evolution under disturbed conditions is similar to the control point KA1755A, though it locates about 100m downward from the point KA1755A. As Table 4-7 and Figure 4-8 shows only saline water from depth seem to intrude into the control point.

According to Table 4-7 and Figure 4-9, a complex evolution occurs in the control point *KAS03* with time. In the undisturbed condition the dry land conditions (cf. Fig. 4-3) are assumed to prevail in the control point. Exceptionally, this assumption can be verified since there is an undisturbed sampling available 40m away from the disturbed sampling point (cf. Table 4-4, Fig. 4-9). Based on disturbed condition calculation results, it seems that groundwater in control point KAS03 has diluted considerably during year 1992. The fraction of saline water diminishes and the fraction of glacial melt increases distinctly. These changes are possibly related to HRL elevator and ventilation shaft excavations, and to excavations of the main tunnel that advanced to the upper spiral of the HRL. In the southern Äspö the hydraulic pressure minimum at depth about 200m below the ground level may have caused in the northern Äspö intrusion of glacial melt rich water into the control point KAS03 at depth about 560m below ground level. In such case, glacial melt rich water was probably drawn down from shallower depths. The situation is inverted later on as the excavations advance to deeper depths. Saline water intrudes into the control point and the fraction of glacial melt begins to diminish. The studied (Fig. 4-9) time span does not clarify whether the salinity increase means a recovery of undisturbed condition or is it a consequence of saline water welling up as a result of HRL pressure minimum.

Table 4-7 Reference water type mixing fractions (in percent) in the studied disturbed KA1755A, SA2074A, SA2783A, KAS03 and KAS07 water samples. The sampling dates given refer to the date 01.01.91. Estimated minimum and maximum fractions are noted after each representative value.

Sample	Day	Meteoric			Baltic Sea			Postgl. Alt.			Litorina Sea			Glacial Melt			"Pregl. Alt."			Saline			Sum
KA1755A	1745	**3.6**	1.6	3.6				**3.1**	1.4	3.1	**1.3**	0.6	0.6	**10.2**	4.4	10.2	**5.5**	2.4	5.5	**76.2**	62.3	100	**100.0**
KA1755A	1967	**1.9**	0.9	1.9				**1.6**	0.8	1.6	**0.7**	0.3	0.3	**5.3**	2.7	5.3	**2.9**	1.5	2.9	**87.7**	81.4	100	**100.0**
SA2074A	766	Contaminated sample																					
SA2074A	1001	**9.9**	9.7	10.3	**26.5**	24.6	27.9	**29.3**	27.8	30.7	**12.4**	11.7	13.0	**9.7**	9.5	10.1	**4.9**	4.8	5.1	**7.3**	7.0	7.6	**100.0**
SA2074A	1253	**10.9**	9.1	12.6	**35.8**	26.4	42.8	**22.6**	15.8	31.2	**9.5**	6.7	13.2	**10.1**	8.2	12.0	**5.1**	4.1	6.1	**6.1**	4.4	8.0	**100.0**
SA2074A	1344	**12.4**	12.2	12.4	**35.9**	34.7	36	**20.5**	20.3	21.4	**8.6**	8.6	9.0	**11.1**	11.0	11.2	**5.6**	5.5	5.6	**5.8**	5.8	6.0	**100.0**
SA2074A	1598	**12.8**	12.6	12.8	**51.1**	51.1	51.6	**11.1**	11.0	11.1	**4.7**	4.7	4.7	**10.9**	10.7	10.9	**5.4**	5.4	5.4	**4.0**	3.9	4.0	**100.0**
SA2783A	1140	**4.1**	3.5	4.1				**11.1**	10.5	11.6	**4.7**	4.4	4.9	**16.8**	14.9	17.8	**9.7**	8.7	10.4	**53.6**	48.9	60.3	**100.0**
SA2783A	1232	**3.4**	0.9	4.0				**11.0**	8.3	14.6	**4.7**	3.5	6.2	**15.8**	7.9	21.1	**9.3**	4.9	12.7	**55.9**	33.1	83.0	**100.0**
SA2783A	1345	**1.5**	0.4	2.6				**13.2**	10.9	15.4	**5.6**	4.6	6.5	**13.3**	8.6	17.9	**8.3**	5.6	11.0	**58.2**	40.9	75.6	**100.0**
SA2783A	1758							**5.1**	4.7	5.1	**2.2**	2.0	2.2	**1.6**	1.5	1.6	**1.0**	0.9	1.0	**90.2**	90.1	91.1	**100.0**
SA2783A	1966							**3.6**	1.1	5.1	**1.5**	0.5	2.2	**1.1**	0.3	1.6	**0.7**	0.2	1.0	**93.0**	88.9	99.2	**100.0**
KAS03	-850							**1.4**	1.2	1.6	**0.6**	0.5	0.7	**30.6**	26.3	34.9	**18.1**	15.6	20.7	**49.2**	43.3	55.2	**100.0**
KAS03	596							**0.6**	0.6	0.6	**0.2**	0.2	0.2	**53.1**	52.9	53.3	**26.1**	26.0	26.3	**19.9**	19.8	20.0	**100.0**
KAS03	768							**0.6**	0.6	0.6	**0.3**	0.3	0.3	**51.8**	51.8	51.9	**25.7**	25.7	25.7	**21.6**	21.6	21.6	**100.0**
KAS03	866							**1.9**	1.9	1.9	**0.8**	0.8	0.8	**46.4**	46.4	46.5	**28.2**	28.2	28.3	**22.6**	22.5	22.6	**100.0**
KAS03	958							**1.7**	1.6	1.7	**0.7**	0.7	0.7	**38.3**	36.1	40.2	**23.0**	21.7	24.2	**36.4**	35.0	38.1	**100.0**
KAS03	980							**1.9**	1.8	1.9	**0.8**	0.8	0.8	**44.7**	44.1	45.7	**27.1**	26.7	27.8	**25.6**	24.5	25.8	**100.0**
KAS03	1197							**1.7**	1.6	1.8	**0.7**	0.7	0.8	**39.4**	36.0	41.4	**23.8**	21.7	24.9	**34.4**	33.5	37.7	**100.0**
KAS07	608							**12.4**	11.9	12.4	**5.2**	5.0	5.2	**26.3**	26.2	26.6	**15.6**	15.6	15.8	**40.4**	40.3	40.9	**100.0**
KAS07	979	**5.2**	5.2	5.5				**17.9**	16.0	18.4	**7.5**	6.8	7.8	**19.0**	18.3	19.9	**10.5**	10.1	11.0	**39.9**	39.0	42.0	**100.0**
KAS07	1197							**16.6**	16.1	16.9	**7.0**	6.8	7.1	**23.3**	18.7	27.2	**13.8**	11.1	16.0	**39.4**	29.8	49.0	**100.0**
KAS07	1344	**5.3**	4.9	5.3				**17.5**	17.2	20.0	**7.4**	7.3	8.4	**19.0**	17.9	19.8	**10.6**	9.9	11.0	**40.2**	37.5	41.0	**100.0**

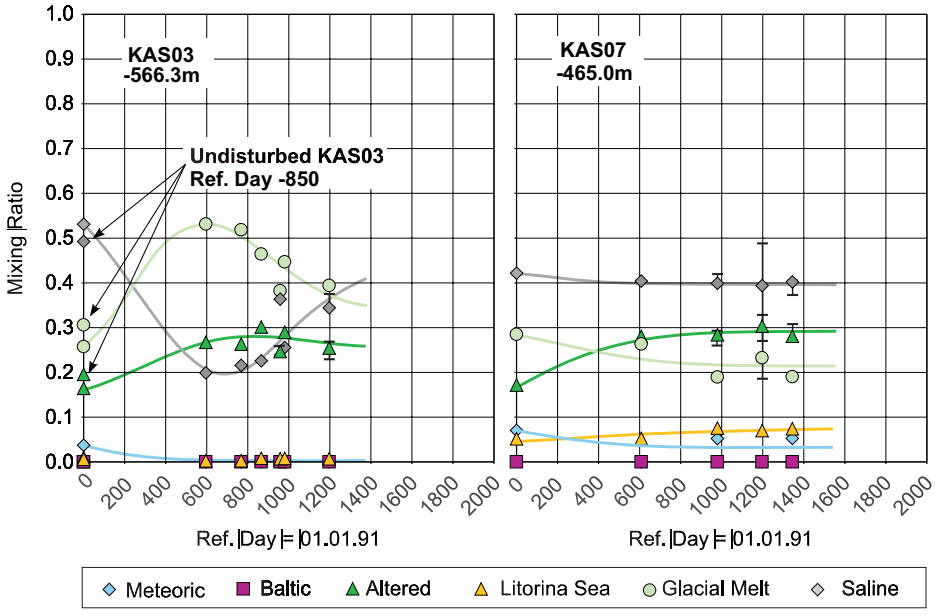

Figure 4-9 Reference water type mixing fractions at control points KAS03 and KAS07 as a function of time. Error bars show cumulative maximum errors in mixing fractions. The mixing fractions on the vertical axes (ref. day = 0) are assumed to be undisturbed fractions based on Figure 4-3. Drawn regressions are visual approximations.

According to the calculations, conditions at the control point KAS07 remain stable in disturbed conditions. In Table 4-7 and Figure 4-9, no significant changes can be identified between the undisturbed assumption and the disturbed samples. As pointed out earlier, the result is interesting because the control points SA1229A, SA1327B and KAS07 are all related to structure NE-1, although the point KAS07 is located almost 300m deeper than the former two.

4.2.3 Mole transfers as a function of mixing fractions

Inverse calculations produce a data set of mole transfers (Appendices 2–6) that can be studied as a function of reference water mixing fractions. In Figures 4-10…4-13 the trends in mole transfers are considered as a function of meteoric, fresh seawater, saline and altered water mixing fractions.

Figure 4-10 considers samples with a high fraction (over 50%) of meteoric water, and shows that precipitation of calcite and pyrite, and dissolution of organic matter tend to increase with an increasing fraction of meteoric water. At the same time Na is depleted, and Ca, Mg and Fe are enriched in the groundwater due to cation exchange processes.

Figure 4-11 shows the mole-transfer processes in samples with a high fraction (over 50%) of fresh Baltic Sea water. As the fresh seawater fraction increases, increasing and significant mole-transfer reactions are needed. Extensive, organic activity-driven redox reactions are bound to happen mostly in sea bottom sediments where the organic activity is strong enough. During infiltration fresh seawater dissolves organic matter and calcite. Simultaneously, Na and Mg concentrations are strongly depleted while Ca and Fe are enriched. A significant part of the dissolved iron subsequently precipitates from the solution as pyrite.

Compared to strong mole transfers related to infiltration of surficial meteoric or seawater water, mole transfers related to saline water welling up from depth are minor. According to Figure 4-12, the processes in samples with a high fraction (over 50%) of saline water are negligible and mixing of saline water is practically a conservative process. This indicates that saline water is mostly well equilibrated for the deep bedrock geochemical conditions.

Finally, there is a disturbed sample group in which none of the reference water type fractions dominates. These samples are presented in Figure 4-13. It would seem that the mole transfers in these samples are almost as negligible as in the case of samples rich in saline water. As in the case of saline samples, it can be concluded that these samples are well equilibrated for the deep bedrock geochemical conditions and only small or negligible mole-transfer reactions occur during groundwater mixings.

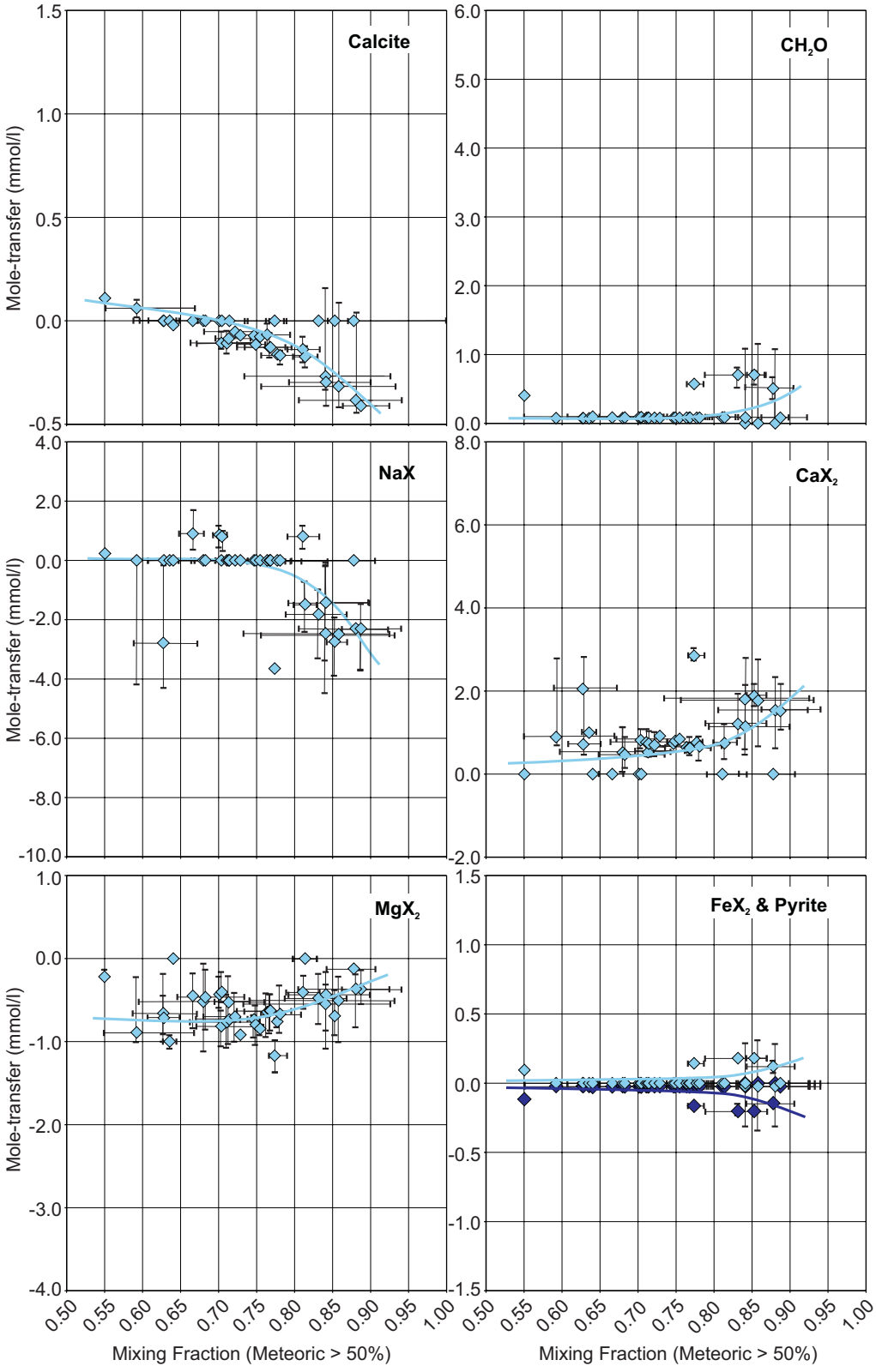

Figure 4-10 Mole transfers as a function of meteoric water fraction in samples containing over 50% meteoric water. Cumulative maximum errors in mixing fractions and maximum errors related to mole transfers are shown with error bars. Drawn regressions are visual approximations. Pyrite mole transfers are shown with dark blue diamonds.

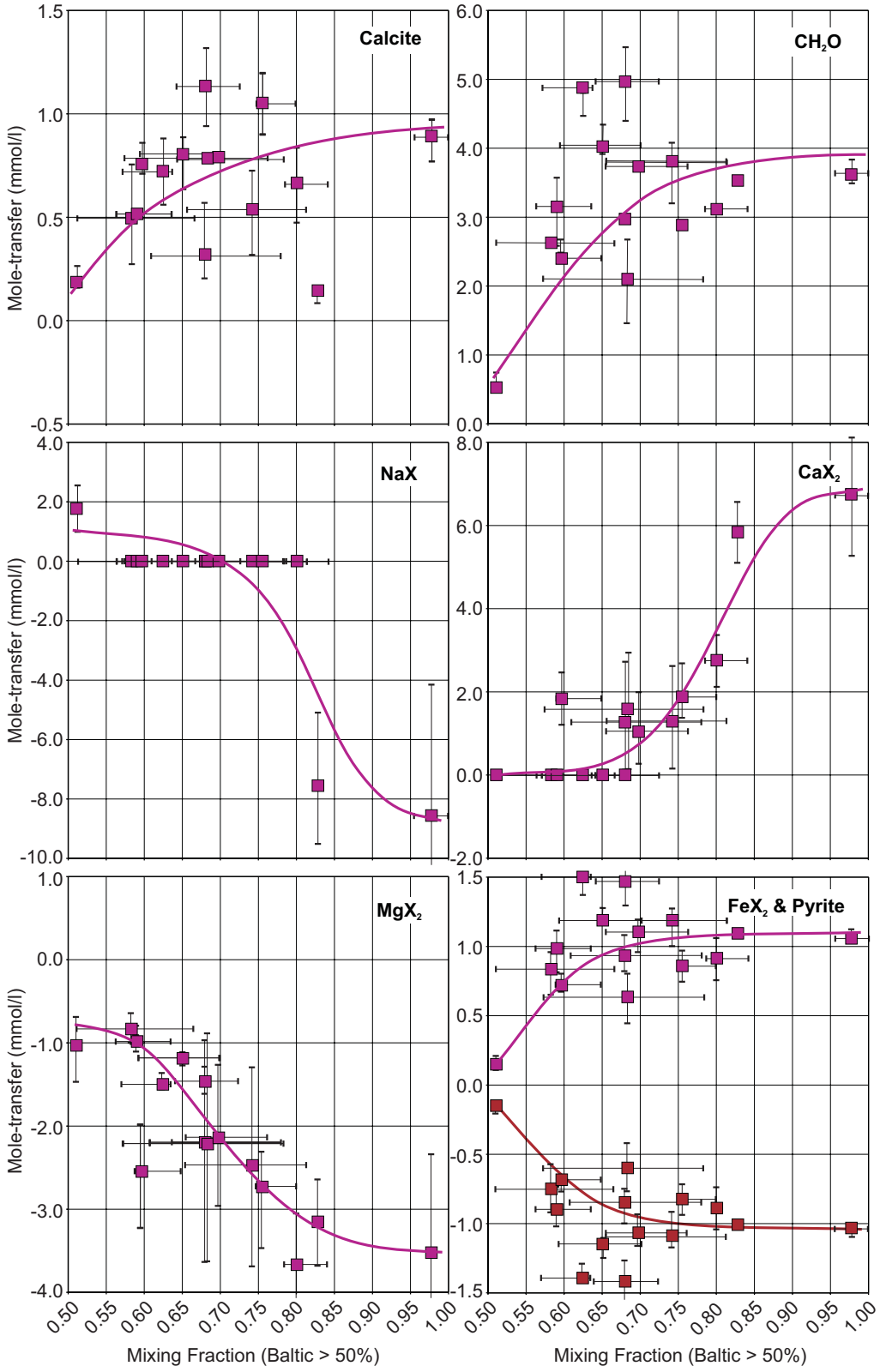

Figure 4-11 Mole transfers as a function of fresh Baltic Sea fraction in samples containing over 50% seawater. Cumulative maximum errors in mixing fractions and maximum errors related to mole transfers are shown with error bars. Drawn regressions are visual approximations. Pyrite mole transfers are shown with brown squares.

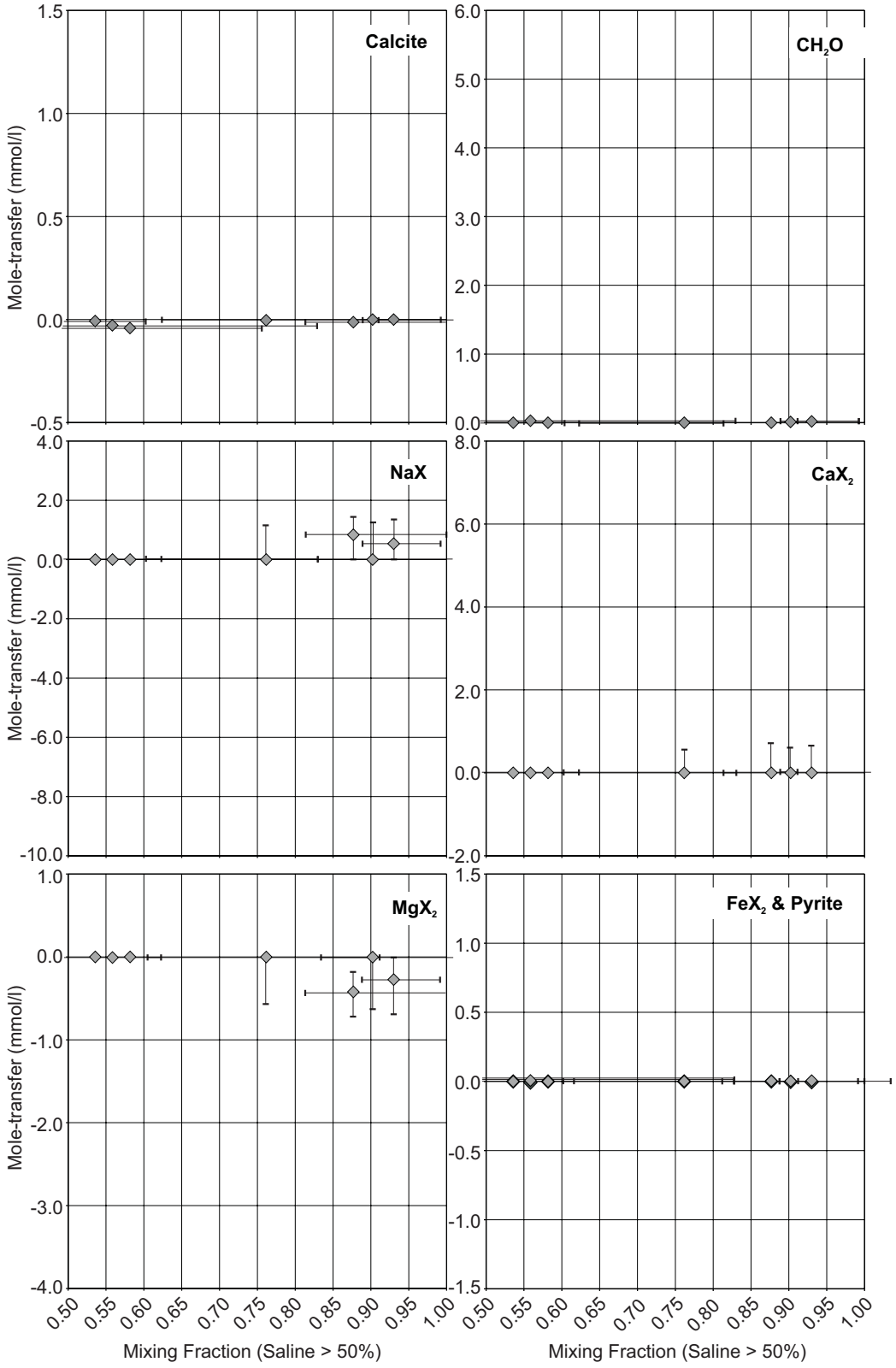

Figure 4-12 Mole transfers as a function of saline fraction in samples containing over 50% saline water. Cumulative maximum errors in mixing fractions and maximum errors related to mole transfers are shown with error bars. Drawn regressions are visual approximations. Pyrite mole transfers are shown with black diamonds.

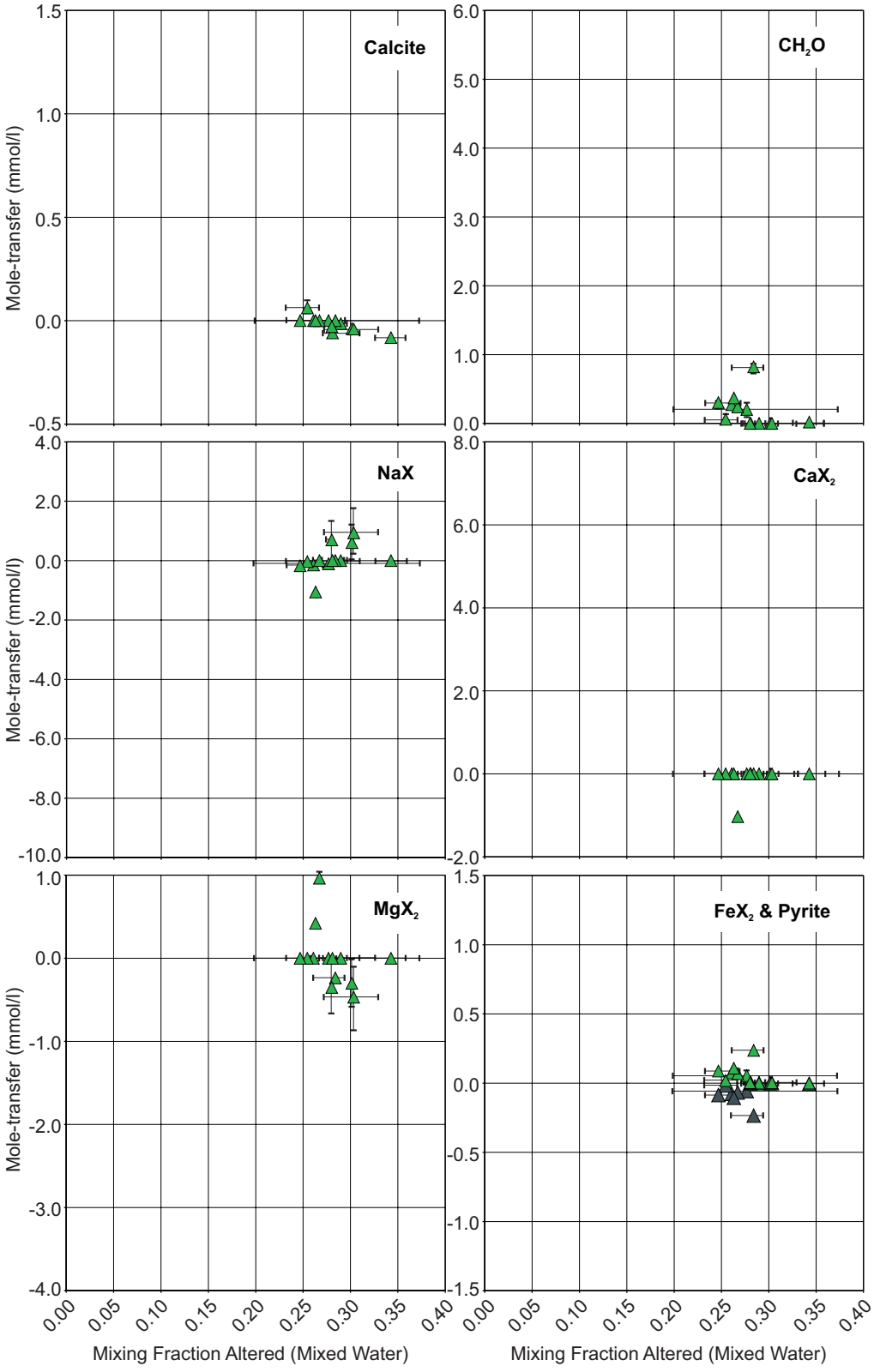

Figure 4-13 Mole transfers as a function of "pre- and postglacial altered" sum fraction in samples containing less than 50% meteoric, fresh Baltic Sea and saline water. Cumulative maximum errors in mixing fractions and maximum errors related to mole transfers are shown with error bars. Pyrite mole transfers are shown with dark green triangles.

5 Discussion

5.1 Error estimations of mixing fractions

The current results are based on the assumption that in undisturbed conditions the hydrodynamic flow field is quiet and the mixing-driven geochemical mole-transfer reactions have plenty of time to react. The error limit calculations for undisturbed conditions, on the other hand, indicate (cf. Table 4-1 and Fig. 4-2) that there are significant uncertainties in postglacial, glacial melt, preglacial and saline reference water fractions for samples from depths -200m – -600m. However, these uncertainties can be attributed mostly to calculatory technical facts and deficient analytical data.

The mixing fractions for samples at moderate depths are inevitably the result of several inverse calculation steps, and the error limits gradually widen during each step of the calculation chain. Tightening the default uncertainties defined for the used conservative parameters (ΔCl = 7%, $\Delta\delta^{18}O$ = 0.1 units) would damp down the error limit propagation. However, such "systematic improvement of analytical precision" for conservative parameters only is without solid basis.

The current mixing fractions were defined in the x(Cl)–y(^{18}O) field (e.g. Fig. 3-4). The calculations would be more robust, and in most cases error limits would strongly converge towards estimate values, if mixing fractions could be defined in the x(Cl,Br)–y(^{18}O,^{2}H) field. Both Cl and Br, and ^{18}O and ^{2}H are known to correlate strongly with each other. Therefore the location of a sample in the x-y field would be a best fit of four variables.

Table 5-1 gives an example of this. The first result column is analogous to Appendix 1, and the mixing fractions for KAS06/-331.9m have been defined with parameters Cl and ^{18}O only. In the next result column Br has been added to conservative parameters. However, in the present data, analytical uncertainties for Br are known to be large (e.g. Banwart et al. 1995), and for current purposes the Br uncertainty for samples was defined as 20%. As Table 5-1 shows, this large uncertainty has no effect on the present calculations. In the third result column, the sample locations in the y-direction were defined as the best fit of given values and uncertainties for ^{18}O and ^{2}H. The results show such a large decrease in mixing fraction uncertainties that the uncertainty ranges do not show up in two digit fractions. The fourth result column in Table 5-1 is analogous to the second column; i.e. the addition of Br, with the uncertainties considered, makes no improvements over the previous calculation (third column).

Table 5-1 Mole-transfer results for the undisturbed sample KAS06/-331.9m. The four result columns have been calculated with different sets of conservative parameters. The uncertainties of the parameters are indicated in the bottom of each column. The reference days given with the sample ID indicate the sampling date and refer to Jan. 1, 1991. The upper part shows mixing fractions of initial water samples for each final water. All mole and redox transfers are in mmol/l. A negative value indicates precipitation/cation uptake and a positive value dissolution/cation release. Minimum and maximum fractions and mole transfers possible within given analytical uncertainties are denoted after the representative values.

Final Water

Initial Water	Sample		KAS06/-331.9m			KAS06/-331.9m			KAS06/-331.9m			KAS06/-331.9m		
		Date	-566			-566			-566			-566		
	Litorina Sea		0.10	0.03	0.14	0.10	0.03	0.14	0.03	0.03	0.03	0.03	0.03	0.03
	KAS06/-433.3	-559	0.64	0.45	0.71	0.64	0.45	0.71	0.48	0.48	0.48	0.48	0.48	0.48
	HAS13/-42.0	-547	0.26	0.16	0.51	0.26	0.16	0.51	0.49	0.49	0.49	0.49	0.49	0.49
	Transfers (mmol/l)													
	Calcite		-0.03	-2.06	-0.03	-0.03	-2.06	-0.03	-0.58	-0.85	-0.34	-0.58	-0.85	-0.34
	CH_2O		0.00	0.00	2.10	0.00	0.00	2.10	0.09	0.05	0.16	0.09	0.05	0.16
	NaX		2.59	0.62	6.44	2.59	0.62	6.44	3.28	0.99	5.59	3.28	0.99	5.59
	CaX_2													
	MgX_2		-1.29	-2.74	-0.29	-1.29	-2.74	-0.29	-1.27	-2.26	-0.29	-1.27	-2.26	-0.29
	Goethite		0.00	0.00	1.59	0.00	0.00	1.59	0.36	0.19	0.54	0.36	0.19	0.54
	FeX_2		0.00	-1.14	0.00	0.00	-1.14	0.00	-0.37	-0.55	-0.21	-0.37	-0.55	-0.21
	Pyrite		0.00	-0.49	0.00	0.00	-0.49	0.00	0.00	-0.01	0.00	0.00	-0.01	0.00
	Redox (mmol/l)													
	Fe(3)		0.00			0.00			0.00			0.00		
	H(0)		0.00			0.00			0.00			0.00		
	S(-2)													
			ΔCl = 7%			ΔCl = 7%			ΔCl = 7%			ΔCl = 7%		
			$\Delta\delta^{18}O$ = 0.1			ΔBr = 20%			$\Delta\delta^{18}O$ = 0.1			ΔBr = 20%		
						$\Delta\delta^{18}O$ = 0.1			$\Delta\delta^{2}H$ = 0.1			$\Delta\delta^{18}O$ = 0.1		
												$\Delta\delta^{2}H$ = 0.1		

Although the addition of ^2H among the conservative parameters seems to improve mixing fraction interpretations, ^2H information has not been included in the inverse modelling calculations. ^2H data refine the location of the samples in the y-direction, whereas the Br data available do not add precision in the x-direction. It was decided at the start of the inverse calculations that the mixing calculations would be carried out solely with Cl and ^{18}O.

5.2 Confidence of mole transfer results

At the start of the calculations, the inverse-modelling approach was simplified as much as possible. Only cation balances among ions Na, Ca, Mg and Fe were considered, excluding potassium. In view of the current results, it is possible that the mole-transfer results would be more realistic if potassium were included among the ion-exchange phases. Furthermore, only the essential reacting phases were defined for the study, i.e. dissolvable silicate phases were not considered (deficiencies in the delivered data). However, all additions to variables probably render mole-transfer interpretations based on 25 undisturbed samples increasingly cumbersome (cf. Tables 4-2 and 4-3). The basic issue is that there is an even higher demand for a larger number of undisturbed samples than there is a need to include more variables in the analyses. Specifically, in the delivered data there were no undisturbed samples available from the areas below the present Baltic Sea. These data would support the depth distribution interpretations of reference water types below sea areas, now done solely with bedrock groundwater data below the dry land areas.

An important aspect of increasing the reliability of inverse modelling results is to include carbon and sulphur isotopic modellings in the studies. As noted in Chapter 2, several assumptions were made as to the origin and processes related to HCO_3 and SO_4 concentrations in groundwater. In respect of HCO_3, it was assumed that the main processes producing bicarbonate are anaerobic oxidation of organic matter (CH_2O) and dissolution of calcite. The main process consuming bicarbonate is precipitation of calcite. Similarly, in the case of SO_4 it was assumed that the sulphate dissolved in the shallow groundwater is mostly directly or indirectly contributed by seawater. Sulphate is reduced and precipitated away only as pyrite, and pyrite oxidation is not considered to be a source of aqueous sulphate. In deep groundwater sulphate reduction processes were considered insignificant. However, these assumptions were reasoned, and neither isotopic data nor modelling results on isotopic dilution and fractionation can be used to support the assumptions.

5.3 Choice of reference water types

In the M3 method, the reference water types define a polygon on the PC_1 vs. PC_2 plot. All obtained samples are supposed to plot within this polygon (Laaksoharju et al., 1999a). The logic is clear, if a sample is mixture of the reference water types, it should not plot outside the polygon. However, the contrary possibility, i.e. that a reference water type may plot within the polygon, has been discarded. The practical example of the M3 calculations is the regional groundwater geochemical interpretation from Äspö Hard Rock Laboratory region (e.g. Laaksoharju & Wallin, 1997; Laaksoharju et al., 1999a).

In the inverse modelling approach, the choice of reference water types requires interpretation of the palaeohydrology and -geochemistry of the study area. The relevant

succession of historic events constrains the calculations. No compositional rules are set, i.e. a reference composition may plot also within the data set to be studied. During each of period in history specific reference water types may infiltrate the bedrock. A simplified history of the Äspö site is presented in Figure 3-1 (p. 8).

The amounts of geochemical reactions related to reference water type mixings are largely dependent on how the reference water types are defined. Figure 5-1 illustrates the differences between the reference water compositions between the M3 and inverse approach. The Baltic Sea and glacial melt water compositions between the approaches are practically similar. However, the meteoric reference used in the M3 method is an estimate of 1960's precipitation (Laaksoharju & Wallin, 1997), while in the inverse approach it is dilute shallow level groundwater from the centre of the Äspö Island. The difference between these two meteoric references is minimal if measured with conservative variables (Fig. 5-1) but quite important if non-conservative variables are studied. Significant reactions occur while fresh rainwater (e.g. 1960's precipitation) infiltrates into the bedrock and becomes dilute shallow level bedrock groundwater. As an example the undoubtedly highest alkalinity concentrations (affecting PC_1 and PC_2 orientations) found from Äspö are present in shallow level bedrock, until concentrations decrease step by step with depth. The inverse approach attempts to take into account this gradual fade out, but by default M3 lumps together the abrupt increase and the gradual fade out and looses the reaction path changing the meteoric water composition.

An important difference among the approaches is how the saline reference type has been chosen. The M3 method uses a brine sample (depth –1656 m) found from the main land (Laaksoharju & Wallin, 1997), while the inverse approach uses the most saline undisturbed sample (depth –914 m) found below the Äspö Island. The compositional gap between these two is clearly visible in Figure 5-1. From the viewpoint of the inverse modelling, the gap brings forward two questions: when and what kind of "steady-state steps" there has been occurred? A study from Olkiluoto, Finland (Pitkänen et al., 1999a) indicates that similar brine water at depth contains prominent amounts of very old water hydrothermal in nature and the dilution of this water likely has taken an extensive time span well beyond the historical scope presented in Figure 3-1. Anyway, from the viewpoint of the present exercise it is likely that the excavated Äspö laboratory system causes an effective flow system that likely does not extend deeper downwards than it is away from the ground level. The laboratory tunnel extends to depth –450 m, and so a saline reference from depth –914 m seems suitable.

The original M3 calculation example (Laaksoharju et al., 1999a) from Äspö contains five different reference water types (meteoric, Baltic Sea, altered marine, glacial, and brine). Laaksoharju et al. revised this set of reference waters to four reference types (1960's precipitation, Baltic Sea, glacial melt water, and brine) for the current modelling task. However, the analysis of geochemical data and interpretation of relevant historic events of Äspö led in the inverse approach to seven reference types that is two more than in the original M3 solution (Fig. 5-1).

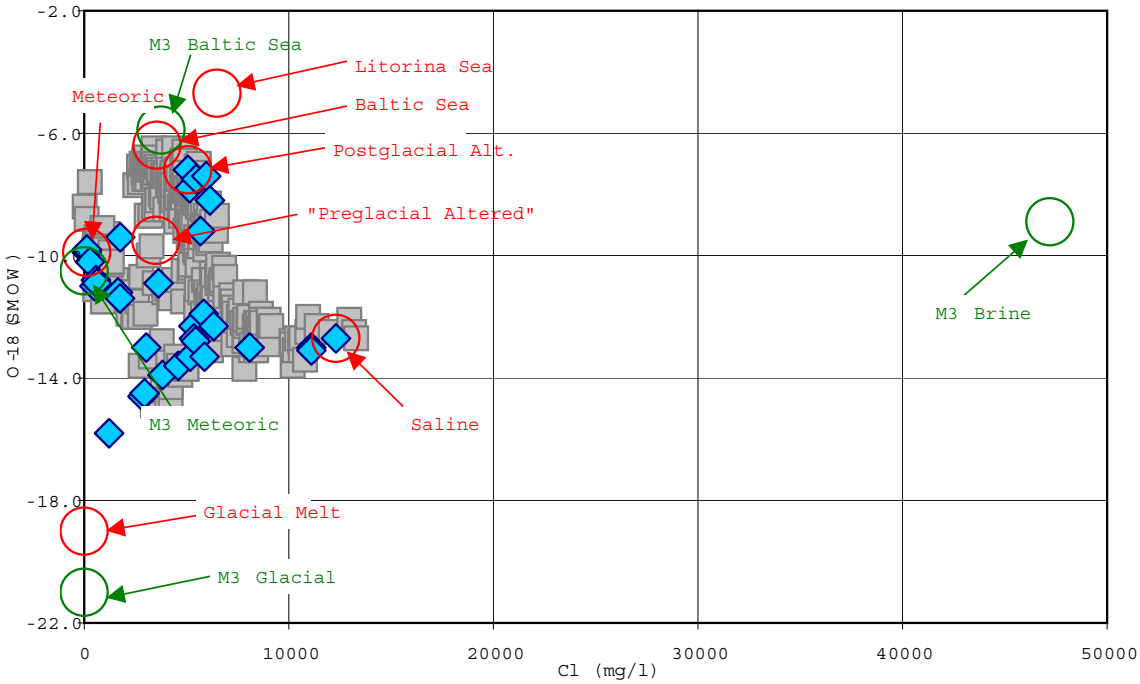

Figure 5-1 Reference water types of the M3 (green circles), the inverse approach (red circles), undisturbed samples before the tunnel construction (blue diamonds) and disturbed samples during and after the tunnel construction (grey squares) from Äspö in the Cl-^{18}O plot.

The choice of reference water types has large significance to the model sensitivity. A generalised example shows how a choice of saline reference affects to the readiness of a method to reflect changes in the system. The saline reference water in the M3 approach contains 47 200 mg/l Cl (Laaksoharju & Wallin, 1997), while in the inverse approach Cl concentration is 12 300 mg/l. Suppose a binary mixture of meteoric and saline water with Cl concentration 10 000 mg/l that dilutes to 8 000 mg/l. In the inverse approach this dilution indicates a 16.3 % change in the saline reference water fraction, while in the M3 approach the change is approximately only 4.2 %.

The significance of the choice of reference water types has been noticed also by Laaksoharju (1999, p. 89). If the original reference waters of M3 (Laaksoharju et al., 1999a), in this case meteoric and glacial, are changed to the currently used more extreme 1960's precipitation and glacial melt water, the variations of mixing fractions are damped down with an average of 8 % within the studied data.

As a further practical example of the significance of the choice of reference water compositions are the mixing fraction estimations for the control point SA2783A (Fig. 4-8). During the time-span from Feb. '94 to May '96 the Cl concentration (from 8 030 mg/l to 12 050 mg/l) and the inversely calculated saline component mixing fraction increases about 50 %. However, the M3 calculated mixing fraction estimate of the brine component rises only about 8 %. According to the inverse interpretation (Fig. 4-8) it is evident that the saline source is the only possibility for Cl concentration increase. Anyway, the 8 % is within the ±10 % uncertainty of the M3 method (Laaksoharju et al., 1999a) manifesting that nothing happens in the control point.

Ideally, in the current inverse modelling approach the choice of reference water types can be condensed to a couple of principles – how to define and/or find reference water types so that they equilibrate as closely as possible with current prevailing conditions in the bedrock, and so that they represent a sensible succession of the historical events identified. At the same time, it is important that reference water types have mixed with each other as little as possible.

5.4 Usage of mole-transfer results in hydrological simulations

Figures 4-10…4-12 illustrate mole-transfer trends as a function of three principal reference water types (meteoric, fresh Baltic Sea and saline water) potentially intruding into the simulated repository depth during disturbed open tunnel conditions at Äspö. In view of the precision of the current approach, chemical reactions can be considered significant when the fraction of used meteoric or fresh Baltic reference exceeds 50% in the final water.

The mixing fraction results of reference water types are considered as water-conservative parameters similarly to Cl or ^{18}O concentrations in groundwater. Mixing fractions can be transported like conservative parameters in hydrological simulations, and the mole-transfer results obtained in the inverse calculations may be coupled indirectly to hydrological transport. The conservative transport results are corrected using the trends shown in Figures 4-10…4-12, that were fitted to a sample set solved earlier.

As an example, we may assume that a hydrological simulation predicts 70% fresh Baltic Sea, 6% meteoric, 10% postglacial altered, 4% fresh Litorina Sea, 5% glacial melt, 3% "preglacial altered" and 2% saline reference water at a location in the hydrogeological model (Table 5-2). By knowing the reference water compositions (Table 3-1), an "uncorrected conservative water composition" can be calculated in accordance with the percentages (Table 5-2). Since the fresh seawater clearly dominates the simulated composition, Figure 4-11 can be used to correct the simulated "conservative water composition". The corrected results are shown in Table 5-2. As indicated, the alkalinity concentration is tripled and the sulphate concentration is almost decreased to half. Similarly, the Ca concentration is increased by about 17% and Mg decreased by almost 27%. The increase in dissolved Fe seems somewhat too high and indicates that perhaps more pyrite should be precipitated.

Table 5-2 Example where a hydrological simulation predicts a fresh Baltic seawater-dominated final water composition. "Uncorrected conservative final water composition" is calculated as the mixing fraction weighted average from reference water compositions (Table 3-1). Chemical reaction corrected results have been calculated using the mole transfer trends illustrated in Figure 4-11. Concentrations subject to modifications are shown in bold type. Values not estimated and deduced numbers containing these values are in brackets.

Reference water type	Fraction		"Conservative result"			Corrected result	
Fresh Baltic Sea	70%		pH	7.6		pH	(7.6)
Meteoric	6%		Na	1797		Na	1797
Postglacial altered	10%		K	60		K	(60)
Fresh Litorina Sea	4%		Ca	**276**		Ca	**334**
Glacial melt	5%		Mg	**203**		Mg	**149**
"Preglacial altered"	3%		Fe	**0.5**		Fe	**6.1**
Saline	2%		Alkalinity	**105**		Alkalinity	**334**
			Cl	3619		Cl	3619
			SO_4	**427**		SO_4	**254**
			^{18}O	-7.5		^{18}O	-7.5
			Sum(Cat)	110.2		Sum(An)	(108.8)
			Sum(An)	-112.7		Sum(An)	(-112.8)
			E.N.(%)	-1.1		E.N.(%)	(-1.8)

6 Conclusions

The current study implemented an inverse-modelling approach to solving the problem of how to find mixing fractions of identified reference water types and geochemical reactions related to groundwater mixing processes in collected and analysed samples. The problem is inverse, both on the scale of an individual sample and on that of the whole Äspö area. In the case of an individual sample, the inverse calculation step quantitatively describes what geochemical phase reactions are needed to reach existing final water from a feasible set of initial water samples. As regards the whole area, chained inverse calculations need an interpretation of the succession of historical events that have affected bedrock groundwater compositions at Äspö.

The calculations carried out were divided into subsets based on excavations of the Äspö tunnel system. The undisturbed sample set was used for identifying the reference water types that have been active in the Äspö HRL volume, for describing the general evolution of water in the bedrock, and for defining the depth relations and distributions of reference water types in the undisturbed model volume. The disturbed sample set was collected from 10 control points, and samples were used to monitor the effects of tunnel construction on groundwater compositions. The results show that there are three extensive sources of water in the disturbed condition that attempt to intrude into the repository during open tunnel conditions. These reference water types are meteoric, fresh Baltic Sea and saline water. Geochemical reactions related to these intruding water types are strong in the case of fresh Baltic Sea water, moderate for meteoric water, and practically insignificant for the saline reference water type.

In summary, the *inverse*-modelling calculation results presented here form the basis for *forward*-modelling calculations presented elsewhere in this volume (Kattilakoski & Luukkonen 2000). The forward groundwater mixing and transport modelling is based on two steps. The first step is conservative mixing and transport, and the second is a single net reaction step based on earlier inverse-modelling calculation results.

References

Andersson, K., 1996. Mineralogy of the Äspö site. Swedish Nuclear Power Inspectorate (SKI), SKI Report 96:33, Stockholm. 10 p.

Appelo, C.A.J. & Postma, D., 1993. Geochemistry, groundwater and pollution. A.A. Balkema, Rotterdam. 536 p.

Banwart, S.A., 1997. Aqueous speciation at the interface between geological solids and groundwater. In: (Grenthe, I. & Puigdomenech, I., eds.) Modelling in aquatic chemistry. Organisation for Economic Co-operation and Development (OECD), Nuclear Energy Agency (NEA), Paris, 245–287.

Banwart, S., Laaksoharju, M., Gustafsson, E., Pitkänen, P., Snellman, M., Landström, O., Aggeryd, I., Mathiasson, L. & Sundblad, B., 1995. The hydrochemistry of conservative natural tracers. In: (Banwart, S., ed.) The redox experiment in block scale. Swedish Nuclear Fuel and Waste Management Co. (SKB), Progress Report 25-95-06, Stockholm, 3-47…3-80.

Burton, C.J. & Viani, B.E., 1997. Ion sorption onto hydrous ferric oxides: effect on major element fluid chemistry at Äspö, Sweden. In: (Laaksoharju, M & Wallin, B., eds.) Evolution of the groundwater chemistry at the Äspö Hard Rock Laboratory, Proceedings of the second Äspö International Geochemistry Workshop, June 6-7, 1995. Swedish Nuclear Fuel and Waste Management Co. (SKB), International Cooperation Report 97-04, Stockholm, Paper #2.

Canfield, D.E., Thamdrup, B. & Hansen, J.W., 1993. The anaerobic degradation of organic matter in Danish coastal sediments: Iron reduction, manganese reduction and sulfate reduction. Geochimica et Cosmochimica Acta 57, 3867–3883.

Eronen, M., 1988. A scrutiny of the late Quaternary history of the Baltic Sea. Geological Survey of Finland, Special Paper 6, Espoo, 11–18.

Kankainen, T., 1986. Loviisa power station, final disposal of reactor waste. On the age and origin of groundwater from the rapakivi granite on the island of Hästholmen. Nuclear Waste Commission of Finnish Power Companies, Report YJT-86-29, Helsinki. 56 p.

Laaksoharju, M., 1988. Shallow groundwater chemistry at Laxemar, Äspö and Ävrö. Swedish Nuclear Fuel and Waste Management Co. (SKB), Progress Report 25-88-04, Stockholm. 15 p.

Laaksoharju, M., 1999. Groundwater characterisation and modelling: problems, facts and possibilities. Academic Dissertation. Stockholm, Sweden: Royal Institute of Technology, Department of Civil and Environmental Engineering. 144 p.

Laaksoharju, M. & Wallin, B. (eds.), 1997. Evolution of the groundwater chemistry at the Äspö Hard Rock Laboratory. Proceedings of the second Äspö International Geochemistry Workshop, June 6-7, 1995. Swedish Nuclear Fuel and Waste Management Co. (SKB), International Cooperation Report 97-04, Stockholm.

Laaksoharju, M., Skårman, C. & Skårman, E., 1999a. Multivariate mixing and mass-balance (M3) calculations, a new tool for decoding hydrogeochemical information. Applied Geochemistry 14, 861–871.

Laaksoharju, M., Andersson, C., Tullborg, E.-L., Wallin, B., Ekwall, K., Pedersen, K. & Nilsson, A.-C., 1999b. Re-sampling of the KLX02 deep borehole at Laxemar. Swedish Nuclear Fuel and Waste Management Co. (SKB), Report R-99-09, Stockholm. 31 p.

Kattilakoski, E. & Luukkonen, A., 2000. Task 5 – Mixing proportions of glacial, Litorina, altered, saline, meteoric and Baltic Sea waters in the Äspö tunnel. In Part IV(this volume), Stockholm. IPR-02-41.

Luukkonen, A., Pitkänen, P., Ruotsalainen, P., Leino-Forsman, H. & Snellman, M., 1999. Hydrogeochemical conditions at the Hästholmen site. Posiva Oy, Report POSIVA 99-26, Helsinki. 64 p.

Nilsson, A.-C., 1999. Resultat av upprepade tritiumanalyser, utförda vid årsskiftet 1998/1999-10-14, Äspö och Laxemar (In Swedish). Swedish Nuclear Fuel and Waste Management Co. (SKB), Djupförvarsteknik, IPR-02-60. (in press)

Parkhurst, D.L., 1997. Geochemical mole-balance modeling with uncertain data. Water Resources Research 33, 1957-1970.

Parkhurst, D.L. & Appelo, C.A.J., 1999. User's guide to PHREEQC (Version 2) – A computer program for speciation, batch-reaction, one dimensional transport, and inverse geochemical calculations. U.S. Geological Survey, Water-Resources Investigations Report 99-4259, Denver. 312 p.

Parkhurst, D.L. & Plummer, L.N., 1993. Geochemical models. In: (ed. Allen, W.M.) Regional ground-water quality. Van Nostrand Reinhold, New York, 199–225.

Pitkänen, P., Luukkonen, A., Ruotsalainen, P., Leino-Forsman, H. & Vuorinen, U., 1999a. Geochemical modelling of groundwater evolution and residence time at the Olkiluoto site. Posiva Oy, Report POSIVA 98-10, Helsinki. 184 p.

Pitkänen, P., Löfman, J., Koskinen, L., Leino-Forsman, H., Snellman, M., 1999b. Application of mass-balance and flow simulation calculations to interpretation of mixing at Äspö, Sweden. Applied Geochemistry 14, 893–905.

Plummer, L.N., Prestemon, E.C., and Parkhurst, D.L., 1994. An interactive code (NETPATH) for modeling NET geochemical reactions along a flow PATH. Version 2.0. U.S. Geological Survey, Water-Resources Investigations Report 94-4169, Reston. 130 p.

Runnells, D.D., 1993. Inorganic chemical processes and reactions. In: (ed. Allen, W.M.) Regional ground-water quality. Van Nostrand Reinhold, New York. 131–153.

Stumm, W., 1992. Chemistry of the solid-water interface. John Wiley & Sons, New York. 428 p.

Wang, Y. & Van Cappellen, P., 1996. A multicomponent reactive transport model of early diagenesis: Application to redox cycling in coastal marine sediments. Geochimica et Cosmochimica Acta 60, 2993–3014.

Appendices

Appendix 1. Summary of mole-transfer results for undisturbed samples. The reference days given with the sample ID indicate the sampling date with respect to Jan. 1, 1991. The upper part shows mixing fractions of initial water samples for each final water. All mole and redox transfers are in mmol/l. A negative value indicates precipitation/cation uptake and a positive value dissolution/cation release. The minimum and maximum fractions and mole transfers possible within given analytical uncertainties are denoted after the representative values.

Appendix 2. Summary of mole-transfer results for the disturbed control point at KR0012B. The reference days given with the sample ID indicate the sampling date with respect to Jan. 1, 1991. The upper part shows mixing fractions of initial water samples for each final water. All mole and redox transfers are in mmol/l. A negative value indicates precipitation/cation uptake and a positive value dissolution/cation release. The minimum and maximum fractions and mole transfers possible within given analytical uncertainties are denoted after the representative values.

Appendix 3. Summary of mole-transfer results for the disturbed control points at SA0850B and SA0813B. The reference days given with the sample ID indicate the sampling date with respect to Jan. 1, 1991. The upper part shows mixing fractions of initial water samples for each final water. All mole and redox transfers are in mmol/l. A negative value indicates precipitation/cation uptake and a positive value dissolution/cation release. The minimum and maximum fractions and mole transfers possible within given analytical uncertainties are denoted after the representative values.

Appendix 4. Summary of mole-transfer results for the disturbed control points at SA1327A and SA1229A. The reference days given with the sample ID indicate the sampling date with respect to Jan. 1, 1991. The upper part shows mixing fractions of initial water samples for each final water. All mole and redox transfers are in mmol/l. A negative value indicates precipitation/cation uptake and a positive value of dissolution/cation release. The minimum and maximum fractions and mole transfers possible within given analytical uncertainties are denoted after the representative values.

Appendix 5. Summary of mole-transfer results for the disturbed control points at KA1755A, SA2074A and SA2873A. The reference days given with the sample ID indicate the sampling date with respect to Jan. 1, 1991. The upper part shows mixing fractions of initial water samples for each final water. All mole and redox transfers are in mmol/l. A negative value indicates precipitation/cation uptake and a positive value dissolution/cation release. The minimum and maximum fractions and mole transfers possible within given analytical uncertainties are denoted after the representative values.

Appendix 6. Summary of mole-transfer results for the disturbed control points at KAS03 and KAS07. The reference days given with the sample ID indicate the sampling date with respect to Jan. 1, 1991. The upper part shows mixing fractions of initial water samples for each final water. All mole and redox transfers are in mmol/l. A negative value indicates precipitation/cation uptake and a positive value dissolution/cation release. The minimum and maximum fractions and mole transfers possible within given analytical uncertainties are denoted after the representative values.

		Meteoric									Litorina						Glacial					
	Sample	KAS04/-185.2			HAS06/-65.1			HAS07/-75.1			KAS06/-200.1			KAS06/-331.9			KAS06/-433.3			KAS06/-284.4			KAS12/-276.0			KAS04/-376.8			KAS03/-121.8			KAS02/-199.8			KAS03/-239.0		
	Date	-624 (a			-1242 (b			-1247			-580			-566			-559			-573			-209 (c			-638			-679			-720			-856		
Saline Glacial Alt. Litorina Meteoric	Seawater Average	0.12	0.10	0.13	0.27	0.27	0.28																												
	HAS05/-56.3 -1243	0.88	0.87	0.90	0.47	0.45	0.47	0.42	0.42	0.43																									
	KAS04/-185.2 -624																																		
	HAS07/-75.1 -1247										0.62	0.61	0.63																						
	KAS06/-200.1 -580				0.26	0.26	0.27																												
	Litorina Sea													0.10	0.03	0.14	0.23	0.15	0.31																
	KAS06/-331.9 -566							0.21	0.20	0.21										0.75	0.75	0.75	0.72	0.65	0.74										
	KAS06/-433.3 -559													0.64	0.45	0.71																			
	KAS06/-284.4 -573										0.33	0.30	0.33													0.29	0.29	0.30							
	KAS04/-376.8 -638										0.05	0.05	0.07																						
	HAS13/-42.0 -547													0.26	0.16	0.51	0.50	0.36	0.59																
	Glacial Melt Water																												0.68	0.68	0.68	0.21	0.152	0.241	0.37	0.33	0.39
	KAS03/-121.8 -679							0.38	0.36	0.38																									
	KAS02-199.8 -720																			0.25	0.25	0.25	0.28	0.26	0.35										
	KAS03/-239.0 -856																																		
	"Preglacial Altered"																												0.32	0.32	0.32	0.16	0.02	0.20	0.25	0.18	0.32
	KAS03/-914.1 -657																																		
	KAS02/-881.3 -700																																		
	KAS03/-830.1 -845																0.27	0.22	0.34																
	KAS02/-523.0 -971																																		
	KAS03/-602.5 -850																									0.71	0.70	0.71							
	KAS03/-348.6 -868																															0.63	0.60	0.82	0.38	0.28	0.45
	KAS03/-454.3 -862																																		
	KAS04/-275.6 -614																																		
	KAS02/-317.2 -826																																		
	Transfers (mmol/l)																																		
	Calcite	-2.31	-3.34	-1.48	-1.29	-1.81	-0.70	-1.30	-1.37	-1.28	0.08	0.05	0.09	-0.03	-2.06	-0.03	-0.82	-4.37	-0.43	-0.31	-0.31	-0.22	-0.43	-1.12	-0.26	0.01	0.01	0.01	0.04	0.04	0.04	-2.21	-2.98	-1.65	-2.91	-3.88	-2.24
	CH_2O	0.34	0.22	0.79	0.19	0.10	0.29	0.23	0.22	0.29	0.21	0.20	0.25	0.00	0.00	2.10	0.12	0.06	3.71	0.05	0.03	0.13	0.07	0.04	0.61	0.00	0.00	0.00	0.02	0.02	0.03	2.77	2.38	4.07	2.87	2.13	3.78
	NaX	-2.48	-4.20	-0.98				-0.11	-0.24	-0.03	-0.09	-0.12	-0.08	2.59	0.62	6.44				0.41	0.28	0.44	0.53	0.30	1.32				1.15	0.83	1.49				1.87	0.76	3.57
	CaX_2	3.75	2.71	4.98	1.98	1.21	2.73	0.00	0.00	0.00							4.44	2.60	7.89																	
	MgX_2	-1.11	-1.34	-0.82	-1.26	-1.72	-0.83	0.78	0.72	0.82				-1.29	-2.74	-0.29	-3.93	-5.76	-2.19										-0.57	-0.74	-0.41	1.15	0.82	1.51	0.65	0.15	1.10
	Goethite	1.38	0.88	2.06	0.78	0.42	1.10	0.76	0.73	0.79				0.00	0.00	1.59	0.49	0.24	3.24	0.20	0.14	0.22	0.26	0.15	0.78	0.00	0.00	0.00				1.81	1.41	2.50	2.24	1.71	2.98
	FeX_2	-1.40	-2.01	-0.91	-0.71	-1.04	-0.35	-0.73	-0.76	-0.70	0.05	0.04	0.06	0.00	-1.14	0.00	-0.51	-2.42	-0.25	-0.21	-0.22	-0.14	-0.26	-0.66	-0.15							-1.15	-1.51	-0.82	-1.58	-2.11	-1.22
	Pyrite	0.00	-0.08	0.00	0.00	-0.01	0.00	-0.01	-0.03	-0.01	-0.06	-0.07	-0.06	0.00	-0.49	0.00	0.00	-0.83	0.00	0.00	-0.02	0.00	0.00	-0.12	0.00	0.00	0.00	0.00	-0.01	-0.01	-0.01	-0.66	-0.98	-0.58	-0.66	-0.87	-0.48
	Redox (mmol/l)																																		
	Fe(3)	1.38			0.75			0.76						0.00			0.49			0.20			0.26			0.00			0.00			1.81			2.24		
	H(0)	0.00			0.00			0.00			0.00			0.00			0.00			0.00			0.00			0.00			-0.01			0.00			0.00		
	S(-2)							-0.02			-0.12																					-1.33			-1.32		

a) Mix Cl only b) ΔS(6) = 12% HAS06 c) Mix Cl only

		Saline					Saline+Glacial				Met+Lit+Gla+Sal				
Sample		KAS02/-881.3	KAS03/-830.1	KAS02/-523.0	KAS05/-483.0	KAS03/-602.5	KAS03/348.6	KAS03/-454.3	KAS03/-566.3	KAS04/-275.6	KAS02/-307.7	KAS02/317.2	KAS02/456.2	KAS05/-339.5
	Date	-700	-845	-971	-209 (d	-850	-868 (e	-862	-218 (f	-614	-995 (g	-826	-981	-209 (h
	Seawater Average													
Saline Glacial Alt. Litorina Meteoric	HAS05/-56.3 -1243													
	KAS04/-185.2 -624									0.34 0.29 0.40				
	HAS07/-75.1 -1247													
	KAS06/-200.1 -580			0.28 0.238 0.323							0.51 0.49 0.53	0.22 0.22 0.26		0.32 0.151 0.518
	Litorina Sea													
	KAS06/-331.9 -566						0.09 0.06 0.10							
	KAS06/-433.3 -559													
	KAS06/-284.4 -573													
	KAS04/-376.8 -638													
	HAS13/-42.0 -547													
	Glacial Melt Water	0.10 0.03 0.14												
	KAS03/-121.8 -679		0.19 0.17 0.19				0.39 0.33 0.42	0.21 0.15 0.22						
	KAS02-199.8 -720					0.41 0.34 0.47			0.30 0.27 0.33					
	KAS03/-239.0 -856									0.35 0.22 0.39				
	"Preglacial Altered"	0.07 0.00 0.14												
	KAS03/-914.1 -657	0.83 0.76 0.97												
	KAS02/-881.3 -700		0.81 0.81 0.83											
	KAS03/-830.1 -845			0.72 0.677 0.762		0.59 0.53 0.66	0.52 0.48 0.60				0.23 0.22 0.42	0.18 0.13 0.19		0.23 0.127 0.366
	KAS02/-523.0 -971				1.00 1.00 1.00									
	KAS03/-602.5 -850							0.65 0.60 0.67	0.70 0.67 0.73	0.31 0.25 0.45				
	KAS03/-348.6 -868													
	KAS03/-454.3 -862										0.26 0.09 0.27	0.60 0.55 0.64		0.45 0.134 0.71
	KAS04/-275.6 -614							0.14 0.11 0.24						
	KAS02/-317.2 -826												1.00 1.00 1.00	
	Transfers (mmol/l)													
	Calcite	-0.28 -5.86 -0.15	-1.23 -2.31 -0.81	-0.47 -2.33 -0.39	-0.02 -0.03 -0.01	-0.51 -2.33 -0.42	-0.46 -3.37 -0.37	-0.01 -0.02 0.00		-0.54 -2.80 -0.15	-0.61 -4.29 -0.50	-0.02 -0.03 -0.01	-0.22 -1.25 -0.15	-0.35 -0.71 -0.05
	CH_2O	0.04 0.02 5.82	1.09 0.65 2.15	0.07 0.06 1.95	0.07 0.04 0.10	0.08 0.06 1.92	0.07 0.05 2.99	0.00 0.00 0.07	0.00 0.00 0.00	0.08 0.02 2.28	0.09 0.08 3.76	0.00 0.00 0.05	0.04 0.03 1.00	0.05 0.00 0.10
	NaX	0.0 0.0 8.2	0.0 0.0 1.4	1.67 1.06 4.10		1.89 1.22 4.27	0.5 0.43 3.7	-0.55 -1.02 -0.11	0.00 0.00 0.00	0.61 0.14 3.06	0.73 0.59 4.71	-2.07 -2.80 -1.18	0.31 0.20 1.43	0.37 0.00 0.82
	CaX_2	0.93 0.00 4.12	0.00 0.00 0.81											
	MgX_2	-0.75 -1.16 -0.36	0.66 0.43 0.87	-0.56 -0.91 -0.21		-0.63 -0.95 -0.32		0.27 0.05 0.51				1.03 0.59 1.40		
	Goethite	0.18 0.10 4.51	0.90 0.58 1.74	0.28 0.23 1.71	0.02 0.01 0.03	0.31 0.25 1.72	0.27 0.21 2.51	0.00 0.00 0.02		0.31 0.08 2.04	0.38 0.31 3.21	0.01 0.01 0.02	0.16 0.11 0.93	0.19 0.01 0.41
	FeX_2	-0.18 -3.17 -0.10	-0.66 -1.24 -0.43	-0.28 -1.28 -0.23		-0.31 -1.29 -0.26	-0.27 -1.83 -0.21		0.00 0.00 0.00	-0.30 -1.53 -0.07	-0.37 -2.36 -0.29		-0.15 -0.71 -0.10	-0.19 -0.41 0.00
	Pyrite	0.00 -1.34 0.00	-0.25 -0.49 -0.14	0.00 -0.43 0.00	-0.02 -0.03 -0.01	0.00 -0.43 0.00	0.00 -0.68 0.00	0.00 -0.02 0.00		0.00 -0.51 0.00	0.00 -0.85 0.00	0.00 -0.01 0.00	0.00 -0.22 0.00	
	Redox (mmol/l)													
	Fe(3)	0.18	0.90	0.28	0.02	0.31	0.27	0.00		0.31	0.38	0.01	0.16	0.19
	H(0)	0.00	0.00	0.00	0.00	0.00	0.00	0.00		0.00	0.00	0.00	0.00	0.00
	S(-2)		-0.49		-0.04									

d) Mix Cl only; 5%

e) $\Delta^{18}O$ = 0.2 in final

f) Mix Cl & SO4

e) $\Delta^{18}O$ = 0.15

h) Mix Cl & SO4; 5%

	Sample		KR0012B			KR0012B			KR0012B			KR0012B			KR0012B			KR0012B			KR0012B			KR0012B			KR0012B			KR0012B			KR0012B		
	Date		169			463			477			491 (*			505			519 (*			542			554			567			583			595			611		
	Seawater Average					0.10	0.08	0.11	0.11	0.07	0.11	0.12	0.12	0.12	0.09	0.06	0.12				0.06	0.06	0.08	0.07	0.03	0.12	0.06	0.04	0.09	0.04	0.04	0.04	0.07	0.05	0.08	0.05	0.04	0.06
Meteoric	HAS05/-56.3	-1243	0.37	0.36	0.37	0.37	0.36	0.44	0.44	0.41	0.46	0.46	0.45	0.47	0.43	0.42	0.43	0.38	0.38	0.38	0.47	0.46	0.48	0.50	0.45	0.55	0.50	0.49	0.54	0.52	0.52	0.52	0.56	0.55	0.57	0.52	0.52	0.53
	KAS04/-185.2	-624																																				
	HAS07/-75.1	-1247	0.44	0.44	0.45	0.53	0.45	0.55	0.46	0.44	0.52	0.42	0.41	0.42	0.48	0.44	0.52	0.62	0.62	0.62	0.47	0.46	0.48	0.43	0.35	0.51	0.44	0.38	0.48	0.43	0.43	0.44	0.37	0.36	0.41	0.42	0.42	0.43
	KAS06/-200.1	-580																																				
Glacial Alt. Litorina	Litorina Sea																																					
	KAS06/-331.9	-566																																				
	KAS06/-433.3	-559																																				
	KAS06/-284.4	-573																																				
	KAS04/-376.8	-638																																				
	HAS13/-42.0	-547																																				
	Glacial Melt Water																																					
	KAS03/-121.8	-679	0.19	0.19	0.19																																	
	KAS02-199.8	-720																																				
	KAS03/-239.0	-856																																				
	"Preglacial Altered"																																					
Saline	KAS02/-881.3	-700																																				
	KAS03/-830.1	-845																																				
	KAS02/-523.0	-971																																				
	KAS03/-602.5	-850																																				
	KAS03/-348.6	-868																																				
	KAS03/-454.3	-862																																				
	KAS04/-275.6	-614																																				
	KAS02/-317.2	-826																																				
	Transfers (mmol/l)																																					
	Calcite		0.11	0.11	0.11	0.06	0.02	0.10										-0.02	-0.02	-0.02													-0.09	-0.12	-0.05			
	CH_2O		0.40	0.40	0.41	0.08	0.07	0.09	0.07	0.07	0.09	0.07	0.06	0.08	0.08	0.07	0.09	0.10	0.10	0.10	0.08	0.08	0.09	0.08	0.07	0.09	0.08	0.07	0.10	0.09	0.08	0.09	0.08	0.08	0.09	0.08	0.08	0.09
	NaX		0.24	0.08	0.24	0.00	-4.17	0.00	-2.79	-4.31	-0.17										0.90	0.35	1.69							0.81	0.33	1.01				0.86	0.43	1.17
	CaX_2					0.89	0.66	2.79	2.05	0.78	2.80	1.00	0.93	1.08	0.71	0.45	1.00							0.52	0.05	1.12	0.47	0.12	0.87				0.53	0.21	0.68			
	MgX_2		-0.21	-0.22	-0.14	-0.89	-1.01	-0.22	-0.66	-0.91	-0.19	-1.00	-1.08	-0.93	-0.71	-1.00	-0.45				-0.45	-0.84	-0.17	-0.52	-1.12	-0.05	-0.47	-0.87	-0.12	-0.40	-0.51	-0.16	-0.53	-0.68	-0.21	-0.43	-0.58	-0.21
	FeX_2		0.09	0.09	0.10																																	
	Pyrite		-0.12	-0.12	-0.12	-0.02	-0.02	-0.02	-0.02	-0.02	-0.02	-0.02	-0.02	-0.02	-0.02	-0.02	-0.02	-0.03	-0.03	-0.03	-0.02	-0.03	-0.02	-0.02	-0.03	-0.02	-0.02	-0.03	-0.02	-0.03	-0.03	-0.02	-0.02	-0.03	-0.02	-0.02	-0.03	-0.02
	Redox (mmol/l)																																					
	Fe(3)		0.00			0.00			0.00			0.00			0.00			0.00			0.00			0.00			0.00			0.00			0.00			0.00		
	H(0)		0.00			0.00			0.00			0.00			0.00			0.00			0.00			0.00			0.00			0.00			0.00			0.00		
	S(-2)		-0.23			-0.04			-0.04			-0.04			-0.04			-0.06			-0.05			-0.04			-0.05			-0.05			-0.05			-0.05		

*) changeables Δ = 10%

*) changeables Δ = 10%

	Sample	KR0012B			KR0012B			KR0012B			KR0012B			KR0012B			KR0012B			KR0012B			KR0012B			KR0012B			KR0012B			KR0012B		
	Date	625			638			650			666			679			693			701			709 (*			720			734			749			768			806 (*		
	Seawater Average	0.11	0.10	0.13	0.10	0.08	0.14	0.11	0.10	0.13	0.09	0.08	0.13	0.12	0.11	0.12	0.09	0.09	0.12	0.09	0.09	0.11	0.19	0.19	0.20	0.10	0.10	0.11	0.08	0.08	0.11	0.08	0.08	0.11	0.09	0.08	0.12	0.09	0.05	0.11
Meteoric	HAS05/-56.3 -1243	0.57	0.55	0.58	0.58	0.55	0.60	0.58	0.56	0.60	0.59	0.57	0.60	0.62	0.61	0.62	0.63	0.63	0.64	0.63	0.62	0.64	0.75	0.75	0.76	0.65	0.65	0.66	0.66	0.65	0.68	0.66	0.64	0.68	0.66	0.64	0.68	0.69	0.68	0.70
	KAS04/-185.2 -624																																							
	HAS07/-75.1 -1247	0.32	0.28	0.33	0.32	0.27	0.35	0.31	0.27	0.33	0.32	0.27	0.34	0.27	0.26	0.27	0.28	0.25	0.28	0.27	0.25	0.29	0.05	0.05	0.06	0.24	0.23	0.25	0.26	0.22	0.27	0.25	0.21	0.27	0.25	0.20	0.28	0.23	0.19	0.27
	KAS06/-200.1 -580																																							
Glacial Alt. Litorina	Litorina Sea																																							
	KAS06/-331.9 -566																																							
	KAS06/-433.3 -559																																							
	KAS06/-284.4 -573																																							
	KAS04/-376.8 -638																																							
	HAS13/-42.0 -547																																							
	Glacial Melt Water																																							
	KAS03/-121.8 -679																																							
	KAS02-199.8 -720																																							
	KAS03/-239.0 -856																																							
	"Preglacial Altered"																																							
Saline	KAS02/-881.3 -700																																							
	KAS03/-830.1 -845																																							
	KAS02/-523.0 -971																																							
	KAS03/-602.5 -850																																							
	KAS03/-348.6 -868																																							
	KAS03/-454.3 -862																																							
	KAS04/-275.6 -614																																							
	KAS02/-317.2 -826																																							
	Transfers (mmol/l)																																							
	Calcite	-0.11	-0.13	-0.05	-0.11	-0.16	-0.05				-0.05	-0.09	0.00	-0.07	-0.08	-0.06	-0.07	-0.10	-0.07	-0.11	-0.13	-0.07				-0.08	-0.09	-0.07	-0.13	-0.15	-0.07	-0.13	-0.18	-0.07	-0.07	-0.12	-0.01	-0.17	-0.21	-0.14
	CH_2O	0.08	0.07	0.09	0.08	0.07	0.09	0.08	0.07	0.09	0.08	0.07	0.09	0.08	0.07	0.08	0.08	0.07	0.09	0.08	0.07	0.09	0.57	0.55	0.59	0.08	0.07	0.09	0.08	0.07	0.09	0.08	0.07	0.09	0.08	0.07	0.09	0.08	0.07	0.09
	NaX																						-3.65	-4.26	-3.19															
	CaX_2	0.81	0.63	1.06	0.76	0.43	1.09	0.73	0.56	1.03	0.70	0.42	1.00	0.92	0.89	0.95	0.73	0.68	0.95	0.80	0.56	1.04	2.85	2.74	3.02	0.85	0.80	0.93	0.63	0.44	0.87	0.63	0.42	0.90	0.64	0.41	0.95	0.67	0.32	0.90
	MgX_2	-0.81	-1.06	-0.63	-0.76	-1.09	-0.43	-0.73	-1.03	-0.56	-0.70	-1.00	-0.42	-0.92	-0.95	-0.89	-0.73	-0.95	-0.68	-0.80	-1.04	-0.56	-1.17	-1.34	-0.99	-0.85	-0.93	-0.80	-0.63	-0.87	-0.44	-0.63	-0.90	-0.42	-0.64	-0.95	-0.41	-0.67	-0.90	-0.32
	FeX_2																						0.14	0.14	0.15															
	Pyrite	-0.02	-0.02	-0.02	-0.02	-0.03	-0.02	-0.02	-0.02	-0.02	-0.02	-0.03	-0.02	-0.02	-0.02	-0.02	-0.02	-0.03	-0.02	-0.02	-0.03	-0.02	-0.16	-0.17	-0.16	-0.02	-0.02	-0.02	-0.02	-0.03	-0.02	-0.02	-0.03	-0.02	-0.02	-0.03	-0.02	-0.02	-0.03	-0.02
	Redox (mmol/l)																																							
	Fe(3)	0.00			0.00			0.00			0.00			0.00			0.00			0.00			0.00			0.00			0.00			0.00			0.00			0.00		
	H(0)	0.00			0.00			0.00			0.00			0.00			0.00			0.00			0.00			0.00			0.00			0.00			0.00			0.00		
	S(-2)	-0.04			-0.05			-0.04			-0.05			-0.04			-0.05			-0.05			-0.33			-0.05			-0.05			-0.05			-0.05			-0.05		

*) ΔCl = 5%

*) ΔCl = 5%

	Sample		KR0012B			KR0012B			KR0012B			KR0012B			KR0012B			KR0012B			KR0012B			KR0012B			KR0012B			KR0012B		
		Date	813 (*			866 (*			892 (*			916 (*			958 (*			1042 (*			1317 (*			1343 (*			1598 (*			1743			1967 (*		
	Seawater Average		0.09	0.09	0.10	0.05	0.04	0.06	0.05	0.04	0.06	0.07	0.04	0.11	0.10	0.08	0.16	0.10	0.08	0.15	0.07	0.05	0.08	0.08	0.07	0.13	0.15	0.13	0.16	0.11	0.10	0.14	0.02	0.02	0.03
Meteoric	HAS05/-56.3	-1243	0.68	0.68	0.69	0.72	0.71	0.73	0.71	0.70	0.73	0.78	0.76	0.81	0.80	0.73	0.86	0.83	0.76	0.87	0.86	0.85	0.88	0.85	0.81	0.89	0.85	0.84	0.87	0.79	0.77	0.82	0.81	0.78	0.83
	KAS04/-185.2	-624																																	
	HAS07/-75.1	-1247	0.22	0.21	0.22	0.23	0.22	0.24	0.24	0.23	0.25	0.16	0.09	0.20	0.10	0.00	0.17	0.08	0.00	0.15	0.07	0.04	0.10	0.07	0.00	0.12				0.11	0.05	0.12	0.17	0.14	0.19
	KAS06/-200.1	-580																																	
Glacial Alt. Litorina	Litorina Sea																																		
	KAS06/-331.9	-566																																	
	KAS06/-433.3	-559																																	
	KAS06/-284.4	-573																																	
	KAS04/-376.8	-638																																	
	HAS13/-42.0	-547																																	
	Glacial Melt Water																																		
	KAS03/-121.8	-679																																	
	KAS02-199.8	-720																																	
	KAS03/-239.0	-856																																	
Saline	"Preglacial Altered"																																		
	KAS02/-881.3	-700																																	
	KAS03/-830.1	-845																																	
	KAS02/-523.0	-971																																	
	KAS03/-602.5	-850																																	
	KAS03/-348.6	-868																																	
	KAS03/-454.3	-862																																	
	KAS04/-275.6	-614																																	
	KAS02/-317.2	-826																																	
	Transfers (mmol/l)																																		
	Calcite		-0.16	-0.18	-0.15	-0.17	-0.22	-0.15	-0.14	-0.20	-0.08	-0.30	-0.41	-0.25	-0.27	-0.33	0.16	-0.32	-0.42	0.09	-0.41	-0.50	-0.39	-0.38	-0.45	0.04									
	CH_2O		0.08	0.07	0.09	0.08	0.08	0.09	0.08	0.08	0.09	0.08	0.07	0.09	0.00	0.00	1.08	0.00	0.00	1.16	0.08	0.07	0.09	0.00	0.00	1.07	0.70	0.56	0.76	0.70	0.51	0.80	0.51	0.35	0.66
	NaX					-1.48	-2.40	-0.72	0.81	0.40	1.18	-1.42	-3.39	-0.18	-2.46	-4.46	-0.06	-2.49	-4.63	-0.44	-2.30	-3.71	-1.47	-2.30	-3.96	-0.61	-2.74	-3.87	-1.91	-1.82	-3.29	-0.97			
	CaX_2		0.76	0.68	0.83	0.74	0.36	1.20				1.15	0.48	2.15	1.80	0.60	2.80	1.77	0.66	2.75	1.52	1.06	2.16	1.54	0.63	2.33	1.88	1.63	2.16	1.21	0.87	1.93			
	MgX_2		-0.76	-0.83	-0.68				-0.40	-0.59	-0.20	-0.43	-0.87	-0.16	-0.55	-1.12	-0.31	-0.50	-1.00	-0.22	-0.37	-0.54	-0.12	-0.37	-0.82	-0.18	-0.69	-0.93	-0.37	-0.48	-0.79	-0.18	-0.12	-0.17	-0.07
	FeX_2														-0.02	-0.03	0.29	-0.02	-0.03	0.31				-0.02	-0.03	0.29	0.18	0.14	0.20	0.18	0.12	0.21	0.12	0.07	0.17
	Pyrite		-0.02	-0.03	-0.02	-0.02	-0.03	-0.02	-0.02	-0.03	-0.02	-0.02	-0.03	-0.02	0.00	-0.31	0.00	0.00	-0.33	0.00	-0.02	-0.03	-0.02	0.00	-0.31	0.00	-0.20	-0.22	-0.16	-0.20	-0.23	-0.15	-0.14	-0.19	-0.10
	Redox (mmol/l)																																		
	Fe(3)		0.00			0.00			0.00			0.00			0.00			0.00			0.00			0.00			0.00			0.00			0.00		
	H(0)		0.00			0.00			0.00			0.00			0.00			0.00			0.00			0.00			0.00			0.00			0.00		
	S(-2)		-0.05			-0.05			-0.05			-0.05									-0.05						-0.40			-0.40			-0.29		
			*) ΔCl = 5%			*) ΔCl = 5%			*) ΔCl = 5%			*) ΔCl = 5%			*) ΔCl = 5%			*) ΔCl = 5%			*) ΔCl = 5%			*) ΔCl = 5%			*) ΔCl = 5%						*) ΔCl = 5%		

	Sample		SA0850B			SA0813B			SA0813B			SA0813B			SA0813B			SA0813B			SA0813B			SA0813B			SA0813B		
	Date		231 (*			309 (*			768 (*			980 (*			1002 (*			1253 (*			1343 (*			1597 (*			1745 (*			1967 (*		
	Seawater Average					0.39	0.36	0.42	0.62	0.57	0.64	0.74	0.66	0.81	0.59	0.56	0.64	0.68	0.61	0.78	0.83	0.82	0.83	0.58	0.51	0.67	0.68	0.57	0.78	0.80	0.79	0.84
Saline Glacial Alt. Litorina Meteoric	HAS05/-56.3	-1243							0.21	0.20	0.23	0.14	0.10	0.18	0.23	0.20	0.23	0.19	0.14	0.24	0.17	0.17	0.18	0.27	0.21	0.31	0.23	0.19	0.29	0.16	0.15	0.17
	KAS04/-185.2	-624																														
	HAS07/-75.1	-1247																														
	KAS06/-200.1	-580	0.32	0.29	0.34	0.07	0.05	0.08																								
	Litorina Sea																															
	KAS06/-331.9	-566	0.20	0.20	0.26	0.55	0.52	0.58	0.17	0.15	0.20	0.12	0.06	0.20	0.18	0.15	0.20	0.13	0.07	0.20				0.14	0.11	0.18	0.08	0.02	0.16	0.04	0.01	0.06
	KAS06/-433.3	-559																														
	KAS06/-284.4	-573																														
	KAS04/-376.8	-638																														
	HAS13/-42.0	-547	0.48	0.41	0.48																											
	Glacial Melt Water																															
	KAS03/-121.8	-679																														
	KAS02-199.8	-720																														
	KAS03/-239.0	-856																														
	"Preglacial Altered"																															
	KAS02/-881.3	-700																														
	KAS03/-830.1	-845																														
	KAS02/-523.0	-971																														
	KAS03/-602.5	-850																														
	KAS03/-348.6	-868																														
	KAS03/-454.3	-862																														
	KAS04/-275.6	-614																														
	KAS02/-317.2	-826																														
	Transfers (mmol/l)																															
	Calcite		0.38	0.34	0.47	6.69	6.43	7.14	0.72	0.56	0.88	0.54	0.32	0.73	0.52	0.32	0.72	0.32	0.21	0.58	0.15	0.09	0.16	0.49	0.27	0.76	0.78	0.53	1.01	0.67	0.48	0.84
	CH_2O		0.72	0.71	0.98	6.75	6.08	7.51	4.88	4.46	4.91	3.81	3.19	4.08	3.15	2.58	3.56	2.97	2.62	3.47	3.53	3.46	3.53	2.63	2.00	3.22	2.10	1.46	2.67	3.11	2.58	3.62
	CO_2					8.39	7.59	9.74																								
	NaX		-0.46	-0.62	-0.44																-7.56	-9.50	-5.08									
	CaX_2					-5.02	-5.76	-4.23				1.29	0.17	2.63				1.27	0.12	2.72	5.84	5.13	6.59				1.58	0.16	2.95	2.76	2.12	3.38
	MgX_2					3.04	2.23	3.64	-1.50	-1.52	-1.37	-2.48	-3.69	-1.30	-0.98	-1.11	-0.81	-2.20	-3.63	-0.97	-3.15	-3.67	-2.65	-0.83	-1.01	-0.65	-2.22	-3.62	-0.89	-3.67	-4.19	-3.07
	FeX_2		0.23	0.22	0.31	1.98	1.78	2.20	1.50	1.37	1.52	1.19	1.00	1.28	0.98	0.81	1.11	0.93	0.82	1.08	1.09	1.07	1.10	0.83	0.65	1.01	0.63	0.45	0.80	0.91	0.76	1.06
	Pyrite		-0.21	-0.28	-0.20	-1.93	-2.15	-1.74	-1.39	-1.40	-1.28	-1.09	-1.17	-0.91	-0.90	-1.02	-0.74	-0.85	-0.99	-0.75	-1.01	-1.01	-0.99	-0.75	-0.92	-0.57	-0.60	-0.76	-0.42	-0.89	-1.03	-0.74
	Redox (mmol/l)																															
	Fe(3)								0.00			0.00			0.00			0.00			0.00			0.00			0.00			0.00		
	H(0)		0.00			0.00			0.00			0.00			0.00			0.00			0.00			0.00			0.00			0.00		
	S(-2)		-0.41			-3.86			-2.79			-2.18			-1.80			-1.70			-2.02			-1.50			-1.20			-1.78		
			*) ΔS(6) 30% in HAS13 & SA0850B			*) ΔCl = 2% *) $\Delta^{18}O$ = .05 *) ΔNa, Ca, S(6) 20% in SA813B			*) ΔCl = 5% *) ΔS(6) = 15%			*) ΔCl = 5%			*) ΔCl = 5% *) ΔS(6) = 10%			*) ΔCl = 5%			*) ΔCl = 5%			*) ΔCl = 5%			*) ΔCl = 5%			*) ΔCl = 5%		

	Sample	Date	SA1327A 653 (*			SA1229A 966 (*			SA1229A 1253 (*			SA1229A 1598 (*			SA1229A 1744 (*			SA1229A 1967 (*		
	Seawater Average		0.60	0.59	0.65	0.68	0.64	0.72	0.65	0.59	0.70	0.70	0.66	0.76	0.76	0.76	0.80	0.98	0.96	1.00
Meteoric	HAS05/-56.3	-1243																		
	KAS04/-185.2	-624																		
	HAS07/-75.1	-1247																		
	KAS06/-200.1	-580	0.23	0.22	0.24				0.18	0.12	0.22	0.23	0.20	0.24	0.24	0.20	0.24	0.02	0.00	0.04
Litorina	Litorina Sea																			
	KAS06/-331.9	-566	0.18	0.12	0.18	0.32	0.28	0.36	0.16	0.11	0.25	0.07	0.02	0.13						
	KAS06/-433.3	-559																		
	KAS06/-284.4	-573																		
	KAS04/-376.8	-638																		
Glacial Alt.	HAS13/-42.0	-547																		
	Glacial Melt Water																			
	KAS03/-121.8	-679																		
	KAS02-199.8	-720																		
Glacial	KAS03/-239.0	-856																		
	"Preglacial Altered"																			
	KAS02/-881.3	-700																		
Saline	KAS03/-830.1	-845																		
	KAS02/-523.0	-971																		
	KAS03/-602.5	-850																		
	KAS03/-348.6	-868																		
	KAS03/-454.3	-862																		
	KAS04/-275.6	-614																		
	KAS02/-317.2	-826																		
	Transfers (mmol/l)																			
	Calcite		0.76	0.71	0.86	1.13	0.94	1.32	0.80	0.64	0.89	0.79	0.63	0.94	1.05	0.90	1.20	0.89	0.78	0.98
	CH_2O		2.40	2.39	2.67	4.97	4.39	5.47	4.02	3.93	4.34	3.73	3.25	4.04	2.88	2.50	3.27	3.62	3.48	3.82
	NaX																	-8.56	#####	-4.12
	CaX_2		1.83	1.19	2.48							1.04	0.26	1.99	1.88	1.37	2.69	6.75	5.27	8.12
	MgX_2		-2.55	-3.23	-1.98	-1.47	-1.62	-1.30	1.19	-1.28	-1.16	-2.14	-2.96	-1.26	-2.73	-3.47	-2.31	-3.52	-4.71	-2.36
	FeX_2		0.72	0.71	0.80	1.47	1.30	1.62	1.19	1.16	1.28	1.10	0.96	1.20	0.86	0.75	0.97	1.06	1.02	1.12
	Pyrite		-0.68	-0.76	-0.68	-1.42	-1.56	-1.25	-1.15	-1.24	-1.12	-1.07	-1.15	-0.93	-0.82	-0.93	-0.71	-1.03	-1.09	-0.99
	Redox (mmol/l)																			
	Fe(3)																			
	H(0)		0.00			0.00			0.00			0.00			0.00			0.00		
	S(-2)		1.37			-2.84			-2.30			-2.13			-1.65			-2.07		
			*) ΔCl = 5%			*) ΔCl = 5%			*) ΔCl = 5%			*) ΔCl = 5%			*) ΔCl = 5%			*) ΔCl = 5%		
			*) $\Delta^{18}O$ = 0.05															*) $\Delta^{18}O$ = 0.05		

	Sample	KA1755A	KA1755A	SA2074A	SA2074A	SA2074A	SA2074A	SA2074A	SA2873A	SA2873A	SA2873A	SA2873A	SA2873A
	Date	1745 (*	1967 (*	766 (*	1001 (*	1253 (*	1344 (*	1598 (*	1140	1232 (*	1345 (*	1758 (*	1966 (*
	Seawater Average				0.26 0.25 0.28	0.36 0.26 0.43	0.36 0.35 0.36	0.51 0.51 0.52					
Saline	HAS05/-56.3 -1243												
Saline	KAS04/-185.2 -624												
Saline	HAS07/-75.1 -1247												
Saline	KAS06/-200.1 -580				0.38 0.37 0.39	0.42 0.35 0.48	0.47 0.47 0.47	0.49 0.48 0.49					
Glacial	Litorina Sea												
Glacial	KAS06/-331.9 -566				0.36 0.33 0.37	0.23 0.13 0.35	0.17 0.17 0.18						
Glacial	KAS06/-433.3 -559												
Glacial	KAS06/-284.4 -573								0.17 0.17 0.18	0.18 0.17 0.25	0.27 0.24 0.30	0.11 0.11 0.11	0.08 0.02 0.11
Glacial	KAS04/-376.8 -638												
Alt. Litorina	HAS13/-42.0 -547												
Meteoric	Glacial Melt Water												
Meteoric	KAS03/-121.8 -679												
Meteoric	KAS02-199.8 -720												
Meteoric	KAS03/-239.0 -856												
	"Preglacial Altered"												
	KAS03/-914.1 -657	0.52 0.52 0.79	0.75 0.75 0.87									0.89 0.89 0.89	0.92 0.89 0.98
	KAS02/-881.3 -700								0.28 0.27 0.35	0.36 0.29 0.63	0.53 0.42 0.65		
	KAS03/-830.1 -845												
	KAS02/-523.0 -971	0.48 0.21 0.48	0.25 0.13 0.25						0.55 0.47 0.56	0.46 0.13 0.54	0.20 0.06 0.35		
	KAS03/-602.5 -850												
	KAS03/-348.6 -868												
	KAS03/-454.3 -862												
	KAS04/-275.6 -614												
	KAS02/-317.2 -826												
	Transfers (mmol/l)												
	Calcite	0.00 -0.01 0.00	-0.01 -0.02 -0.01		-0.08 -0.09 -0.08			0.19 0.16 0.27	-0.01 -0.01 -0.01	-0.03 -0.03 -0.03	-0.04 -0.05 -0.03		
	CH_2O	0.00 0.00 0.01	0.00 0.00 0.00		0.02 0.01 0.02	0.20 0.10 0.30	0.27 0.20 0.32	0.52 0.52 0.73	0.00 0.00 0.00	0.03 0.03 0.03	0.00 0.00 0.00	0.01 0.01 0.02	0.02 0.00 0.03
	NaX	0.00 0.00 1.13	0.84 0.00 1.42			-0.11 -0.17 -0.05	-0.15 -0.18 -0.11	1.77 0.98 2.55		0.00 0.00 0.00		0.00 0.00 1.24	0.54 0.00 1.35
	CaX_2	0.00 0.00 0.56	0.00 0.00 0.71							0.00 0.00 0.00		0.00 0.00 0.62	0.00 0.00 0.68
	MgX_2	0.00 -0.56 0.00	-0.42 -0.72 -0.17					-1.03 -1.48 -0.70		-0.01 -0.01 -0.01		0.00 -0.62 0.00	-0.27 -0.68 0.00
	FeX_2	0.00 0.00 0.00	0.00 0.00 0.00			0.05 0.02 0.08	0.07 0.05 0.09	0.15 0.15 0.21		0.01 0.01 0.01		0.00 0.00 0.01	0.01 0.00 0.01
	Pyrite	0.00 0.00 0.00	0.00 0.00 0.00		-0.01 -0.01 0.00	-0.06 -0.09 -0.03	-0.08 -0.09 -0.06	-0.15 -0.21 -0.15	0.00 0.00 0.00	-0.01 -0.01 -0.01	0.00 0.00 0.00	0.00 -0.01 0.00	-0.01 -0.01 0.00
	Redox (mmol/l)												
	Fe(3)												
	H(0)	0.00	0.00		0.00	0.00	0.00	0.00	0.00	0.00	0.00	0.00	0.00
	S(-2)				-0.01	-0.12	-0.15	-0.30		-0.02		-0.01	-0.01
		*) ΔCl = 5%	*) ΔCl = 5%		*) ΔCl = 5%	*) ΔCl = 5%	*) ΔCl = 5%	*) ΔCl = 5%		*) ΔCl = 5%	*) ΔCl = 5%	*) ΔCl = 5%	*) ΔCl = 5%

Contaminated Sample

*) changeables Δ = 10%

	Sample	KAS03			KAS03			KAS03			KAS03			KAS03			KAS03			KAS07			KAS07			KAS07		
	Date	-850			596 (*			768 (*			866 (*			958 (*			980 (*			1197 (*			608 (*			979 (*			1197 (*			1344 (*		
	Seawater Average																														
Meteoric	HAS05/-56.3	-1243																													
Meteoric	KAS04/-185.2	-624																													
Meteoric	HAS07/-75.1	-1247																													
Meteoric	KAS06/-200.1	-580																													
Litorina	Litorina Sea																														
Litorina	KAS06/-331.9	-566																													
Litorina	KAS06/-433.3	-559																													
Litorina	KAS06/-284.4	-573																					0.25	0.24	0.25	0.30	0.26	0.30	0.36	0.35	0.36	0.29	0.29	0.34
Litorina	KAS04/-376.8	-638																													
Alt.	HAS13/-42.0	-547																													
Glacial	Glacial Melt Water																														
Glacial	KAS03/-121.8	-679				0.60	0.59	0.60	0.56	0.56	0.56																				
Glacial	KAS02-199.8	-720	0.41	0.34	0.47																										
Glacial	KAS03/-239.0	-856										0.75	0.75	0.75	0.36	0.33	0.38	0.67	0.67	0.69	0.42	0.35	0.42								
Saline	"Preglacial Altered"																														
Saline	KAS03/-914.1	-657																													
Saline	KAS02/-881.3	-700																													
Saline	KAS03/-830.1	-845	0.59	0.53	0.66																								0.14	0.07	0.23			
Saline	KAS02/-523.0	-971																								0.70	0.70	0.74				0.71	0.66	0.71
Saline	KAS03/-602.5	-850				0.40	0.40	0.41	0.44	0.44	0.44	0.25	0.25	0.25	0.64	0.62	0.67	0.33	0.31	0.33	0.58	0.58	0.65	0.75	0.75	0.76				0.51	0.41	0.57			
Saline	KAS03/-348.6	-868																													
Saline	KAS03/-454.3	-862																													
Saline	KAS04/-275.6	-614																													
Saline	KAS02/-317.2	-826																													
	Transfers (mmol/l)																														
	Calcite		-0.51	-2.33	-0.42							-0.04	-0.05	-0.02				-0.01	-0.02	0.00	0.06	0.04	0.10	-0.03	-0.04	-0.01				-0.04	-0.04	-0.04	-0.06	-0.07	-0.05
	CH_2O		0.08	0.06	1.92	0.24	0.22	0.29	0.37	0.37	0.37	0.00	0.00	0.02	0.30	0.27	0.35	0.00	0.00	0.00	0.06	0.00	0.15	0.00	0.00	0.04	0.82	0.74	0.88	0.00	0.00	0.01	0.00	0.00	0.03
	NaX		1.89	1.22	4.27				-1.06	-1.09	-0.99	0.60	0.02	1.18	-0.17	-0.20	-0.16				-0.04	-0.09	0.00	0.70	-0.02	1.33				0.93	0.20	1.75	0.00	-0.01	0.01
	CaX_2					-1.03	-1.13	-1.01																											
	MgX_2		-0.63	-0.95	-0.32	0.96	0.92	1.04	0.42	0.39	0.44	-0.30	-0.59	-0.02										-0.35	-0.67	0.00	-0.24	-0.25	-0.21	-0.47	-0.88	-0.10			
	Goethite		0.31	0.25	1.72																														
	FeX_2		-0.31	-1.29	-0.26	0.07	0.06	0.08	0.11	0.11	0.11	0.00	0.00	0.00	0.09	0.08	0.10				0.02	0.00	0.04	0.00	0.00	0.01	0.24	0.21	0.25	0.00	0.00	0.00	0.00	0.00	0.01
	Pyrite		0.00	-0.43	0.00	-0.07	-0.08	-0.06	-0.11	-0.11	-0.11	0.00	0.00	0.00	-0.09	-0.10	-0.08	0.00	0.00	0.00	-0.02	-0.04	0.00	0.00	-0.01	0.00	-0.23	-0.25	-0.21	0.00	0.00	0.00	0.00	-0.01	0.00
	Redox (mmol/l)																																		
	Fe(3)		0.31			0.00																													
	H(0)		0.00			-0.14			0.00			0.00			0.00			0.00			0.00			0.00			0.00			0.00			0.00		
	S(-2)								-0.21						-0.17						-0.03						-0.47								
						*) ΔCl = 5%			*) ΔCl = 5%			*) ΔCl = 5%			*) ΔCl = 5%			*) ΔCl = 5%			*) ΔCl = 5%			*) ΔCl = 5%			*) ΔCl = 5%			*) ΔCl = 5%			*) ΔCl = 5%		
						*) ΔNa = 13%						*) ΔS(6) = 15%						*) ΔS(6) = 10%												*) ΔAlk = 30% in KAS07					
																														*) Δ pH = 0.8					

Part IV

Task 5 — Mixing Proportions of Glacial, Litorina, Altered, Saline, Meteoric and Baltic Sea Waters in the Äspö Tunnel

Eero Kattilakoski

VTT Energy

Ari Luukkonen

VTT Building and Transport

March 2001

SUMMARY

Task 5 (Impact of the tunnel construction on the groundwater system at Äspö, a hydrological-hydrochemical model assessment exercise) aims for the comparison and ultimate integration of hydrochemistry and hydrogeology. This work concerned with the groundwater flow modelling part of Task 5.

The dual porosity transport model was applied. The FEFTRA code, which is based on the porous medium concept and the finite element method, was used for the numerical solution.

The flow model was constructed by including the hydrologic connections recognised during the tunnel construction. The observed properties of water and bedrock were included in the simulation model. The initial chloride boundary was fixed in accordance with the observations of the groundwater composition. The groundwater table applied over the Äspö Island was replaced by a flow rate boundary condition in the first updating of the tunnel. The hydraulic data gained during the tunnel construction was utilised to confirm the residual pressure and flow rate boundary conditions in the tunnel and the shaft.

The reference water types were identified on the basis of the analyses of geochemical data and the interpretations of the Quaternary history of the Äspö site in the separate inverse-modelling. In the hydrological simulations the mixing fractions of the reference water types were transported like conservative parameters.

In essence, the simultaneous modelling of flow and transport is a coupled process due to the varying density of groundwater. First, the coupled equations of residual pressure and concentration were solved. Then, the transport equations of the different water types were solved using the residual pressure and concentration fields. The simulation time steps covered the period from the natural conditions until the completion of the tunnel and the shaft.

The groundwater flow simulation aimed to the reproduction of the estimated mixing proportions, and further to predict the mixing proportions in the model. The predictions could be converted into chemical compositions, and the ultimate results were the predictions of chemical compositions in the model.

Detailed performance measures were used for the presentation of the results. The simulated mixing proportions in the control points and at certain cut planes were compared with those from the inverse-modelling. At current stage, the results propose a method for confirming the structural relations, and for refining the spatial hydrological and structural averages for the fracture zones.

TABLE OF CONTENTS

1 INTRODUCTION

1.1 Background

Task 5 (Impact of the tunnel construction on the groundwater system at Äspö, a hydrological-hydrochemical model assessment exercise) aims for the comparison and ultimate integration of hydrochemistry and hydrogeology. The consistency of groundwater flow models and hydrochemical mixing-reaction models is assessed through the integration and comparison of hydraulic and chemical data obtained before and during the tunnel construction. The modelling task will be useful for a stability assessment of the hydrodynamic and hydrochemical conditions at Äspö. A specific objective is the development of a procedure for the integration of hydrological and hydrochemical information which could be used for disposal site assessments — especially in a crystalline bedrock environment. (Wikberg, 1998)

As regards to the contribution of VTT Energy, the groundwater flow simulation on the basis of the geochemical M3 estimations (Gurban et al., 1998) formed the first part of Task 5 (Kattilakoski, 1999). Similar types of simulations were requested on the basis of the estimations done in VTT Communities & Infrastructure. The current work concerns the integration of the hydrological simulations with the geochemical estimations by Luukkonen (2000).

In the present approach the geochemical reference water types differ from the M3 approach (Gurban et al, 1998). Therefore, the approximations of geochemical boundaries have to be re-estimated. The reference types considered relevant for mixing calculations are glacial melt, Litorina Sea, altered, saline, meteoric and Baltic Sea waters. For undisturbed conditions, the redefinition of the boundaries is a fairly straightforward process. By plotting calculated reference water proportions as a function of sampling depths and making smoothed regressions onto depth vs. proportion plots, reasonable estimates for the vertical boundaries of the hydrological model at sea and land areas can be achieved.

1.2 Objectives

This work concerns with the two sides of groundwater flow modelling (transport and geochemical reactions) the main emphasis being on the conservative transport. In the transport simulation no chemical reactions are modelled, only mixing (see Appendix B). Depending on the mixing result of the reference water types a net geochemical correction may be done to the conservative mixing result, if applicable.

Mixing estimations were performed using the reference water types that have been identified based on the analyses of geochemical data and on the

interpretations of the Quaternary history of the Äspö site. In the hydrological simulations the mixing fractions of the reference water types can be transported like conservative parameters. The groundwater flow modelling aims to the determination of the mixing proportions. The mixing proportions simulated give tools to interpret the actual sample compositions for locations of interest (see Appendix C). If certain criteria are fulfilled (cf. Luukkonen, 2000), during the composition calculation step also the net effect of chemical reactions can be estimated.

The flow model is constructed by including the hydrologic connections recognised during the tunnel construction. The observed properties of water and bedrock are included in the simulation model (Rhén et al., 1997). The initial chloride boundary is fixed in accordance with the observations of the groundwater composition. The groundwater table applied over the Äspö Island is replaced by a flow rate boundary condition in the first updating of the tunnel. The hydraulic data gained during the tunnel construction is utilised to confirm the residual pressure and flow rate boundary conditions in the tunnel and the shaft(s).

In essence, the simultaneous modelling of flow and transport is a coupled process. The FEFTRA code, which is based on the porous medium concept and the finite element method, is used to solve both the coupled equations of residual pressure and concentration and the transport equations of the different water types. The dual porosity transport model is applied in the calculations.

The simulation time steps cover the period from the natural conditions until the completion of the tunnel and the shafts. The transport equations of the different groundwater types are solved using the previously simulated residual pressure and concentration fields. The initial concentration boundary condition for the transport equations of the different water types is given on the basis of the geochemical inverse-modelling results (Luukkonen, 2000).

The mixing ratios simulated at the control points and at certain cut planes are compared with those from the geochemical estimations. Detailed performance measures (Rhén et al., 1998) are used for the presentation of the results.

2 MODEL CONCEPTS AND FORMULATION

2.1 Governing equations

The mathematical formulation of flow and transport in the *dual porosity* medium comprises three coupled and non-linear partial differential equations. Two of them describe the flow of water with variable density and the amount of mass transported with flowing water in the water-bearing fractures. The third equation describes the amount of mass transported by diffusion in the matrix blocks. The mathematical formulation of the dual porosity approach is explained in detail by e.g., Löfman and Taivassalo (1995) and Löfman (1996).

The flow equation is expressed in terms of the residual pressure p — the actual pressure minus the hydrostatic component of freshwater (e.g., Bear, 1979; de Marsily, 1986):

$$\nabla \cdot (\frac{\rho \mathbf{k}}{\mu}(\nabla p - (\rho - \rho_0)\mathbf{g})) = \frac{S_S}{g}\frac{dp}{dt} + \phi\frac{d\rho}{dt} - \rho_{in}Q_{in} + \rho Q_{out}\,, \qquad (2.1)$$

where

p	is the residual pressure (Pa),
ρ	is the density of water (kgm^{-3}),
ρ_0	is the freshwater density (kgm^{-3}),
μ	is the viscosity of water (kgm^{-1}s^{-1}),
$\boldsymbol{k}$	is the permeability tensor of the medium (m^2),
$\boldsymbol{g}$	is the gravitational acceleration (ms^{-2}),
S_S	is the specific storage of the medium (m^{-1}),
ϕ	is the total porosity (-),
ρ_{in}	is the density of the inflowing water (kgm^{-3}),
Q_{in}	is the term for sources (s^{-1}) and
Q_{out}	is the term for sinks (s^{-1}).

The permeability tensor $\boldsymbol{k}$ in Eq. (2.1) can be expressed in terms of the hydraulic conductivity $\boldsymbol{K}$ (m/s):

$$\mathbf{k} = \frac{\mathbf{K}\mu}{\rho g}\,. \qquad (2.2)$$

In the dual porosity approach Eq. (2.1) describes the flow in the water-bearing fractures.

The equation describing mass transport in the water-bearing fractures is as follows (Huyakorn et al., 1983):

$$\nabla \cdot (\mathbf{D}\nabla c) - \nabla \cdot (\mathbf{q}c) + Q_{in}c_{in} - Q_{out}c + (1 - \phi_f)\Gamma = \phi_f \frac{\partial c}{\partial t}\,, \qquad (2.3)$$

where c is the concentration of the solute (g/l),
$\boldsymbol{D}$ is the hydrodynamic dispersion coefficient, which includes dispersion and diffusion (m^2s^{-1}),
$\boldsymbol{q}$ is the Darcy velocity (ms^{-1}),
Q_{in} is the term for sources (s^{-1}),
c_{in} is the concentration in the inflowing water (g/l),
Q_{out} is the term for sinks (s^{-1}),
ϕ_f is the flow (fracture) porosity (-) and
Γ is the rate of solute transfer from the matrix block to the fracture ($kgm^{-3}s^{-1}$).

The components of the hydrodynamic dispersion tensor in Eq. (2.3) are

$$D_{ij} = \varepsilon_T |\mathbf{q}| \delta_{ij} + (\varepsilon_L - \varepsilon_T) \frac{q_i q_j}{|\mathbf{q}|} + \phi_d D_0 \delta_{ij} , \tag{2.4}$$

where ε_L is the longitudinal dispersion length (m),
ε_T is the transversal dispersion length (m),
δ_{ij} is the Kronecker delta function (-),
ϕ_d is the diffusion porosity (-) and
D_0 is the molecular diffusion coefficient in water (m^2s^{-1}).

The Darcy velocity $\boldsymbol{q}$ in Eq. (2.3) in terms of the residual pressure p is

$$\mathbf{q} = -\frac{\mathbf{k}}{\mu} (\nabla p - (\rho - \rho_0)\mathbf{g}) . \tag{2.5}$$

The mass transport in the matrix blocks can be described with a one-dimensional diffusion equation

$$\frac{\partial}{\partial z'} (D_e' \frac{\partial c'}{\partial z'}) = \phi' \frac{\partial c'}{\partial t} , \tag{2.6}$$

where c' is the concentration of the solute (g/l),
D_e' is the effective diffusion coefficient (m^2s^{-1}) and
ϕ' is the porosity in the matrix blocks (-).

In accordance with Archie's law (Valkiainen, 1992), the connection between the effective diffusion coefficient and the porosity in the matrix blocks can be stated as

$$D_e' = 0.71 \cdot D_0 \phi'^{1.58} . \tag{2.7}$$

Equations (2.3) and (2.6) are coupled by the continuity of the diffusive mass flux at the interface of the fracture and the matrix block. For a rectangular matrix block unit the rate of solute transfer from the matrix block to the fracture is

$$\Gamma = -\frac{1}{a}(D'_e \frac{\partial c'}{\partial z'}\Big|_{z'=a}), \qquad (2.8)$$

where a (m) is half the fracture spacing, i.e., half the matrix block thickness.

2.2 Numerical tool

The flow equation (2.1) and the transport equation (2.3) are coupled by the density ρ and the Darcy velocity $\boldsymbol{q}$ (Eq. (2.5)). This results in a system of two non-linear partial differential equations that can rarely be solved analytically. The finite element code FEFTRA was used in this work for the numerical solution (Löfman, 1996).

The finite element method with linear elements was employed. The conventional Galerkin technique was applied to the flow equation (2.1). In order to avoid the numerical problems related to highly convective cases the transport equation (2.3) was solved using the streamline-upwind/Petrov-Galerkin (SUPG) method (Brooks and Hughes, 1992; implemented in FEFTRA by Laitinen, 1995). The conventional Galerkin method was applied to the diffusion equation (2.6) in the matrix blocks.

In the coupled cases non-linearities were treated by the Picard iteration scheme (Huyakorn and Pinder, 1983), which applies the finite element procedure for both the flow and the transport equation sequentially. At the end of each iteration sweep the concentration values are updated using an underrelaxation scheme. This way the oscillations of concentration changes from iteration to iteration are reduced. No iteration was needed in the mixing calculations of a single water type, which utilised the previously simulated residual pressure and chloride fields.

An initial estimate for the nodal values of the residual pressure and the concentration at the beginning of the first iteration sweep of each time step was obtained by using a linear time extrapolation formula.

The mass matrices resulting from the finite element formulation were formed by a diagonalization procedure known as ”lumping” (Huyakorn and Pinder, 1983). In practical problems this leads to a more stable solution than with a ”consistent” matrix.

The Gauss-Seidel method (Laitinen, 1994) was used to solve the matrix equation (2.3) in the mixing calculations. In the coupled calculations the conjugate gradient method was used to solve the finite element formulation of Equation (2.1) for residual pressure and the Gauss-Seidel method to solve the finite element formulation of Equation (2.3) for concentration.

3 SIMULATION MODEL

This chapter describes the geometric framework, finite element mesh, material properties and boundary conditions of the simulation model. The properties given by Rhén et al. (1997) and the modifications made in this work are given in Table 3.2. The reference water types used in the inverse modellings are shown in Table 3.5.

3.1 Geometric framework

All the certain, probable and possible structures proposed by Rhén et al. (1997) were included in the model (Figure 3.1).

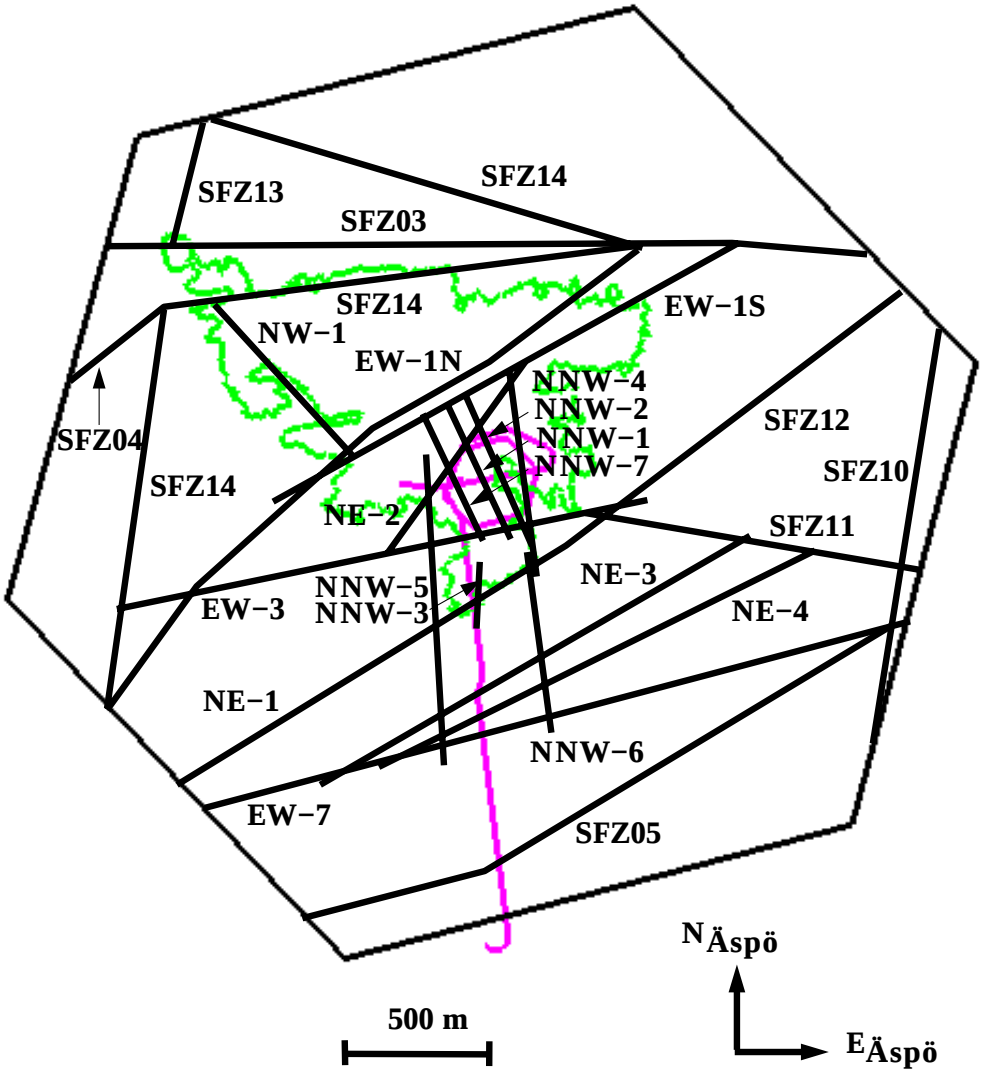

Figure 3.1. Modelling area and fracture zones at the surface. The coastline of the Äspö Island and the tunnel are also shown.

The regional zones SFZ05 and SFZ12 have dip angles of about 70 degrees. The other regional zones are vertical. All the regional zones extend to the depth of 1500 m.

The local zones were defined as quadrangles with corner points as proposed by the three points given by Rhén et al. (1997). The vertical zones were extended to the depth of 1500 m (except on the ground level unexposed NNW-8, which extends from the depth of 300 m to the depth of 700 m).

The hydraulic connections were established as given by Rhén et al. (1997, Fig. 6-31 and Table A2-6).

The definitions of the zones SFZ07 and EW-1N were combined: thus, the zone EW-1N has a regional extension in the model (Fig. 3.1). The geometry of the zone NE-1 was combined with the geometry of SFZ12. The directions of the zones NE-3 and NE-4 were approximated with the average values of X, Y and Z given. In addition, NE-3 was connected with SFZ11 and EW-7.

The zone EW-1S was given an extension as far as SFZ07 and SFZ03. The assumed hydraulic connection of EW-1S with the zones NNW-1, NNW-2 and NNW-4 was formed. The depth extension of EW-1S is the same as that of NNW-2 (about 1150 m; see Appendix A). This is the only difference in the geometry in comparison with the M3-based simulations (Kattilakoski, 1999). EW-3 stops at SFZ14 and SFZ12. The zone EW-7 was continued as far as SFZ12 and SFZ10.

The zones NE-2 and EW-1S were connected. The conductor NW-1 is assumed to terminate to the south at EW-1N. The conductor NNW-4 intersects with EW-1S and SFZ12. In the southern end, NNW-5 was connected with NE-4 and NNW-6 with EW-7. NNW-7 forms a connection with EW-3 and EW-1S. In addition, NNW-7 was extended to the depth of 191 m.

The coordinates of the fracture zones included in the flow model are shown in Appendix A.

3.2 Finite element mesh

The finite elements for the rock blocks are linear hexahedrals and wedges. The base mesh formed by these elements is approximately the same as in the study by Mészáros (1996). Triangles and quadrangles are used for the fracture zones. The mesh contains 58 224 three-dimensional elements and 13 443 two-dimensional elements.

The element mesh extends from the sea level to the depth of 1500 m (as in Mészáros, 1996). The finite element mesh is the same as in the M3-based simulations (Kattilakoski, 1999).

3.3 Material properties

The properties of water and bedrock employed in the simulations are shown in Table 3.1.

Table 3.1. Properties of water and bedrock used in the simulations.

Symbol	Parameter	Value	Reference
μ	Viscosity	$1.0 \cdot 10^{-3}$ kgm^{-1}s^{-1}	Lide (1990)
ρ_0	Freshwater density	998.585 kgm^{-3}	
D_0	Molecular diffusion coefficient	$1.0 \cdot 10^{-9}$ m^{2}s^{-1}	Löfman and Taivassalo (1995)
a_C	Density dependence on chloride	1.16	Löfman (1996)
ε_L	Longitudinal dispersion length	1000 m	
ε_T	Transversal dispersion length	100 m	
ϕ_d	Diffusion porosity	$3.5 \cdot 10^{-3}$	
ϕ'	Porosity in the matrix blocks	$3.5 \cdot 10^{-3}$	Rhén et al. (1997) p. 22, p. 403
C_{vh}	Coefficient for dependence between the volume and hydraulic apertures	10	Vieno et al. (1992)

The properties of the fracture zones are shown in Table 3.2 (Rhén et al., 1997). The transmissivities T (m^2/s), the widths of the zones (m), storage coefficients S (-) and the fracture spacings $2a_0$ (m) at the ground level are shown. There are several indications of the transmissivity vs. depth relations of the fracture zones (e.g. Rhén et al., 1997, Fig. A2-6). In the shallow depth dry land areas transmissivity values seem to *increase* as depth increases. In moderate and profound depths, the transmissivity vs. depth relation seems much more insensitive.

Depth dependencies were given for the transmissivities of the shallow parts of the fracture zones in the land areas down to 200 metres, and for the deep parts of the zones EW-3, SFZ05, SFZ12 and NNW-8 (Fig. 3.2). The deep part depth dependence in the zone EW-3 was suggested by Rhén et al. (1997).

The relationship for the transmissivities of the shallow parts of the fracture zones in the dry land areas down to 200 metres depth is as follows:

$$T = T_0 \cdot 10^{c \log_{10} d}, \qquad (3.1)$$

where T_0 is one thousandth part of the transmissivity given in Table 3.2 (T_0=T(z=-200 m)/1000 for the zone EW-3 due the depth dependent transmissivity throughout the zone), c is the coefficient for the depth dependence (1.30376) and d is the depth (m). The topmost level, at which this formula is applied, is the depth of 15 m, which is approximately the depth of the center line of the uppermost element layer. The other depth dependencies related to the fracture zones are discussed in detail in Section 5.2, where the mixing ratios at the control points are considered.

The depth dependence (3.1) was not applied for the shallow part of the zone SFZ05 in the land areas due to the tendency of the model to underestimate the proportion of meteoric water in the control point KR0012B. The transmissivity of the zone SFZ12 in the land areas down to 200 metres depth is T=7.51·10^{-6} m^2/s. The zone NNW-8 extends from the depth of 300 m to the depth of 700 m. Thus, the transmissivity value given in Table 3.2 for NNW-8 is at the depth of 300 m.

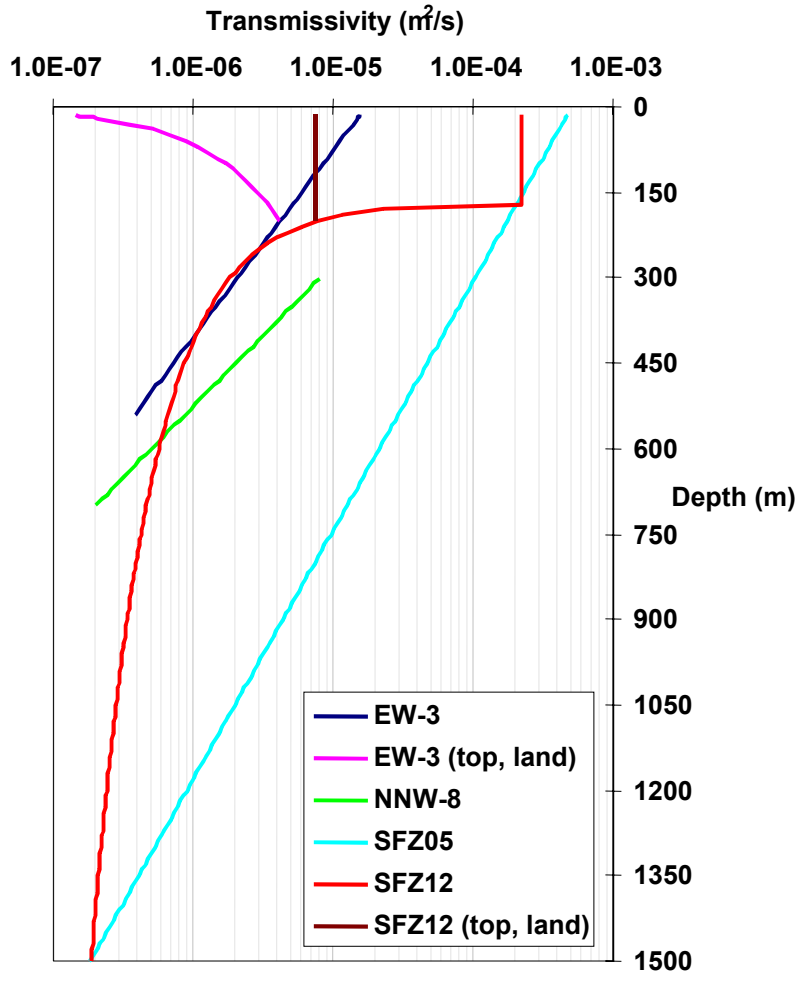

Figure 3.2. The transmissivities of the fracture zones SFZ05, SFZ12, EW-3 and NNW-8.

Rhén et al. (1997) gave the linear relationship between $\log_{10}T$ and $\log_{10}S$. They noticed that the relation seems to give unrealistic low S values for very low T values. For that reason, for S the value $\max(1.0\cdot10^{-6}; aT^b)$ is used in this work. There are also few points for the regression that makes the relation uncertain. However, the variability in S values is probably relatively large.

An assumption is made on the depth dependence of the spacing of the water-bearing fractures:

$$2a = 2a_0 2^{-\frac{z}{500}}, \tag{3.2}$$

where $2a_0$ (m) is the fracture spacing on the surface.

The fracture aperture $2b$ (m) is given as a function of the fracture spacing $2a$ (m) and the hydraulic conductivity K as follows (Taivassalo and Saarenheimo, 1991)

$$2b = C_{vh}\left(\frac{12\mu}{\rho_0 g} K 2a\right)^{1/3}, \tag{3.3}$$

where C_{vh} (Vieno et al., 1992) is the coefficient for the dependence between the volume and the hydraulic fracture aperture, μ the viscosity of water (Lide, 1990), ρ_0 the freshwater density and g the gravitational acceleration (9.81 m/s^2).

The flow porosity ϕ_f (-) is given as follows (as in Löfman, 1996)

$$\phi_f = \frac{b}{a+b}. \tag{3.4}$$

Table 3.2. Properties of fracture zones. The depth dependencies for the transmissivities of the zones EW-3, SFZ05, SFZ12 and NNW-8 are shown in Figure 3.2. The transmissivities of the shallow parts of the other fracture zones in the dry land areas down to 200 metres depth are given by Eq. (3.1). The transmissivity of the uppermost elements of the zone NE-4 below the sea is T=9.3·10^{-9} m^2/s (supposed width 30 m).

Zone	T (m^2/s) according to Rhén et al., 1997 (Mean)	T (m^2/s), modified	width of zone (m) according to Rhén et al., 1997	width of zone (m), modified	a	b	$S=aT^b$ (-) Rhén et al., 1997 p. 214-215	max (1.0·10^{-6}; S)	$2a_0$ (m) Rhén et al., 1997 p. 117
SFZ01	3.0·10^{-6}		20		0.00922	0.785	4.3·10^{-7}	1.0·10^{-6}	0.05
SFZ02	1.0·10^{-4}		20		0.00922	0.785	6.7·10^{-6}	6.7·10^{-6}	0.05
SFZ03	3.0·10^{-6}		20		0.00922	0.785	4.3·10^{-7}	1.0·10^{-6}	0.05
SFZ04	3.0·10^{-6}		20		0.00922	0.785	4.3·10^{-7}	1.0·10^{-6}	0.05
SFZ05	1.0·10^{-4}	5.0·10^{-4}	20		0.00922	0.785	2.4·10^{-5}	2.4·10^{-5}	0.05
SFZ06	3.0·10^{-6}		20		0.00922	0.785	4.3·10^{-7}	1.0·10^{-6}	0.05
SFZ08	3.0·10^{-6}		20		0.00922	0.785	4.3·10^{-7}	1.0·10^{-6}	0.05
SFZ09	3.0·10^{-6}		20		0.00922	0.785	4.3·10^{-7}	1.0·10^{-6}	0.05
SFZ10	1.0·10^{-4}		20		0.00922	0.785	6.7·10^{-6}	6.7·10^{-6}	0.05
SFZ11	3.0·10^{-6}		20		0.00922	0.785	4.3·10^{-7}	1.0·10^{-6}	0.05
SFZ12	2.2·10^{-4}		20		0.00922	0.785	1.2·10^{-5}	1.2·10^{-5}	0.05
SFZ13	3.0·10^{-6}		20		0.00922	0.785	4.3·10^{-7}	1.0·10^{-6}	0.05
SFZ14	3.0·10^{-6}		20		0.00922	0.785	4.3·10^{-7}	1.0·10^{-6}	0.05
SFZ15	1.0·10^{-4}		20		0.00922	0.785	6.7·10^{-6}	6.7·10^{-6}	0.05
EW-1N	5.2·10^{-7}		30	10	0.00922	0.785	1.1·10^{-7}	1.0·10^{-6}	0.05
EW-1S	1.2·10^{-5}		30	10	0.00922	0.785	1.3·10^{-6}	1.3·10^{-6}	0.05
EW-3	1.7·10^{-5}		15		0.00922	0.785	1.7·10^{-6}	1.7·10^{-6}	0.05
EW-7	1.5·10^{-5}		10		0.00922	0.785	1.5·10^{-6}	1.5·10^{-6}	0.05
NE-2	1.2·10^{-7}		5		0.00922	0.785	3.4·10^{-8}	1.0·10^{-6}	0.05
NE-3	3.2·10^{-4}		50		0.00922	0.785	1.7·10^{-5}	1.7·10^{-5}	0.05
NE-4	3.1·10^{-5}		40		0.00922	0.785	2.7·10^{-6}	2.7·10^{-6}	0.05
NW-1	4.1·10^{-7}		10		0.00922	0.785	8.9·10^{-8}	1.0·10^{-6}	0.05
NNW-1	8.6·10^{-6}		20	10	0.00922	0.785	1.0·10^{-6}	1.0·10^{-6}	0.05
NNW-2	2.4·10^{-5}	2.1·10^{-6} (Mean-st. dev)	20	10	0.00922	0.785	1.0·10^{-6}	1.0·10^{-6}	0.05
NNW-3	2.0·10^{-5} (Table A2-7)		20		0.00922	0.785	1.9·10^{-6}	1.9·10^{-6}	0.05
NNW-4	6.5·10^{-5}	1.3·10^{-5}	10		0.00922	0.785	1.4·10^{-6}	1.4·10^{-6}	0.05
NNW-5	4.0·10^{-6}		20	10	0.00922	0.785	5.3·10^{-7}	1.0·10^{-6}	0.05
NNW-6	1.4·10^{-5} (Table A2-7)		20		0.00922	0.785	1.4·10^{-6}	1.4·10^{-6}	0.05

Table 3.2. (cont.) Properties of fracture zones.

Zone	T (m^2/s) according to Rhén et al., 1997 (Mean)	T (m^2/s), modified	width of zone (m) according to Rhén et al., 1997	width of zone (m), modified	a	b	$S=aT^b$ (-) Rhén et al., 1997 p. 214-215	max ($1.0 \cdot 10^{-6}$; S)	$2a_0$ (m) Rhén et al., 1997 p. 117
NNW-7	$7.5 \cdot 10^{-6}$		20		0.00922	0.785	$1.0 \cdot 10^{-6}$	$1.0 \cdot 10^{-6}$	0.05
NNW-8	$8.4 \cdot 10^{-6}$ (depth= 300 m)	$8.0 \cdot 10^{-6}$ (depth= 300 m)	20		0.00922	0.785	$9.2 \cdot 10^{-7}$	$1.0 \cdot 10^{-6}$	0.05

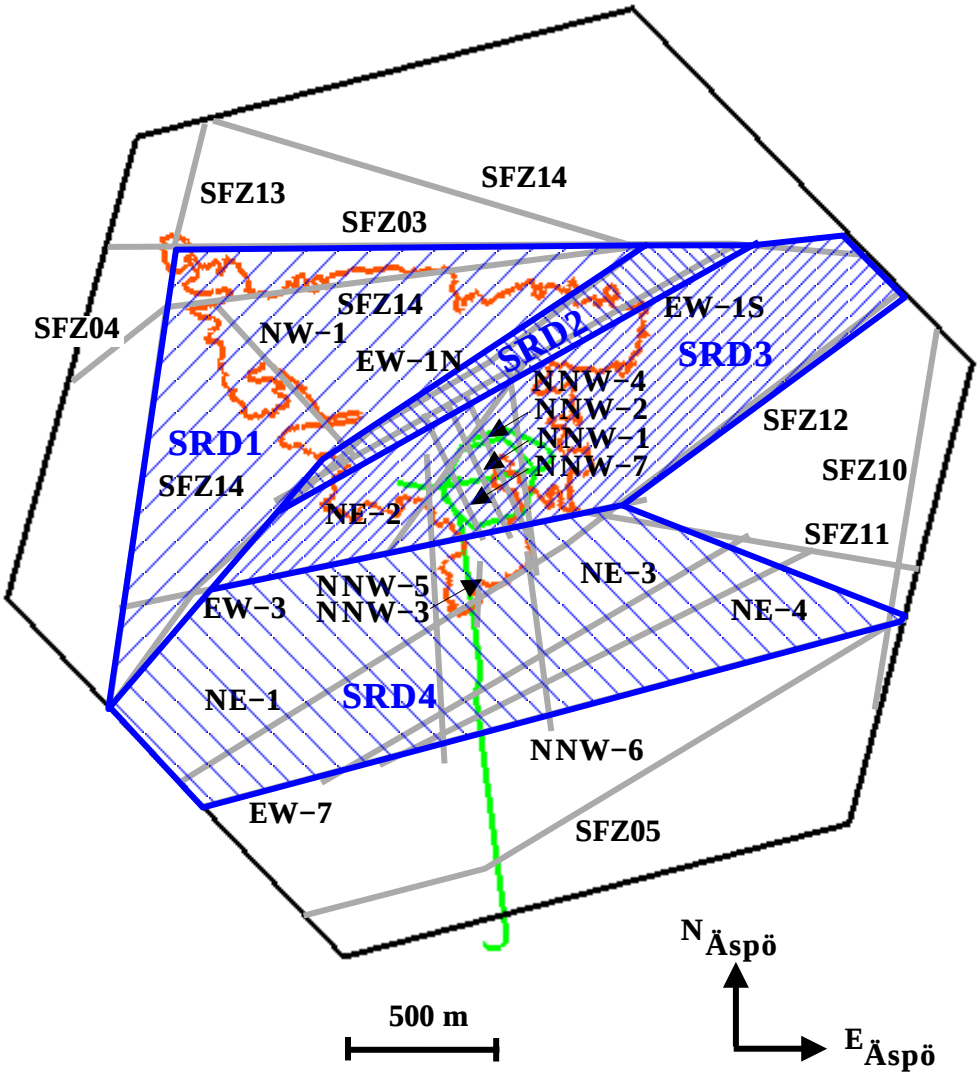

Figure 3.3. The site scale hydraulic rock mass domains (SRD) included in the model.

The properties of the rock are shown in Table 3.3. The specific storage S_S (m^{-1}) can be derived from a linear relationship between $\log_{10}K$ and $\log_{10}S_S$ given by Rhén et al. (1997). Four site scale hydraulic rock mass domains (Rhén et al., 1997) were included in the model (see Figure 3.3):

- SRD1: Northern part of Äspö, bounded to the south by the northern part of EW-1
- SRD2: Volume bounded by the northern and southern parts of EW-1
- SRD3: Southern part of Äspö bounded to the north by the southern part of EW-1 and to the south by EW-3
- SRD4: South of EW-3.

Outside Äspö SRDs 1–4 are assumed to be valid within an area bounded by EW-7 to the south and some 100 metres outside Äspö to the west, north and east. The domains extend to the depth of about 600 m. The hydraulic conductivities K of the site scale hydraulic rock mass domains are the calibrated values given by Svensson (1997). The hydraulic conductivity value used outside the SRD domains in the model is the same as in the M3-based simulations (Kattilakoski, 1999).

Table 3.3. Properties of rock.

rock	K (m/s) Rhén et al., 1997 p. 365, 219	S_S (m^{-1}) Rhén et al., 1997 p. 241-242	$2a_0$ (m) Rhén et al., 1997 p. 131	$2b$ (m) at model surface	ϕ_f (-) at model surface
SRD1	$1.58 \cdot 10^{-8}$	$8.4 \cdot 10^{-7}$	0.45	$2.1 \cdot 10^{-4}$	$4.6 \cdot 10^{-4}$
SRD2	$7.94 \cdot 10^{-8}$	$8.4 \cdot 10^{-7}$	0.45	$3.5 \cdot 10^{-4}$	$7.8 \cdot 10^{-4}$
SRD3	$2.0 \cdot 10^{-9}$	$8.4 \cdot 10^{-7}$	0.45	$1.0 \cdot 10^{-4}$	$2.3 \cdot 10^{-4}$
SRD4	$2.51 \cdot 10^{-8}$	$8.4 \cdot 10^{-7}$	0.45	$2.4 \cdot 10^{-4}$	$5.3 \cdot 10^{-4}$
elsewhere	$9.3 \cdot 10^{-9}$	$8.4 \cdot 10^{-7}$	0.45	$1.7 \cdot 10^{-4}$	$3.8 \cdot 10^{-4}$

3.4 Boundary conditions

Seventeen time steps were chosen. They cover the period from the natural conditions until December 1996 (Table 3.4).

Table 3.4. The modelling period with comments on the tunnel and shaft updating.

Step	Date	Tunnel face (m)	Comments on modelling
0	0.5 years before 1.10.1990	0	Start of modelling period
1	1.10.1990	0	
2	21.05.1991	696	First tunnel updating, release of groundwater table over the land
3	10.02.1992	1212	
4	10.08.1992	1398.8	
5	05.10.1992	1672.5	
6	10.11.1992	1774	First updating of shafts
7	11.02.1993	2100	
8	03.06.1993	2600.1	
9	03.11.1993	2604	No updating of tunnel
10	16.02.1994	2998.8	Second updating of shafts
11	16.06.1994	3192.3	
12	16.09.1994	3600	
13	24.01.1995	3600	Last updating of shafts
14	25.05.1995	3600	
15	24.10.1995	3600	
16	24.04.1996	3600	
17	23.12.1996	3600	

The tunnel and shaft advance is modelled by giving a residual pressure boundary condition for the flow equation (Eq. (2.1)) and a flow rate boundary condition for the transport equation (Eq. (2.3)) to the nodes describing the tunnel and shafts in each time step (see Section 4).

3.4.1 Solving of pressure and concentration fields

The fixing of the initial concentration boundary condition is described in Section 4.2.

The density of water (kg/m^3) is given by the following equation (Rhén et al., 1997)

$$\rho = \rho_0 + a_C C\,, \tag{3.5}$$

where ρ_0 is the freshwater density (998.585 kg/m^3), a_C is the coefficient of the density dependence on the chloride concentration C (g/l) (see Table 3.1).

Thus, the hydraulic pressure (Pa) can be expressed as

$$p = p_{fresh}(d) + a_C g \int_0^d C(d_z)\, dd_z\,, \tag{3.6}$$

where p_{fresh} is the freshwater pressure, g is the gravitational acceleration (9.81 m/s^2) and d is the depth (m).

The residual pressure (Pa) is

$$p_{res} = a_C g \int_0^d C(d_z)\, dd_z\,. \tag{3.7}$$

The initial (t=0) pressure boundary condition for each node of the element mesh under the sea level is calculated with Eq. (3.7), after the initial concentration distribution has been determined (Section 4.2). Zero residual pressure is applied at the sea level, while groundwater table is specified over the land.

In the first time step the pressure and concentration boundary conditions given in the interior nodes of the element mesh are released. The pressure boundary condition in the bottom nodes is also released, because it would not be consistent with the chloride concentration.

In the second time step the progress of the tunnel is taken into account for the first time. The groundwater table boundary condition at the surface of the model is released (see Table 3.4). A flow rate boundary condition giving an infiltration of about 20 mm/a in the shaft area is given for the flow equation (Eq. (2.1)) in the nodes depicting the land.

3.4.2 Transport of water types

In the following, the estimations of mixing proportions of reference water types for groundwater samples (Luukkonen, 2000) are briefly described.

Then, the derivation of boundary conditions for the hydrological modelling is explained.

In the inverse-modelling approach the mixing fractions are based on Cl and ^{18}O values of observed groundwater compositions (Table 3.5). All other chemical values taken into calculations are subject to mole-transfers, i.e. they are dissolved/precipitated from/to reacting phases to satisfy the calculation constraints. The geochemical mole-transfer reactions considered are dissolution/precipitation of calcite, consumption of organic matter (CH_2O), dissolution of goethite, precipitation of pyrite, and in detail undefined exchange processes among pairs Na-Ca, Na-Mg and Na-Fe.

The inverse calculations are done in steps assuming that the steady-state assumption of chemical reactions is valid. In practice this means that a final water composition can be produced from a realistic set of initial water samples with small, moderate or otherwise feasible mole-transfers. The directions of dissolution/precipitation reactions form an important basis for the judgement of the acceptability of the steady state condition. Judgements depend strongly on what kind of initial water samples are being mixed together.

The detailed description of the inverse-modelling approach is presented in Luukkonen (2000). The successfulness of the approach can be extracted into couple principles: the amount of suitable samples, the amount of conservative parameters available, the choice of reference water types and the mole-transfer phases considered.

There is no simple rule for the minimum sample amount. However, the amount of variables increases easily in the calculations to 15–20 (cf. Luukkonen, 2000) and the amount of samples should clearly exceed this number. The precision of mixing fractions increases rapidly if there are more than two conservative parameters available among the variables. The reference water types should be defined and/or found so that they have equilibrated with current prevailing conditions in bedrock as well as possible, and so that they represent sensible succession of historical events identified. At the same time it is important that the reference water types have mixed to each other as little as possible. Finally, the correct choice of the mole-transfer phases depends largely on the amount of samples, analysed variables and reference water type compositions.

Table 3.5. Reference water types used in the inverse modellings. Meteoric, postglacial altered and saline reference water types are actual undisturbed samples. Reference days in the footnotes are given in relation to the sampling date (Ref. day 0 = 01.01.91).

	Meteoric Water a)	Seawater Average b)	Postglacial Alt. c)	Litorina Sea Approx. d)	Glacial Melt Approx. e)	"Preglacial Altered" f)	Saline g)
pH	8.0	7.7	7.3	7.6	5.8	7.7	8.0
Na	237	1904	1880	3764	0.2	1700	3020
K	4.0	72.7	32.8	134	0.2	(4.0)	7.3
Ca	25.0	90.9	1040	151	0.1	450.0	4380
Mg	6.0	226	219	448	0.1	110.0	49.5
Alkalis	370	85.7	132	92.5	0.2	200	11.0
Cl	119	3562	5070	6500	0.7	3500	12300
SO_4	118	505	136	890	0.1	100	709
Si	5.2	0.3	5.0	1.8	0.0	(4.7)	4.2
Fe	1.6	0.08	2.7	0.002	0.0	1.7	0.08
^{18}O	-9.9	-6.4	-7.2	-4.7	-19.0	-9.5	-12.7

a) HAS05/-56.3m. Reference day -1243
b) Average from 6 samples PASSEA01 (28.8.92) & PASSEA01-05 (7.8.93)
c) HAS13/-42.0m. Reference day -547
d) From Pitkänen et al. (1999) & refs. therein
e) From Pitkänen et al. (1999) & refs. therein with reconsidered O-18 value
f) O-18 & Cl values from Pitkänen et al. (1999). Main component concentrations fitted for samples KAS03/-121.8m (Ref. Day -679), KAS02/-199.8m (Ref. Day -720), KAS03/-239.0 (Ref. Day -856) & KAS02/-881.3 (Ref. Day -700)
g) KAS03/-914.1m. Reference day -657

The step-wise calculation processes are presented schematically in Figure 3.4 that illustrates also the choice of the reference water types. In all, the inverse-modelling approach comprises a multiple exercise based on an attempt to understand the geochemical system along a (hypothetical) flow path. In the current approach, a previous successful (assumed steady-state) step leads to the following step, which is to find new sets of initial water samples for previous initial water samples now considered as final water samples, and so on.

The geochemical estimations carried out were divided into subsets in respect of the excavations of the Äspö tunnel system. The undisturbed sample set was used to identify the reference water types that have been active in the Äspö site, for describing the general evolution of water in the bedrock, and for defining the depth relations and the distributions of reference water types in the undisturbed model volume. The hypothetical flow path relations for samples collected during the undisturbed conditions of the Äspö Island are presented in Figure 3.4. The disturbed sample set was collected from 10 control points, and samples were used to monitor the effects of the tunnel construction to groundwater compositions.

In the inverse approach the geochemical reference water types and the mixing calculation procedure differ from the M3 approach. Therefore, the

approximations of geochemical boundaries for the hydrological modelling had to be re-estimated. For undisturbed conditions, the redefinition of the boundaries was a fairly straightforward process. By plotting calculated reference water proportions as a function of sampling depths and making smoothed regressions onto depth vs. proportion plots, reasonable estimates for the vertical boundaries of the hydrological model at sea and land areas were achieved (Fig. 3.5).

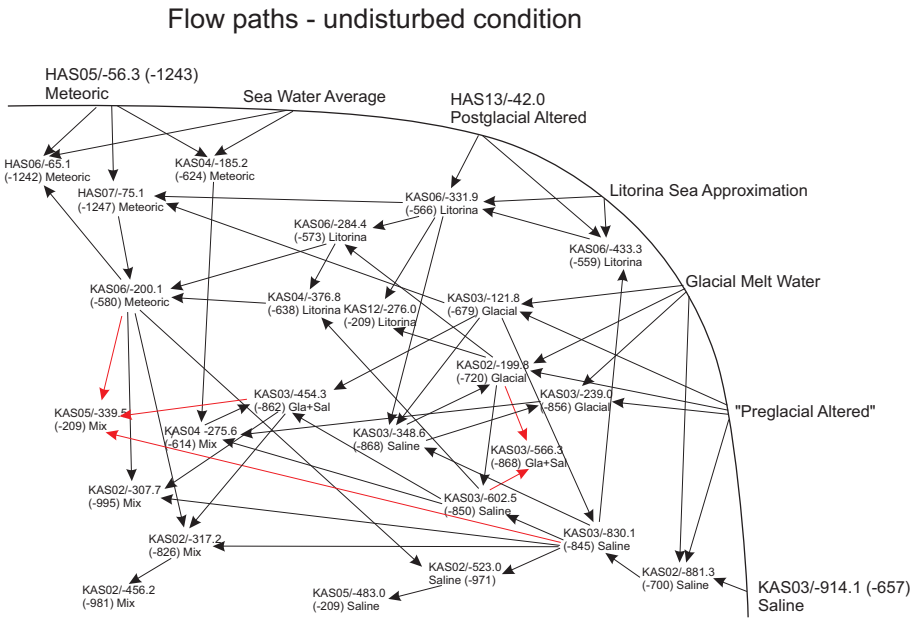

Figure 3.4. Mixing relations among undisturbed samples. (Luukkonen, 2000)

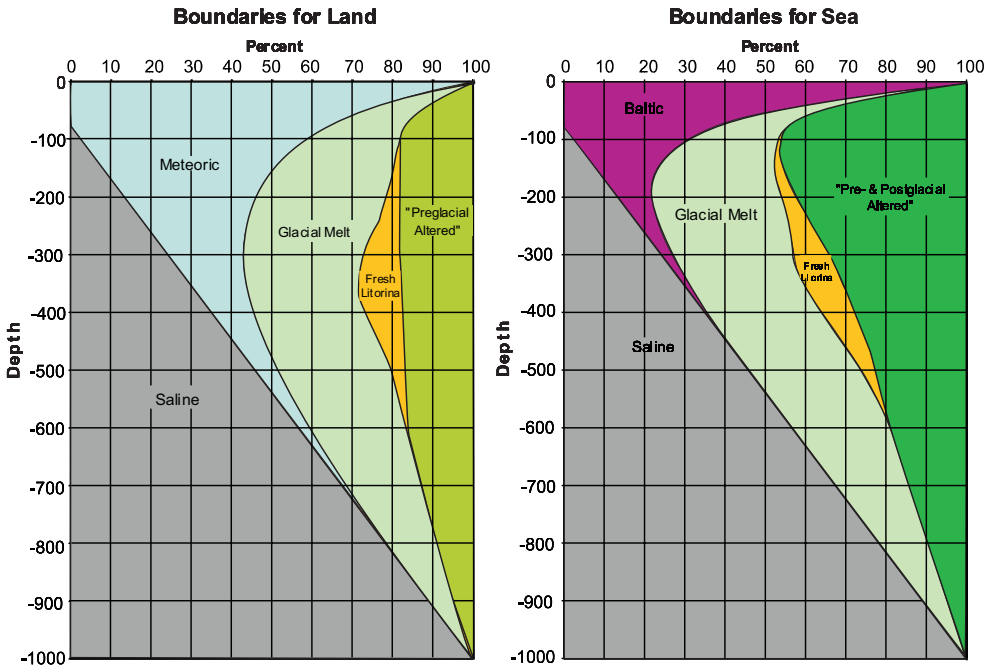

Figure 3.5. Mixing proportions of water types in model boundaries.

In the hydrological simulations the mixing fractions of the reference water types are transported like conservative parameters. The groundwater flow simulation aims to the reproduction of the estimated mixing proportions, and further to predict mixing proportions in the model. The predictions can be converted into chemical compositions, and ultimate results are predictions of chemical compositions at arbitrary locations in the model. The transport equations of the different groundwater types are solved using the previously simulated residual pressure and concentration fields. The initial concentration boundary condition for the transport equations of the different water types is given in each node on the basis of the inverse modelling (Fig. 3.5) depending on whether the node is situated in the land or sea area (Fig. 3.6). The boundary condition given initially in an interior node is released in the first time step.

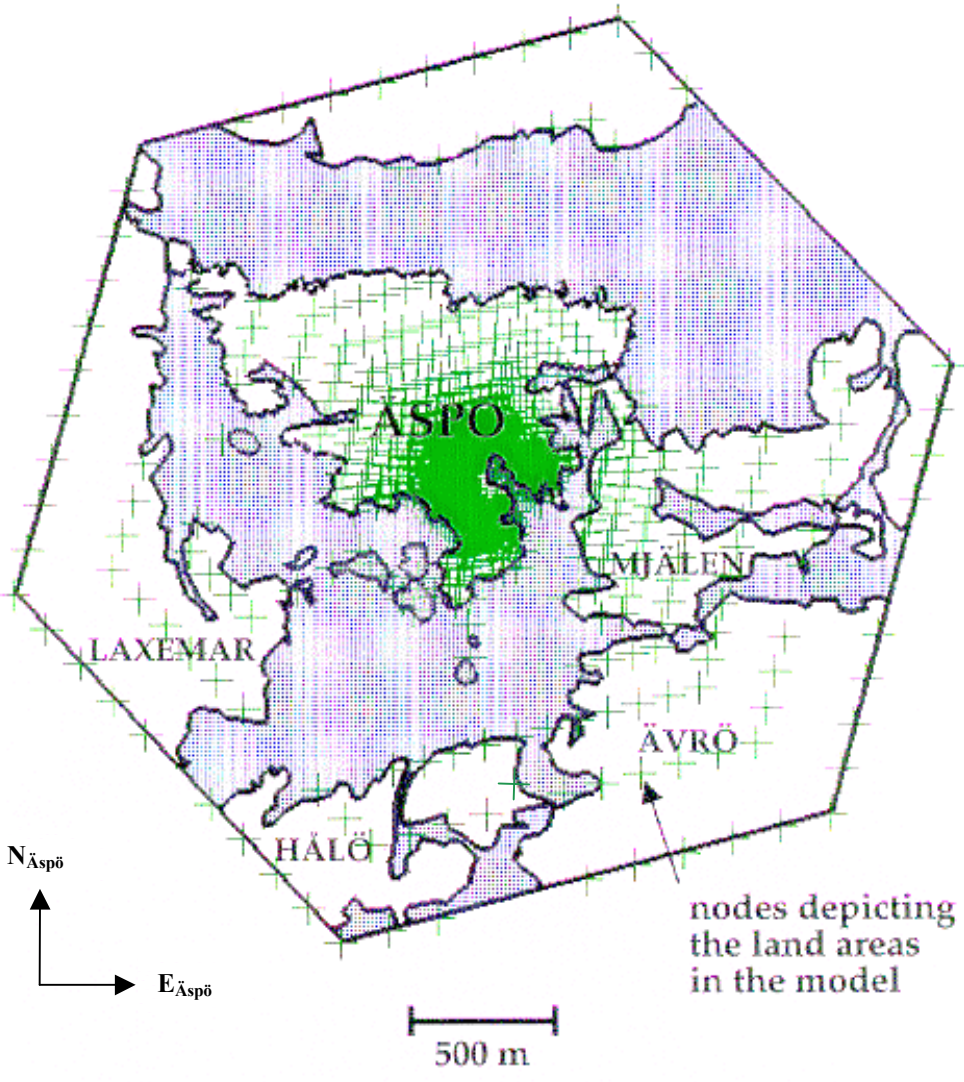

Figure 3.6. Land and sea areas in the model. Nodes in the land areas of the model are also shown. The mesh is denser in the tunnel and shaft area than in the surrounding.

4 CALIBRATION

4.1 Introduction

In the M3-based simulations (Kattilakoski, 1999) the hydrological conditions of the model were calibrated to fit the freshwater heads measured in the boreholes KAS02—KAS09, KAS12 and KAS14 and also the measured flow into the tunnel and the shaft. The hydrological tunnel and shaft boundary conditions given in those simulations were not modified in this work.

The tunnel was modelled without modifying the hydraulic conductivity of the rock around it. The residual pressure boundary condition in the tunnel and the shaft was fixed on the basis of the freshwater head measured in the nearmost borehole sections. In order to get an insight into the boundary condition to be assigned to the nodes pertaining to the tunnel, the measured freshwater heads from borehole sections at certain times (Forsmark and Rhén, 1994) were assigned to the nearest nodes of the tunnel phase. In case many values were obtained in one node an average was calculated. The measured values not farther than 75 metres away the tunnel were used.

In the current simulations, the initial hydrological boundary conditions were supplemented with vertical hydrological density distributions based on initial hydrogeochemical boundaries presented in Fig. 3.5. The details of the density corrections for the model are given below.

4.2 Concentration

The model was given an initial concentration boundary condition in accordance with the natural conditions, which prevailed before the tunnel construction. The initial concentration boundary condition was defined in accordance with the chemical modelling done by Luukkonen (2000). Each node of the element mesh was classified as a land node or a sea node (Fig. 3.6). The chloride distributions in the land and sea areas shown in Fig. 4.1 were used to outline the concentration boundary condition in each node. The boundary conditions were extrapolated linearly to the bottom of the model thus having a chloride concentration of 17.7 g/l. Thus, the residual pressure boundary condition (Eq. 3.7) prevailing on the lateral edges throughout the simulation could be given consistently with the chloride concentration. The concentration boundary conditions initially given in interior nodes were released in the first time step.

Chloride concentration of 0.1 g/l was used over the land due to the freshwater flow into the groundwater system. This is caused by the hydraulic gradient of the water table of the Äspö Island. The chloride concentration used at the sea level was 3.6 g/l.

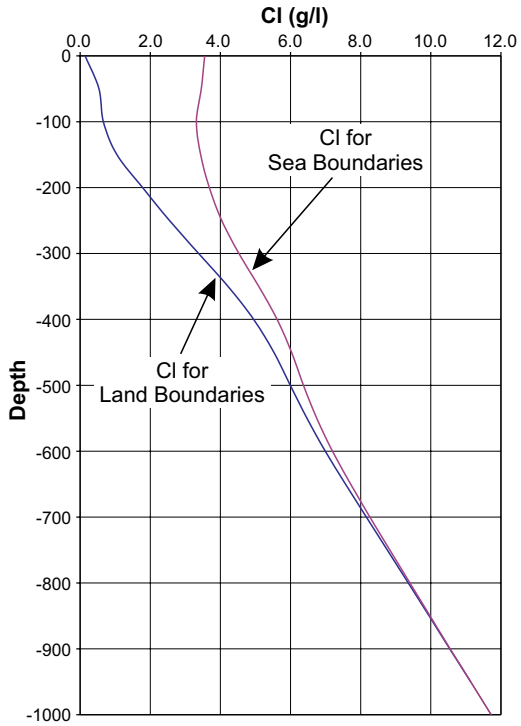

Figure 4.1. Chloride (g/l) for the land and sea boundaries (Luukkonen, 2000).

4.3 Residual pressure

The initial residual pressure boundary condition throughout the model was calculated from the chloride concentration using Eq. 3.7. In the first time step the residual pressure in the interior and bottom nodes was released.

The freshwater head used to calculate the residual pressure boundary condition prevailing in the tunnel nodes is depicted in Figure 4.2. The lowering of the curve in the depth interval 284—348 m is based on a calibration result (Kattilakoski, 1999) in the boreholes KAS05—KAS08.

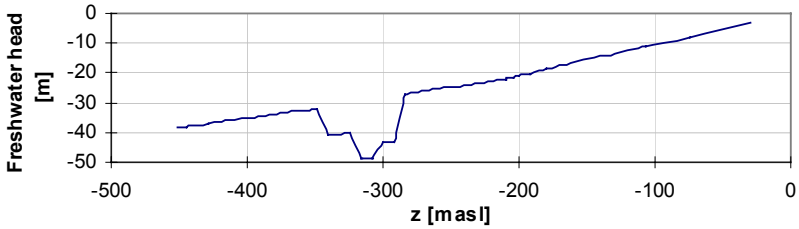

Figure 4.2. The freshwater head (m) used to calculate the residual pressure boundary condition in the tunnel nodes.

The low freshwater head measured in the uppermost packed-off sections of the borehole KAS02 was tried to catch up by assigning the residual pressure corresponding to the freshwater head

$$h_{0,shaft}(z) = -80 \text{ m} \tag{4.1}$$

to the nodes representing the shaft.

The freshwater hydraulic head measured from the boreholes and the residual pressure are related as follows:

$$p_{res}(z) = \rho_0 g h_0(z)\,, \tag{4.2}$$

where ρ_0 is the freshwater density (998.585 kg/m^3), g is the gravitational acceleration (9.81 m/s^2) and $h_0(z)$ is the freshwater head (m) given on the basis of the borehole measurements.

The simulated and measured freshwater head in the boreholes KAS02—KAS09, KAS12 and KAS14 as function of time is shown in Figure 4.3. In spite of the relatively low residual pressure boundary condition assigned to the nodes depicting the shaft, the model is not fully capable of producing the low freshwater head measured in the borehole KAS02.

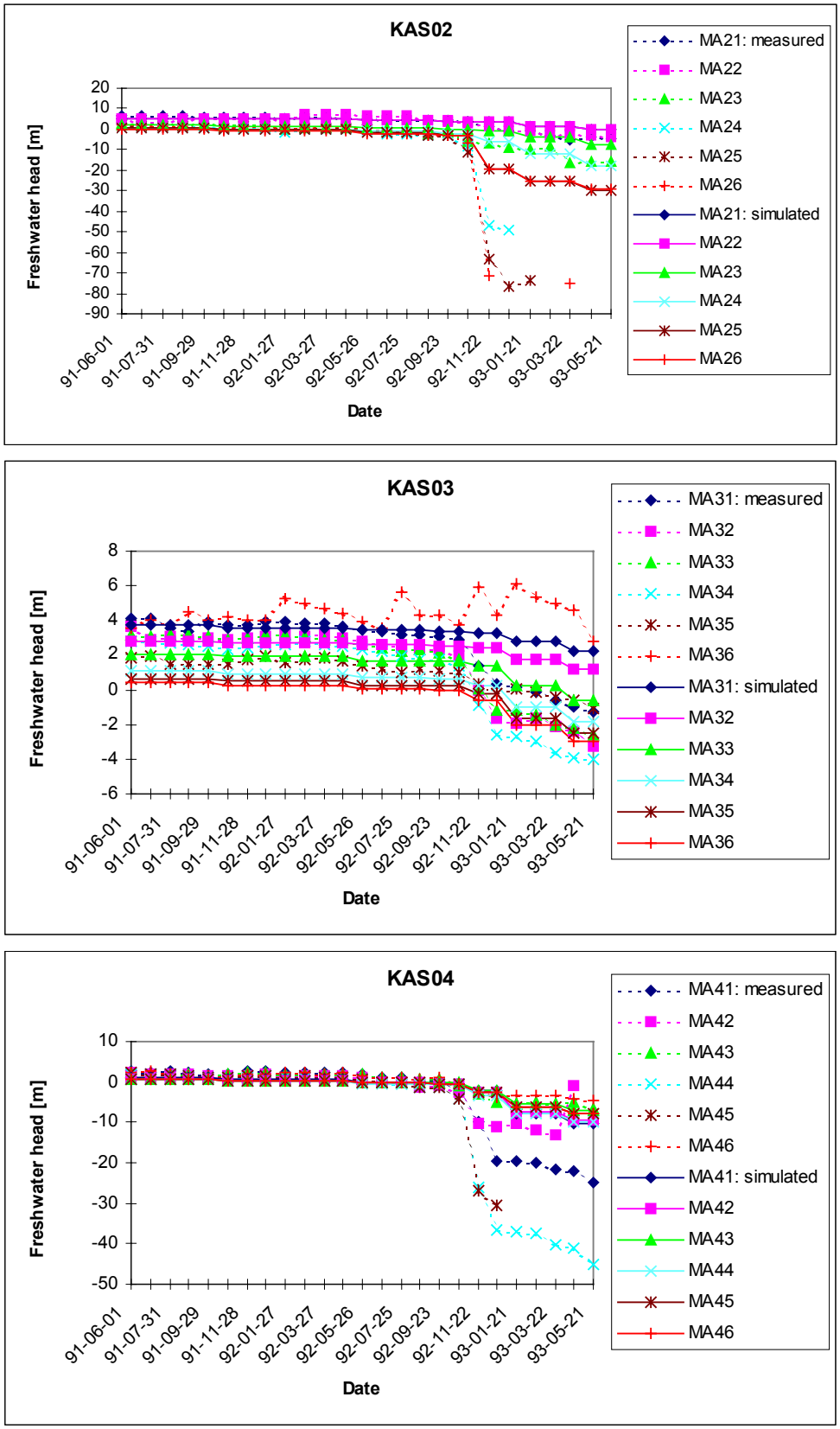

Figure 4.3. Simulated and measured freshwater head (m) in the boreholes KAS02—KAS04 as function of time.

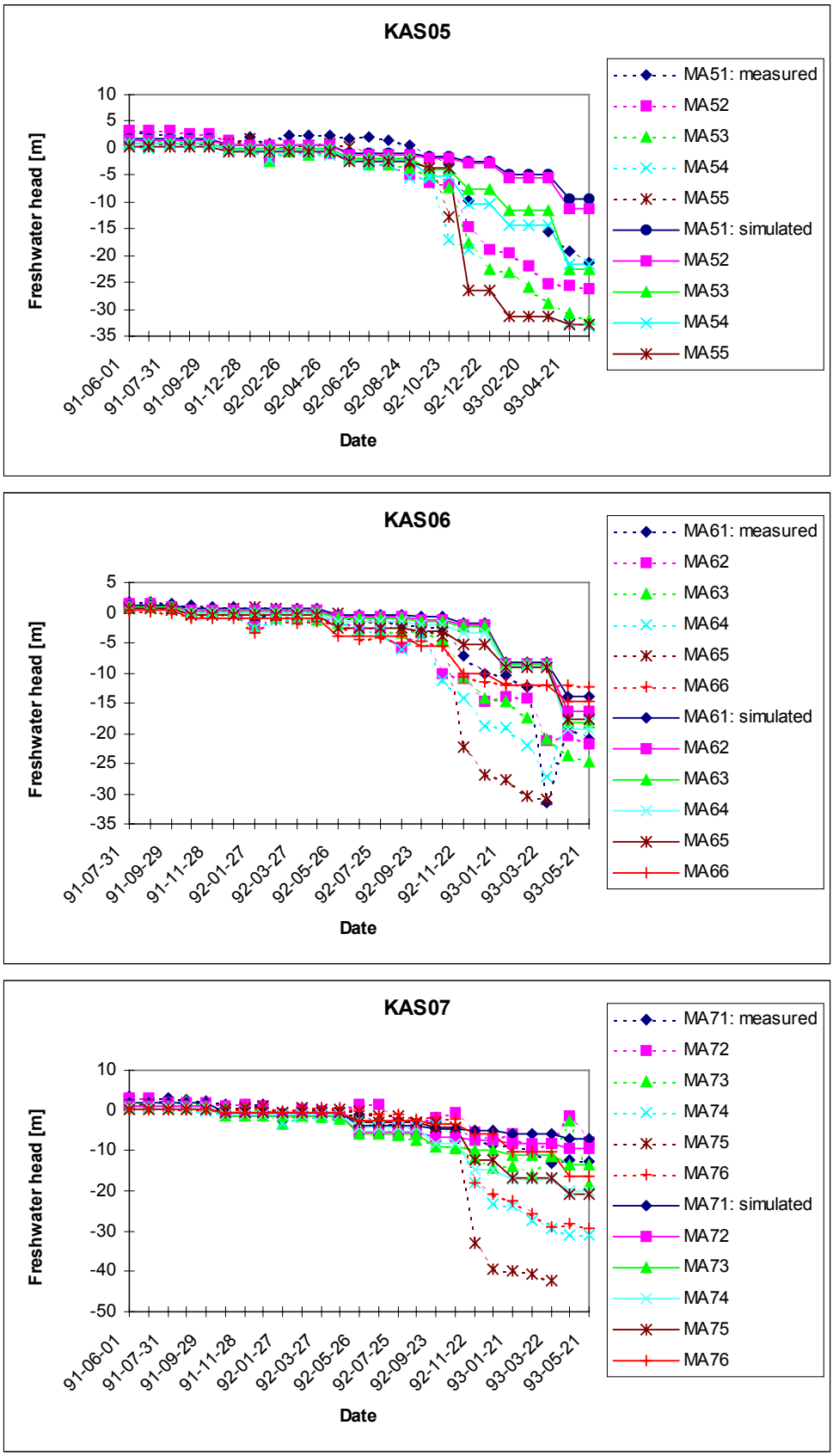

Figure 4.3. (cont.) Simulated and measured freshwater head (m) in the boreholes KAS05—KAS07 as function of time.

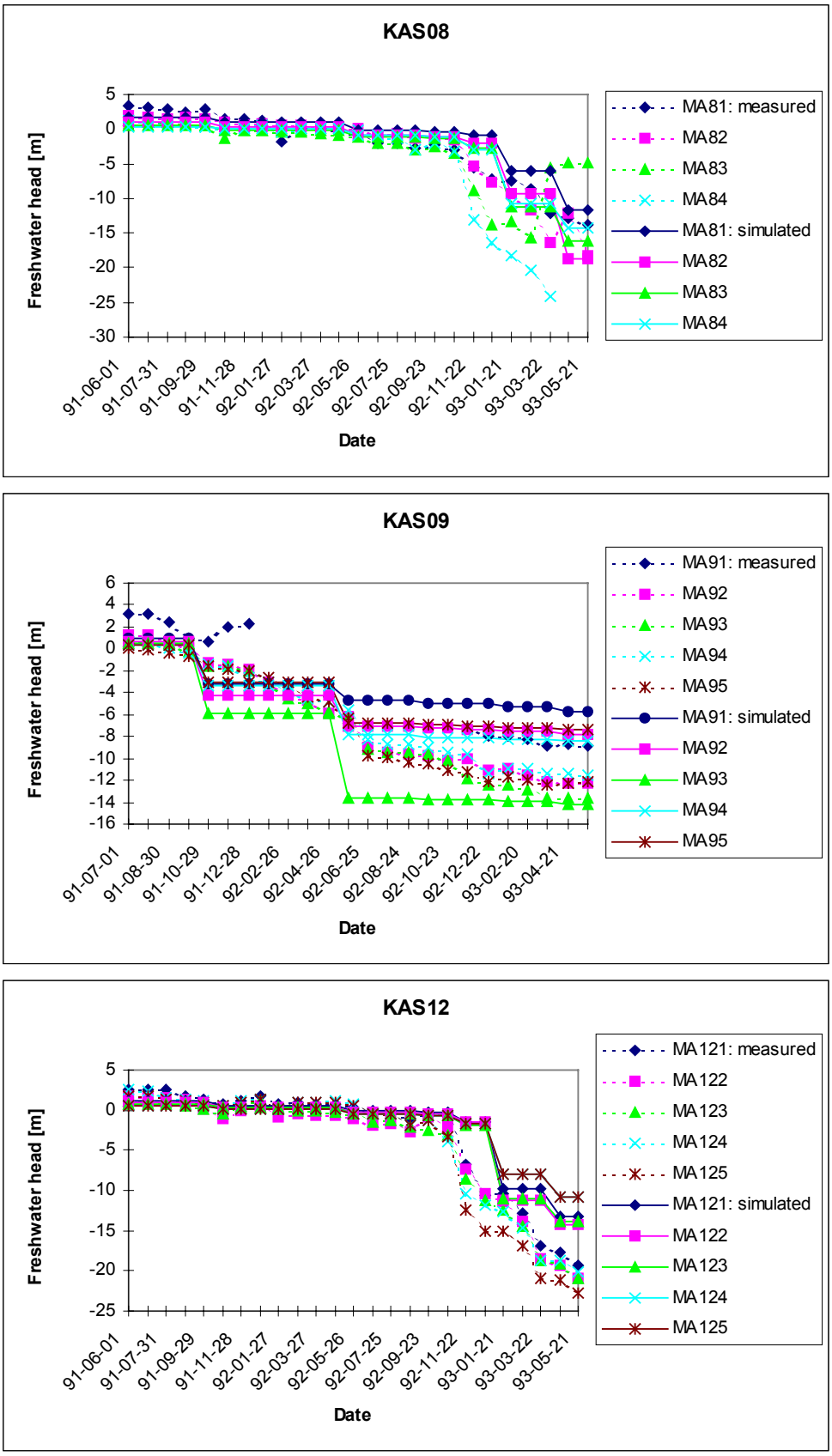

Figure 4.3. (cont.) Simulated and measured freshwater head (m) in the boreholes KAS08, KAS09 and KAS12 as function of time.

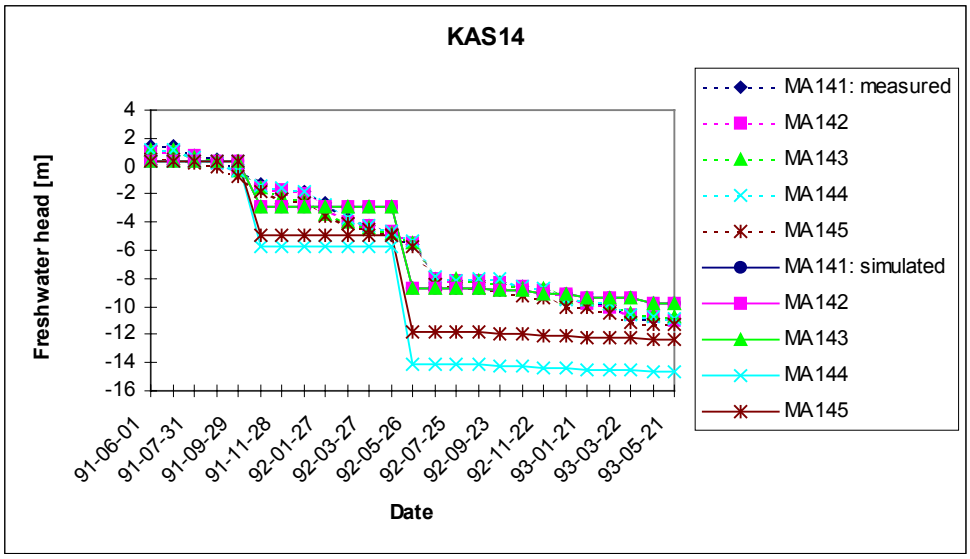

Figure 4.3. (cont.) Simulated and measured freshwater head (m) in the borehole KAS14 as function of time.

4.4 Inflow

Details about the flow measurements can be found in SKB PR 25-95-28, App. 2:4. The flow rates have also been presented by Rhén et al. (1997) (App. 2). However, minor adjustments of the flow rates reported by Rhén et al. (1997) and in SKB PR 25-95-28 have been made after August 1995 in the data delivered.

In each time step the nodes representing the tunnel and the shaft were grouped according to the measurement sections determined by the weirs. The flow rate measured at the weir was then uniformly divided between the nodes. In the coupled calculations of residual pressure and chloride concentration the flow boundary condition was given for the transport equation in each time step during the tunnel construction.

As suggested, the actual measurements at MA1659G, MA2587G and MA3384G have not been used in the modelling. Tunnel F (parallel and close to tunnel A, approximately section 3400-3510 m) being not modelled, the flow rate in MF0061G was added to MA3411G (50 %) and MA3426G (50 %).

4.5 Mean error and accuracy

The mean error and accuracy are defined as follows (Rhén et al., 1998):

MEAN ERROR

$$dh = \frac{\sum_{i=1}^{n} (h_i^m - h_i^c)}{n}, \tag{4.3}$$

$$dh(abs) = \frac{\sum_{i=1}^{n} \left| h_i^m - h_i^c \right|}{n}, \tag{4.4}$$

ACCURACY

$$Dh = \sqrt{\frac{\sum_{i=1}^{n} (h_i^m - h_i^c - dh)^2}{n-1}}, \tag{4.5}$$

where n is the number of points with measured data used to compare with calculated points, h piezometric level (freshwater head) in metres above sea level (masl). Index m refers to a measured value and c to a calculated one.

These quantities are depicted in the following Figure 4.4 in the boreholes KAS02—KAS09, KAS12 and KAS14 separately and in all the boreholes concurrently. The first modelling stage of the shaft in November 1992 impairs the fit between the model result and the measurements. This effect can also be seen in the last figure showing the performance measures calculated from all the borehole results.

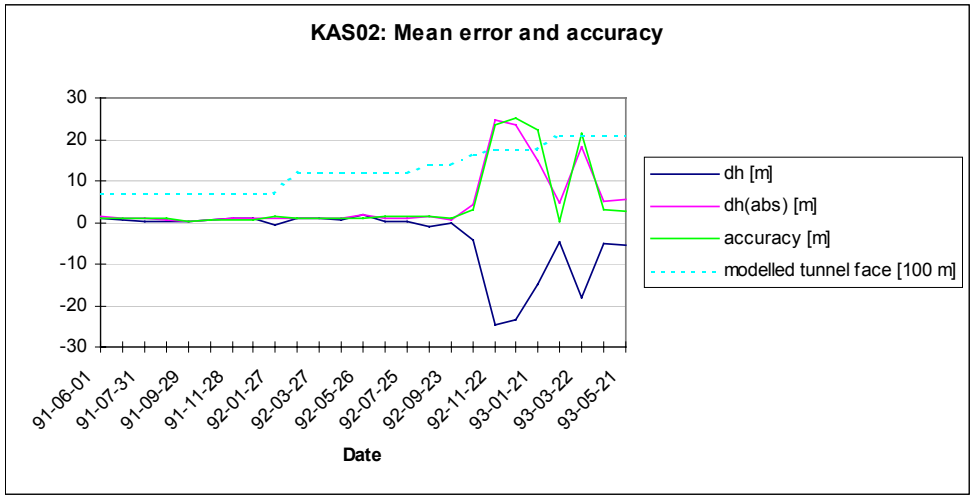

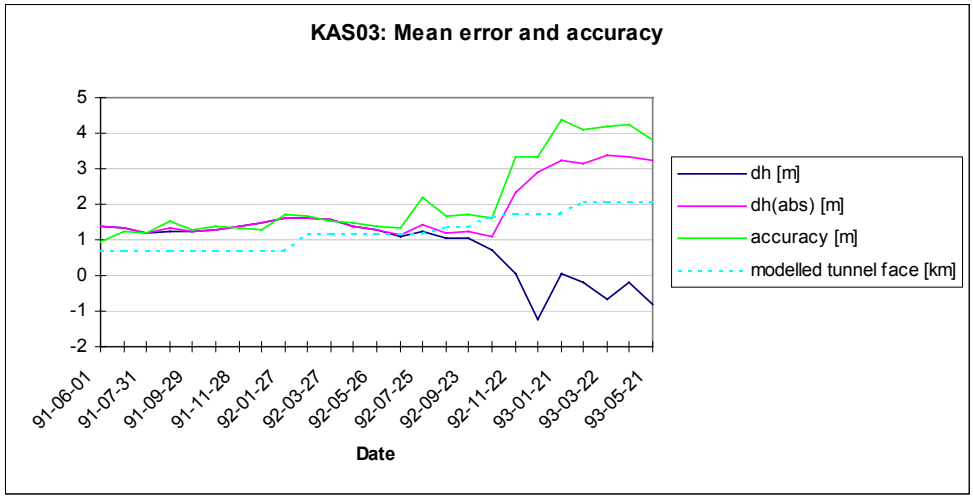

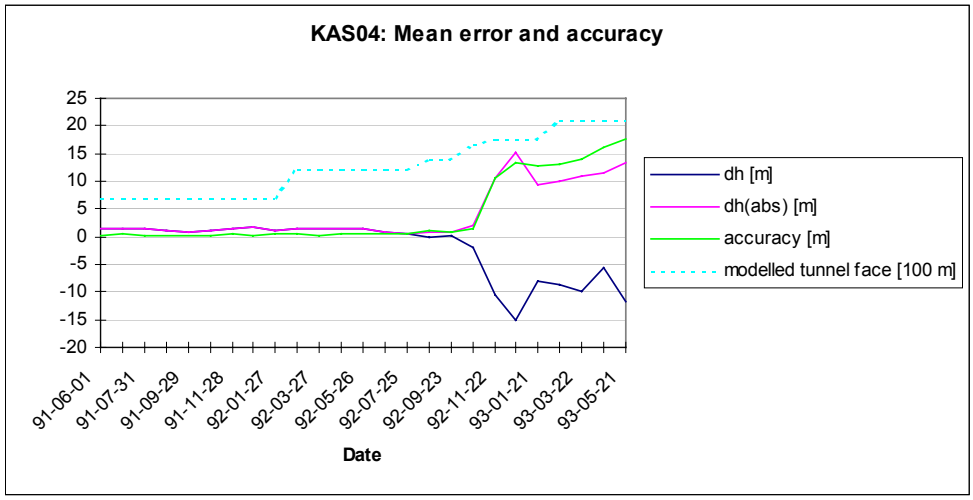

Figure 4.4. Mean error and accuracy (m) in the boreholes KAS02—KAS04 as function of time.

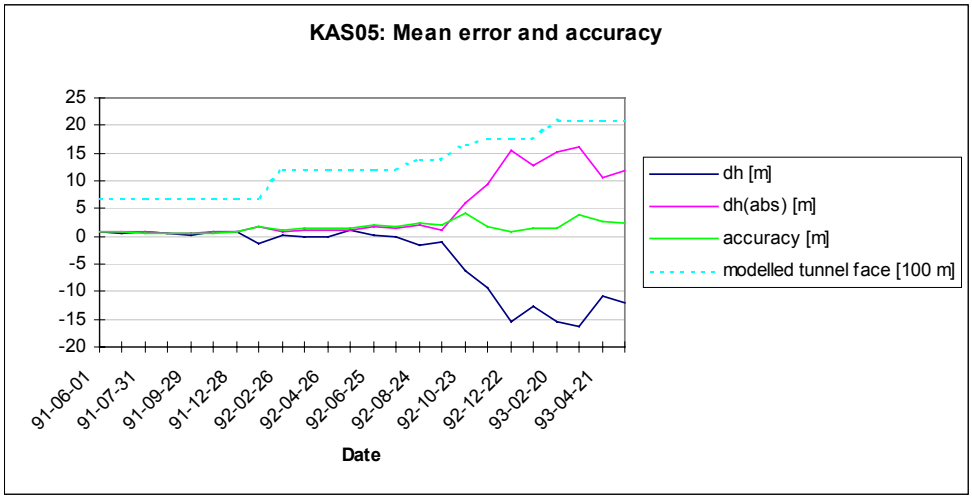

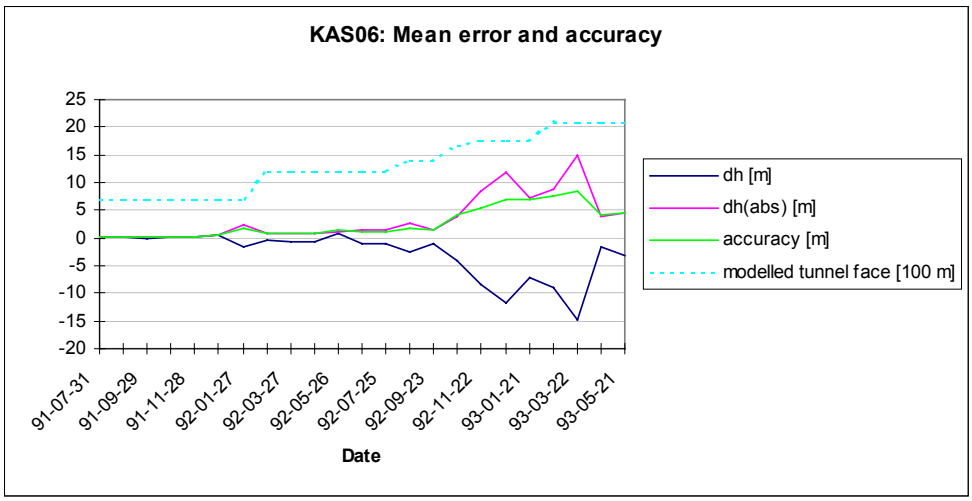

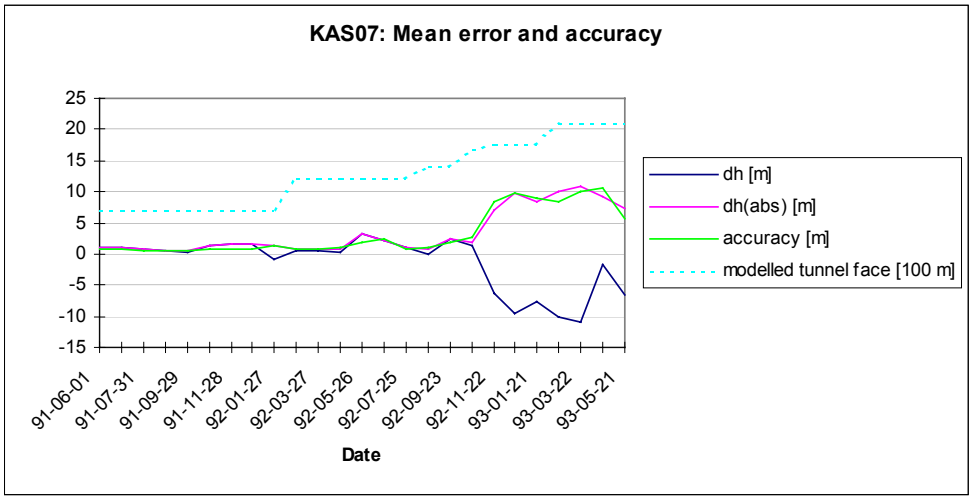

Figure 4.4. (cont.) Mean error and accuracy (m) in the boreholes KAS05—KAS07 as function of time.

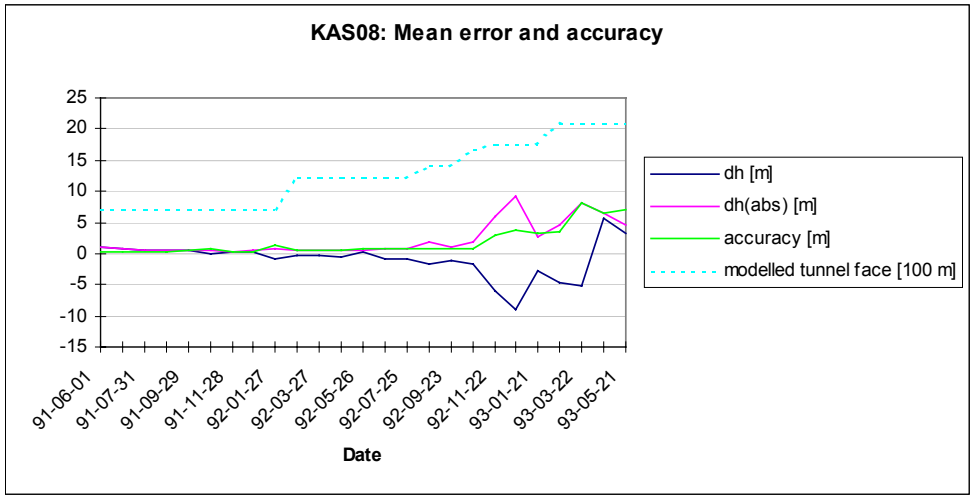

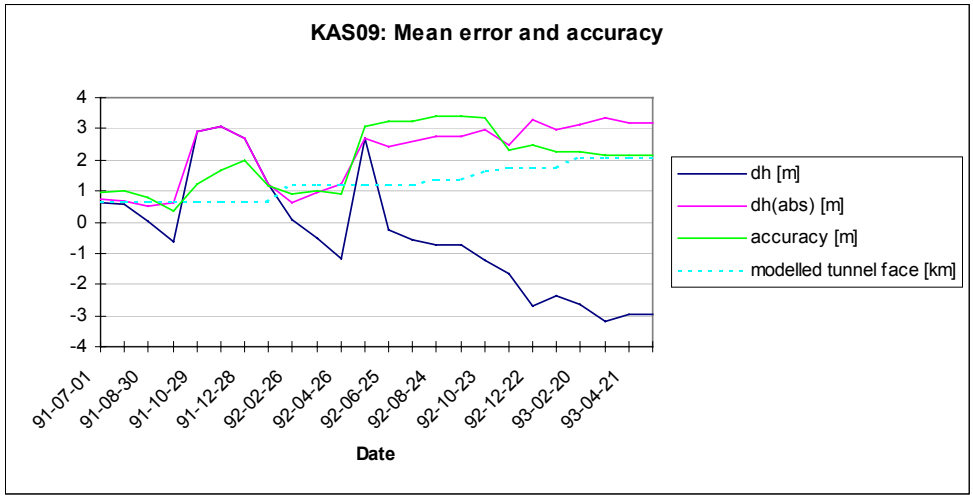

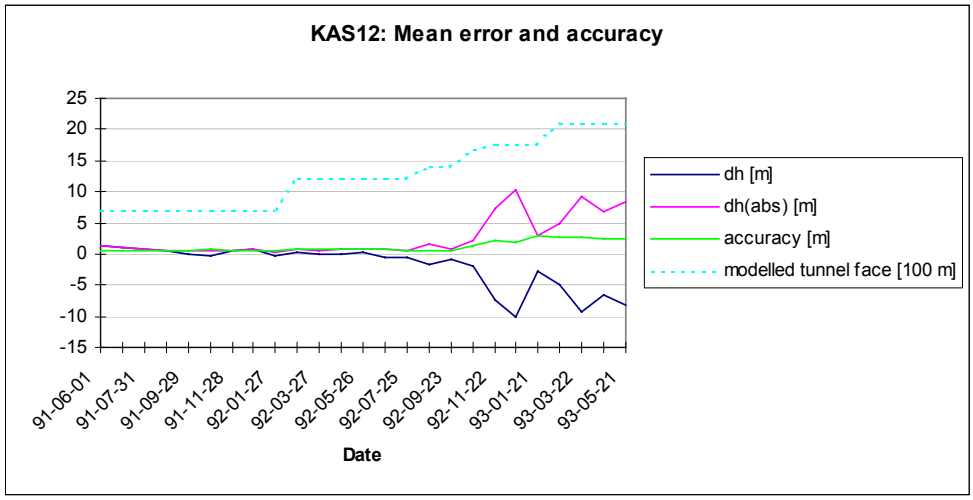

Figure 4.4. (cont.) Mean error and accuracy (m) in the boreholes KAS08, KAS09 and KAS12 as function of time.

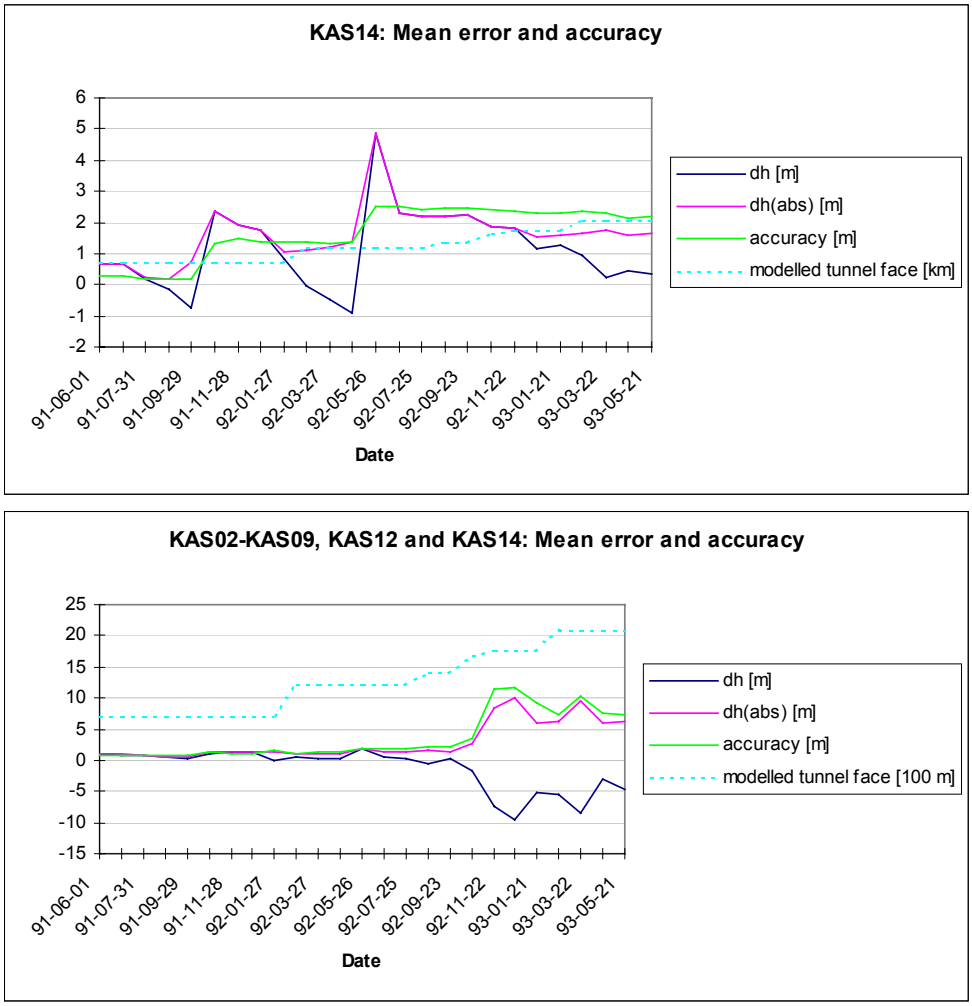

Figure 4.4. (cont.) Mean error and accuracy (m) in the borehole KAS14 and in the whole model as function of time.

5 MAIN RESULTS

5.1 Introduction

In this work, the flow equation is expressed in terms of the residual pressure. The flow direction can not generally be determined from the residual pressure contours, except in a freshwater zone (see Eq. (2.5)).

The surface boundary condition for four tunnel face positions (1400 m, 2100 m, 3000 m and 3600 m) is shown in Figure 5.1 as freshwater head (m). It depicts the groundwater table in the surroundings of the Äspö Island. The lowering of the groundwater table also in the area of Hålö, Ävrö and Mjälen is due to the excavation of the tunnel and the infiltration boundary condition applied over the land. The first modelling stage of the shaft (when the tunnel face was at 1774 metres (see Table 3.4)) lowers the water table down to -80 metres. The strongest drawdown is quite local, however.

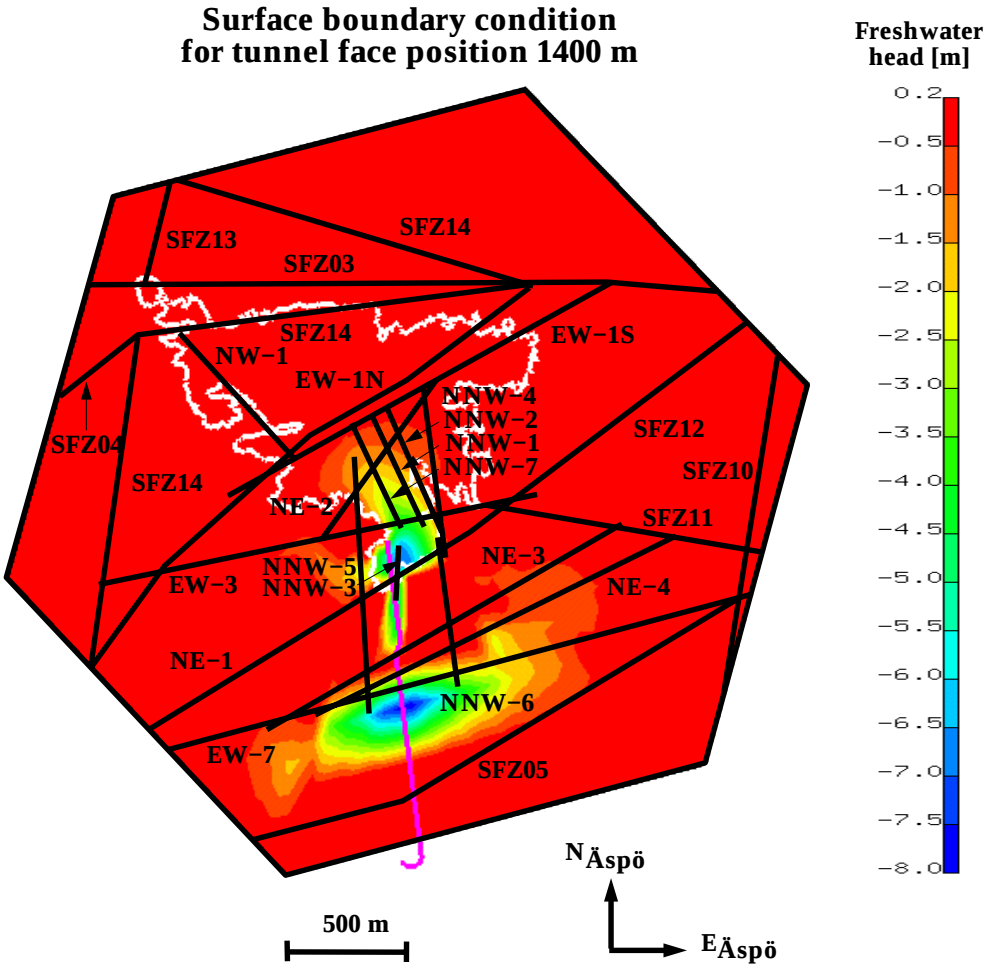

Figure 5.1. Surface boundary condition for tunnel face position 1400 m.

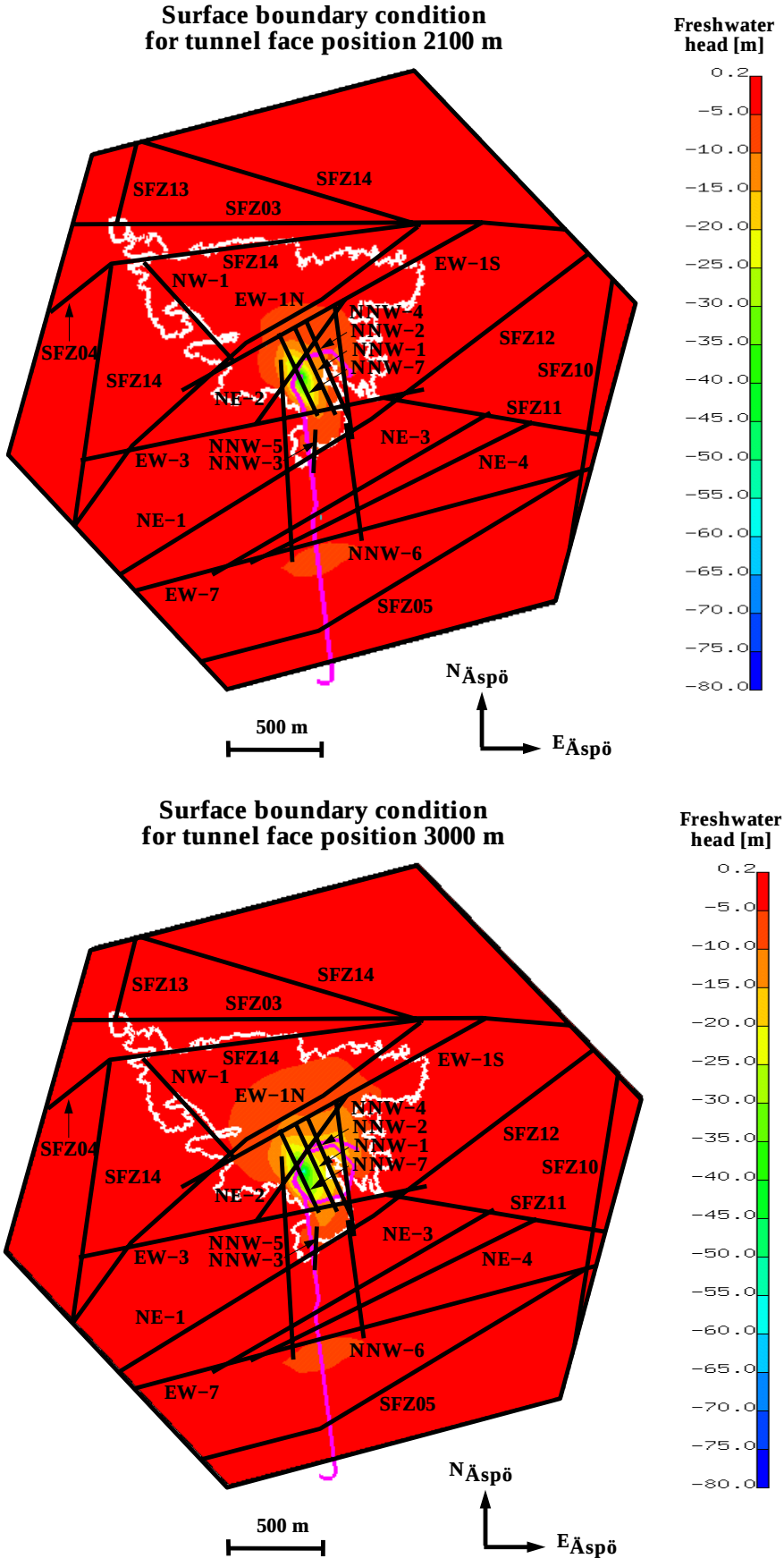

Figure 5.1. (cont.) Surface boundary condition for tunnel face position 2100 m (top) and 3000 m (bottom).

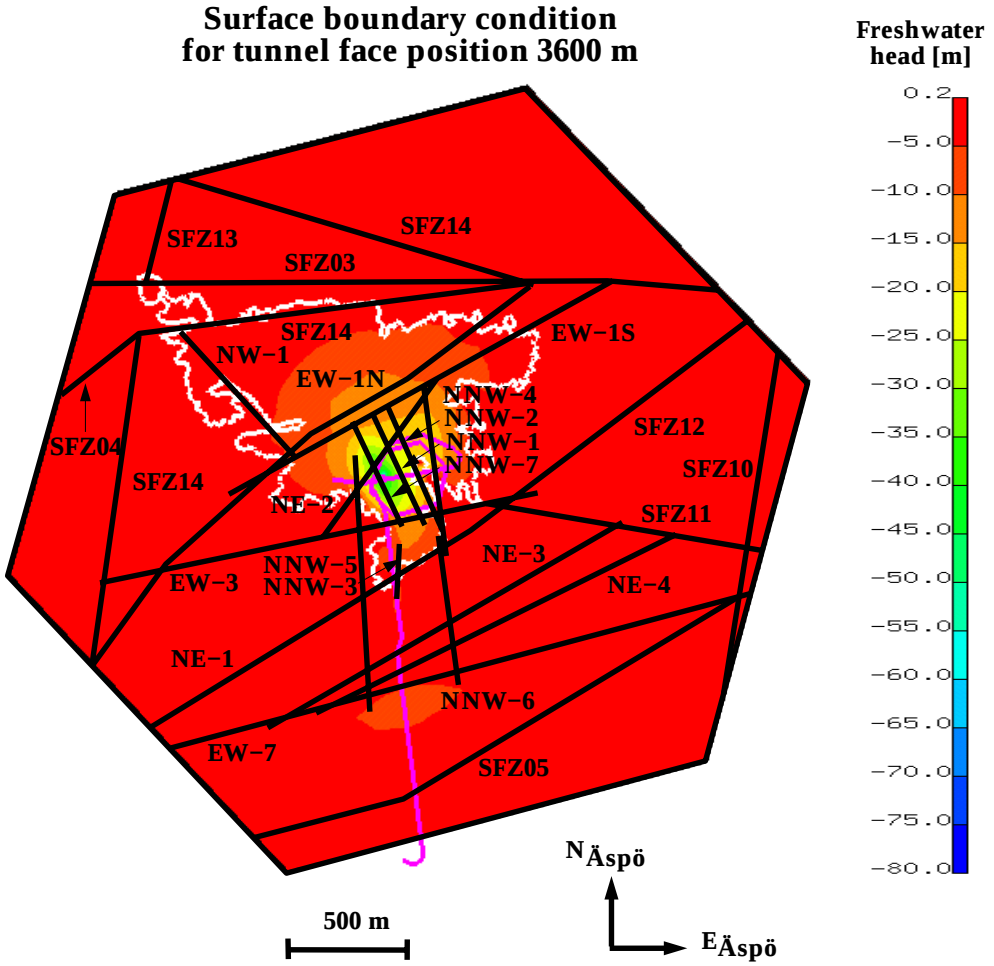

Figure 5.1. (cont.) Surface boundary condition for tunnel face position 3600 m.

5.2 Mixing ratios at control points

The undisturbed hydrogeochemical boundary/initial conditions of the model are presented in Fig. 3.5. The initial depth distributions of the reference water mixing fractions differ for the land and sea areas but no hydrogeochemical boundary differences were made between the fracture zones and the less fractured rock blocks of the modelled volume. The difference between the fracture zones and the less fractured rock volume is governed by the conductivity differences (Tables 3.1 – 3.3). As the modelled volume gradually turns into disturbed condition due to tunnel and shaft excavations, mixing fractions are transported in the simulations similarly as any other conservative element (e.g. ^{18}O or Cl).

In the mixing calculations (see Section 3.4.2) the transport equations of the different groundwater types were solved using the coupled residual pressure and chloride concentration fields (Fig. 5.2).

The control points, in which the mixing proportions are considered, are shown in Table 5.1 and Figure 5.3.

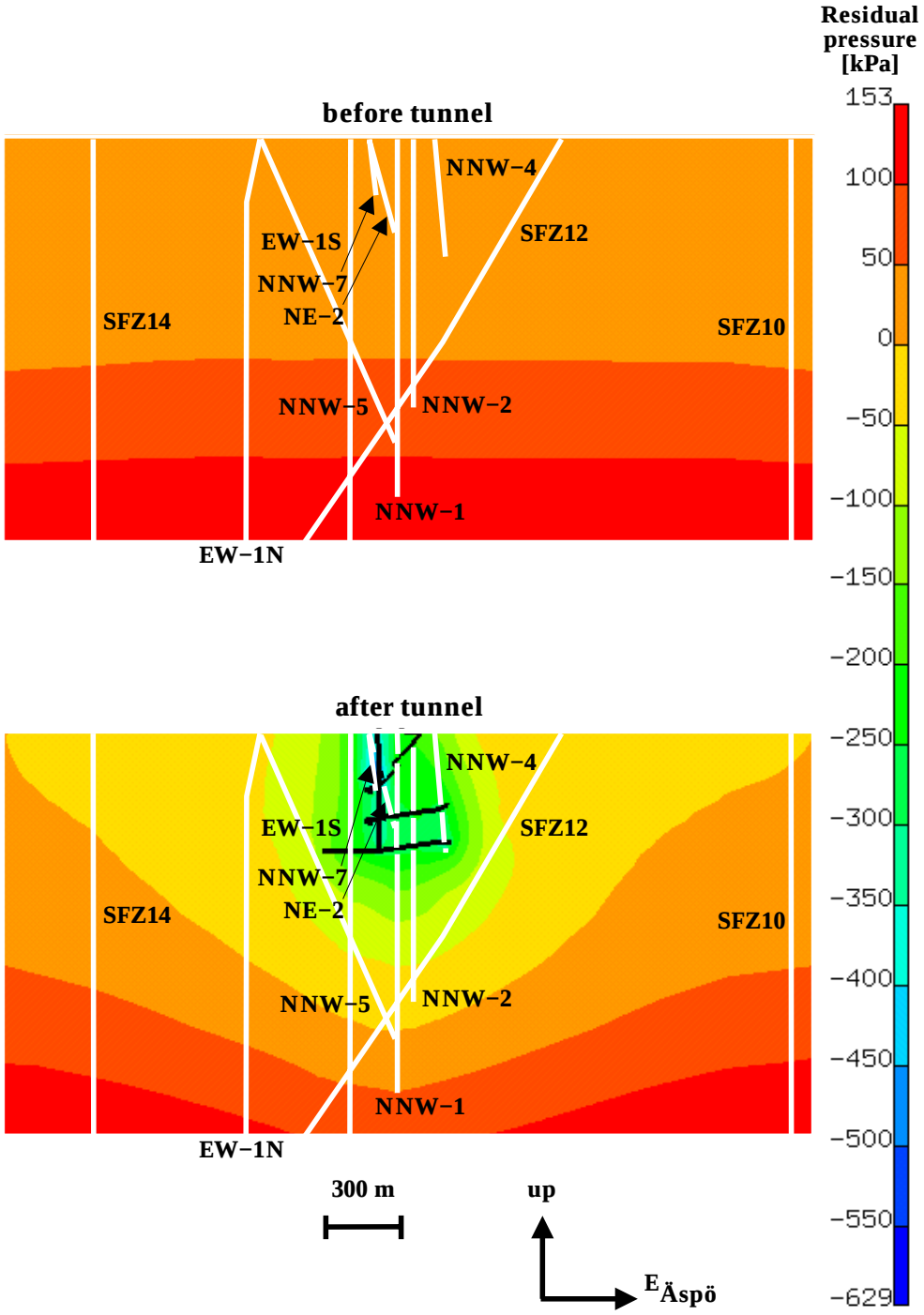

Figure 5.2. Residual pressure (kPa) on an east—west trending cut plane before (October 1st, 1990; see Table 3.4) and after the tunnel construction (January 24th, 1995).

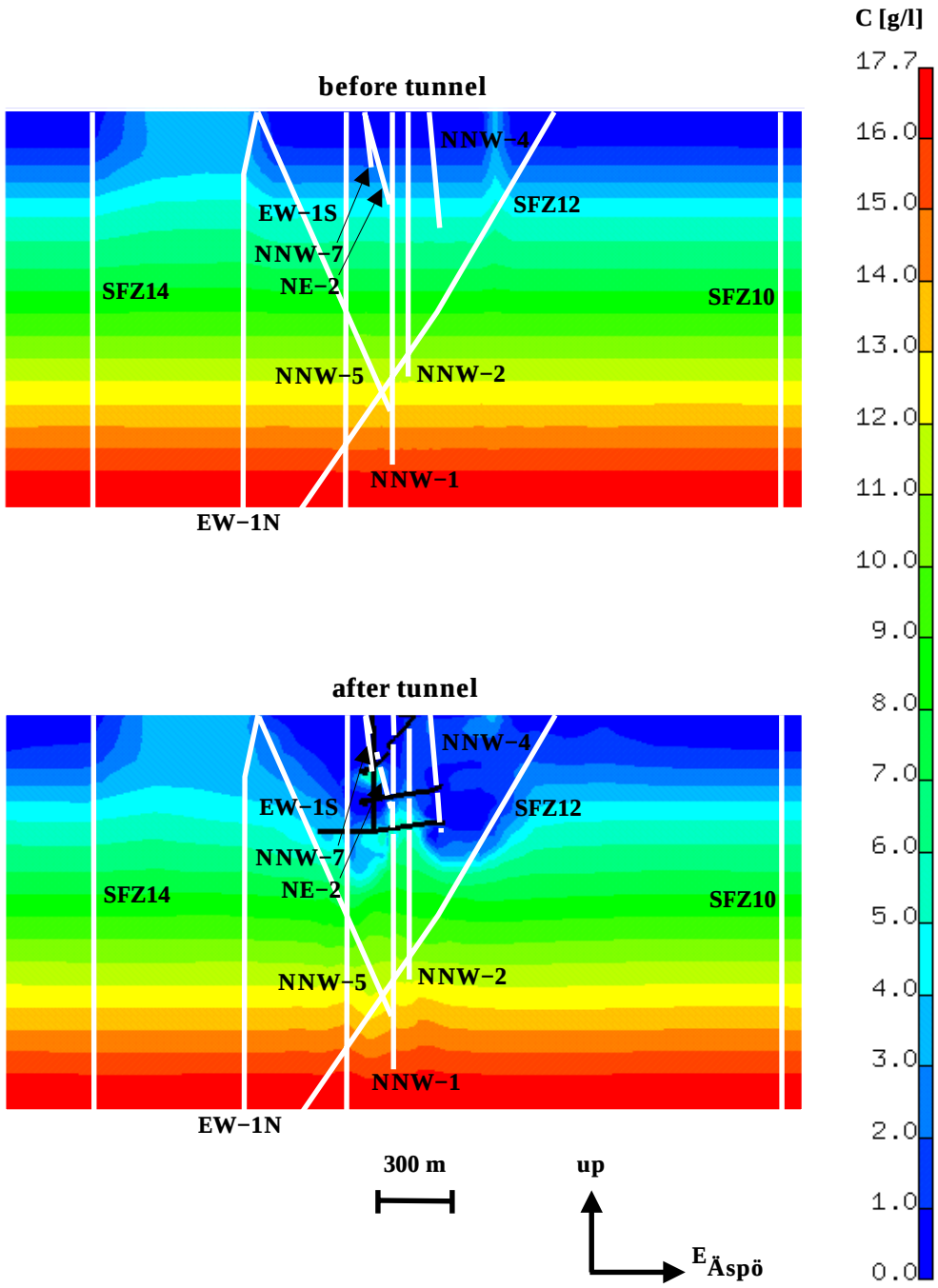

Figure 5.2. (cont.) Chloride (g/l) on an east—west trending cut plane before (October 1st, 1990; see Table 3.4) and after the tunnel construction (January 24th, 1995).

Table 5.1. Control points.

	Control point		Elevation (m)	Fracture zone
Calibration section 0–2900 m	1	KR0012B	-69.2	Redox zone
	2	SA0813B	-112.9	NE-4
	2	SA0850B	-117.7	NE-4
	3	SA1229A	-171.3	NE-1
	3	SA1327B	-184.1	NE-1
	4	SA2074A	-281.7	NNW-4
	5	SA2783A	-371.4	NNW-2
	6	KA1755A	-277.6	EW-1S
Prediction section 2900–3600 m	7	KA3005A	-403.0	Hydraulic Rock mass Domain
	8	KA3110A	-415.9	NNW-4
	9	KA3385A	-448.8	(NNW-7)
Outside tunnel	10	KAS03 (609–623 m)	-602.5	
	10	KAS03 (533–626 m)	-566.3	
	11	KAS07 (501–604 m)	-465.0	NE-1

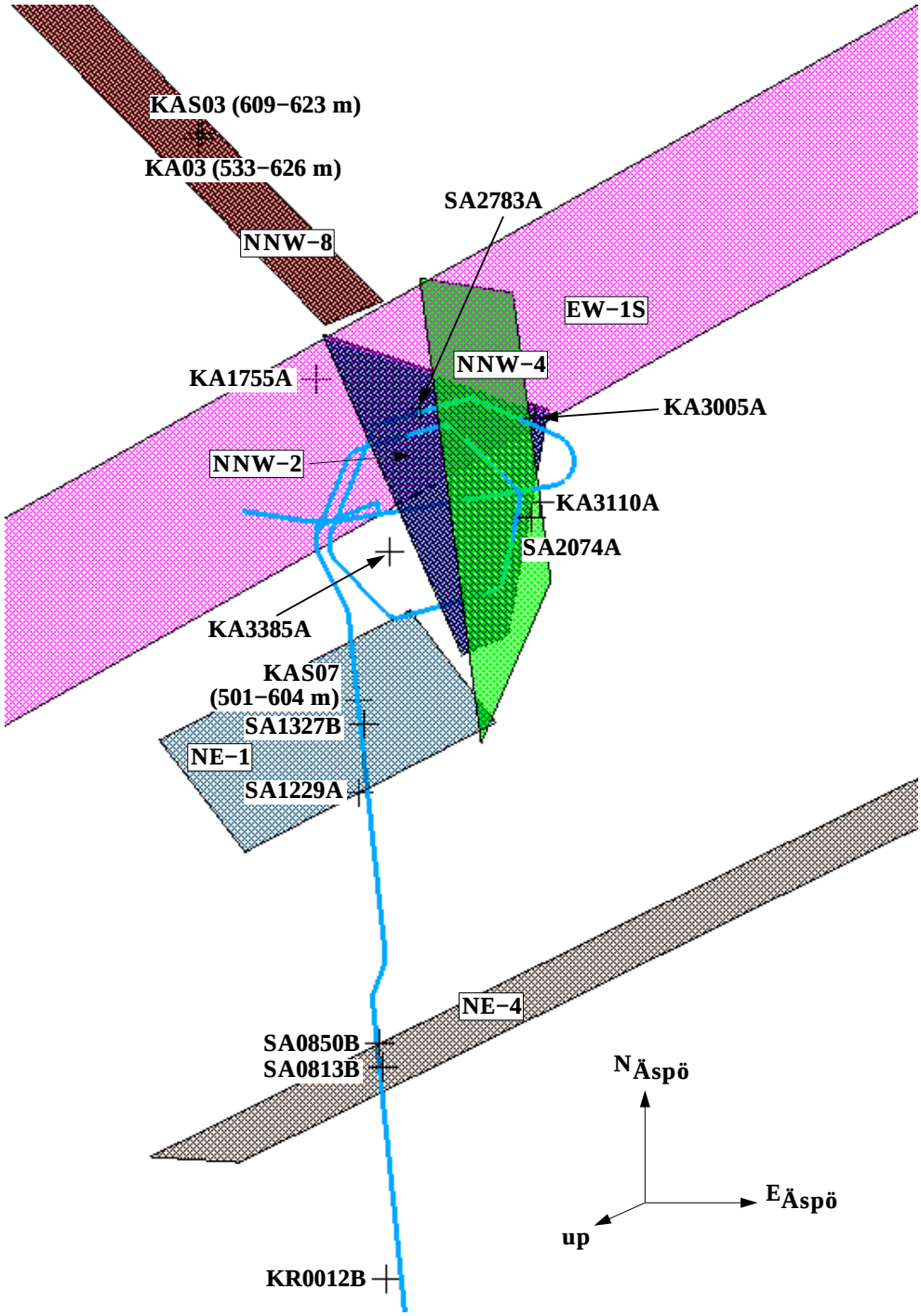

Figure 5.3. Control points and fracture zones pertaining to them.

At first, the model was solved with the same properties as in the M3-based simulations (Kattilakoski, 1999).

Next the site scale hydraulic rock mass domains (SRD) were included in the model (Fig. 3.3. and Table 3.3). The longitudinal and transversal dispersion lengths 5000 m and 500 m, respectively, in the fracture zones NE-2, NNW-1, NNW-2, NNW-4, NNW-5 and NNW-7 used in the M3-based simulations (Kattilakoski, 1999) were shortened to 1000 m and 100 m,

respectively. In order to improve the willingness of saline water to well upwards, the transmissivities of the zones NNW-1 and NNW-7 were modified (Table 3.2). The values from Model 96 (Table 8-1 in Rhén et al., 1997) are used instead of the calibrated values (Svensson, 1997). The infiltration from the sea was not any more restricted as in the M3-based calculations. This resulted in a better fit in the mixing proportions of Baltic water in the control points SA1229A and SA2074A. Also, the chloride distribution given on the basis of the inverse-modelling results (Luukkonen, 2000) was extended down to the model bottom, which has the chloride content of 17.7 g/l.

In order to get better the fit between the mixing proportions from the geochemical estimations and the mixing proportions simulated here for the control point KR0012B, the infiltration from the sea was restricted in the fracture zone SFZ05. The transmissivity of the uppermost elements of the zone SFZ05 below the sea was lowered to the value T=9.3·10^{-9} m^2/s (supposed width 30 m). To increase the mixing proportions of meteoric water in KR0012B the transmissivity of the fracture zone SFZ05 was increased fivefold to T=5.0·10^{-4} m^2/s with a depth dependency (Fig. 3.2). Unfortunately, the mixing proportions of meteoric water in KR0012B did not increase, till the surface boundary condition in the vicinity of the control point KR0012B was modified. One node depicting sea area in the model was changed to a land node thus having no Baltic water. This resulted in that the zone SFZ05 does not anymore run through the sea area.

The somewhat too high mixing proportions of Baltic water in SA0813B were tried to lower by decreasing the infiltration from the sea in the fracture zone NE-4. The transmissivity of the uppermost elements of the zone NE-4 below the sea was lowered to the value T=9.3·10^{-9} m^2/s (supposed width 30 m). The mixing proportions of Baltic water in SA0813B did not decrease significantly, till the surface boundary condition near the coastline of the Äspö Island was modified. Two nodes in the vicinity of the control point SA0813B were given the boundary condition with 70 % Baltic, 25 % meteoric and 5 % altered water.

The control point in KAS03 (533–626 m) is situated near the fracture zone NNW-8. The transmissivity of the fracture zone NNW-8 was given a depth dependency (Fig. 3.2). This did not decrease the mixing proportions of saline water in the control point, however.

Because the infiltration through the sea bottom was not restricted, the mixing proportions of Baltic water became too high in the control point SA2074A. This was corrected by decreasing the transmissivity of the zone NNW-4 to one fifth, T=1.3·10^{-5} m^2/s.

In order to retain the mixing proportions of Baltic water in the control point SA1229A and to decrease them in the control point KAS07 (501–604 m), the fracture zone SFZ12 (including NE-1) was given a depth dependent transmissivity (Fig. 3.2).

The model did not yield the up-welling of saline water, which is apparent on the basis of the geochemical estimations in the control points KA1755A and SA2783A (Figs. 5.7 and 5.9). This was improved a bit by extending the zone EW-1S to the depth of about 1150 metres – as deep as the nearly perpendicular zone NNW-2. The zones EW-1S, EW-1N, NNW-1, NNW-2 and NNW-5 were narrowed. The width of 10 metres resulted in a somewhat more apparent welling up of saline water (Fig. 5.15).

The mixing proportions of meteoric water were lowered by applying an increasing transmissivity in the fracture zones in the land areas down to the depth of 200 metres (see Section 3.3 and Eq. (3.1)). There exist shallow transmissivity measurements only in the land areas.

Figures 5.4—5.9 depict the mixing proportions of glacial, Litorina, altered, saline, meteoric and Baltic waters in the calibration section in the control points KR0012B, SA0813B, SA1229A, KA1755A, SA2074A and SA2783A as function of time. The simulated results are compared to the results of the geochemical estimations. Figures 5.10 and 5.11 show the comparison in the control points outside the Äspö tunnel, namely in KAS03 (section 533—626 m) and KAS07 (section 501—604 m). Table 5.2 summarizes the single results in the control points KAS03 (section 609—623 m; preinvestigations), SA0850B and SA1327B.

Figures 5.12—5.14 show the mixing proportions in the prediction points KA3005A, KA3110A and KA3385A in the section 2900—3600 m of the tunnel. Looking at the results in the prediction section (Figures 5.12, 5.13 and 5.14), the common feature is the increase in the mixing proportions of Baltic water. Similarly, the mixing proportions of glacial, Litorina and altered water types decrease in all prediction points. Only the most shallow prediction point KA3005A exhibits an indistinct increase in meteoric water as a function of time. In the other prediction points the proportion of meteoric water remains nearly constant. Analogously, only the deepest prediction point KA3385A shows an increase in saline water as a function of time. In KA3005A and KA3110A the saline proportion decreases.

All the simulated and estimated mixing proportions for the control points in the tunnel section 0–2900 m are tabulated in Appendix B. In the case of the prediction points, all the simulated proportions and water composition estimations evaluated from these proportions are presented in Appendix C. The details, how the water compositions are calculated from the simulated proportions, and how the geochemical mole-transfer reactions are taken into account in these calculations are presented by Luukkonen (2000).

Figure 5.15 shows the mixing proportions of each water type on an east—west trending cut plane before (October 1st, 1990; see Table 3.4) and after the tunnel construction (January 24th, 1995). The tunnel construction caused the welling up of saline water and the decrease of glacial, Litorina and altered waters in the tunnel area.

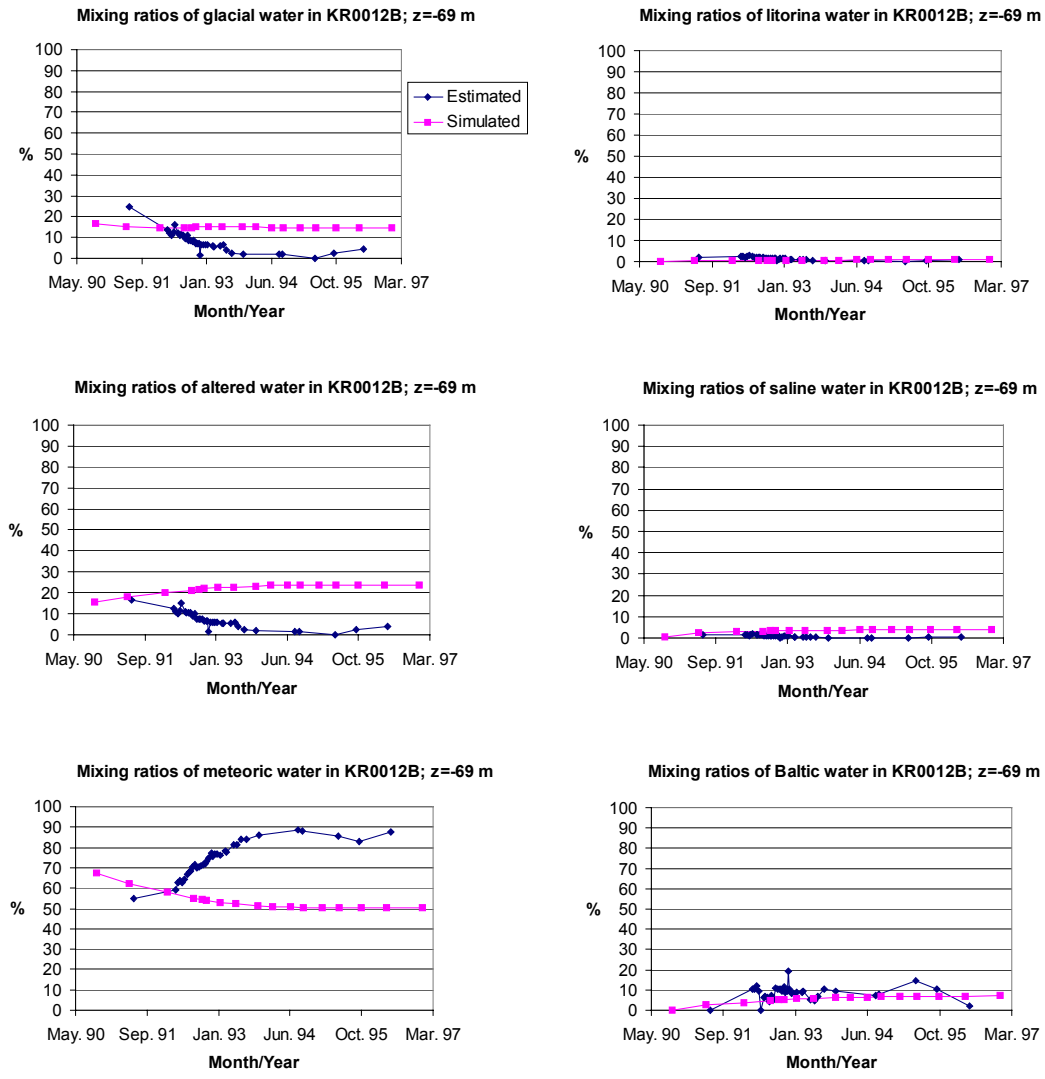

Figure 5.4. The mixing ratios of glacial, Litorina, altered, saline, meteoric and Baltic water in KR0012B as function of time.

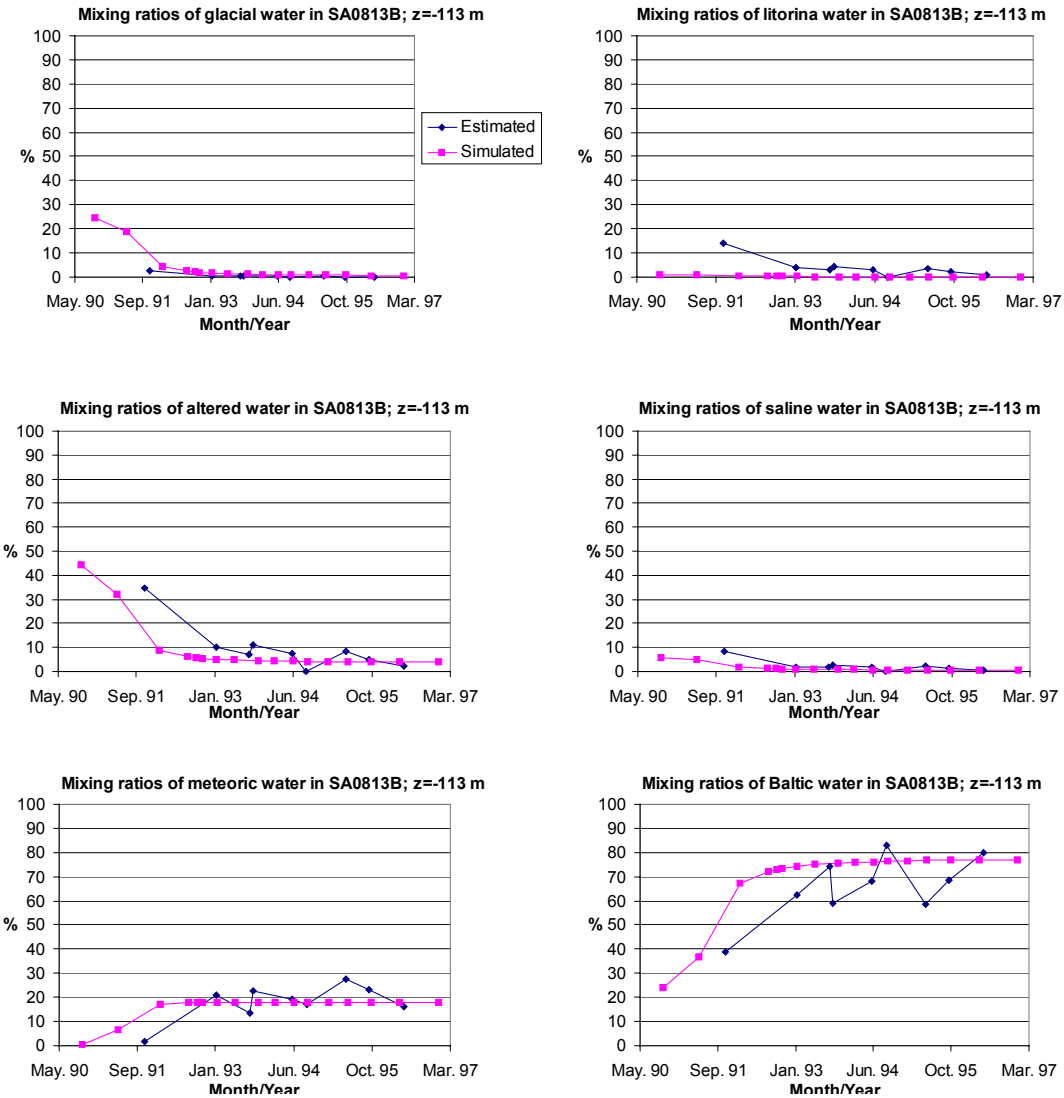

Figure 5.5. The mixing ratios of glacial, Litorina, altered, saline, meteoric and Baltic water in SA0813B as function of time.

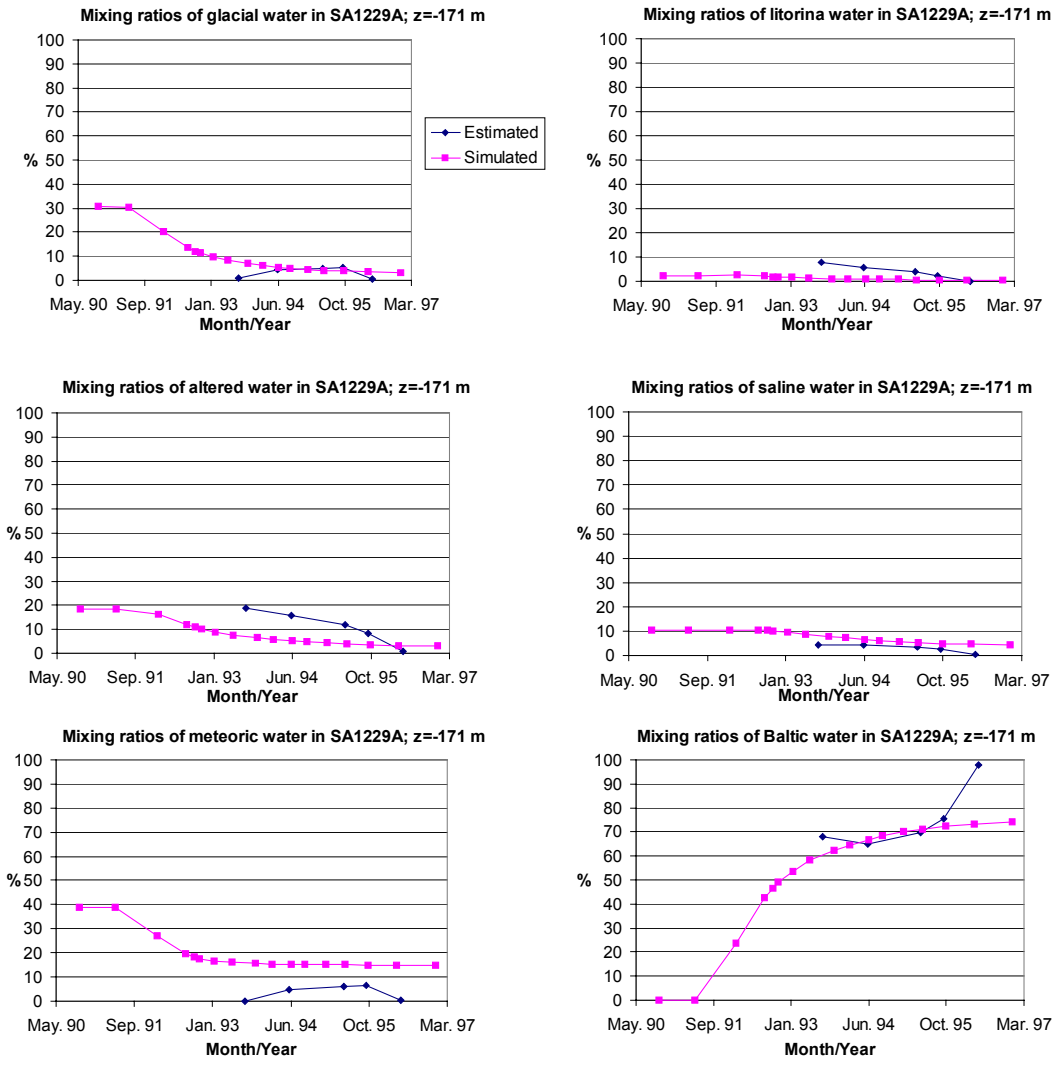

Figure 5.6. The mixing ratios of glacial, Litorina, altered, saline, meteoric and Baltic water in SA1229A as function of time.

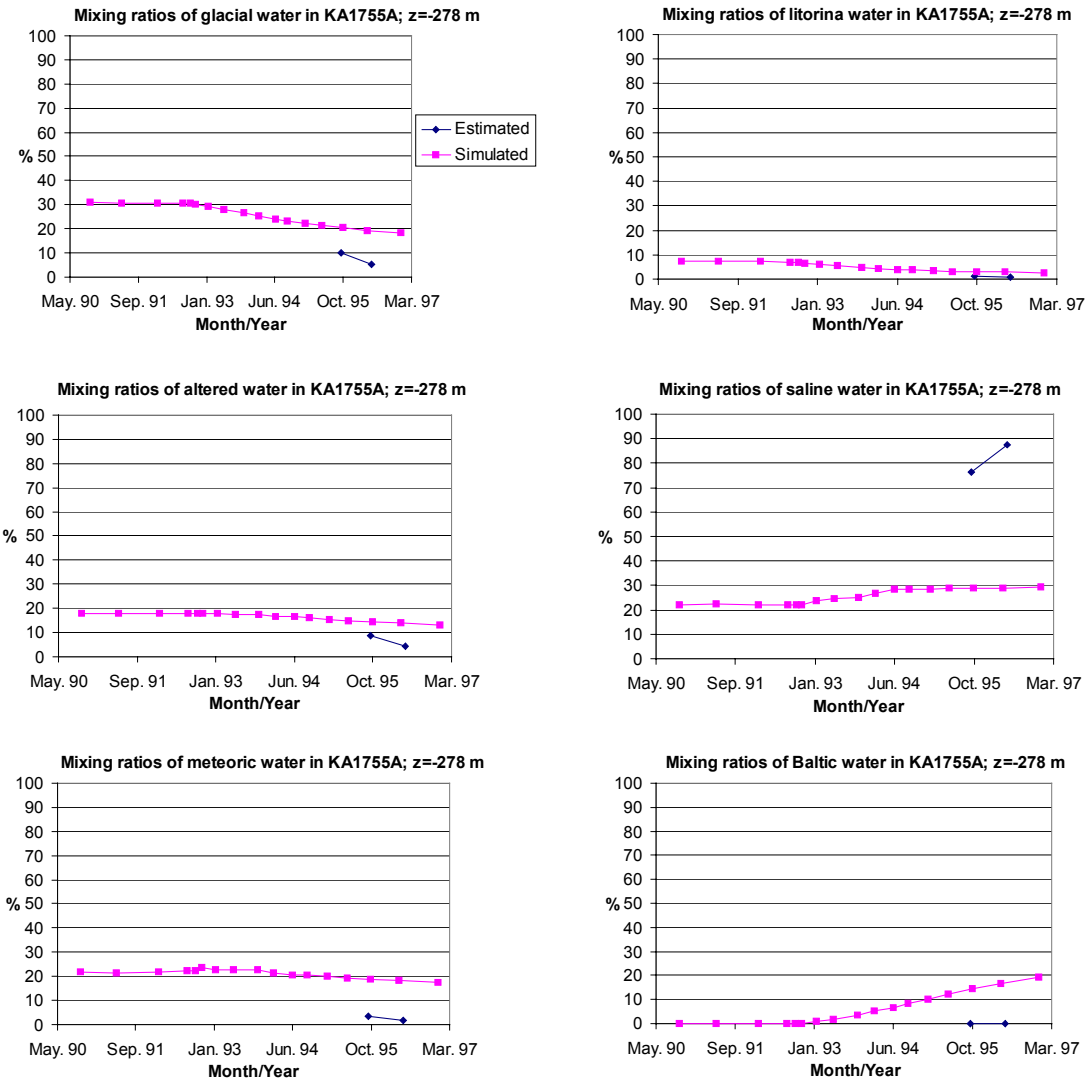

Figure 5.7. The mixing ratios of glacial, Litorina, altered, saline, meteoric and Baltic water in KA1755A as function of time.

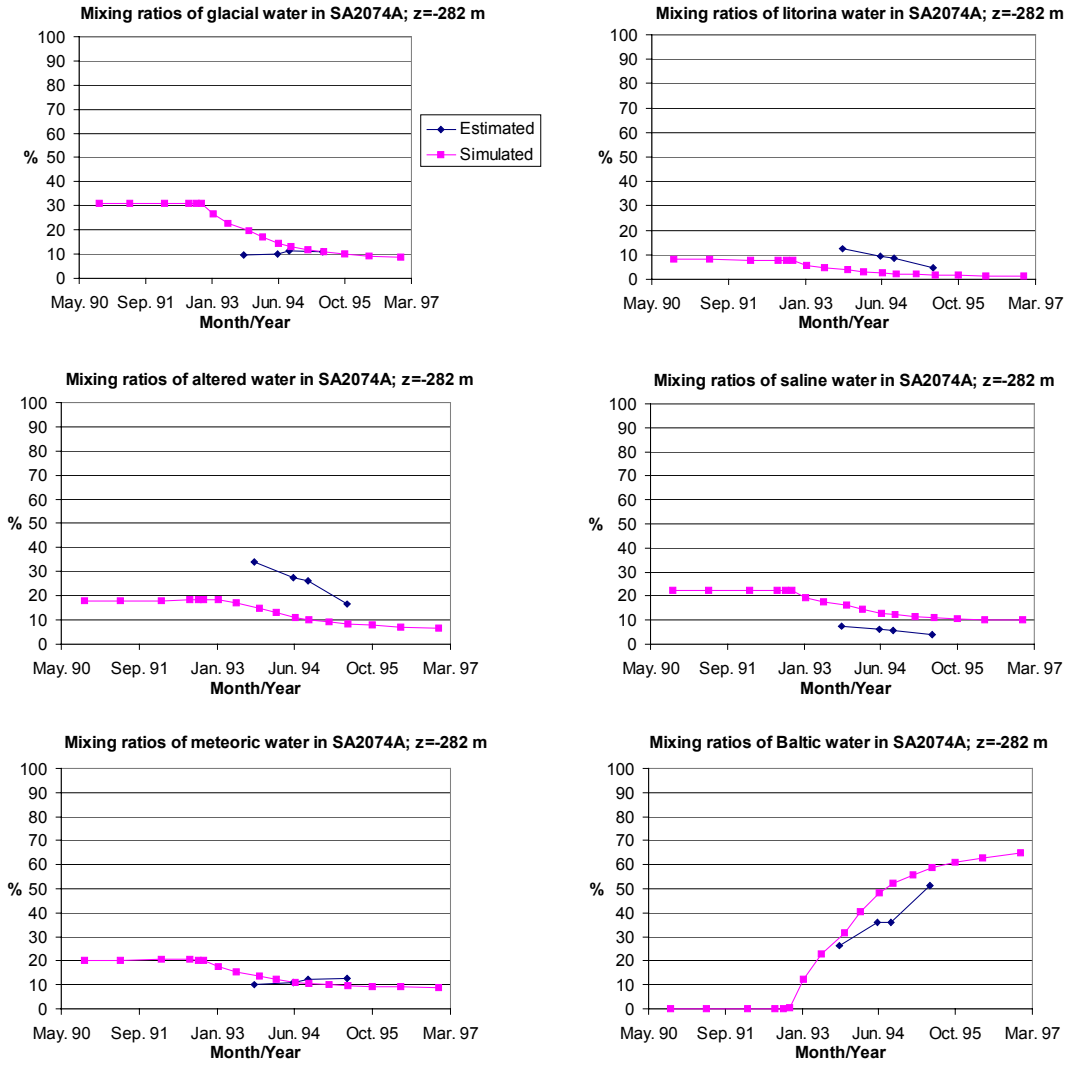

Figure 5.8. The mixing ratios of glacial, Litorina, altered, saline, meteoric and Baltic water in SA2074A as function of time.

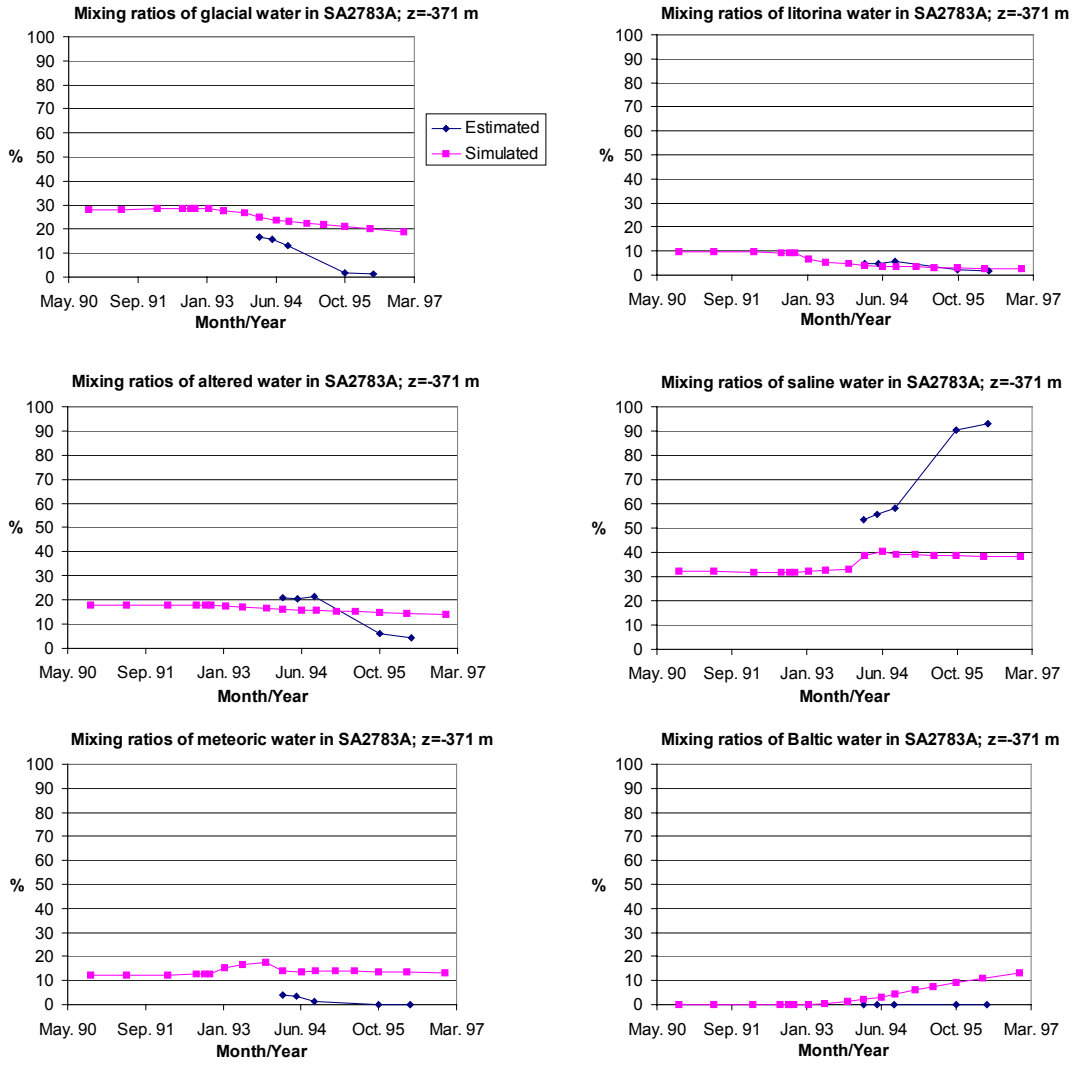

Figure 5.9. The mixing ratios of glacial, Litorina, altered, saline, meteoric and Baltic water in SA2783A as function of time.

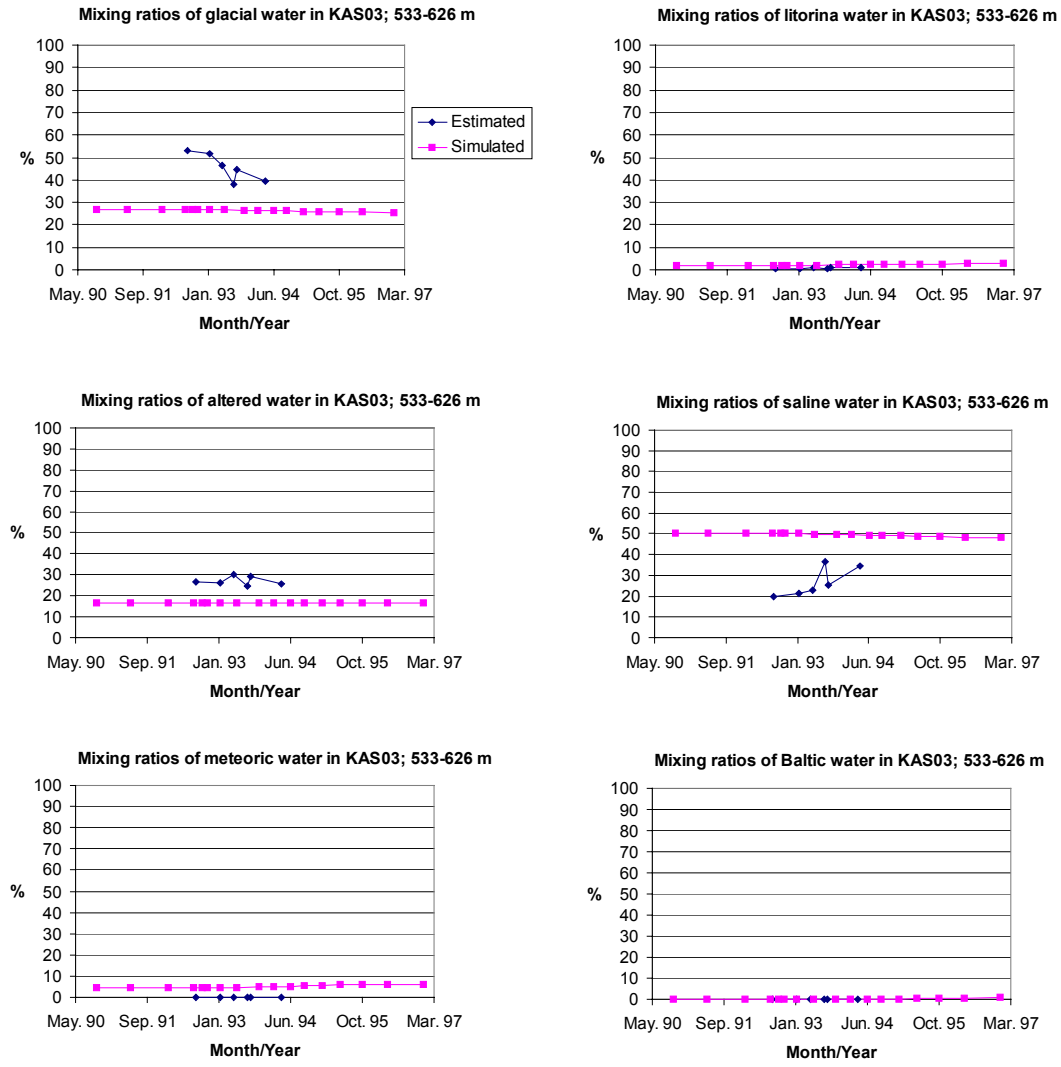

Figure 5.10. The mixing ratios of glacial, Litorina, altered, saline, meteoric and Baltic water in KAS03 (section 533—626 m) as function of time.

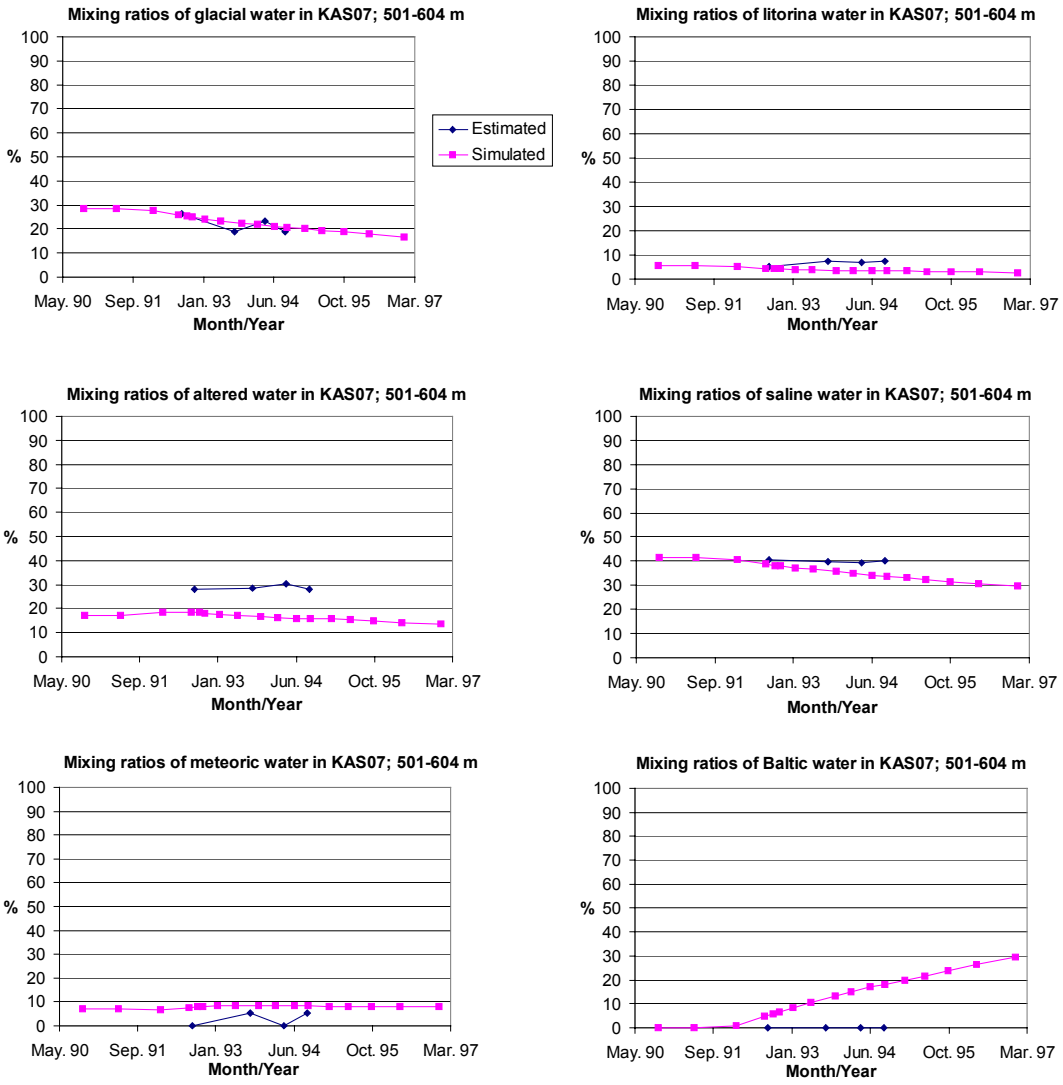

Figure 5.11. The mixing ratios of glacial, Litorina, altered, saline, meteoric and Baltic water in KAS07 (section 501—604 m) as function of time.

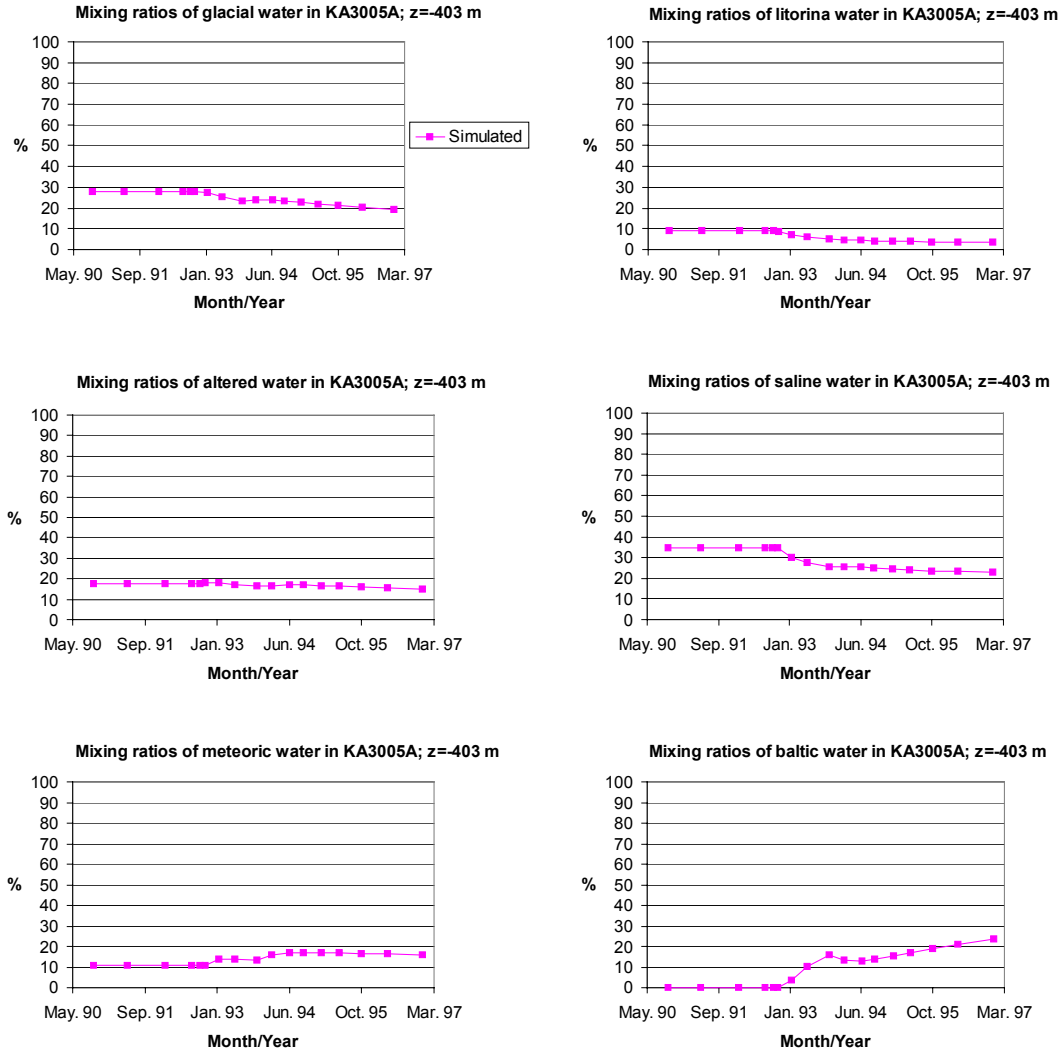

Figure 5.12. The mixing ratios of glacial, Litorina, altered, saline, meteoric and Baltic water in KA3005A as function of time.

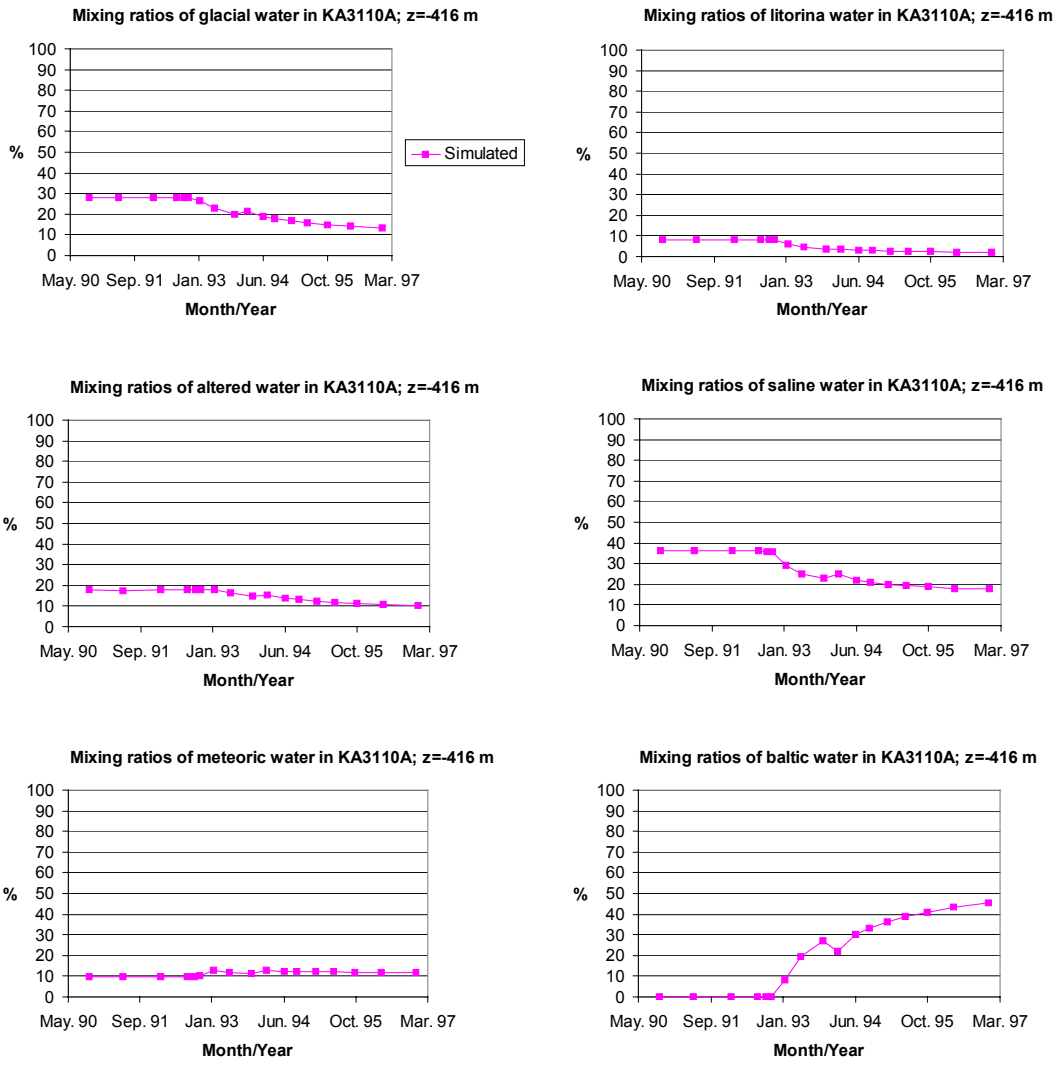

Figure 5.13. The mixing ratios of glacial, Litorina, altered, saline, meteoric and Baltic water in KA3110A as function of time.

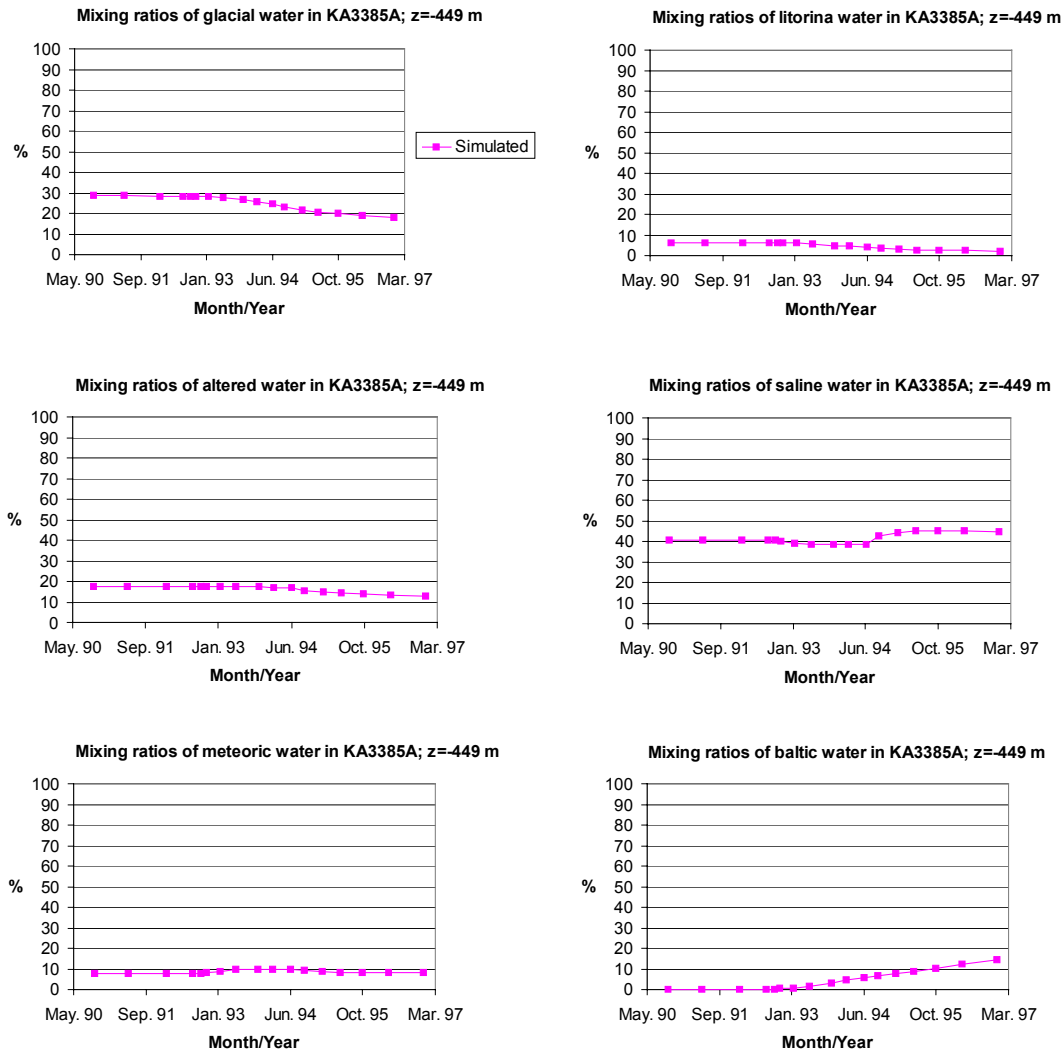

Figure 5.14. The mixing ratios of glacial, Litorina, altered, saline, meteoric and Baltic water in KA3385A as function of time.

Table 5.2. The mixing ratios of glacial, Litorina, altered, saline, meteoric and Baltic water in KAS03 (section 609—623 m; preinvestigations), SA0850B and SA1327B.

		Estimated						*Simulated*					
	Date	*Glacial*	*Litorina*	*Altered*	*Saline*	*Meteoric*	*Baltic*	*Glacial*	*Litorina*	*Altered*	*Saline*	*Meteoric*	*Baltic*
KAS03	*Sep. 88*	31	1	20	49	0	0	24	0	16	57	3	0
SA0850B	*Aug. 91*	7	8	71	6	8	0	19	1	32	5	7	37
SA1327B	*Oct. 92*	5	6	18	5	6	60	15	2	13	10	21	38

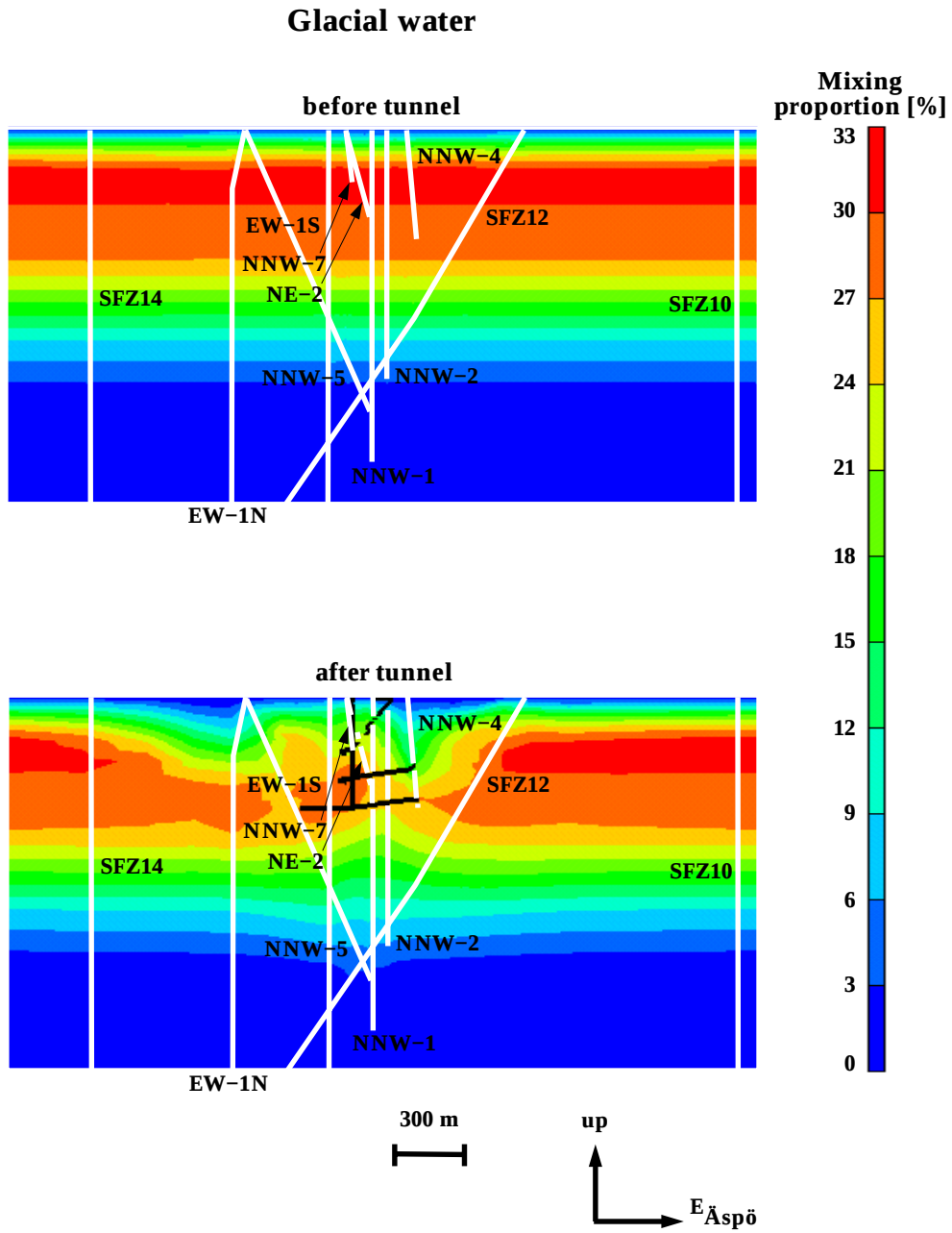

Figure 5.15. The mixing ratio of glacial water on an east—west trending cut plane before and after the tunnel construction.

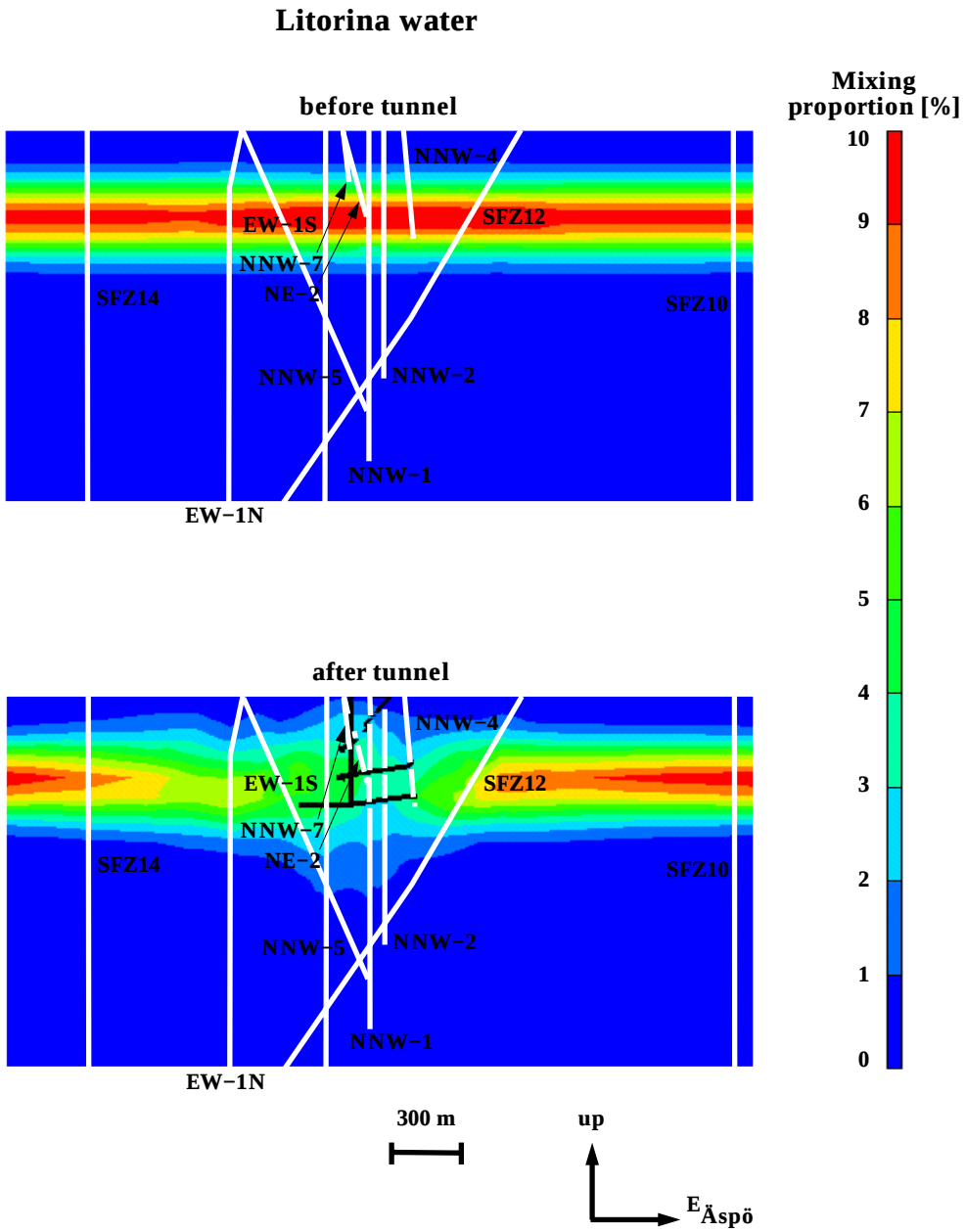

Figure 5.15. (cont.) The mixing ratio of Litorina water on an east—west trending cut plane before and after the tunnel construction.

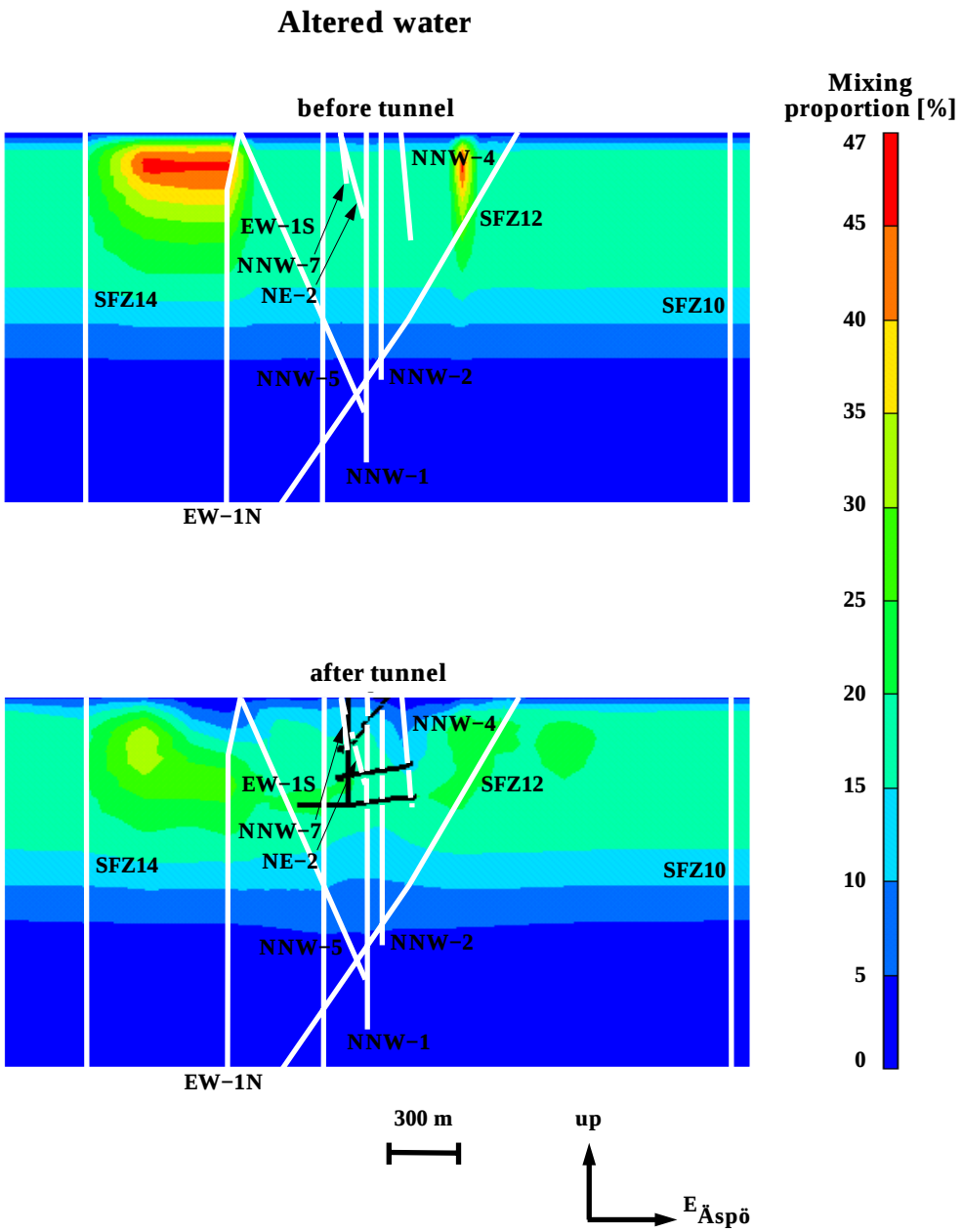

Figure 5.15. (cont.) The mixing ratio of altered water on an east—west trending cut plane before and after the tunnel construction.

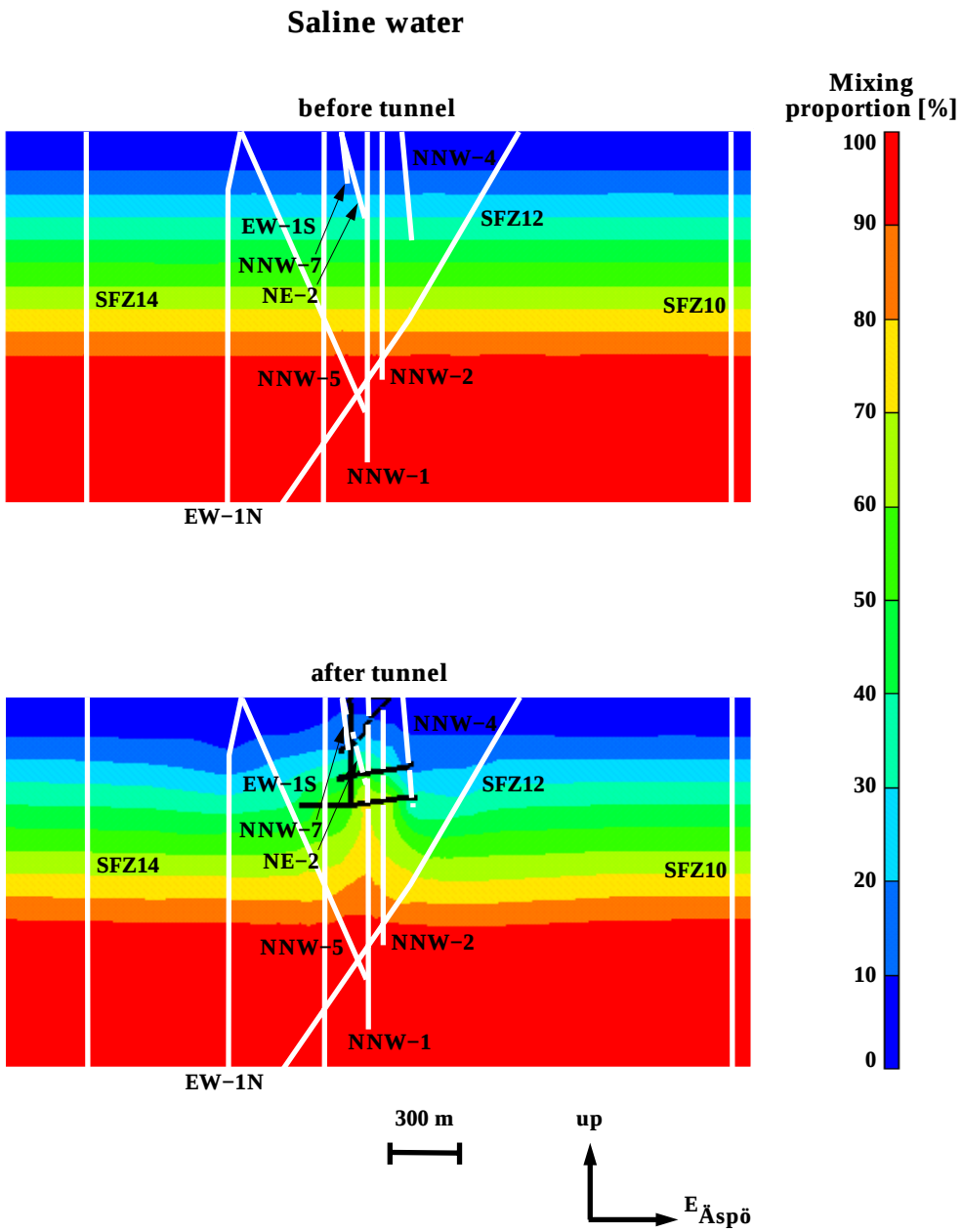

Figure 5.15. (cont.) The mixing ratio of saline water on an east—west trending cut plane before and after the tunnel construction.

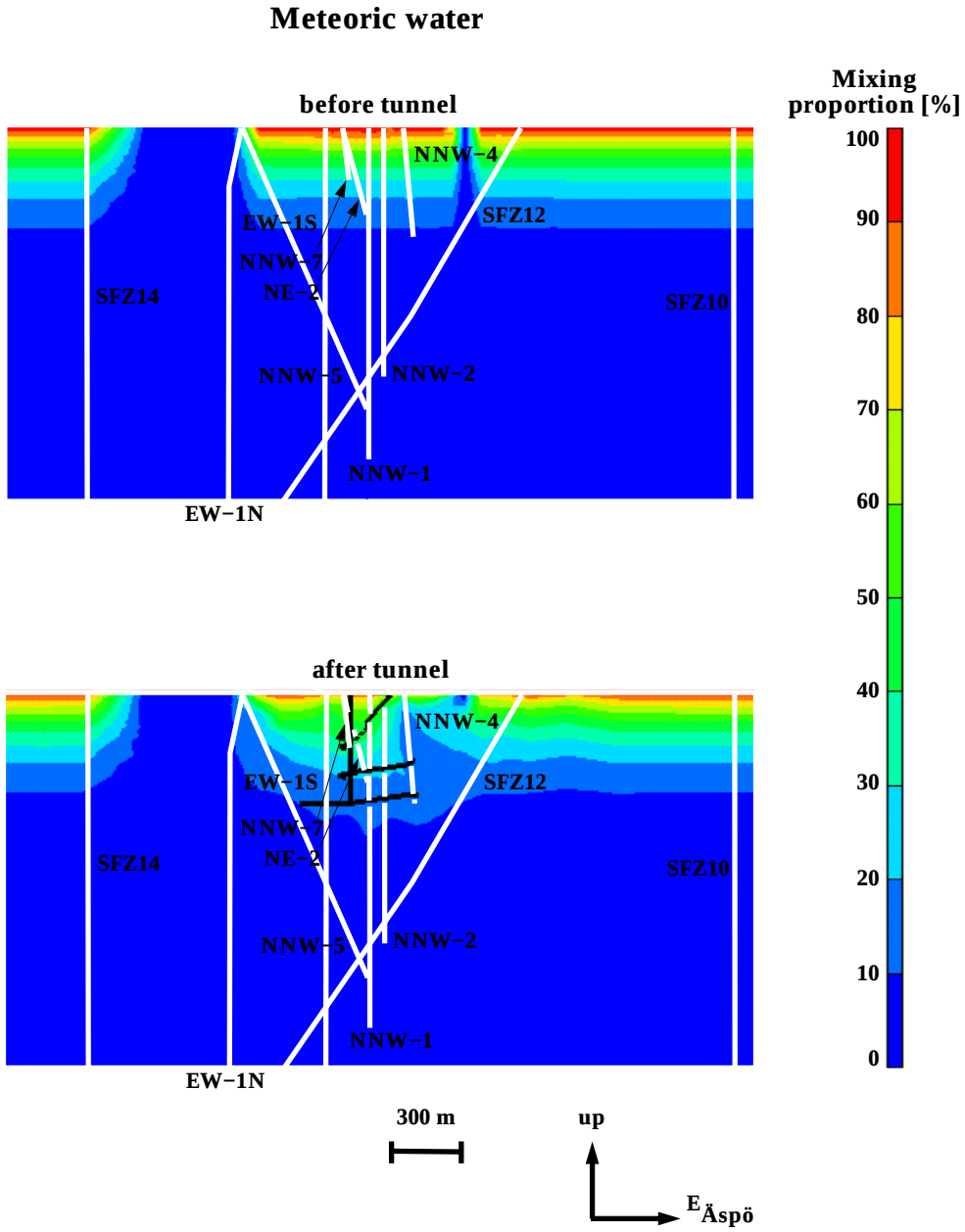

Figure 5.15. (cont.) The mixing ratio of meteoric water on an east—west trending cut plane before and after the tunnel construction.

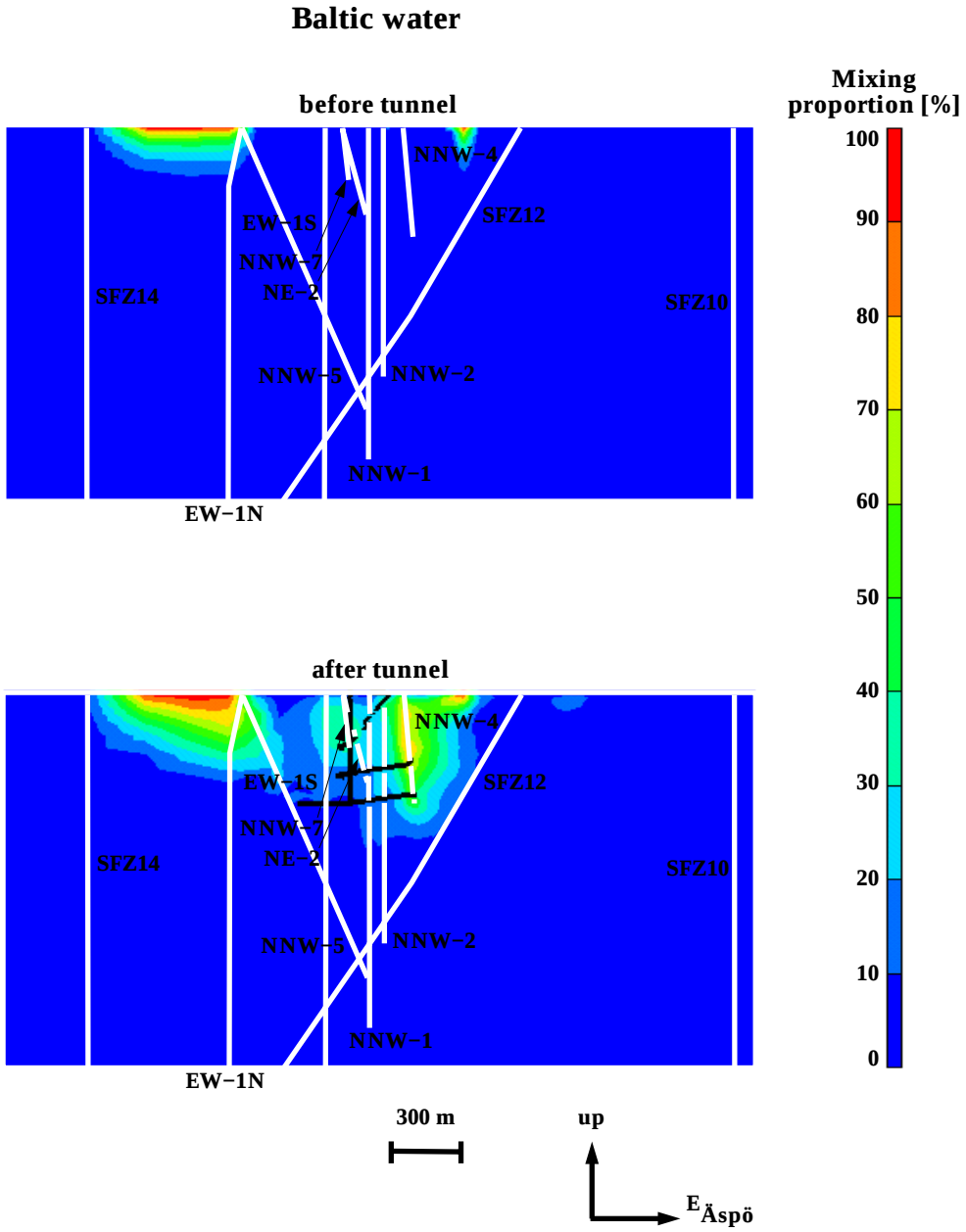

Figure 5.15. (cont.) The mixing ratio of Baltic water on an east—west trending cut plane before and after the tunnel construction.

6 DISCUSSION

6.1 Hydrological simulations

Although several step-wise modifications and additions were made to the calibrated hydrological model (cf. Chapter 5.2), the finally accepted model succeeds variously in reproducing the geochemical estimation results as shown in Figures 5.4–5.11.

The control point KR0012B is situated near the surface and on the edge of the model. The mixing results depend strongly on the surface boundary condition associated with each water type (Fig. 5.4). The mixing result in KR0012B is only roughly adjusted due to the large element size of the model in the boundary area (Fig. 3.6). The simulation difficulties in this control point can be largely addressed to the local coarseness of the model. Therefore, these results do not indicate difficulties in the central tunnel area.

In the control point SA0813B altered water was the dominant type in the undisturbed conditions. The tunnel construction caused the dominance in the mixing proportions of meteoric and Baltic waters (Fig. 5.5). The meteoric water intrusion into SA0813B likely originates either from the small islands between Hålö and Äspö or from the Hålö Island via the fracture zone NE-4. As Figure 5.5 shows, the agreement between the simulated and estimated results is quite successful in the case of SA0813B.

In the estimated results for the control point SA0850B in August 1991 the high proportion of altered water can be seen (Table 5.2). In the case of SA0850B it is evident that the sum of simulated altered and Baltic fractions (32 % + 37 %) resembles closely the estimated altered fraction (71 %). The estimated results are based on a single sample. Therefore, no far-going conclusions are to be made.

The control points SA1229A and SA1327B in the fracture zone NE-1 are situated below the southern parts of Äspö near the coastline of the island. They are, however, easily influenced by seawater because the water-bearing zone NE-1 and the perpendicular NNW-3 (Fig. 5.1) cause the strong increase in the mixing proportions of Baltic water (Fig. 5.6 and Table 5.2). With the exception of meteoric water the simulated evolution trends between SA0813B and SA1229A exhibit similar character. In all, the simulated trends for SA1229A repeat relatively well the estimated mixing fractions. However, towards the end of the time-series, the estimations indicate higher and lower proportions of Baltic Sea and meteoric water, respectively, than the simulation results give. In the case of the single SA1327B simulation results it can be concluded that they fit almost exactly to the simulated SA1229A time-series trends. The major deviation between the simulated and estimated SA1327B values is among the Baltic Sea fractions (Table 5.2).

The control point SA2074A in the upper spiral of the tunnel is also under the influence of the marine boundaries like the control points SA1229A and SA1327B, which again results in an increment in the mixing proportions of the Baltic water type as a function of time (Fig. 5.8). The difference between these points is that SA2074A resides about 100 m deeper down in the bedrock than the other two control points. Therefore, it can be expected that seawater intrusion into SA2074A is more peaceful. According to Figure 5.8, the simulated and estimated fractions coincide relatively well with each other, though certain distinct differences can be pointed out.

The control points KA1755A and SA2783A locate below the Äspö Island. The points lie within the fracture zones EW-1S and NNW-2 as indicated in Figure 6.1. Both locations are supposed to be under the influence of the dry land boundaries (cf. Fig. 3.5) in the undisturbed conditions (Figs. 5.7 and 5.9). The undisturbed boundary assumption predicts saline water fractions about 25 % for the control points. In principle, both the control points have connections to surficial meteoric and seawater via the named structures, and it can be assumed that both meteoric and seawater may intrude into the control points in the disturbed condition. However, the estimated and simulated reference-water fractions deviate a lot in the disturbed condition.

The tunnel face position passed the sampling location KA1755A in the beginning of November ’92, and the location SA2783A about one year later in the beginning of year ’94 (Table 3.4). The first estimations for the location SA2783A are for a sample taken soon after the excavations passed the sampling point (Fig. 5.9). Indeed, the deviation between the estimations and the simulations is quite satisfactory for this sample.

In the case of KA1755A, the first estimated sample (Oct. 12th, ’95) has been taken approximately three years after the tunnel excavations passed the sampling location. However, the first available incompletely analysed sample from this location dates back to over a 1.5 years earlier date (March 16th, ’94). In this sample Cl concentration is about 78 % of the first estimated sample. As an approximation this indicates decrease in saline reference water fraction from 76 % to about 54 %. If this fraction is plotted on Figure 5.7 the increasing trend in the saline reference water estimations with time becomes more evident. From the date March 16th, ’94 there is still about 1.5 years to go to the tunnel passage date. If the dilution back in time would remain similar (March 16th, ’94 → Nov. ’92) as in the later step (Oct. 12th, ’95 → March 16th, ’94), a similar conclusion as for the location SA2783A could be made, i.e. when the tunnel passed the control point the estimations and simulations approximately coincide.

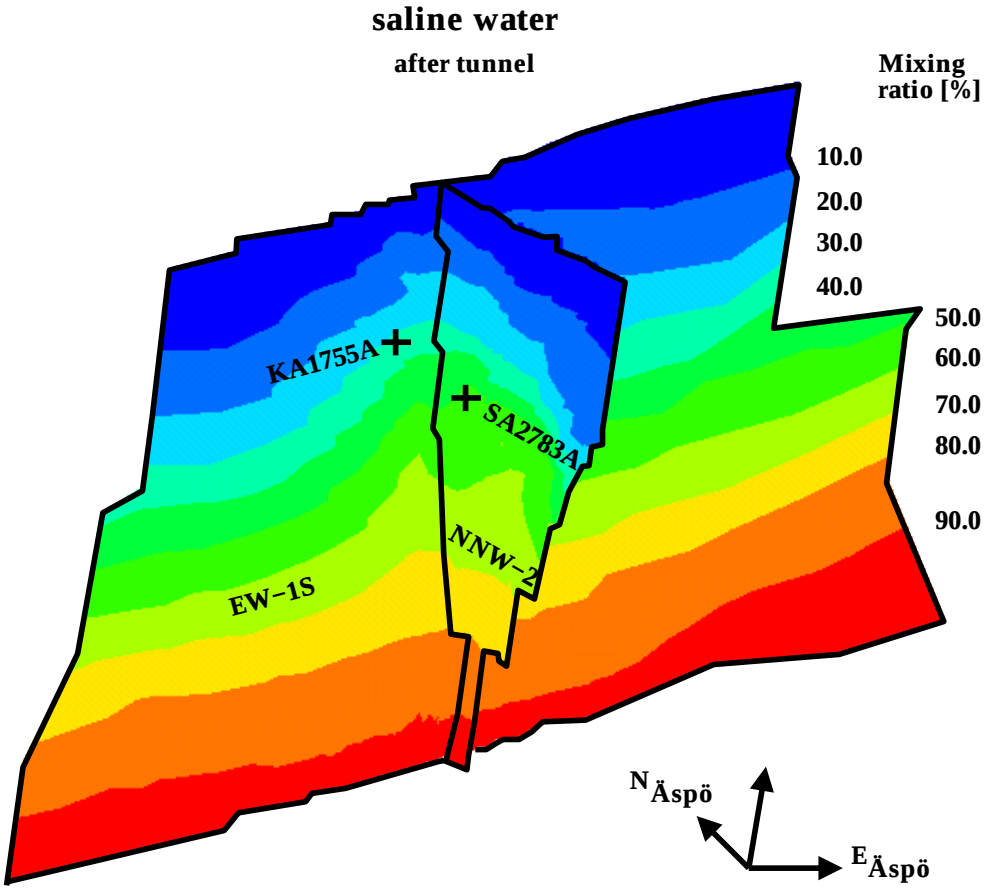

Figure 6.1. Locations of control points KA1755A and SA2783A within structures EW-1S and NNW-2, and simulated distribution of saline reference water within the structures after the Äspö HRL construction (the disturbed condition).

In all, however, the simulation results follow poorly the estimated mixing fractions in the control points KA1755A and SA2783A (Figs. 5.7 and 5.9). Furthermore, the deviation between the estimated and simulated fractions seems to broaden with time. Specifically, in the case of meteoric and Baltic Sea water, the hydrological simulations seem to exaggerate these sources. The geochemical estimations indicate that contributions from both the sources are negligible, though the structural model indicates potential connections to the source areas. In the case of saline reference water the difference between the estimated and simulated fractions becomes very large with time. The simulations cannot repeat the high increase of saline reference water in the control points KA1755A and SA2783A. From the Figures 5.7 and 5.9 it can be seen that the simulated welling up of saline reference starts approximately when the tunnel passes the control point. The simulated welling up is shown in Figure 6.1.

Two of the control points are situated north–west of the tunnel area in the borehole KAS03. They are the deepest control points examined here. The disturbed samples from KAS03 were sampled from the depth interval 533–626 m (average depth of 566 m) and the undisturbed sample was sampled from the depth interval 609–623 m (average depth 603 m). The disturbed

results are shown in Figure 5.10 and the undisturbed results in Table 5.2. The packed-off sampling intervals of these control points are partially overlapping. Furthermore, there is a good chance that both the control points receive the major part of their water from the fracture zone NNW-8 (Fig. 5.3). Therefore, from the hydrological point of view, it is useful to consider these control points together.

In the undisturbed conditions (Table 5.2) the estimated and simulated fractions for KAS03 coincide well. If the fractions presented in Table 5.2 are plotted to Figure 5.10, the estimated and simulated values plot very close to the first fractions of the simulated disturbed trends of KAS03 as expected (because the undisturbed estimations are in accordance with the undisturbed geochemical boundaries). Major difficulties start when the disturbed estimated and simulated trends are compared to each other. The first estimated disturbed sample has been taken on August 19th, '92. The differences between the estimated and simulated fractions are large (Fig. 5.10), though the differences decrease with time.

Based on the disturbed estimations, it seems that groundwater in the control point KAS03 diluted considerably during year 1992. The fraction of saline water diminishes and the fraction of glacial melt increases distinctly compared to the undisturbed sample presented in Table 5.2. These changes could be related to the excavations of the main tunnel that advanced to the upper spiral of the laboratory during summer '92. The tunnel face position 1400 m shown in Figure 5.1 represents the situation on August 10th, '92 (Table 3.4). In the southern Äspö the hydraulic pressure minimum was then at the depth of about 200 m. In order to be effective, this southern minimum should cause the intrusion of glacial melt rich water into the northern control point KAS03 at the depth of about 570 m. According to the boundary assumptions (Fig. 3.5), more glacial melt rich water was available only at shallower depths, from where it should be drawn down. According to this speculation, the situation inverted later on as the excavations advanced deeper. Saline water welled then up into the control point and the fraction of glacial melt water began to diminish.

Without knowing the exact history of the borehole KAS03, the preceding speculation is quite questionable. Although, a year earlier (July 9th, '91) an incomplete sampling from KAS03 indicates that the sampling point diluted in respect of chlorine 36 % in one year. In all, according to the simulations the disturbed conditions in KAS03 remain quite steady. The excavations have no significant effect to the mixing fractions, i.e. only lateral transport is possible/expected at the control point. There are two ways to explain the difference between the estimated and simulated values. The gradual estimated salinity increase in KAS03 (cf. Fig. 5.10) might indicate gradual recovery of the undisturbed condition at the control point. Then, the compositional changes detected were caused by earlier or other activities done *in* the borehole KAS03. The other explanation is that the hydrological simulation model behaves too stiffly in time, and the detected increase in salinity is a consequence of saline water welling up from depth.

The control point of the borehole KAS07 is situated in the fracture zone NE-1 as the upper SA1229A and SA1327B. According to the estimations, the conditions in the control point KAS07 remain stable in the disturbed conditions. The first estimated sample dates back to August 31st, '92 when the excavated tunnel front was passed the sampling location. However, there are incomplete analyses available also from the undisturbed conditions and these analyses indicate stable conditions as well in the control point. There are practically no changes in the groundwater composition as a consequence of the tunnel excavations. The estimation results are interesting because the control points SA1229A, SA1327B and KAS07 are all connected to the sea via the structure NE-1, though the point KAS07 locates almost 300 m deeper than the former two. According to the estimations, Baltic Sea has a significant effect to the control points SA1229A (Fig. 5.6) and SA1327B (Table 5.2), while the control point KAS07 (Fig. 5.11) remains untouched. The simulation results for KAS07, however, predict decreasing glacial, altered and saline, and increasing Baltic proportions.

The differences between the estimated and simulated fractions in the control point KAS07 give similar indications as disparities detected in the control points KA1755A and SA2783A. It seems that when the tunnel passes the control point in KAS07 the estimations and simulations approximately coincide. Thereafter the deviations in some water types start to grow larger with time.

As the preceding discussion already indicates the simulation difficulties in the deep control points do not build up confidence in the prediction point (KA3005A, KA3110A and KA3385A) simulation results. The control points KA3005A and KA3385A reside in the hydraulic rock mass domain (SRD3, Fig. 3.3), though KA3385A is relatively close to the fracture zone NNW-7 (cf. Table 5.1). The control point set used for the calibrations of the hydraulic model does not have any control points either from SRD3 or from NNW-7. KA3385A is the deepest prediction point considered and it exhibits a small increase in the saline water proportion as a function of time. It could be expected that the saline proportion would increase more distinctly at this depth. However, our calibration simulations elsewhere were not successful in respect of saline water, and furthermore, the predictions do not have any decent a priori knowledge about the relationships between the fracture zone (i.e. hydraulic conductor) vs. the rock mass domain.

The predictions for the point KA3110A are on the most solid basis. The KA3110A is located in the fracture zone NNW-4 and this fracture zone has been calibrated with one control point (SA2074A). The locations of the points SA2074A and KA3110A are shown in Figure 5.3 and the calibrated simulation results vs. the geochemically estimated proportions for SA2074A are shown in Figure 5.8. Most aspects of the predicted results for KA3110A (Fig. 5.13) are similar to the control point SA2074A, though the changes and the rate of changes are more damped at depth.

6.2 Evaluation of hydrological simulation results

As the preceding discussion indicates, there are several disparities between the estimated and simulated modelling results. The most obvious reasons for these problems will be pointed out in the following. However, before that a comparison between the M3- and inverse-modelling based simulations is necessary.

Kattilakoski (1999) has presented the M3-based hydrological simulation results. As a summary, the M3 estimations indicate calm geochemical changes or practically static geochemical conditions, while the Äspö tunnel excavations gradually turn the initial undisturbed hydrological–geochemical conditions into the disturbed conditions. Similarly, the M3-based simulations produce smooth trends that coincide in most cases relatively well with the M3 estimations.

When the inverse-modelling results (Luukkonen, 2000) are compared to the M3 estimation results on a qualitative level, it becomes evident that the inverse estimation results give impression of more brisk geochemical changes as a response to the system disturbance. In most cases there are three distinct water sources (meteoric, Baltic Sea, saline) potentially intruding into a control point. Other water type fractions tend to diminish as a function of time as they do not have any extensive sources.

The detailed comparison between the geochemical estimation methods is a complicated task not to be presented here. However, a generalised example shows how a choice of saline reference affects to the readiness of a method to reflect changes in the system. The saline reference water in the M3 approach contains 47 200 mg/l Cl (Laaksoharju & Wallin, 1997), while in the inverse approach Cl concentration is 12 300 mg/l. Suppose a binary mixture of meteoric and saline water with Cl concentration 10 000 mg/l that dilutes to 8 000 mg/l. In the inverse approach this dilution indicates a 16.3 % change in the saline reference water fraction, while in the M3 approach the change is approximately only 4.2 %.

Considering the inverse-modelling based simulation results presented in Figures 5.4–5.11, it can be concluded that the simulations at shallow depths (SA0813B, SA0850B, SA1229A and SA1327B) gave good or fair results compared to the estimated results. All these control points are also strongly influenced by seawater. Deeper two major problems can be pointed out in the simulations. In certain control points (KA1755A, SA2783A, KAS07) the difference between the estimations and simulations begins systematically enlarge after the control point actually experiences the effect of the neighbouring open tunnel. At least in one case (KAS03) it seems that the hydrological model may behave too stiffly in time compared to the geochemically estimated fractions.

There are a couple of factors that can be addressed as sources for growing differences between the estimations and simulations, and the supposed exaggerated stiffness of the hydrological model. A primary concern is that

the hydrological properties of the individual structures taken into account in the model are not correctly calibrated. Rhén et al. (1997) have estimated the essential hydraulic properties of the structures used in this study. However, within the margins given there, considerable possibilities are left to vary the structural properties. For example, in this study several functional depth relations were assumed (Fig. 3.2 and Eqs. 3.1–3.4). Particularly, the reluctantly arising saline water (Fig. 6.1) gives an impression that the pathways upward from depth should be more efficient. Also, more considerations should be given to the structural relations. Especially, in the case of the control point KAS03 a question arises whether all the structural connections are correct in the present model. Finally, the question whether the open tunnel effect is taken into account correctly should be brought forward. For example, the response simulated in KAS07 is essentially a result of the modelled properties of the fracture zone NE-1 and how the open tunnel modifies the hydraulic conditions in NE-1.

There is also a conceptual problem in the hydrological simulation process itself. The mixing fractions for each reference water type have to be calculated in separate independent runs. As a consequence the initial results collected and summed up for a certain sample do not necessarily add up to 100 % but frequently to some figure over 100 %. This problem was tried to control mainly by adjusting the dispersion lengths (Kattilakoski, 1999) and ultimately recalculating the initial mixing fractions to 100 % as presented in Appendix B. In all, however, this problem is basically related to the hydrological properties of the structures that were noted already above as a primary concern.

As a conclusion it can be said that the attempt to associate geochemical estimation results into hydrological simulations is a challenging task. The geochemical modelling tools are sensitive instruments that sum up information from the behaviour of several analysed chemical components. If this extracted information contains conservative parameters such as mixing fractions, the geochemical modelling then actually produces natural tracers for the hydrological simulations. In fact, this chain of reasoning proposes the Äspö open tunnel condition as an areal tracer and interference test laboratory. The hydrological simulations and geochemical estimations could be used together to adjust the Äspö structural model and the hydraulic properties of the individual structures.

6.3 Evaluation of geochemical estimation results

In addition to hydrological-structural considerations, certain geochemical aspects need attention as well. The geochemical calculations utilised here are results of iterative calculation processes (c.f. Luukkonen, 2000). Calculations are done in small steps (from a sample to another) presuming that the steady-state assumption of chemical reactions is valid, i.e. the mixing driven geochemical mole-transfer reactions have enough time to react.

However, the calculated mixing fractions for analysed samples in the moderate depths (200 m–600 m) are inevitably results of several calculation steps and the error limits get wider during each step in the calculation chain. In the current hydrological simulations the expansion of the error limits has an effect especially on the assumed geochemical boundaries presented in Figure 3.5. The distributions of the Litorina, altered and saline reference water types proposed for the moderate depth interval must be considered as approximations. The original undisturbed data behind these diagrams (Fig. 3.5) contains uncertainties especially in the altered reference type fraction estimations (c.f. Luukkonen, 2000). This uncertainty is further reflected to the disturbed hydrological simulations. In the case of the disturbed calibration section control points (Table 5.1) both the geochemical estimations and the hydrological simulations of mixing fractions have the same undisturbed data in the background. Therefore, there is no simple way to estimate the uncertainties. However, since the geochemical uncertainties for the estimations and simulations stem from the same source, it is probable that the uncertainties at least partially compensate each other.

Considering further the possible uncertainties related to the proposed undisturbed geochemical boundaries, it has to be pointed out certain deficiencies in the background data of the diagrams presented in Figure 3.5. In the delivered data, there were no undisturbed samples available from the areas below the present Baltic Sea. These data would support the depth distribution interpretations of the reference water types below the sea areas, now done solely with bedrock groundwater data below the dry land areas. In the delivered undisturbed data there are also certain analytical insufficiencies. The reported Br values in the data have been proven to be imprecise (e.g. Banwart et al., 1995), and mostly useless in geochemical calculations. However, Br would be an important parameter in the error limit reduction attempts (Luukkonen, 2000). As well, the addition of carbon and sulphur isotopic values into the data would increase significantly the reliability of the geochemical modelling results.

In the view of geochemical-structural considerations Figure 6.2 shows an example how the mixing fractions of the estimated undisturbed samples distribute in the single fracture zone NE-2. Figure 6.2 proposes that the fracture zone NE-2 can be divided at least into two vertical parts. In the southwestern part of the fracture zone undisturbed samples (HAS05/-56.3 m, KAS02/-307.7 m, KAS02/-317.2 m, KAS05/-339.5 m, KAS02/-456.2 m and KAS05/-483.0 m) seem to contain fair fractions of meteoric water. The meteoric fraction decreases as a function of depth while at the same time the saline fraction in these samples increases. The two samples (KAS12/-276.0 m and KAS06/-433.3 m) in the middle of the fracture zone NE-2, however, exhibit a completely different character. The samples seem to lack the meteoric fraction completely. The fractions of altered water types are high and the fractions of glacial melt seem to diminish as a function of depth. It seems clear that the crosscutting structure NNW-2 has fed the sample locations with altered water having a distinct postglacial seawater affinity.

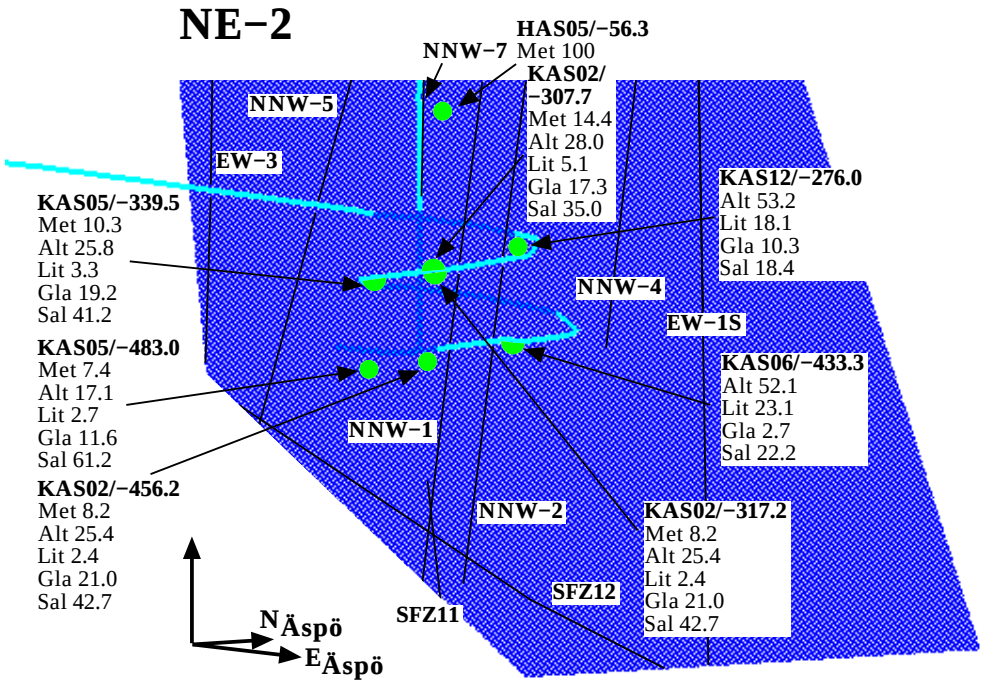

Figure 6.2. Undisturbed condition in the fracture zone NE-2 according to geochemical estimations for samples indicated.

Figure 6.2 emphasises the importance of correct structural connections in the structural model as already pointed out in the hydrological-structural considerations in the former chapter. Figure 6.2 hints also that clear hydrological heterogeneities affecting a fracture zone should be taken into account while modelling and calibrating the properties of the fracture zone. The situation presented in Figure 6.2 describes the fracture zone NE-2 in the undisturbed condition. There are, however, plenty of data (from the presented sampling points, Fig. 6.2) in the delivered dataset, while the fracture zone gradually turns into the disturbed condition. Evidently, if hydrological studies are concentrated, for example, into this single fracture zone, and simulations are gradually calibrated in space and time to geochemical estimations, the results should give good hydrological spatial averages for the fracture zone.

7 CONCLUSIONS

The difficulties related to the calibration points can be roughly divided to problems close to the surface and at depth. Adjusting the surface boundary conditions and the transmissivities suitably usually solved the shallow problems. The adjustments of the node types were generally entitled because of the coarseness of the model and the re-estimations of the transmissivity values usually by lack of measurement values. At depth, the simulations exhibit either a systematically growing difference to the geochemically estimated values, or hint to an exaggerated stiffness of the hydrological model. These difficulties raised three principal questions: "are the hydrological/structural properties of the fracture zones correctly estimated at depth, are the structural relations between the fracture zones correctly defined, and is the open tunnel effect taken correctly into account in the hydrological model?"

The confidence of the simulation results for the prediction points is not considered high. The primary reason is the amount of calibration points. Only eight calibration points with time-series data were used for the model calibrations. In four deep points the calibrations were not successful.

Large volumes of the model are assumed to behave homogeneously or according to harmonic functions of depth. There are several fracture zones and hydraulic conductor domains that are not monitored during the simulations. Therefore, the current approach presented here must be considered more as a feasibility study of the coupling of geochemical inverse-modelling estimations and areal hydrological simulations. The results show that the method is feasible, though there are couple aspects in the method demanding further refinement.

Methodological uncertainties are related to the hydrological transport of conservative mixing proportions and to the geochemical estimation of these proportions. At present the distribution of each reference water type within the model has to be simulated in a separate run. Consequently, the separate simulations do not necessarily add up to 100 %. In view of the geochemical estimations as well, the uncertainties can be addressed mostly to calculation technical facts and deficient analytical data. The amount of available (chemically analysed) conservative parameters has a very large effect to the precision and confidence of the geochemical estimations. In all, the geochemical inverse-modelling approach is a sensitive tool if correctly used, and with favourable amount of data it produces truly conservative parameters (mixing proportions) that can be used as natural tracers.

The hydrological simulations on the aerial scale are difficult tasks. There are several traps and sources of uncertainties. Nevertheless, the Äspö site with extensive data sets from both undisturbed and disturbed conditions is an exceptional target for these studies. As pointed out in the discussion, there are plenty of unstudied geochemical data within the delivered dataset. The open tunnel condition, causing considerable drawdown on a scale beyond

any formal interference tests, gives possibilities to simulate and fit spatial hydrological properties and relations of fracture zones in the geological site model.

Inevitably, the iterative hydrological simulations, even if they are concentrated in single fracture zones at a time, are laborious. It is apparent that the fracture zones of the Äspö site have spatial properties that cannot be bypassed only with simple generalisations. Furthermore, in the case of an aerial conductive fracture zone, the physical dimensions of rock mechanically weak and the hydrologically conductive zone are frequently considered equal, though almost without exception the former has clearly larger dimensions than the latter. Usually, this happens simply because only the mechanically weak zone can be measured during the geological mapping.

In the case of need of geochemical transport modelling, the present exercise encourages more than suppresses similar exercises in the future. At current stage, the results propose a method for confirming structural relations, and for refining spatial hydrological and structural averages for the fracture zones.

REFERENCES

S Banwart, M Laaksoharju, E Gustafsson, P Pitkänen, M Snellman, O Landström, I Aggeryd, L Mathiasson & B Sundblad, 1995. The Hydrochemistry of Conservative Natural Tracers. In: (S Banwart, ed.) The Redox Experiment in Block Scale. Swedish Nuclear Fuel and Waste Management Co. (SKB), Stockholm. Progress Report 25-95-06, 3-47…3-80.

J Bear, 1979. Hydraulics of Groundwater. McGraw-Hill, Israel.

A N Brooks and T J R Hughes, 1992. Streamline Upwind/Petrov-Galerkin Formulations for Convection Dominated Flows with Particular Emphasis on the Incompressible Navier-Stokes Equations. Computer Methods in Applied Mechanics and Engineering, 32, pp. 199-259.

T Forsmark and I Rhén, 1994. SKB - ÄSPÖ HARD ROCK LABORATORY. Information for Numerical Modelling 1994. PR-25-94-16.

I Gurban, M Laaksoharju and C Andersson, 1998. Influences of the Tunnel Construction on the Groundwater Chemistry at Äspö. Hydrochemical Initial and Boundary Conditions: WP D1, WP D2. Part 2. Äspö Hard Rock Laboratory, IPR-02-59. (in press)

P S Huyakorn, B H Lester and J W Mercer, 1983. An Efficient Finite Element Technique for Modelling Transport in Fractured Porous Media, 1, Single Species Transport. Water Resources Research, vol. 19, no. 3, pp. 841-854.

P S Huyakorn and G F Pinder, 1983. Computational Methods in Subsurface Flow. Academic Press INC, Orlando.

E Kattilakoski, 1999. Task 5 — Mixing Proportions of Brine, Glacial, Meteoric and Baltic Sea Waters in the Äspö Tunnel. In Part II (this volume) IPR-02-41.

M Laitinen, 1994. Developing an Iterative Solver for the FEFLOW Package. VTT Energy, Espoo. Technical Report, POHJA-2/94. (in Finnish)

M Laitinen, 1995. Modelling Convection Dominated Transport Problems with Improved Galerkin Finite Element Formulations. Technical Research Centre of Finland, Espoo. VTT Julkaisuja - Publikationer 804. (in Finnish)

D R Lide (ed.), 1990. CRC Handbook of Chemistry and Physics. 71st Edition 1990-1991. CRC Press Inc., Boston.

M Laaksoharju and B Wallin (eds.), 1997. Evolution of the Groundwater Chemistry at the Äspö Hard Rock Laboratory. Proceedings of the Second Äspö International Geochemistry Workshop, June 6-7, 1995. Swedish Nuclear Fuel and Waste Management Co. (SKB), Stockholm. International Cooperation Report 97-04.

A Luukkonen, 2000. Groundwater Mixing and Geochemical Reactions – An Inverse Modelling Approach. In Part III (this volume). Stockholm. IPR-02-41.

J Löfman, 1996. Groundwater Flow Modelling at the Olkiluoto Site. Flow under Natural Conditions. Posiva Oy, Helsinki. Work report PATU-96-76e.

J Löfman and V Taivassalo, 1995. Simulations of Pressure and Salinity Fields at Äspö. SKB ICR 95-01.

G de Marsily, 1986. Quantitative Hydrogeology — Groundwater Hydrology for Engineers. Academic Press INC, Orlando.

F Mészáros, 1996. Simulation of the Transient Hydraulic Effect of the Access Tunnel at Äspö. Äspö International Cooperation Report ICR 96-06.

P Pitkänen, A Luukkonen, P Ruotsalainen, H Leino-Forsman and UVuorinen, 1999. Geochemical Modelling of Groundwater Evolution and Residence Time at the Olkiluoto Site. Posiva Oy, Report POSIVA 98-10, Helsinki. 184 p.

I Rhén (ed.), G Gustafson, R Stanfors and P Wikberg, 1997. ÄSPÖ HRL — Geoscientific Evaluation 1997/5. Models Based on Site Characterization 1986-1995. SKB TR 97-06.

I Rhén, J Smellie and P Wikberg, 1998. Äspö HRL Task Force on Modelling of Groundwater Flow and Transport of Solutes. Task 5, Performance Measures, Version 1. November 1998.

U Svensson, 1997. A Site Scale Analysis of Groundwater Flow and Salinity Distribution in the Äspö Area. SKB TR 97-17.

V Taivassalo and A Saarenheimo, 1991. Groundwater Flow Analysis for the VLJ Repository. Nuclear Waste Commission of Finnish Power Companies, Helsinki. YJT-91-10.

M Valkiainen, 1992. Diffusion in the Rock Matrix — A Review of Laboratory Tests and Field Studies. Nuclear Waste Commission of Finnish Power Companies, Helsinki. YJT-92-04.

T Vieno, A Hautojärvi, L Koskinen and H Nordman, 1992. TVO-92 Safety Analysis of Spent Fuel Disposal. Nuclear Waste Commission of Finnish Power Companies, Helsinki. YJT-92-33E.

P Wikberg, 1998. Äspö Task Force on Modelling of Groundwater Flow and Transport of Solutes. Plan for Modelling Task # 5: Impact of the Tunnel Construction on the Groundwater System at Äspö, a Hydrological-Hydrochemical Model Assessment Exercise. Äspö Hard Rock Laboratory Progress Report HRL-98-07.

EW-1N

-3570.0	2545.0	0.0
-480.0	5285.0	0.0
-480.0	5285.0	-1600.0
-3570.0	2545.0	-1600.0
-480.0	5285.0	0.0
905.0	6525.0	0.0
905.0	6525.0	-1600.0
-480.0	5285.0	-1600.0
905.0	6525.0	0.0
1215.0	6950.0	0.0
1215.0	6950.0	-1600.0
905.0	6525.0	-1600.0
1215.0	6950.0	0.0
1614.4	7359.1	-327.4
1614.4	7359.1	-1600.0
1215.0	6950.0	-1600.0
1215.0	6950.0	0.0
1614.4	7359.1	-327.4
1811.5	7482.0	0.0
1215.0	6950.0	0.0
1811.5	7482.0	0.0
2197.1	7698.3	0.0
2000.0	7575.4	-327.4
1614.4	7359.1	-327.4
1614.4	7359.1	-327.4
2000.0	7575.4	-327.4
2000.0	7575.4	-1600.0
1614.4	7359.1	-1600.0
2000.0	7575.4	-1600.0
2000.0	7575.4	-327.4
2690.0	8080.0	0.0
2690.0	8080.0	-1600.0
2690.0	8080.0	0.0
2197.1	7698.3	0.0
2000.0	7575.4	-327.4
2690.0	8080.0	0.0

EW-1S

3006.0	8088.1	0.0
1453.1	7217.4	0.0
1031.7	6709.5	-1164.0
3428.5	8053.3	-1164.0

EW-3

2703.6	7229.1	0.0
938.8	6863.0	0.0
920.1	6751.4	-542.2
2166.5	7010.0	-542.2

EW-7

743.3	6075.7	0.0
279.4	5913.4	-231.8
3571.8	6795.9	-231.8
3590.5	6838.9	0.0

NE-2

1829.9	7038.5	0.0
2325.1	7720.0	0.0
2389.6	7671.5	-349.4
1718.4	6747.8	-349.4

NE-3

1621.3	6288.3	0.0
1290.7	6171.2	-227.6
2939.8	7123.4	-227.6
3040.3	7107.6	0.0

NE-4

1818.6	6349.8	0.0
3267.3	7064.3	0.0
3368.7	7044.4	-228.3
1905.5	6322.8	-228.3

NW-1

1257.6	7882.0	0.0
1725.7	7373.8	0.0
2091.3	7607.4	-246.6
1447.6	8306.2	-246.6

NNW-1

2033.4	7551.8	0.0
2240.6	7104.5	0.0
2374.7	6814.7	-1600.0
2161.3	7275.6	-1600.0

NNW-2

2091.2	7583.1	0.0
2300.2	7106.1	0.0
2300.2	7106.1	-319.2
2184.3	7370.7	-1144.1

NNW-3

2143.6	7025.4	0.0
2136.9	6812.9	0.0
2136.9	6812.9	-1600.0
2143.6	7025.4	-1600.0

NNW-4

2240.2	7668.4	0.0
2286.2	7609.0	-436.7
2340.9	7178.9	-436.7
2328.3	6975.0	0.0

NNW-5

1962.8	7394.1	0.0
2025.1	6348.5	0.0
2025.1	6348.5	-1600.0
1962.8	7394.1	-1600.0

NNW-6

2298.7	7058.1	0.0
2382.9	6464.0	0.0
2382.9	6464.0	-1600.0
2298.7	7058.1	-1600.0

NNW-7

1988.5	7486.7	-191.2
1957.1	7515.0	0.0
2146.8	7105.3	0.0
2180.4	7072.3	-191.5

NNW-8

1540.0	8060.0	-300.0
2030.0	7570.0	-300.0
2030.0	7570.0	-700.0
1540.0	8060.0	-700.0

SFZ01

-3190.0	13380.0	0.0
-1475.0	12910.0	0.0
-1475.0	12910.0	-1600.0
-3190.0	13380.0	-1600.0
-1475.0	12910.0	0.0
760.0	12380.0	0.0
760.0	12380.0	-1600.0
-1475.0	12910.0	-1600.0
760.0	12380.0	0.0
2620.0	12000.0	0.0
2620.0	12000.0	-1600.0
760.0	12380.0	-1600.0
2620.0	12000.0	0.0
4760.0	11620.0	0.0
4760.0	11620.0	-1600.0
2620.0	12000.0	-1600.0
4760.0	11620.0	0.0
8550.0	10950.0	0.0
8550.0	10950.0	-1600.0
4760.0	11620.0	-1600.0

SFZ02

-1095.0	14250.0	0.0
-1475.0	12910.0	0.0
-1475.0	12910.0	-1600.0
-1095.0	14250.0	-1600.0
-1475.0	12910.0	0.0
-1830.0	11760.0	0.0
-1830.0	11760.0	-1600.0
-1475.0	12910.0	-1600.0
-1830.0	11760.0	0.0
-2050.0	10640.0	0.0
-2050.0	10640.0	-1600.0
-1830.0	11760.0	-1600.0
-2050.0	10640.0	0.0
-2190.0	9760.0	0.0
-2190.0	9760.0	-1600.0
-2050.0	10640.0	-1600.0
-2190.0	9760.0	0.0
-2380.0	8905.0	0.0
-2380.0	8905.0	-1600.0
-2190.0	9760.0	-1600.0
-2380.0	8905.0	0.0
-2570.0	8310.0	0.0
-2570.0	8310.0	-1600.0
-2380.0	8905.0	-1600.0
-2570.0	8310.0	0.0
-3025.0	7285.0	0.0
-3025.0	7285.0	-1600.0
-2570.0	8310.0	-1600.0
-3025.0	7285.0	0.0
-3571.0	5335.0	0.0
-3571.0	5335.0	-1600.0
-3025.0	7285.0	-1600.0
-3571.0	5335.0	0.0
-3740.0	4690.0	0.0
-3740.0	4690.0	-1600.0
-3571.0	5335.0	-1600.0
-3740.0	4690.0	0.0
-3950.0	3620.0	0.0
-3950.0	3620.0	-1600.0
-3740.0	4690.0	-1600.0
-3950.0	3620.0	0.0
-4140.0	2640.0	0.0
-4140.0	2640.0	-1600.0
-3950.0	3620.0	-1600.0

SFZ03

-4140.0	8785.0	0.0
-2570.0	8310.0	0.0
-2570.0	8310.0	-1600.0
-4140.0	8785.0	-1600.0
-2570.0	8310.0	0.0
-1950.0	8210.0	0.0
-1950.0	8210.0	-1600.0
-2570.0	8310.0	-1600.0
-1950.0	8210.0	0.0
-1330.0	8120.0	0.0
-1330.0	8120.0	-1600.0
-1950.0	8210.0	-1600.0
-1330.0	8120.0	0.0
1120.0	8070.0	0.0
1120.0	8070.0	-1600.0
-1330.0	8120.0	-1600.0
1120.0	8070.0	0.0
1120.0	8070.0	-1600.0
2690.0	8080.0	-1600.0
2690.0	8080.0	0.0
2690.0	8080.0	0.0
3000.0	8085.0	0.0
3000.0	8085.0	-1600.0
2690.0	8080.0	-1600.0
3000.0	8085.0	0.0
3710.0	8020.0	0.0
3710.0	8020.0	-1600.0
3000.0	8085.0	-1600.0
3710.0	8020.0	0.0
5200.0	7900.0	0.0
5200.0	7900.0	-1600.0
3710.0	8020.0	-1600.0
5200.0	7900.0	0.0
5800.0	7930.0	0.0
5800.0	7930.0	-1600.0
5200.0	7900.0	-1600.0
5800.0	7930.0	0.0
8330.0	8000.0	0.0
8330.0	8000.0	-1600.0
5800.0	7930.0	-1600.0

SFZ04

-5240.0	3520.0	0.0
-3740.0	4690.0	0.0
-3740.0	4690.0	-1600.0
-5240.0	3520.0	-1600.0
-3740.0	4690.0	0.0
-3050.0	5285.0	0.0
-3050.0	5285.0	-1600.0
-3740.0	4690.0	-1600.0

-3050.0	5285.0	0.0
-2570.0	5570.0	0.0
-2570.0	5570.0	-1600.0
-3050.0	5285.0	-1600.0
-2570.0	5570.0	0.0
-590.0	6670.0	0.0
-590.0	6670.0	-1600.0
-2570.0	5570.0	-1600.0
-590.0	6670.0	0.0
200.0	7160.0	0.0
200.0	7160.0	-1600.0
-590.0	6670.0	-1600.0
200.0	7160.0	0.0
1095.0	7860.0	0.0
1095.0	7860.0	-1600.0
200.0	7160.0	-1600.0

SFZ05

-5310.0	2880.0	0.0
-1000.0	5140.0	0.0
-754.1	4651.1	-1503.5
-5048.5	2399.3	-1503.5
-1000.0	5140.0	0.0
-754.1	4651.1	-1503.5
2316.6	5474.2	-1503.5
2165.0	6000.0	0.0
2165.0	6000.0	0.0
2316.6	5474.2	-1503.5
3800.8	6340.3	-1503.5
3520.0	6810.0	0.0
3520.0	6810.0	0.0
3800.8	6340.3	-1503.5
7133.0	7974.4	-1503.5
5800.0	7930.0	0.0

SFZ06

-1950.0	8210.0	0.0
-760.0	8830.0	0.0
-760.0	8830.0	-1600.0
-1950.0	8210.0	-1600.0
-760.0	8830.0	0.0
-50.0	9140.0	0.0
-50.0	9140.0	-1600.0
-760.0	8830.0	-1600.0
-50.0	9140.0	0.0
715.0	9360.0	0.0
715.0	9360.0	-1600.0
-50.0	9140.0	-1600.0
715.0	9360.0	0.0
2285.0	9450.0	0.0
2285.0	9450.0	-1600.0
715.0	9360.0	-1600.0
2285.0	9450.0	0.0
4285.0	9740.0	0.0
4285.0	9740.0	-1600.0
2285.0	9450.0	-1600.0
4285.0	9740.0	0.0
5595.0	9920.0	0.0
5595.0	9920.0	-1600.0
4285.0	9740.0	-1600.0

5595.0	9920.0	0.0
8330.0	10230.0	0.0
8330.0	10230.0	-1600.0
5595.0	9920.0	-1600.0

SFZ08

-70.0	3095.0	0.0
2380.0	2260.0	0.0
2380.0	2260.0	-1600.0
-70.0	3095.0	-1600.0
2380.0	2260.0	0.0
2785.0	2190.0	0.0
2785.0	2190.0	-1600.0
2380.0	2260.0	-1600.0
2785.0	2190.0	0.0
6545.0	1240.0	0.0
6545.0	1240.0	-1600.0
2785.0	2190.0	-1600.0

SFZ09

1165.0	1570.0	0.0
2380.0	2260.0	0.0
2380.0	2260.0	-1600.0
1165.0	1570.0	-1600.0
2380.0	2260.0	0.0
2810.0	2525.0	0.0
2810.0	2525.0	-1600.0
2380.0	2260.0	-1600.0
2810.0	2525.0	0.0
7240.0	4640.0	0.0
7240.0	4640.0	-1600.0
2810.0	2525.0	-1600.0

SFZ10

2670.0	1260.0	0.0
2785.0	2190.0	0.0
2785.0	2190.0	-1600.0
2670.0	1260.0	-1600.0
2785.0	2190.0	0.0
2810.0	2525.0	0.0
2810.0	2525.0	-1600.0
2785.0	2190.0	-1600.0
2810.0	2525.0	0.0
3550.0	7000.0	0.0
3550.0	7000.0	-1600.0
2810.0	2525.0	-1600.0
3550.0	7000.0	0.0
3710.0	8020.0	0.0
3710.0	8020.0	-1600.0
3550.0	7000.0	-1600.0
3710.0	8020.0	0.0
4285.0	9740.0	0.0
4285.0	9740.0	-1600.0
3710.0	8020.0	-1600.0
4285.0	9740.0	0.0
4760.0	11620.0	0.0
4760.0	11620.0	-1600.0
4285.0	9740.0	-1600.0
4760.0	11620.0	0.0
5050.0	13000.0	0.0
5050.0	13000.0	-1600.0
4760.0	11620.0	-1600.0

SFZ11

2512.7	7182.4	0.0
3550.0	7000.0	0.0
3550.0	7000.0	-1600.0
1665.9	7331.3	-1600.0
3550.0	7000.0	0.0
3810.0	6975.0	0.0
3810.0	6975.0	-1600.0
3550.0	7000.0	-1600.0
3810.0	6975.0	0.0
7570.0	6165.0	0.0
7570.0	6165.0	-1600.0
3810.0	6975.0	-1600.0

SFZ12

3899.5	8448.2	-1503.5
3760.2	8080.1	0.0
3367.2	8446.5	-1503.5
3899.5	8448.2	-1503.5
2420.0	7070.0	0.0
2212.8	7576.5	-1503.5
3367.2	8446.5	-1503.5
3760.2	8080.1	0.0
2212.8	7576.5	-1503.5
2420.0	7070.0	0.0
-706.0	5145.9	0.0
-992.9	5611.9	-1503.5

SFZ13

-50.0	9140.0	0.0
1230.0	8500.0	0.0
1230.0	8500.0	-1600.0
-50.0	9140.0	-1600.0
1230.0	8500.0	0.0
1120.0	8070.0	0.0
1120.0	8070.0	-1600.0
1230.0	8500.0	-1600.0

SFZ14

905.0	6525.0	0.0
1095.0	7860.0	0.0
1095.0	7860.0	-1600.0
905.0	6525.0	-1600.0
1095.0	7860.0	0.0
2670.0	8070.0	0.0
2670.0	8070.0	-1600.0
1095.0	7860.0	-1600.0
2670.0	8070.0	0.0
1230.0	8500.0	0.0
1230.0	8500.0	-1600.0
2670.0	8070.0	-1600.0

SFZ15

2285.0	9450.0	0.0
2620.0	12000.0	0.0
2620.0	12000.0	-1600.0
2285.0	9450.0	-1600.0
2620.0	12000.0	0.0
2810.0	13430.0	0.0
2810.0	13430.0	-1600.0
2620.0	12000.0	-1600.0

Control point	Date	Geochemical estimation						Hydrological simulation					
		Glacial	Litorina	Altered	Saline	Meteoric	Baltic	Glacial	Litorina	Altered	Saline	Meteoric	Baltic
KR0012B	19.Jun.91	24.7	2.2	16.7	1.3	55.0	0.0	15.0	0.5	17.9	2.3	62.0	2.4
KR0012B	08.Apr.92	13.7	2.6	12.6	1.5	59.2	10.3	14.7	0.5	20.1	2.9	57.9	3.9
KR0012B	22.Apr.92	12.0	2.3	11.0	1.3	62.7	10.7	14.7	0.5	20.1	2.9	57.9	3.9
KR0012B	06.May.92	10.9	2.1	10.0	1.2	63.6	12.2	14.7	0.5	20.1	2.9	57.9	3.9
KR0012B	20.May.92	12.6	2.4	11.6	1.4	62.8	9.2	14.8	0.6	21.3	3.2	55.2	4.8
KR0012B	03.Jun.92	16.2	3.1	14.9	1.8	64.0	0.0	14.8	0.6	21.3	3.2	55.2	4.8
KR0012B	26.Jun.92	12.2	2.3	11.2	1.4	66.6	6.3	14.8	0.6	21.3	3.2	55.2	4.8
KR0012B	08.Jul.92	11.2	2.2	10.3	1.3	68.0	7.0	14.8	0.6	21.3	3.2	55.2	4.8
KR0012B	21.Jul.92	11.4	2.2	10.5	1.3	68.3	6.3	14.8	0.6	21.3	3.2	55.2	4.8
KR0012B	06.Aug.92	11.3	2.2	10.4	1.3	70.4	4.4	14.8	0.6	21.3	3.2	55.2	4.8
KR0012B	18.Aug.92	9.7	1.9	8.9	1.1	71.3	7.1	14.8	0.6	21.3	3.2	55.2	4.8
KR0012B	03.Sep.92	11.0	2.1	10.1	1.2	70.1	5.4	14.8	0.6	21.3	3.2	55.2	4.8
KR0012B	17.Sep.92	8.4	1.6	7.7	0.9	70.4	10.9	14.9	0.6	21.7	3.3	54.5	5.0
KR0012B	30.Sep.92	8.4	1.6	7.7	0.9	71.1	10.3	14.9	0.6	21.7	3.3	54.5	5.0
KR0012B	12.Oct.92	8.1	1.6	7.5	0.9	71.4	10.5	14.9	0.6	21.7	3.3	54.5	5.0
KR0012B	28.Oct.92	8.3	1.6	7.7	0.9	72.2	9.3	14.9	0.6	22.0	3.4	53.9	5.1
KR0012B	10.Nov.92	7.0	1.4	6.5	0.8	72.9	11.5	14.9	0.6	22.0	3.4	53.9	5.1
KR0012B	24.Nov.92	7.3	1.4	6.7	0.8	74.7	9.1	14.9	0.6	22.0	3.4	53.9	5.1
KR0012B	02.Dec.92	7.2	1.4	6.6	0.8	74.9	9.2	14.9	0.6	22.0	3.4	53.9	5.1
KR0012B	10.Dec.92	1.4	0.3	1.3	0.2	77.4	19.5	14.9	0.6	22.0	3.4	53.9	5.1
KR0012B	21.Dec.92	6.4	1.2	5.8	0.7	75.5	10.4	14.9	0.6	22.0	3.4	53.9	5.1
KR0012B	04.Jan.93	6.7	1.3	6.2	0.8	76.8	8.2	14.9	0.7	22.4	3.4	53.0	5.6
KR0012B	19.Jan.93	6.7	1.3	6.1	0.7	76.7	8.5	14.9	0.7	22.4	3.4	53.0	5.6
KR0012B	07.Feb.93	6.7	1.3	6.1	0.7	76.4	8.8	14.9	0.7	22.4	3.4	53.0	5.6
KR0012B	17.Mar.93	6.0	1.2	5.5	0.7	78.1	8.6	14.9	0.7	22.4	3.4	53.0	5.6
KR0012B	24.Mar.93	5.8	1.1	5.3	0.6	77.7	9.5	14.9	0.7	22.4	3.4	53.0	5.6
KR0012B	16.May.93	6.1	1.2	5.6	0.7	81.4	5.0	15.0	0.7	22.8	3.5	52.2	5.8
KR0012B	11.Jun.93	6.4	1.2	5.9	0.7	81.1	4.7	15.0	0.7	22.8	3.5	52.2	5.8
KR0012B	05.Jul.93	4.1	0.8	3.8	0.5	84.1	6.7	15.0	0.7	22.8	3.5	52.2	5.8
KR0012B	16.Aug.93	2.6	0.5	2.3	0.3	84.1	10.2	15.0	0.7	22.8	3.5	52.2	5.8
KR0012B	08.Nov.93	2.1	0.4	1.9	0.2	85.8	9.6	15.0	0.7	23.2	3.7	51.3	6.2
KR0012B	10.Aug.94	1.9	0.4	1.7	0.2	88.7	7.1	14.9	0.8	23.6	3.7	50.5	6.6
KR0012B	05.Sep.94	1.8	0.4	1.7	0.2	88.1	7.9	14.9	0.8	23.6	3.7	50.5	6.6
KR0012B	18.May.95	0.0	0.0	0.0	0.0	85.3	14.7	14.7	0.8	23.7	3.8	50.3	6.8
KR0012B	10.Oct.95	2.8	0.5	2.5	0.3	83.2	10.7	14.6	0.8	23.7	3.9	50.1	7.0
KR0012B	21.May.96	4.5	0.9	4.1	0.5	87.8	2.2	14.6	0.8	23.7	3.9	50.1	7.0
SA0813B	06.Nov.91	2.6	14.0	34.5	8.4	1.7	38.7	4.3	0.5	8.7	1.9	17.1	67.5

Control point	Date	Geochemical estimation						Hydrological simulation					
		Glacial	Litorina	Altered	Saline	Meteoric	Baltic	Glacial	Litorina	Altered	Saline	Meteoric	Baltic
SA0813B	07.Feb.93	0.6	4.1	9.9	2.0	21.0	62.5	1.7	0.3	5.0	1.0	17.9	74.1
SA0813B	07.Sep.93	0.3	3.0	7.1	1.7	13.7	74.3	1.2	0.2	4.4	0.8	18.0	75.5
SA0813B	29.Sep.93	0.4	4.5	10.9	2.6	22.5	59.1	1.2	0.2	4.4	0.8	18.0	75.5
SA0813B	07.Jun.94	0.3	3.1	7.5	1.8	19.2	68.0	0.9	0.2	4.2	0.6	18.0	76.2
SA0813B	05.Sep.94	0.0	0.0	0.0	0.0	17.2	82.9	0.8	0.2	4.1	0.6	18.0	76.3
SA0813B	17.May.95	0.3	3.5	8.5	2.0	27.3	58.3	0.8	0.1	4.0	0.5	18.0	76.7
SA0813B	12.Oct.95	0.2	2.0	4.9	1.2	23.4	68.4	0.7	0.1	3.9	0.5	18.0	76.8
SA0813B	21.May.96	0.1	0.9	2.3	0.6	16.0	80.1	0.6	0.1	3.9	0.4	18.0	77.0
SA0850B	20.Aug.91	7.2	7.9	70.6	6.0	8.3	0.0	18.7	1.0	32.1	5.0	6.6	36.6
SA1229A	24.Aug.93	0.7	7.8	18.9	4.5	0.0	68.1	6.9	1.1	6.4	7.6	15.6	62.4
SA1229A	07.Jun.94	4.3	5.8	15.8	4.2	4.8	65.1	5.4	0.8	5.1	6.7	15.3	66.6
SA1229A	18.May.95	5.0	4.0	11.9	3.3	6.0	69.8	4.1	0.6	3.9	5.2	15.1	71.2
SA1229A	11.Oct.95	5.2	2.4	8.1	2.4	6.4	75.6	3.7	0.6	3.6	4.9	15.0	72.2
SA1229A	21.May.96	0.5	0.2	0.7	0.2	0.6	97.8	3.4	0.5	3.3	4.6	14.9	73.2
SA1327B	15.Oct.92	5.2	6.5	17.9	4.7	5.9	59.7	15.4	2.3	13.0	10.1	21.5	37.7
SA2074A	05.Feb.93	0.0	0.0	0.0	0.0	0.0	0.0	26.5	5.7	18.3	19.4	17.7	12.3
SA2074A	28.Sep.93	9.7	12.4	34.3	7.3	9.9	26.5	19.8	3.7	15.0	16.4	13.7	31.4
SA2074A	07.Jun.94	10.1	9.5	27.7	6.1	10.9	35.8	14.4	2.5	11.1	12.9	11.1	48.0
SA2074A	06.Sep.94	11.1	8.6	26.1	5.8	12.4	35.9	13.0	2.2	10.1	12.1	10.4	52.1
SA2074A	18.May.95	10.9	4.7	16.6	4.0	12.8	51.1	10.9	1.7	8.3	10.9	9.6	58.6
SA2783A	14.Feb.94	16.8	4.7	20.8	53.6	4.1	0.0	24.8	3.9	16.0	38.8	14.1	2.3
SA2783A	17.May.94	15.8	4.7	20.3	55.9	3.4	0.0	23.8	3.6	15.6	40.3	13.6	3.2
SA2783A	07.Sep.94	13.3	5.6	21.5	58.2	1.5	0.0	23.3	3.5	15.6	39.3	13.9	4.4
SA2783A	25.Oct.95	1.6	2.2	6.0	90.2	0.0	0.0	21.0	3.0	14.8	38.5	13.7	9.0
SA2783A	20.May.96	1.1	1.5	4.3	93.0	0.0	0.0	20.1	2.8	14.4	38.3	13.5	10.9
KA1755A	12.Oct.95	10.2	1.3	8.7	76.2	3.6	0.0	20.4	3.1	14.5	29.0	18.8	14.3
KA1755A	21.May.96	5.3	0.7	4.5	87.7	1.9	0.0	19.4	2.9	13.9	29.1	18.3	16.5
KAS07	31.Aug.92	26.3	5.2	28.0	40.4	0.0	0.0	26.0	4.5	18.4	38.7	7.6	4.7
KAS07	06.Sep.93	19.0	7.5	28.4	39.9	5.2	0.0	22.3	3.6	16.7	35.8	8.5	13.1
KAS07	12.Apr.94	23.3	7.0	30.3	39.4	0.0	0.0	21.7	3.5	16.3	35.1	8.5	14.8
KAS07	06.Sep.94	19.0	7.4	28.1	40.2	5.3	0.0	20.7	3.4	15.9	33.8	8.2	18.0
KAS03	19.Aug.92	53.1	0.2	26.7	19.9	0.0	0.0	26.8	1.8	16.8	50.1	4.5	0.0
KAS03	07.Feb.93	51.8	0.3	26.3	21.6	0.0	0.0	26.7	1.9	16.7	50.1	4.6	0.0
KAS03	16.May.93	46.4	0.8	30.1	22.6	0.0	0.0	26.6	2.1	16.7	50.0	4.7	0.0
KAS03	16.Aug.93	38.3	0.7	24.7	36.4	0.0	0.0	26.6	2.1	16.7	50.0	4.7	0.0
KAS03	07.Sep.93	44.7	0.8	29.0	25.6	0.0	0.0	26.4	2.2	16.7	49.8	4.9	0.0
KAS03	12.Apr.94	39.4	0.7	25.4	34.4	0.0	0.0	26.3	2.3	16.7	49.6	5.1	0.0
KAS03	03.Sep.88	30.6	0.6	19.6	49.2	0.0	0.0	23.9	0.5	15.8	56.8	3.0	0.0

Control Point	Date	Simulated proportion						Estimated chemical composition											Charge balance		
		Glacial (%)	Litorina (%)	Altered (%)	Saline (%)	Meteoric (%)	Baltic (%)	pH -	Na (mg/l)	K (mg/l)	Ca (mg/l)	Mg (mg/l)	Alk. (mg/l)	Cl (mg/l)	SO_4 (mg/l)	Si (mg/l)	Fe (mg/l)	^{18}O (‰)	Σ(Cat) (meq/l)	Σ(An) (meq/l)	E.N. (%)
KA3005A	01.Oct.90	28.0	9.0	17.7	34.8	10.6	0.0	7.3	1725	17.6	1655	84	82	5590	359	3.0	0.6	-12.7	165.1	-166.5	**-0.4**
KA3005A	21.May.91	28.0	8.9	17.7	34.7	10.6	0.0	7.3	1722	17.5	1654	84	83	5583	358	3.0	0.6	-12.7	164.8	-166.3	**-0.4**
KA3005A	10.Feb.92	28.0	8.9	17.7	34.7	10.6	0.0	7.3	1722	17.5	1654	84	83	5583	358	3.0	0.6	-12.7	164.8	-166.3	**-0.4**
KA3005A	10.Aug.92	28.0	8.9	17.7	34.6	10.7	0.0	7.3	1719	17.5	1650	84	83	5571	357	3.0	0.6	-12.7	164.5	-165.9	**-0.4**
KA3005A	05.Oct.92	28.1	8.9	17.8	34.6	10.7	0.0	7.3	1718	17.4	1647	84	83	5564	357	3.0	0.6	-12.7	164.3	-165.7	**-0.4**
KA3005A	10.Nov.92	28.1	8.8	17.8	34.5	10.7	0.0	7.3	1714	17.3	1646	84	83	5556	356	3.0	0.6	-12.8	164.0	-165.5	**-0.4**
KA3005A	11.Feb.93	27.6	7.1	17.8	30.0	14.0	3.5	7.3	1588	17.4	1447	82	96	5014	330	3.0	0.6	-12.5	148.5	-149.9	**-0.5**
KA3005A	03.Jun.93	25.6	6.0	17.2	27.4	13.7	10.2	7.3	1582	20.4	1334	90	98	4833	334	2.8	0.6	-12.1	143.3	-144.9	**-0.6**
KA3005A	03.Nov.93	23.6	5.0	16.4	25.7	13.3	16.0	7.3	1590	23.2	1258	97	99	4736	342	2.7	0.6	-11.7	140.5	-142.3	**-0.6**
KA3005A	16.Feb.94	24.0	4.7	16.7	25.3	15.8	13.6	7.3	1529	21.0	1241	90	107	4592	327	2.8	0.6	-11.9	136.4	-138.1	**-0.6**
KA3005A	16.Jun.94	23.9	4.5	16.9	25.3	16.7	12.8	7.3	1513	20.2	1241	88	109	4561	322	2.9	0.6	-11.9	135.5	-137.2	**-0.6**
KA3005A	16.Sep.94	23.4	4.3	16.8	24.9	17.0	13.6	7.4	1509	20.6	1223	88	111	4525	322	2.9	0.6	-11.8	134.5	-136.2	**-0.6**
KA3005A	24.Jan.95	22.6	4.1	16.6	24.4	17.0	15.3	7.4	1516	21.5	1201	91	112	4504	326	2.8	0.6	-11.7	133.9	-135.6	**-0.7**
KA3005A	26.May.95	22.0	3.9	16.3	24.0	16.9	17.0	7.4	1523	22.4	1184	93	112	4491	329	2.8	0.6	-11.6	133.5	-135.4	**-0.7**
KA3005A	25.Oct.95	21.1	3.7	15.9	23.6	16.6	19.0	7.4	1535	23.5	1166	96	112	4488	334	2.7	0.6	-11.4	133.5	-135.4	**-0.7**
KA3005A	24.Apr.96	20.3	3.5	15.5	23.2	16.3	21.2	7.4	1548	24.7	1148	99	111	4485	339	2.7	0.6	-11.3	133.4	-135.4	**-0.8**
KA3005A	24.Dec.96	19.3	3.3	14.9	22.8	15.9	23.8	7.4	1566	26.2	1127	103	111	4489	347	2.6	0.6	-11.1	133.5	-135.7	**-0.8**
KA3110A	01.Oct.90	28.1	8.2	17.6	36.4	9.6	0.0	7.3	1742	16.5	1725	81	78	5737	363	3.0	0.5	-12.8	169.0	-170.7	**-0.5**
KA3110A	21.May.91	28.1	8.2	17.6	36.4	9.7	0.0	7.3	1741	16.5	1723	81	79	5731	362	3.0	0.5	-12.8	168.8	-170.5	**-0.5**
KA3110A	10.Feb.92	28.2	8.2	17.6	36.3	9.7	0.0	7.3	1738	16.5	1718	81	79	5718	362	3.0	0.5	-12.8	168.5	-170.1	**-0.5**
KA3110A	10.Aug.92	28.2	8.2	17.7	36.0	9.9	0.0	7.3	1731	16.5	1706	81	80	5685	360	3.0	0.5	-12.8	167.6	-169.2	**-0.5**
KA3110A	05.Oct.92	28.2	8.2	17.8	35.8	9.9	0.1	7.3	1729	16.6	1699	81	80	5670	359	3.0	0.5	-12.8	167.1	-168.7	**-0.5**
KA3110A	10.Nov.92	28.2	8.2	17.8	35.6	10.0	0.1	7.3	1725	16.6	1692	81	80	5651	358	3.0	0.6	-12.8	166.6	-168.2	**-0.5**
KA3110A	11.Feb.93	26.3	5.9	17.7	29.0	13.0	8.1	7.3	1596	18.9	1407	86	95	4973	334	2.9	0.6	-12.3	147.2	-148.8	**-0.6**
KA3110A	03.Jun.93	22.8	4.5	16.3	25.2	12.0	19.2	7.4	1613	24.6	1237	101	97	4749	348	2.6	0.6	-11.6	140.8	-142.8	**-0.7**
KA3110A	03.Nov.93	20.1	3.7	14.7	23.2	11.1	27.2	7.4	1643	29.0	1144	112	96	4667	365	2.4	0.5	-11.1	138.5	-140.8	**-0.8**
KA3110A	16.Feb.94	21.3	3.8	15.3	24.8	12.7	22.0	7.4	1611	25.5	1216	102	99	4718	353	2.6	0.6	-11.4	139.9	-142.1	**-0.8**
KA3110A	16.Jun.94	18.8	3.2	13.8	22.1	12.3	29.9	7.4	1628	30.1	1092	114	101	4560	366	2.4	0.5	-10.8	135.5	-137.9	**-0.9**
KA3110A	16.Sep.94	17.7	3.0	13.2	20.9	12.3	32.9	7.4	1632	31.8	1040	118	102	4486	370	2.3	0.5	-10.6	133.4	-135.9	**-0.9**
KA3110A	24.Jan.95	16.7	2.7	12.4	20.0	12.1	36.1	7.5	1640	33.6	996	123	103	4435	376	2.2	0.5	-10.4	132.0	-134.6	**-1.0**
KA3110A	26.May.95	15.8	2.5	11.8	19.2	12.0	38.6	7.5	1647	35.0	961	126	103	4393	381	2.2	0.5	-10.3	130.8	-133.5	**-1.0**
KA3110A	25.Oct.95	15.0	2.4	11.2	18.7	11.9	40.9	7.5	1656	36.3	933	129	103	4370	386	2.1	0.5	-10.1	130.2	-133.0	**-1.1**
KA3110A	24.Apr.96	14.1	2.2	10.6	18.1	11.7	43.3	7.5	1667	37.7	905	133	103	4347	392	2.0	0.5	-9.9	129.6	-132.5	**-1.1**
KA3110A	24.Dec.96	13.3	2.0	10.0	17.7	11.6	45.5	7.5	1679	38.9	886	136	103	4341	398	2.0	0.4	-9.8	129.4	-132.4	**-1.1**

Control Point	Date	Simulated proportion						Estimated chemical composition											Charge balance		
		Glacial (%)	Litorina (%)	Altered (%)	Saline (%)	Meteoric (%)	Baltic (%)	pH -	Na (mg/l)	K (mg/l)	Ca (mg/l)	Mg (mg/l)	Alk. (mg/l)	Cl (mg/l)	SO_4 (mg/l)	Si (mg/l)	Fe (mg/l)	^{18}O (‰)	Σ(Cat) (meq/l)	Σ(An) (meq/l)	E.N. (%)
KA3385A	01.Oct.90	28.5	6.0	17.2	40.7	7.6	0.0	7.3	1775	13.6	1902	72	69	6089	370	3.0	0.5	-13.1	178.4	-180.6	**-0.6**
KA3385A	21.May.91	28.5	6.0	17.2	40.7	7.6	0.0	7.3	1775	13.6	1902	72	69	6089	370	3.0	0.5	-13.1	178.4	-180.6	**-0.6**
KA3385A	10.Feb.92	28.5	6.0	17.2	40.7	7.6	0.0	7.3	1775	13.6	1901	72	69	6089	370	3.0	0.5	-13.1	178.4	-180.6	**-0.6**
KA3385A	10.Aug.92	28.4	5.9	17.3	40.5	7.7	0.1	7.3	1772	13.5	1895	72	70	6073	369	3.0	0.5	-13.1	177.9	-180.1	**-0.6**
KA3385A	05.Oct.92	28.3	5.9	17.3	40.4	7.9	0.2	7.3	1770	13.6	1889	72	70	6058	369	3.0	0.5	-13.1	177.5	-179.7	**-0.6**
KA3385A	10.Nov.92	28.2	6.0	17.3	40.0	8.1	0.3	7.3	1765	13.8	1873	73	71	6025	368	3.0	0.5	-13.1	176.6	-178.8	**-0.6**
KA3385A	11.Feb.93	28.2	6.1	17.3	39.2	8.9	0.3	7.3	1744	13.8	1838	73	74	5928	363	3.1	0.5	-13.0	173.9	-176.0	**-0.6**
KA3385A	03.Jun.93	27.4	5.5	17.5	38.3	9.7	1.6	7.3	1724	14.0	1800	73	78	5833	359	3.1	0.5	-12.9	171.2	-173.3	**-0.6**
KA3385A	03.Nov.93	26.4	4.8	17.2	38.6	9.6	3.3	7.3	1736	14.3	1813	73	78	5879	364	3.0	0.5	-12.8	172.4	-174.7	**-0.7**
KA3385A	16.Feb.94	25.7	4.6	17.0	38.6	9.8	4.4	7.3	1742	14.7	1811	74	79	5887	367	3.0	0.5	-12.7	172.6	-175.0	**-0.7**
KA3385A	16.Jun.94	24.8	4.2	16.7	38.7	9.9	5.7	7.4	1752	15.1	1814	75	80	5912	371	3.0	0.5	-12.6	173.3	-175.8	**-0.7**
KA3385A	16.Sep.94	22.9	3.4	15.5	42.5	9.1	6.6	7.4	1831	14.9	1971	74	75	6309	393	3.1	0.5	-12.6	184.5	-187.4	**-0.8**
KA3385A	24.Jan.95	21.8	3.1	15.0	44.2	8.6	7.4	7.4	1874	15.0	2042	74	73	6502	405	3.1	0.5	-12.5	189.9	-193.0	**-0.8**
KA3385A	26.May.95	20.7	2.8	14.4	45.0	8.4	8.8	7.4	1901	15.5	2074	76	72	6604	413	3.1	0.5	-12.4	192.8	-196.1	**-0.8**
KA3385A	25.Oct.95	19.8	2.6	14.0	45.0	8.2	10.4	7.5	1919	16.4	2076	78	72	6642	420	3.1	0.5	-12.3	193.9	-197.3	**-0.9**
KA3385A	24.Apr.96	18.9	2.4	13.5	44.9	8.2	12.1	7.5	1934	17.4	2070	80	72	6659	426	3.0	0.4	-12.2	194.4	-197.9	**-0.9**
KA3385A	24.Dec.96	17.8	2.2	12.9	44.6	8.2	14.2	7.5	1948	18.6	2054	83	73	6661	432	3.0	0.4	-12.0	194.5	-198.1	**-0.9**

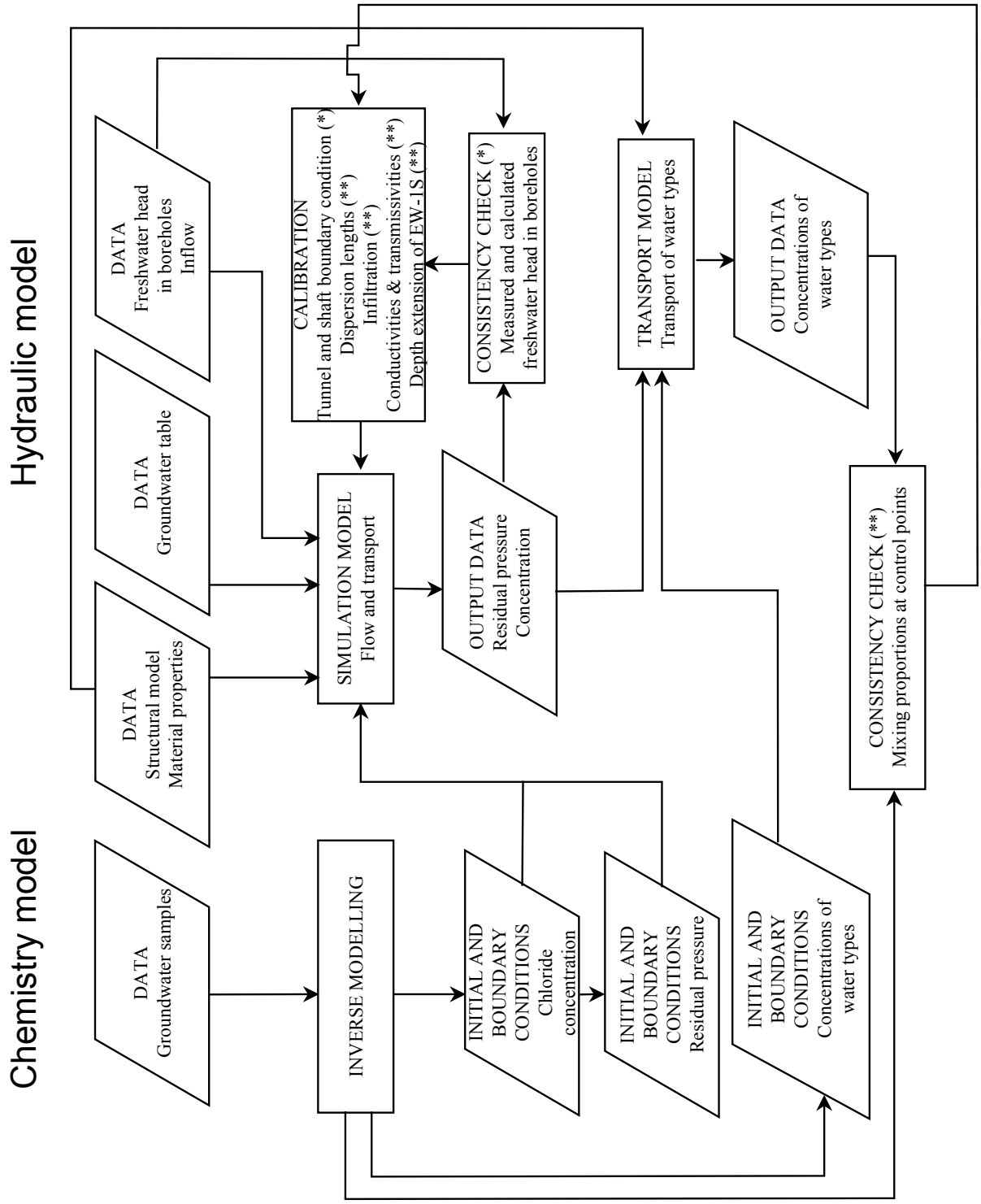
Hydraulic model
Chemistry model
DATA
Freshwater head
in boreholes
Inflow
DATA
Groundwater table
DATA
Structural model
Material properties
DATA
Groundwater samples
CALIBRATION
Tunnel and shaft boundary condition (*)
Dispersion lengths (**)
Infiltration (**)
Conductivities & transmissivities (**)
Depth extension of EW-1S (**)
SIMULATION MODEL
Flow and transport
CONSISTENCY CHECK (*)
Measured and calculated
freshwater head in boreholes
OUTPUT DATA
Residual pressure
Concentration
TRANSPORT MODEL
Transport of water types
OUTPUT DATA
Concentrations of
water types
CONSISTENCY CHECK (**)
Mixing proportions at control points
INVERSE MODELLING
INITIAL AND
BOUNDARY
CONDITIONS
Chloride
concentration
INITIAL AND
BOUNDARY
CONDITIONS
Residual pressure
INITIAL AND
BOUNDARY
CONDITIONS
Concentrations of
water types

Part V

MODELLING QUESTIONNAIRE FOR TASK #5

MODELLING QUESTIONNAIRE FOR TASK 5 (Posiva)

worked October 1999

This is a Modelling Questionnaire prepared by SKB based on discussions within the Task Force group. It should be answered when reporting Task 5 in order to simplify the evaluation process of the modelling exercise. Preferably, include this response in an appendix to your forthcoming report.

1. SCOPE AND ISSUES

a) What was the purpose for your participation in Task 5?
The purpose was to integrate the hydrodynamic model with two chemical models (M3 and inverse modelling) and to predict the conditions at Äspö.

b) What issues did you wish to address through participation in Task 5?
The comparison of two chemical models: M3 and the inverse modelling.

2. CONCEPTUAL MODEL AND DATA BASE

a) Please describe your models using the tables 1-3 in the appendix.

b) To what extent have you used the data sets delivered? Please fill in Table 4 in the appendix.

c) Specify more exactly what data in the data sets you actually used? Please fill in "Comments" in Table 4.

d) What additional data did you use if any and what assumptions were made to fill in data not provided in the Data Distributions but required by your model? Please add in the last part of Table 4.

e) Which processes are the most significant for the situation at the Äspö site during the simulation period?
Advection and hydrodynamic dispersion. Coupled flow and transport by variable density and Darcy velocity.

3. MODEL GEOMETRY/STRUCTURAL MODEL

a) How did you geometrically represent the ÄSPÖ site and its features/zones?
Fracture zones are represented as combined quadrilaterals (see Appendix A in the reports). In the finite element mesh the fracture zones are described with 2D elements and the rock between them with 3D elements.

b) Which features were considered the most significant for the understanding of flow and transport in the ÄSPÖ site, and why?
The fracture zones NNW-2 and EW-1S seem to be important as regards to the upconing of saline water.

c) Motivate selected numerical discretization in relation to used values of correlation length and/or dispersion length.
The dispersivity is somewhat high in relation to the test scale, judging from Fig. 8-31 in SKB TR 97-06, where the longitudinal dispersivity (m) versus test scale (m) is presented.

4a. MATERIAL PROPERTIES - HYDROGEOLOGY

a) How did you represent the material properties in the hydraulic units used to represent the ÄSPÖ SITE?
The material properties are given in the elements of the hydraulic units. Values are given for each fracture zone and for the site scale rock mass domains (SRD) (inverse modelling-based hydraulic simulations) and the rock mass outside them.

b) What is the basis for your assumptions regarding material properties?
Homogeneous and isotropic conductivity K and transmissivity T (SKB TR 97-06). Depth dependent transmissivity for the fracture zone EW-3 (SKB TR 97-06). Widths of the fracture zones, storage coefficients S, specific storage S_S and the fracture spacings at the surface $2a_0$ judged from SKB TR 97-06. The longitudinal (ε_L) and transversal (ε_T) dispersion lengths are adjusted in the calibration process. An assumption is made on the depth dependence of the spacing of the water-

bearing fractures based on the estimations of the size of matrix blocks: $2a = 2a_0 2^{-\frac{z}{500}}$. In the dual porosity approach the flow porosity ϕ_f is defined as the volume of fractures per unit volume of the entire rock: $\phi_f = \frac{b}{a+b}$, where experimentally $2b = 10(\frac{12\mu}{\rho_0 g} K 2a)^{1/3}$. The matrix porosity is based on the measured porosity of rock samples from the Äspö HRL (SKB TR 97-06).

In the inverse modelling-based hydrologic simulations in attempt to adjust the mixing proportions in the control points, depth dependent transmissivities were also given for the zones SFZ05, SFZ12 (including NE-1) and NNW-8. Somewhat more based on the measured transmissivities a depth dependence was also given for the transmissivities of the surface parts of the fracture zones in the land areas down to 200 metres to calibrate the mixing proportions of meteoric water in the control points.

c) Which assumptions were the most significant, and why?
The need to increase the dispersion lengths reflects the deficiencies of the model, but was appreciated to adjust the model due to lack of resources.

4b. CHEMICAL REACTIONS - HYDROCHEMISTRY

a) What chemical reactions did you include?
The geochemical mole-transfer reactions, considered in the inverse modelling, are dissolution/ precipitation of calcite, consumption of organic matter (CH_2O), dissolution of goethite, precipitation of pyrite, and in detail undefined ion exchange processes among pairs Na-Ca, Na-Mg and Na-Fe.

b) What is the basis for your assumptions regarding the chosen chemical reactions?
The inverse-modelling approach was simplified as much as possible. Only cation balances among ions Na, Ca, Mg and Fe were considered excluding potassium, i.e. dissolvable silicate phases were not considered. In respect HCO_3, it was assumed that the main processes producing bicarbonate are anaerobic oxidation of organic matter (CH_2O) and dissolution of calcite. The main process consuming bicarbonate is precipitation of calcite. Similarly, in the case of SO_4 it was assumed that sulphate dissolved into shallow groundwater is mostly directly or indirectly contributed from seawater. Sulphate is reduced and precipitated away only as pyrite, and pyrite oxidation is not considered as a source of aqueous sulphate.

c) Which reactions were the most significant, and why?
The reactions and the amounts of reactions depend on where in the model the study point is located. The modelled reactions among undisturbed, well-mixed and well-equilibrated samples in the moderate depth of the Äspö model indicate that mole-transfers are in these cases small. Frequent reactions, such as dissolution/precipitation of *calcite*, precipitation of *goethite*, and Na-Mg and Na-Fe *exchanges* are small, usually clearly less than 0.5 mmol/l in a steady-state step. In many cases, mixing of well-equilibrated samples is practically conservative.

With the reference waters used in the current inverse modelling, the large mixing proportions of *fresh* seawater in final water indicate considerable dissolution of organic matter and calcite, precipitation of pyrite, dissolution of Ca, Fe, and precipitation of Na, Mg. All reactions defined are vital. Anion balances (HCO_3^-, SO_4^{2-}) are adjusted with significant dissolution of calcite and organic matter, and precipitation of pyrite. Adjustments in anion concentrations require significant counterbalancing among cations to fulfil the electroneutrality and observed concentrations.

The question of significant reactions is strongly related to the question: how the reference water types are found and/or can be defined? In the optimum case, all reference waters have equilibrated with the currently prevailing conditions in bedrock as well as possible, and at the same time they have mixed to each other as little as possible. If it would be possible to find or define reasonable average *altered* seawater the reactions considered above would be significantly smaller.

5a. BOUNDARY CONDITIONS FOR HYDROGEOLOGICAL MODEL

a) What boundary conditions were used in the modelling of the ÄSPÖ site tests?
Salinity (M3-based simulations) or chloride (inverse modelling-based simulations) was given on the sides of the model. The residual pressure boundary condition on the vertical edges was calculated on the basis of the salinity/chloride distribution. The boundary conditions given initially in the interior nodes were released in the first time step. The residual pressure boundary condition at the bottom was also released.

Groundwater table was initially applied over the Äspö island, but was replaced by a flow rate boundary condition in the second time step, when the tunnel was modelled for the first time. The residual pressure boundary condition for the flow equation and the flow rate boundary condition for the transport equation were given in the tunnel and the shaft.

The concentration boundary condition for the transport equation of each water type was derived from the chemical model. The boundary condition given initially in the interior nodes was released in the first time step.

b) What was the basis for your assumptions regarding boundary conditions?
The salinity or chloride boundary condition was given on the basis of the corresponding chemical model. Groundwater table applied over the Äspö island had to be replaced by a flow rate boundary condition due to the tunnel excavation. The residual pressure boundary condition in the tunnel and the shaft was fixed utilising the measured freshwater head in the nearest borehole sections. The flow rate boundary condition in the tunnel and the shaft was given on the basis of the measured flow at the weirs.

c) Which assumptions were the most significant, and why?
The tunnel and shaft effect was modelled by giving the above mentioned boundary conditions in the tunnel and the shaft. Thus, the assumptions concerning these boundary conditions are very important.

5b. BOUNDARY/INITIAL CONDITIONS FOR HYDROCHEMICAL MODEL

a) What boundary conditions were used in the modelling of the ÄSPÖ site tests?
The water samples used for inverse calculations, were divided into two subsets (undisturbed and disturbed) in respect of the excavations of the Äspö tunnel system. The undisturbed sample set, were used for identification of the reference water types that have been active in the Äspö HRL volume, for describing the general evolution of water in the bedrock, and for defining the depth relations and distributions of reference water types in the undisturbed model volume.

The depth distributions of the reference water types form the initial condition for the simulation exercise. At the vertical and bottom boundaries of the model these undisturbed conditions are assumed to be valid throughout the exercise. The depth distribution of chloride (cf. item 5a-a) is calculated from the depth distributions of the reference water types. The depth distribution of chloride (i.e. density) is assumed be constant within the model volume during the exercise.

b) What was the basis for your assumptions regarding boundary conditions?
It is assumed that the Quaternary history of the Äspö area is reflected in the general evolution of water in the bedrock, and in the depth distributions of reference water types.

c) Which assumptions were the most significant, and why?
The undisturbed sample set utilised in the depth distribution estimations is collected solely from the Äspö Island, though also the reference water type distributions below the sea areas are also estimated. Furthermore, it is assumed that the undisturbed depth distributions of reference water types can present the areal model boundaries also during the disturbed part of the exercise. This is reasonable if the model boundaries remain undisturbed during the disturbed condition simulations and the detected local depth distribution can be extended to the areal scale.

The density distribution does not change during simulations. However, inverse calculations exhibit significant drawdown of meteoric and fresh seawater, and moreover considerable up welling of saline water during the disturbed conditions.

6. MODEL CALIBRATION

a) To what extent did you calibrate your model on the provided hydraulic information? (Steady state and transient hydraulic head etc.)
The residual pressure boundary condition in the tunnel and the shaft was fixed utilising the measured freshwater head in the nearest borehole sections. Groundwater table was replaced by the flow rate boundary condition, which adjusts the infiltration.

b) To what extent did you calibrate your model on the provided "transport data"? (Breakthrough curves etc.)

c) To what extent did you calibrate your model on the provided hydrochemical data? (Mixing ratios; density/salinity etc.)
The salinity or chloride boundary condition was given on the basis of the M3 modelling and the inverse modelling, respectively. The mixing ratios delivered from the chemical models were utilised to fix the concentration boundary condition for the transport equation of each water type.

d) What parameters did you vary?
Dispersion lengths, infiltration from the sea, transmissivities, the depth extension of the zone EW-1S, classification of sea and land nodes, the widths of some fracture zones. Some attempts with the specific storage S_S, the matrix porosity ϕ' and the fracture spacing $2a$ were not reported.

e) Which parameters were the most significant, and why?
The dispersion lengths, the infiltration from the sea and the transmissivities to adjust the concentration in the control points.

f) Compare the calibrated model parameters with the initial data base - comments?
The dispersion lengths were not delivered in the initial data base. In the M3-based modelling the transmissivities were taken either from Model 96 or the calibrated model, which are reported in SKB TR 97-06. However, for the zone NNW-2 the mean minus standard deviation value T=2.1e-6 m^2/s was used. Additional transmissivity modifications were made in the inverse modelling-based simulations. The depth dependencies for the transmissivities of the fracture zones NNW-8, SFZ05 and SFZ12 (including NE-1) are perhaps not fully supported by the measurements.

7. SENSITIVITY ANALYSIS

Identify the sensitivity in your model output to:

a) the discretization used
not studied

b) the transmissivity/hydraulic conductivity (distribution) used
The changing of the transmissivities of the zones NNW-2 and EW-1S tenfold resulted in a change of at most 20 percentage units in the mixing proportions. The changing of the transmissivities of the zones NNW-2 and EW-1S to one tenth resulted in a change of at most 5 percentage units in the mixing proportions.

c) transport parameters used
The mixing proportions are sensitive to the dispersion lengths. The changing of the dispersion lengths tenfold throughout the model resulted in a change of tens percentage units in the mixing proportions.

d) chemical mixing parameters used
The mixing proportions for most studied undisturbed samples are results of several inverse calculation steps, and the error limits gradually get wider during each step in the calculation chain. In the case of the disturbed calibration section control points both the geochemical estimations (calculations utilise undisturbed data) and the hydrological simulations of mixing proportions (based on undisturbed depth distributions – cf. item 5b-a) have the same undisturbed geochemical data in the background. Therefore, there is no simple way to estimate the uncertainties. However, since the geochemical uncertainties for the estimations and simulations stem from the same source, it is probable that the uncertainties at least partially compensate each other.
The precision of the mixing proportions is presented in the supplement report concentrating to geochemical modelling. The maximum deviations, based on assumed analytical uncertainty of the conservative parameters used (ΔCl = 7%, $\Delta\delta^{18}O$ = 0.1 units), are tabulated together with the given best estimates. The addition of conservative parameters to four (Cl, Br, ^{18}O, ^{2}H), without tightening the assumed uncertainties, would greatly improve the robustness of the mixing proportion results.

The deficiencies in the analytical data did not allow the usage of more than two conservative parameters as basis of mixing calculations.

e) chemical reaction parameters used
The geochemical reactions are supposed to have no role to the sensitivity of the hydrological simulations. The residual pressure boundary condition is based on the estimated conservative chloride distribution, and the mixing portions transported are conservative. The geochemical mixing portion calculations are based solely on conservative parameters, and appropriate geochemical adjustments to hydrological simulation results are made in one post-simulation reaction step.

The maximum deviations of mole-transfers related to phases (calcite, CH_2O, goethite, pyrite, NaX, CaX_2, MgX_2 and FeX_2) were calculated, based on the assumed analytical uncertainty of the chemical parameters (uncertainty for Na, Ca, Mg, Fe_{tot}, HCO_3 and SO_4 7%, and for pH 0.1 units) subject to mole-transfer reactions. The deviations are presented in the supplementary report.

8. LESSONS LEARNED

a) Given your experience in implementing and modelling the ÄSPÖ site, what changes do you recommend with regards to:

- Experimental site characterisation?
In the view of inverse modelling based estimations and simulations, distinct deviations in hydrological performance measures, as well as in estimated and simulated mixing proportion results were detected. In both cases deviations seem to start as a control point turns into the disturbed condition. These difficulties raised three principal questions: “are the hydrological/structural properties of the fracture zones correctly estimated at depth, are the structural relations between the fracture zones correctly defined, and is the open tunnel effect taken correctly into account in the hydrological model?”
- Presentation of characterisation data?
mainly good enough this way
- Performance measures and presentation formats?

b) What additional site-specific data would be required to make a more reliable prediction of the tracer experiments?
Considering the site scale model there may be a need of more accurate definition of hydrological/structural properties of the fracture zones.

c) What conclusions can be made regarding your conceptual model utilised for the exercise?
It involves a large number of somewhat uncertain parameters, also due to the dual porosity approach.

d) What additional generic research results are required to improve the ability to carry out predictive modelling of transport on the site scale?
See items 8a and b.

9. RESOLUTION OF ISSUES AND UNCERTAINTIES

a) What inferences did you make regarding the descriptive structural-hydraulic model on the site scale for the ÄSPÖ site?
The inverse modelling based simulations run into several difficulties. The main reasons were interpreted to result from the problems indicated in the item 8a. In our model also several functional hydrological depth relations were assumed for the fracture zones and were not calibrated to measured values.

In the case of an aerial conductive fracture zone, the physical dimensions of rock mechanically weak and the hydrologically conductive zone are perhaps frequently (?) considered as equal, though almost without exception the former has clearly larger dimensions than the latter. Possibly, this happens simply because only the mechanically weak zone can be measured during the geological mapping.

b) What inference did you make regarding the active hydrochemical processes, hydrochemical data provided and the hydrochemical changes calculated?
The important geochemical processes that should be taken into account in the modellings and the extent of hydrochemical changes in these processes depend strongly on the choice of the reference water types.

If the meteoric water reference composition is defined according to an average precipitation, large mole-transfers can be expected to occur during infiltration through organically active Quaternary sedimentary cover and upper parts of bedrock. Similarly, if *fresh* Baltic Sea water reference could be substituted with an *altered* Baltic Sea reference, sampled below the sea bottom sediments, significantly smaller mole-transfers could be expected than presented in the supplement geochemical report for *fresh* Baltic Sea. The choice problem in the case of saline reference is analogous to the former two reference water types and is discussed in more detail in the supplement report.

There were two significant analytical deficiencies considering the hydrochemical data. The reported Br values in the data have been proven to be imprecise, and mostly useless in geochemical calculations. However, Br would be an important parameter in the mixing-proportion error reduction attempts. As well, the addition of carbon and sulphur isotopic values into the data would increase significantly the reliability of the geochemical modelling results.

The processes related to Na, Ca, Mg and Fe were not defined in detail. More or less likely reacting phases, in addition to normal exchange processes, are montmorillonite, kaolinite and chlorite that are usual alteration products of feldspars and biotite. These mineral phases have not been included into inverse calculations because Al concentrations in the samples were not reported. Therefore, ion-exchange processes utilised must be considered as lumped approximations.

There was deficiency of undisturbed samples available for inverse-modelling calculations, basically because ^{18}O values were not available for all analysed samples. However, the amount of variables in the inverse calculations may easily increase to 15–20 (reference water types + reacting phases) and the amount of samples should clearly exceed this number. This was an important reason as well to minimise reactions considered and use lumped phases.

c) What issues did your model application resolve?
Generally in the M3-based simulations, the brine water seems to remain steady, except in the prediction section, where it is mildly increasing. The glacial water decreases, because it is a relict component in the present-day groundwater conditions. In the control point KA3385A the future condition of the glacial component seems nearly unvarying. The meteoric water generally increases. In the control points SA2783A and KA3385A it remains steady in the near future, however. The overall future condition of the Baltic water seems quite steady. These results are fairly well in line with those of the M3 model.

d) What additional issues were raised by the model application?
In the inverse modelling-based simulations the hydrological model did not yield the up-coning of saline water, which is apparent on the basis of the inverse modelling results in the control points KA1755A and SA2783A. Overall, the trends in the mixing proportions calculated in the inverse model appear more clearly than in the M3 results.

10. INTEGRATION OF THE HYDROGEOLOGICAL AND HYDROCHEMICAL MODELLING

a) How did you integrate the hydrogeological and hydrochemical work?
They were integrated by defining the salinity/chloride and the water type boundary conditions of the hydrogeological model on the basis of the hydrochemical models. In the case of inverse-modelling approach the simulated proportions are recalculated first to the “conservative chemical compositions”. These compositions are further transferred to “corrected chemical compositions” in a reaction step discussed in more detail in the geochemical supplement report.

b) How can the integration of the hydrogeological and hydrochemical work be improved?
The calibration stage should be done more carefully. More attention should be paid to the hydraulic conductivities and the transmissivities in the upper and lower parts of the model. This could result in a better fit between the calculated and “measured” mixing proportions.

In the view of inverse-modelling results, more careful definition of undisturbed condition and considerable increase of control points with time-series data would give tools for confirming structural relations, and for refining spatial hydrological and structural averages for the fracture zones.

c) Hydrogeologist: How has the hydrochemistry contributed to your understanding of the hydrogeology around the Äspö site?
   It has raised questions upon the needs and usability of hydrogeological data and thus increased the understanding of the hydrogeology around the Äspö site.
d) Hydrochemist: How has the hydrogeology contributed to your understanding of the hydrochemistry around the Äspö site?
   Off-focusing the detailed geochemical modelling may produce, coupled with hydrological simulations, interpretations and generalisations that may have a role in refining the site scale structural-hydrological model.

Table 1 Description of model for water flow calculations

TOPIC	Example	Our Model
Type of model	Stochastic continuum model	Porous medium, dual porosity
Process description	Darcy´s flow including density driven flow. (Transport equation for salinity is used for calculation of the density)	Advection, dispersion, molecular and matrix diffusion Coupled flow and transport by density and Darcy velocity
Geometric framework and parameters	Model size: 1.8x1.8x1 km^3 . Deterministic features: All deterministic features provided in the data set. Rock outside the deterministic features modelled as stochastic continuum.	Model size: cross-section hexahedron with diameter about 3.3 km, depth 1.5 km Fracture zones provided in SKB TR 97-06 Rock between the fracture zones Both the fracture zones and the rock between them modelled as dual porosity medium
Material properties and hydrological properties	Deterministic features: Transmissivity (T), Storativity (S) Rock outside deterministic features: Hydraulic conductivity(K), Specific storage (Ss)	Fracture zones: Transmissivity (T), widths (w), storage coefficients (S), total porosity (ϕ) as sum of kinematic porosity (ϕ_f) and diffusion porosity (ϕ_d) Rock between the fracture zones: Hydraulic conductivity (K), specific storage (S_S), total porosity (ϕ) as sum of kinematic porosity (ϕ_f) and diffusion porosity (ϕ_d) Diffusion porosity (ϕ_d), fracture spacing ($2a$), matrix porosity (ϕ'), longitudinal (ε_L) and transversal (ε_T) dispersion lengths for the fracture zones and the rock between them
Spatial assignment method	Deterministic features: Constant within each feature (T,S). No changes due to calibration. Rock outside deterministic features: (K,Ss) lognormal distribution with correlation length xx. Mean, standard deviation and correlation based on calibration of the model	Properties given for each element in the model Depth dependence for the transmissivity of the fracture zone EW-3 (both M3-based and inverse modelling-based simulations) and NNW-8, SFZ05 and SFZ12 (including NE-1) (the inverse modelling-based simulations only) Depth dependent fracture spacing Kinematic porosity calculated from the hydraulic conductivity/transmissivity and the fracture spacing
Boundary conditions	Surface: Constant flux. Sea: Constant head Vertical-North: Fixed pressure based on vertical salinity distribution. Vertical-East: Fixed pressure based on vertical salinity distribution. Vertical-South: Fixed pressure based on vertical salinity distribution. Vertical-West: Fixed pressure based on vertical salinity distribution. Bottom: No flux. Linear change by time based regional simulations for undisturbed conditions and with Äspö tunnel present.	Land: zero salinity (M3-based simulations), chloride 0.1 g/l (inverse modelling-based simulations), initially and time step #1: groundwater table, time steps #2–#17: constant flow rate Sea: zero residual pressure, constant salinity (M3-based simulations) or constant chloride concentration (inverse modelling-based simulations) Vertical edges: residual pressure on the basis of a salinity (M3-based simulations) or chloride distribution (inverse modelling-based simulations), constant in time Bottom: salinity (M3-based simulations) or chloride concentration (inverse modelling-based simulations), constant in time Tunnel and shaft: residual pressure and flow rate in each time step Residual pressure initially also in the interior and bottom nodes and concentration in the interior nodes, released in the first time step
Numerical tool	PHOENICS	FEFTRA
Numerical method	Finite volume method	Finite element method
Output parameters	Head, flow and salinity field.	Residual pressure and concentration fields

Table 2 Description of model for tracer transport calculations

TOPIC	EXAMPLE	Our model
Type of model	Stochastic continuum model	Porous medium, dual porosity
Process description	Advection and diffusion, spreading due to spatially variable velocity and molecular diffusion.	Advection, dispersion, molecular and matrix diffusion
Geometric framework and parameters	Model size: 1.8x1.8x1 km^3 . Deterministic features: All deterministic features provided in the data set. Rock outside the deterministic features modelled as stochastic continuum.	Model size: cross-section hexahedron with diameter about 3.3 km, depth 1.5 km Fracture zones provided in SKB TR 97-06 Rock between the fracture zones Both the fracture zones and the rock between them modelled as dual porosity medium
Material properties	Flow porosity (ne)	Diffusion porosity (ϕ_d), fracture spacing ($2a$), matrix porosity (ϕ'), longitudinal (ε_L) and transversal (ε_T) dispersion lengths
Spatial assignment method	ne based on hydraulic conductivity value (TR 97-06) for each cell in model, including deterministic features and rock outside these features.	Properties given for each element in the model Depth dependent fracture spacing Kinematic porosity (ϕ_f) calculated from the hydraulic conductivity/transmissivity and the fracture spacing
Boundary conditions	Mixing ratios for endmembers as provided as initial conditions in data sets.	Land, sea, vertical edges and bottom: concentration for endmembers on the basis of the mixing ratios as provided by M3 and the inverse modelling Concentration for endmembers initially also in the interior nodes based on the mixing ratios as provided by M3 and the inverse modelling, released in the first time step
Numerical tool	PHOENICS	FEFTRA
Numerical method	Particle tracking method or tracking components by solving the advection/diffusion equation for each component	Finite element method, the previously simulated residual pressure and concentration fields used
Output parameters	Breakthrough curves	Concentration

Table 3 Description of model for chemical reactions calculations

TOPIC	EXAMPLE	Our model
Type of model	xxx	Inverse-modelling approach
Process description	Mixing. Reactions: Xx, Yy,Zz,Dd…..	Stepwise mixing calculations based on conservative Cl and ^{18}O. Reactions: Dissolution/precipitation of calcite, consumption of organic matter (CH_2O), dissolution of goethite, precipitation of pyrite, and in detail undefined ion exchange processes among pairs Na-Ca, Na-Mg and Na-Fe.
Geometric framework and parameters	Modelling reactions within one fracture zone, NE-1.	The reaction flow paths considered are hypothetical in the sense that no physical path between the interrelated samples was required. The aim is to describe the general evolution of water in the bedrock. It is assumed that if there would be stepwise data available along all physical flow paths related to the chosen samples, we would find analogous chemical evolution of groundwater as described with hypothetical flow paths.
Reaction parameters	Xx: a=ff, b=gg,… Yy: c=. Zz: d=...	Detailed thermodynamic rationality or reaction rates are not taken into account but reactions take place irreversibly in one step. Modelling produces quantitative reaction amounts for predefined phases that are required to reproduce the final water composition from the defined initial water samples.
Spatial distribution of reactions assumed	Xx: seafloor sediments Yz: Bedrock below sea, superficial Dd: Bedrock ground surface, superficial Yz: Bedrock below sea, at depth Zz: Bedrock ground surface, at depth Yy, Zz: near tunnel	The *altered* meteoric reference (HAS05/-56m) has been modified in the sedimentary cover and upper parts of bedrock. Following reactions are still expected in meteoric mixing: consumption of organic matter (close to ground level we still have organic matter available), moderate or strong precipitation of calcite (meteoric reference is high in HCO_3) and small overall mole-transfers among other dissolved ions are expected. If the *fresh* seawater dominates mixing, strong consumption of organic matter, dissolution of calcite, dissolution of Ca and Fe from CaX_2 and FeX_2/goethite, precipitation of Na and Mg to NaX and MgX_2, and precipitation of pyrite are expected. The saline reference water is well equilibrated with its environment. Only small organic matter consumption (restricted microbial activity at depth) and small overall mole-transfers among other dissolved ions are expected.
Boundary/initial conditions for the reactions	Xx: aaa… Yy: bbb…	Inverse-modelling approach is based on an attempt to understand the geochemical system along a flow path. Calculations continue until acceptable set of initial water samples and reactions are found for certain final water. A previous successful (assumed steady-state) step leads to the following step, which is to find new sets of initial water samples for previous initial water samples now considered as final water samples, and so on. Steps are ultimately extended to the reference water types and then mixing fractions of the reference water types in each sample, considered in the calculation chain, can be solved.
Numerical tool	Phreeque	PHREEQC-2
Numerical method	xx	*Iterative approach* aiming to contemporaneous solution of: a) mole-balance equations for each element or element redox state, alkalinity, and electrons b) charge balance equation c) an equation that relates the uncertainty terms for pH, alkalinity, and total dissolved inorganic carbon d) inequality constraints on the size of the uncertainty terms
Output parameters	xx	Mixing proportions of reference water types for each sample involved in the calculations. Estimations of mole-transfers required reaching the final water composition in question.

Table 4a Summary of data usage

Data del. No	Data	Importance of data (see notes)	Comment
1	Hydrochemical data 1		
1a	Surface boreholes- undisturbed conditions, Äspö-Laxemar	**P**	Only data from the Äspö Island used
1b	Surface boreholes- disturbed conditions (by tunnel excavation), Äspö	**P**	Only KAS03 and KAS07
1c	Surface boreholes- undisturbed conditions, Ävrö	X	
1d	Surface boreholes- sampled during drilling, Äspö	X	
1e	Data related to the Redox experiment	**P**	
1f	Tunnel and tunnel boreholes- disturbed conditions	**P**	
2	Hydrogeological data 1		
2a1	Annual mean air temperature	-	
2a2	Annual mean precipitation	-	
2a3	Annual mean evapotranspiration	-	
2b1	Tunnel front position by time	**P**	
2b2	Shaft position by time	**P**	
2c1	Geometry of main tunnel	**P**	
2c2	Geometry of shafts	**P**	
2d	Hydrochemistry at weirs (Cloride, pH, Electrical conductivity, period: July 1993- Aug 1993)	-	
2e	Geometry of the deterministic large hydraulic features (Most of them are fracture zones)	-	data from SKB TR 97-06

Table 4b Summary of data usage

Data del. No	Data	Importance of data (see notes)	Comment
3	Hydrogeological data 2		
3a	Monthly mean flow rates measured at weirs. Tunnel section 0-2900m, period May 1991 – January 1994	-	Data delivery #9 was used instead.
3b	Piezometric levels for period June 1st 1991 – May 21st 1993. Values with 30 days interval (Task 3 data set)	**P**	Freshwater head used
3c	Salinity levels in borehole sections for period -Sept 1993. (Task 3 data set)	**P**	Undisturbed values used in the comparison with the model outcome in the M3-based modelling
3d	Undisturbed piezometric levels	**P**	Values used in the comparison with the model outcome in the M3-based modelling
3e	Co-ordinates for borehole sections	**P**	
3f	Piezometric levels for period July 1st 1990 – January 24st 1994. Daily values.	-	
4	Hydrochemical data 2		This was used before delivery #7.
4a	Chemical components, mixing proportions and deviations for all borehole sections used in the M3 calculations	**P**	The mixing proportions in the control points were used in the comparison with the model outcome.
4b	Boreholes with time series, > 3 samples (part of 4a)	-	
4c	Borehole sections interpreted to intersect deterministic large hydraulic features (Most of them are fracture zones) (part of 4a)	-	
4d	Chemical components, mixing proportions and deviations. Grid data based on interpolation. Undisturbed conditions	**P**	The mixing proportions were used in the fixing of the initial boundary conditions for the water types.
4e	Chemical components, mixing proportions and deviations. Grid data based on interpolation. Disturbed conditions (by tunnel excavation)	-	
4f	Boundary and initial conditions. Chemical components, mixing proportions and deviations (1989). Grid data for vertical boundaries based on interpolation. Undisturbed conditions	**P**	4d was used, 4f & 4g were compared.
4g	Boundary conditions after tunnel construction (1996) Chemical components, mixing proportions and deviations. Grid data for vertical boundaries based on interpolation. Disturbed conditions (by tunnel excavation)	**P**	

Table 4c Summary of data usage

Data del. No	Data	Importance of data (see notes)	Comment
5	Geographic data 1		
5a	Äspö coast line	**P**	
5b	Topography of Äspö and the nearby surroundings	p	This data was used in a test case in the M3-based simulations.
6	Hydro tests and tracer tests		
6a	Large scale interference tests (19 tests)	-	
6b	Long time pump and tracer test, LPT2	-	
7	Hydrochemical data 3, update of data delivery 4 based on new endmembers. Recommended to be used instead of 4.		This data was used instead of delivery #4.
7a	Chemical components, mixing proportions and deviations for all borehole sections used in the M3 calculations	**P**	The mixing proportions in the control points were used in the comparison with the model outcome.
7b	Boreholes with time series, > 3 samples (part of 7a)	-	
7c	Borehole sections interpreted to intersect deterministic large hydraulic features (Most of them are fracture zones) (part of 7a)	-	
7d	Chemical components, mixing proportions and deviations. Grid data based on interpolation. Undisturbed conditions	**P**	The mixing proportions were used in the fixing of the initial boundary conditions for the water types.
7e	Chemical components, mixing proportions and deviations. Grid data based on interpolation. Disturbed conditions (by tunnel excavation)	-	
7f	Boundary and initial conditions. Chemical components, mixing proportions and deviations (1989). Grid data for vertical boundaries based on interpolation. Undisturbed conditions	-	7d was used.
7g	Boundary conditions after tunnel construction (1996). Chemical components, mixing proportions and deviations. Grid data for vertical boundaries based on interpolation. Disturbed conditions (by tunnel excavation)	-	

Table 4d Summary of data usage

Data del. No	Data	Importance of data (see notes)	Comment
8	Performance measures and reporting 1		
8a	Performance measures	**P**	
8b	Suggested control points. 6 points in tunnel section 0-2900m and 3 points in tunnel section 2900-3600m.	**P**	This data was replaced by data deliveries #12 and #15.
8c	Suggested flowchart for illustration of modelling	**P**	
9	Hydrogeological data 3		
9a	Monthly mean flow rates measured at weirs. Tunnel section 0-3600m, period: May 1991- Dec 1996.	**P**	
10	Geographic data 2		
10a	Topography of Äspö and the nearby surroundings (larger area than 5b)	**M**	see 5b
10b	Co-ordinates for wetlands	-	
10c	Co-ordinates for lakes	-	
10d	Co-ordinates for catchments	-	
10e	Co-ordinates for streams	-	
10f	Co-ordinate transformation Äspö system- RAK	-	
11	Boundary and initial conditions		
11a	Pressure before tunnel construction, from the regional SKB model (TR 97-09)	-	
11b	Salinity before tunnel construction, from the regional SKB model (TR 97-09)	-	
11c	Pressure after tunnel construction, from the regional SKB model (TR 97-09)	-	
11d	Salinity after tunnel construction, from the regional SKB model (TR 97-09)	-	

Table 4e Summary of data usage

Data del. No	Data	Importance of data (see notes)	Comment
12	Performance measures and reporting 2		
12a	Suggested control points. 6 points in tunnel section 0-2900m and 3 points in tunnel section 2900-3600m (same as 8b) and 2 outside the tunnel.	**P**	
13	Transport parameters compiled		
13a	LPT2 tracer tests	-	
13b	Tracer test during passage of fracture zone NE-1	-	
13c	Redox tracer tests	-	
13d	TRUE-1 tracer tests	-	
14	Hydrochemical data 4		
14a	Groundwater reactions to consider within TASK5 modelling (Description of how M3 calculates the contribution of reactions and identifying dominating reactions based on the M3 calculations.	**M**	
15	Co-ordinates for the test sections defining the control points	**P**	
16	Co-ordinates for boreholes drilled from the tunnel	-	

Table 4f Summary of data usage

Data del. No	Data	Importance of data (see notes)	Comment
17	Hydrogeological data - prediction period		
17a	Hydrochemistry at weirs (Cloride, pH, Electrical conductivity, period: July 1993- Dec 1995)	-	
17b	Piezometric levels for period July 1st 1990 – Dec 1996. Daily values.	-	
18	Hydrochemical data - prediction period.		
18a	Chemical components, mixing proportions and deviations for all borehole sections used in the M3 calculations. Data for tunnel section 2900-3600m.	**P**	
18b	Boreholes with time series, > 3 samples (part of 18a)	-	
18c	Boreholes sections interpreted to intersect deterministic large hydraulic features (Most of them are fracture zones) (part of 18a)	-	
	Other data (part of data to Task 1, 3 and 4)		
	Fracture orientation, fracture spacing and trace length – tunnel data	-	
	Fracture orientation, fracture spacing– mapping of cores	-	
	Fracture orientation, fracture spacing and trace length – mapping of outcrops	-	
	Groundwater table over the Äspö island	**P**	This was taken from a previous modelling exercise and was used in the beginning and in the first time step.

P = data of great importance for quantitative estimation of model parameters
p = data of less importance for quantitative estimation of model parameters
M = data of great importance used qualitatively for setting up model
m = data of less importance used qualitatively for setting up model
X = data useful as general background information
- = data not used

Acknowledgements

The geochemical mixing results and the boundary conditions used in the simulations reported in Part II were produced with the M3 method by Ioana Gurban, Marcus Laaksoharju and Cecilia Andersson (all from Intera KB) and distributed to all modelling groups of the Task #5. Early distribution of these results has been in the crucial role in the fluent progress of the project.
Our manuscripts were reviewed by Peter Jackson (AEA Technology) and Adrian Bath (Intellisci). We would like to thank the reviewers for the constructive criticism and good pieces of advice how to improve the texts.
The project was steered by Peter Wikberg (SKB), Ingvar Rhén (VBB VIAK) and John Smellie (Conterra). They guaranteed the fluent co-operation in the project, and have made excellent suggestions and comments to the manuscripts as well.
Most indebted we are, however, to Aimo Hautojärvi ja Margit Snellman (both from Posiva). Their support made our participation in this project financially possible. During the years of project activities, both Aimo and Margit also commented several times our work.